PB89-207955

Evaluation of Internally Staged Coal Burners and Sorbent Jet Aerodynamics for Combined SO2/NOx Control in Utility Boilers Volume 1. Testing in a 10 Million Btu/hr Experimental Furnace

Energy and Environmental Research Corp., Irvine, CA

Prepared for:

Environmental Protection Agency, Research Triangle Park, NC

Jun 89

U.S. Department of Commerce
National Technical Information Service
NTIS

TECHNICAL REPORT DATA

(Please read Instructions on the reverse before completing)

1. REPORT NO. EPA/600/7-89/007	2.	3. RECIPIENT'S ACCESSION NO.

4. TITLE AND SUBTITLE Evaluation of Internally Staged Coal Burners and Sorbent Jet Aerodynamics for Combined SO_2/NO_x Control in Utility Boilers; Volume 1. Testing in a *	5. REPORT DATE June 1989
	6. PERFORMING ORGANIZATION CODE
7. AUTHOR(S) B. Cetegen, J. Clough, G. England, T. Johnson, Y. Kwan, and R. Payne	8. PERFORMING ORGANIZATION REPORT NO.
9. PERFORMING ORGANIZATION NAME AND ADDRESS Energy and Environmental Research Corporation 18 Mason Irvine, California 92718-2798	10. PROGRAM ELEMENT NO.
	11. CONTRACT/GRANT NO. 68-02-3923
12. SPONSORING AGENCY NAME AND ADDRESS EPA, Office of Research and Development Air and Energy Engineering Research Laboratory Research Triangle Park, NC 27711	13. TYPE OF REPORT AND PERIOD COVERED Final; 10/82 - 6/85
	14. SPONSORING AGENCY CODE EPA/600/13

15. SUPPLEMENTARY NOTES AEERL project officer is D. Bruce Henschel, Mail Drop 54, 919/541-4112. (*) 10 Million Btu/hr Experimental Furnace.

16. ABSTRACT The document gives results of tests conducted in a 2 MWt experimental furnace to: (1) investigate ways to reduce NOx emissions from utility coal burners without external air ports (i.e., with internal fuel/air staging); and (2) improve the performance of calcium-based sorbents for SO2 control, by modifying the design and operation of the sorbent jets. NOx emissions could be reduced by 50-60% (to 300-500 ppm) without external ports by using two secondary air channels in the burner throat, and by modifying the coal nozzle. A baffle in the outer secondary air channel also appears necessary where high secondary air velocities cannot be avoided. Sorbent testing confirmed that jet design/operation must focus on protecting the sorbent from seeing high peak temperatures: a peak temperature of 1230-1290 C gave optimum sorbent performance. SO2 removals of 80% at Ca/S = 2 were achieved with a pressure-hydrated lime at this temperature. Jet design to increase sorbent heating rate might also have a secondary effect in improving performance.

17. KEY WORDS AND DOCUMENT ANALYSIS

a. DESCRIPTORS		b. IDENTIFIERS/OPEN ENDED TERMS	c. COSATI Field/Group	
Pollution	Calcium Oxides	Pollution Control	13B	
Coal	Jets	Stationary Sources	21D	20D
Combustion	Aerodynamics	Utility Boilers	21B	
Nitrogen Oxides	Utilities		07B	
Sulfur Dioxide	Boilers			13A
Sorbents			11G	

18. DISTRIBUTION STATEMENT Release to Public	19. SECURITY CLASS *(This Report)* Unclassified	21. NO. OF PAGES 296
	20. SECURITY CLASS *(This page)* Unclassified	22. PRICE

EPA Form 2220-1 (9-73)

PB89-207955

EPA/600/7-89/007
June 1989

EVALUATION OF INTERNALLY STAGED COAL BURNERS AND SORBENT JET AERODYNAMICS FOR COMBINED SO_2/NO_x CONTROL IN UTILITY BOILERS

Volume 1. Testing in a 10 Million Btu/hr Experimental Furnace

by

B. M. Cetegen
J. Clough
G. C. England
T. R. Johnson
Y. Kwan
R. Payne

Energy and Environmental Research Corporation
18 Mason
Irvine, California 92718-2798

EPA Contract 68-02-3923

EPA Project Officer: D. Bruce Henschel
Air and Energy Engineering Research Laboratory
Office of Environmental Engineering and Technology Demonstration
Research Triangle Park, NC 27711

AIR AND ENERGY ENGINEERING RESEARCH LABORATORY
OFFICE OF RESEARCH AND DEVELOPMENT
U.S. ENVIRONMENTAL PROTECTION AGENCY
RESEARCH TRIANGLE PARK, NC 27711

REPRODUCED BY
U.S. DEPARTMENT OF COMMERCE
NATIONAL TECHNICAL INFORMATION SERVICE
SPRINGFIELD, VA. 22161

NOTICE

This document has been reviewed in accordance with U.S. Environmental Protection Agency policy and approved for publication. Mention of trade names or commercial products does not constitute endorsement or recommendation for use.

ABSTRACT

As part of EPA's Limestone Injection/Multistage Burner (LIMB) program, testing was conducted on a 10 million Btu/hr experimental furnace to explore the potential for designing utility coal burners to achieve reduced NO_x emissions through staging of the combustion air internally within the burner. Such internal staging would avoid the need for external tertiary air ports, and thus simplify the retrofit of such a low-NO_x burner into existing utility furnaces. Testing also addressed the potential for SO_2 removal through the injection of calcium-based sorbents (such as limestone) in conjunction with coal-fired internally-staged burners, to provide combined SO_2/NO_x control. Particular emphasis was placed upon understanding the sorbent jet design parameters which could improve the activation and SO_2 removal performance of sorbents, through control of sorbent heating rate and the peak temperature seen by the sorbent. The sorbent jet testing considered injection near the burners (using large, double concentric jets), and injection under upper-furnace conditions, remote from the burners.

Testing of alternative internally-staged burner designs showed that -- if a particular retrofit situation offers the flexibility to increase the burner throat diameter, in order to reduce velocity -- NO_x emissions of 300-500 ppm appear achievable with two secondary air channels and coal nozzle modifications. This emission represents approximately the desired 50 to 60 percent reduction in the emissions characteristic of pre-NSPS burners (typically 500-750 ppm). However, where there is not flexibility to increase the throat and reduce velocity, then additional steps (e.g., a baffle in the outer secondary air channel to direct the air away from the fireball) are necessary to reduce NO_x to 400-550 ppm, approaching the reduction objective.

Sorbent jet testing confirmed that the peak temperature seen by the sorbent is a key variable in determining sorbent reactivity. A peak temperature of 2250 to 2350 °F appears to be optimum for all five sorbents tested (a limestone, a dolomite, two atmospheric hydrates and a pressure hydrate). At this peak temperature, the most reactive sorbent (the pressure hydrate) gave 80 percent SO_2 removal at Ca/S = 2, the least reactive (the limestone) gave 30 percent. The apparent effect of sorbent heating rate was not consistent over the full range of temperatures tested, but at the optimum peak sorbent temperature, the higher heating rate (higher sorbent jet velocity) consistently produced somewhat higher SO_2 removals. The experimental furnace was too small to permit an effective test of whether double concentric jets (with an annular air jet surrounding the sorbent jet) could protect the sorbent from overheating during near-burner injection. Testing of controlled sorbent precalcination followed by immediate injection into the furnace showed little clear benefit of close-coupled precalcination.

TABLE OF CONTENTS

Section Page

Abstract iii
List of Figures ix
List of Tables xvii
Metric Conversion Factors xix

EXECUTIVE SUMMARY E-1

E.1 Low-NO_x Internally-Staged Burners. E-2
E.2 Sorbent Jet Investigations - Double Concentric Jets. E-7
E.3 Sorbent Jet Investigations - Small Jets. . . E-7
E.4 Testing of a Close-Coupled Precalciner . . . E-11

1.0 INTRODUCTION - INTERNALLY-STAGED BURNERS. 1-1

1.1 Considerations in Low-NO_x Burner Design. . . 1-3
1.2 Considerations in Sorbent Injection Testing. 1-13

2.0 EQUIPMENT, MATERIALS AND TEST MATRICES FOR INTERNALLY-STAGED BURNER TESTING 2-1

2.1 Experimental Furnace, Fuels and Sorbents . . 2-1
2.2 Burner Configurations for Internally-Staged Burner Tests 2-4
  2.2.1 HV1 Burner 2-4
  2.2.2 LV1 Burner 2-9
  2.2.3 HV2 Burner 2-15
2.3 Experimental Arrangement for Sorbent Injection Testing. 2-23
  2.3.1 Sorbent Injection with Internally-Staged Burners. . . 2-25
  2.3.2 Measurements for Sorbent Injection Tests. 2-27

3.0 LOW-NO_x INTERNALLY-STAGED BURNER TEST RESULTS . . 3-1

3.1 High Velocity Burner 1 (HV1) 3-1
  3.1.1 HV1 Tests with Natural Gas . . . 3-1
  3.1.2 HV1 Tests with Utah Coal 3-5

TABLE OF CONTENTS (continued)

Section Page

3.2 Low Velocity Burner 1 (LV1). 3-8
3.2.1 LV1 Tests with Conventional Coal Transport 3-9
3.2.2 LV1 Tests with Dense-Phase Coal Transport 3-19
3.3 High-Velocity Burner 2 (HV2) 3-24
3.3.1 HV2 Tests with Conventional Coal Transport 3-25
3.3.2 HV2 Tests with Dense-Phase Coal Transport 3-35
3.4 Summary of NO_x Results from Internally-Staged Burners 3-43

4.0 SORBENT INJECTION WITH INTERNALLY-STAGED LOW-NO_x BURNERS 4-1

4.1 Natural Gas Flames Doped with SO_2. 4-1
4.1.1 Effect of Injection Location . . 4-2
4.1.2 Effect of Injection Velocity (Wall Injection) 4-5
4.1.3 Effect of Burner Load (Wall Injection) 4-7
4.1.4 Effect of Initial SO_2 Concentration 4-10
4.2 Coal Flames. 4-11
4.2.1 HV1 Burner 4-11
4.2.2 LV1 Burner 4-13
4.3 Potential for Sulfur Capture with Near-Burner Sorbent Injection 4-19

5.0 CONCLUSIONS FROM INTERNALLY-STAGED BURNER TESTS . 5-1

6.0 INTRODUCTION - SORBENT JET AERODYNAMICS 6-1

7.0 EQUIPMENT, MATERIALS AND TEST MATRICES FOR STUDIES OF SORBENT JET AERODYNAMICS 7-1

7.1 Experimental Furnace, Fuels and Sorbents . . 7-1
7.2 Sorbent Jet Experiments. 7-2
7.2.1 Non-Symmetric Jet Arrangement . 7-2
7.2.2 Symmetric Co-Flowing Jet Arrangement. 7-7
7.2.3 Cross-Flow Jet Injection 7-16

TABLE OF CONTENTS (continued)

Section Page

7.3 Close-Coupled Precalciner. 7-21
7.4 Measurements for Sorbent Jet Studies 7-24

8.0 SORBENT INJECTION WITH DOUBLE CONCENTRIC JETS . . 8-1

8.1 Jet Experiments in Non-Axisymmetric Configuration 8-2
8.2 Jet Experiments in Axisymmetric Configuration. 8-10
8.2.1 Double Concentric Jets in Co-Flow. 8-12
8.2.2 Sorbent Surface Area and Calcium Utilization. 8-23
8.2.3 Effect of Ash Interaction. . . . 8-29
8.2.4 Single-Pipe Sorbent Jets 8-29
8.3 Double Concentric Jets in Cross-Flow 8-34

9.0 SORBENT HEATING RATE STUDIES WITH SMALL JETS. . . 9-1

9.1 SO_2 Capture Results with 2-Inch Single-Pipe Jets. 9-2
9.2 SO_2 Capture Results with 1-Inch Single-Pipe Jets. 9-10
9.3 Small-Diameter Co-Axial Jets 9-12
9.4 Temperature Measurements in Jets 9-17
9.5 Effect of Temperature on SO_2 Capture 9-30
9.6 Sorbent Surface Area 9-32
9.7 Summary of Sorbent Heating Rate Studies. . . 9-38

10.0 CLOSE-COUPLED PRECALCINER INVESTIGATION 10-1

10.1 SO_2 Capture with the Precalciners 10-1
10.1.1 Regular Refractory, Long Version 10-1
10.1.2 Regular Refractory, Short Version 10-3
10.1.3 Chrome Refractory, Long version 10-3
10.1.4 Chrome Refractory, Short Version. 10-3
10.2 Sorbent Surface Areas 10-7

TABLE OF CONTENTS (continued)

Section Page

11.0 CONCLUSIONS FROM SORBENT JET INVESTIGATIONS . . . 11-1

11.1 Large Diameter Jet Studies. 11-1
11.2 Sorbent Heating Rate Studies. 11-2

12.0 REFERENCES 12-1

APPENDIX

A QUALITY ASSURANCE: SWS INVESTIGATIONS A-1

LIST OF FIGURES

Figure Page

E-1 Summary of NO_x emissions for low-NO_x coal nozzles tested with low-velocity and high-velocity burners . E-4

E-2 NO_x reductions achieved by secondary air baffles with high-velocity burner E-5

E-3 SO_2 capture with Vicron 45-3 sorbent in HV1 burner (natural gas flames)--effect of injection location . E-6

E-4 Effect of peak sorbent temperature on SO_2 capture at different sorbent initial heating rates E-9

E-5 SO_2 capture with Vicron limestone injected through a 2-inch single-pipe jet -- heating rate studies . . E-10

E-6 Effect of peak temperature and heating rate on sorbent surface area E-12

1-1 Air and fuel staging 1-4

1-2 Air staging effects with a distributed mixing burner utilizing external tertiary air ports 1-5

1-3 An internal conical baffle between inner and outer secondary air channels of a divided register burner. 1-9

1-4 Alternative approaches for coal nozzle modifications 1-10

2-1 Component parts of SWS furnace and exhaust system. . 2-2

2-2 High-velocity burner with three secondary air channels (HV1) 2-7

2-3 Peabody gas nozzle used in HV1 testing 2-8

2-4 Sketch of an axial vane swirler. 2-10

2-5 Low-velocity burner (LV1). 2-11

2-6 Sketch of divergent splitters. 2-13

2-7 Sketch of dense phase coal nozzles 2-14

2-8 Coal splitters/spreaders tested for LVI burner . . . 2-16

2-9 Burner operating parameters investigated on the LV1 and HV2 burner configurations. 2-17

LIST OF FIGURES (continued)

Figure / Page

2-10 High-velocity burner with two secondary air channels (HV2) 2-18

2-11 Secondary air baffle installed in the HV2 burner configuration. 2-20

2-12 Burner modifications tested during HV2 burner tests. 2-21

2-13 Schematic diagram of sorbent feed system 2-24

2-14 Sorbent injection locations for tests with internally-staged burners 2-26

3-1 NO_x emissions versus furnace exit temperature during coal combustion tests with HV1 burner 3-7

3-2 Summary of NO_x emissions at baseline burner settings for LV1 with axial vane coal swirlers . . . 3-10

3-3 Flame shapes for baseline flames with axial swirlers in LV1 burner (NO_x and CO emission values are dry and corrected to 0% O_2, at 2000 °F furnace exit temperature). 3-12

3-4 Summary of NO_x emissions at baseline burner settings for LV1 with divergent splitter nozzles . . 3-15

3-5 Flame shapes for baseline flames with T and 3T splitters in LV1 burner (NO_x and CO emissions values are dry and corrected to 0% O_2, at 2000 °F furnace exit temperature). 3-16

3-6 Summary of NO_x emission at baseline burner settings for LV1 with dense phase nozzles 3-20

3-7 Flame shapes for baseline flames with dense phase coal nozzles in LV1 burner (NO_x and CO emission values are dry and corrected to 0% O_2 at 2000 °F exit temperature 3-21

3-8 Summary of NO_x emissions at baseline burner settings for HV2 with 15° axial swirler (with and without baffles). LV1 results with 15° swirler shown for comparison 3-26

LIST OF FIGURES (continued)

Figure Page

3-9 Comparison of baseline flame shapes for LV1 and HV2 burners with 15° axial swirler (NO_x and CO emissions values are dry and corrected to 0% O_2, at 2000 °F furnace exit temperature) 3-28

3-10 Summary of NO_x emissions at baseline burner settings for HV2 with T-15° splitter (with and without baffles). LV1 results for T-15° splitter shown for comparison 3-31

3-11 Comparison of baseline flame shapes for LV1 and HV2 flames with T-15° splitter (NO_x and CO emissions values are dry and corrected to 0% O_2 at 2000 °F furnace exit temperature). 3-33

3-12 Summary of NO_x emissions at baseline burner settings for HV2 with swirler (with and without baffle). LV1 results with dense-phase swirler shown for comparison 3-36

3-13 Comparison of baseline flame shapes for LV1 and HV2 burners with 30° axial swirler in dense phase and nozzle 3-38

3-14 Summary of NO_x emissions at baseline burner settings for HV2 with dense phase 30° cone spreader (with and without baffle). LV1 results with dense-phase cone shown for comparison 3-40

3-15 Comparison of baseline flame shapes for LV1 and HV2 burner with 30° cone spreader in dense phase coal nozzle (NO_x and CO emissions values are dry and corrected to 0% O_2 at 2000 °F furnace exit temperature) 3-42

3-16 Summary of baseline NO_x emissions for low-NO_x coal nozzles tested with low velocity and high velocity burners (without secondary air baffles). 3-45

3-17 NO_x reductions achieved by secondary air baffles with HV2 burner 3-47

3-18 Correlation of NO_x emissions with flame shape factor (2000 °F furnace exit temperature) 3-48

3-19 Correlation of LV1 NO_x emissions using parameter accounting for flame volume and thermal characteristics. 3-50

LIST OF FIGURES (continued)

Figure Page

4-1 Sorbent injection locations for low-NO_x burners. . . 4-3

4-2 SO_2 capture in HV1 burner (doped natural gas flames) -- effect of sorbent injection location . . 4-4

4-3 SO_2 capture in HV1 burner (doped natural gas flames) -- effect of sorbent injection velocity . . 4-6

4-4 SO_2 capture in HV1 burner (doped natural gas flames) -- effect of burner load 4-8

4-5 Mean time-temperature profiles on the axis of the SWS furnace at full load and half load 4-9

4-6 SO_2 capture in HV1 burner (Utah coal flame) -- effect of sorbent injection location and fuel type . 4-12

4-7 SO_2 capture results with low-NO_x burner conditions . 4-16

4-8 SO_2 capture in LV1 burner as a function of SWS furnace exit temperature, with Vicron 45-3 at Ca/S = 2.0 4-17

7-1 Sorbent particle size distributions. 7-4

7-2 Commercial hydrate particle size distributions . . . 7-5

7-3 SWS configuration for preliminary jet experiment . . 7-6

7-4 SWS configuration for double-concentric jet experiments with uniform bulk gas flow field 7-9

7-5 SWS configuration for single-pipe jet experiments with uniform bulk gas flow field 7-11

7-6 Calculated mean jet bulk temperatures as a function of time for 1-inch and 2-inch diameter single-pipe jets in an environment with falling background temperature T_B (initial T_B = 2600 °F) -- used in design of jet heating rate Tests 7 and 8 7-15

7-7 Calculated mean jet bulk temperatures as a function of time for 2-inch single-pipe jets at initial T_B = 2500 °F, for two values of jet velocity -- used in design of jet heating rate Tests 7 and 8 7-17

LIST OF FIGURES (continued)

Figure Page

7-8 Calculated mean jet bulk temperature as a function of time for 1-inch and 2-inch single-pipe jets, for various jet velocities and background temperatures resulting in a peak sorbent temperature of 2250 °F. 7-18

7-9 Calculated mean jet bulk temperature as a function of time for 2-inch single-pipe jets reaching peak sorbent temperatures of 2040 and 2250 °F at approximately the same heating rate 7-19

7-10 SWS arrangement for cross-flow sorbent injection into uniform gas flow field. 7-20

7-11 Schematic for SWS precalciner. 7-23

8-1 SO_2 capture with double concentric jets around V-10 externally-staged distributed mixing burner -- effect of sorbent injection velocity 8-3

8-2 SO_2 capture with double concentric jets during preliminary (non-axisymmetric) testing -- effects of sorbent jet velocity and annular air jet velocity, with 12-inch air jet (oil firing) 8-5

8-3 SO_2 capture with double concentric jets during preliminary (non-axisymmetric) testing -- effects of sorbent jet velocity and annular air jet velocity, with 10-inch air jet (oil firing) 8-6

8-4 SO_2 capture with double concentric jets during preliminary (non-axisymmetric) testing -- effects of sorbent and annular air jet velocities, and effect of coal vs. oil, with 10-inch jet (coal firing) 8-9

8-5 SO_2 capture with double concentric jets in uniform flow (axisymmetric) testing -- 12-inch annular air jet (co-flow) 8-13

8-6 Radial and axial temperature profiles for 12-inch double concentric air jet. 8-15

8-7 SO_2 capture with double concentric jets in uniform flow (axisymmetric) testing -- 10-inch annular air jet (co-flow) 8-17

LIST OF FIGURES (continued)

Figure		Page
8-8	SO_2 capture with double concentric jets in uniform flow (axisymmetric) testing -- 6-inch annular air jet (co-flow)	8-19
8-9	SO_2 capture as a function of furnace exit temperature for double-concentric jet experiments. .	8-22
8-10	Sorbent surface area along the center-line of the 6-inch double concentric air jet (co-flow, uniform flow field)	8-24
8-11	Profiles along the center-line of the 6-inch double concentric air jet	8-25
8-12	Calcium utilization and surface area along the center-line of the 6-inch double concentric jet . .	8-27
8-13	Effect of coal ash on SO_2 capture in gas flames -- 10-inch and 6-inch double concentric jets (co-flow, uniform flow conditions)	8-30
8-14	SO_2 capture with single-pipe sorbent jet at 2200 °F background temperature -- effect of sorbent injection velocity	8-32
8-15	SO_2 capture with single-pipe sorbent jet at injection velocity of 100 ft/sec -- effect of background temperature	8-35
8-16	SO_2 capture with double concentric jet in cross-flow -- effect of air and sorbent jet velocities . .	8-37
8-17	Estimated center-line trajectories of cross-flow jets in SWS furnace	8-39
9-1	SO_2 capture with Vicron limestone injected through a 2-inch single-pipe jet -- heating rate studies . .	9-3
9-2	SO_2 capture for Colton atmospheric-pressure calcitic hydrate injected through 2-inch single-pipe jets -- heating rate studies	9-5
9-3	SO_2 capture for Longview atmospheric-pressure calcitic hydrate injected through 2-inch single-pipe jet -- heating rate studies	9-6
9-4	SO_2 capture for D3002 dolomite injected through 2-inch single-pipe jet -- heating rate studies . . .	9-8

LIST OF FIGURES (continued)

Figure		Page
9-5	SO_2 capture for Genstar Type-S dolomitic pressure hydrate injected through 2-inch single-pipe jet -- heating rate studies	9-8
9-6	Effect of heating rate and peak temperature on SO_2 capture in 1-inch single-pipe jets (Vicron limestone, Longview atmospheric hydrate and Type-S pressure hydrate) -- heating rate studies	9-13
9-7	SO_2 capture with Vicron limestone injected through 4-inch double concentric jet -- heating rate study .	9-15
9-8	SO_2 capture with Longview atmospheric calcitic hydrate injected through 4-inch double concentric jet -- heating rate study	9-16
9-9	SO_2 capture with Genstar Type-S dolomitic pressure hydrate injected through 4-inch double concentric jet -- heating rate study	9-18
9-10	Temperature distribution measured in 2-inch jet (jet velocity = 50 ft/sec; background temperature 2500 °F)	9-19
9-11	Change in mean temperature with distance along jet .	9-23
9-12	Estimated temperature and Ca/S ratio histories for 2-inch jet injected at 50 ft/sec into SWS with 2500 °F background temperature	9-25
9-13	Estimated temperature and Ca/S ratio histories for 2-inch jet injected at 100 ft/sec into SWS with 2500 °F background	9-26
9-14	SO_2 captures predicted for 2-inch single-pipe jets at jet velocities of 50 and 100 ft/sec, based upon sulfation model of Silcox et al.	9-28
9-15	Effect of peak sorbent temperature on SO_2 capture at different sorbent initial heating rates	9-31
9-16	Effect of peak temperature and heating rate on sorbent surface area	9-35
9-17	Sorbent surface area in 2-inch jet for Longview Lime sorbent	9-37

LIST OF FIGURES (continued)

Figure | Page

10-1 SO_2 capture with Vicron limestone using a close-coupled precalciner -- standard alumina refractory, long version 10-2

10-2 SO_2 capture with Vicron limestone using a close-coupled precalciner -- standard alumina refractory, short version 10-4

10-3 SO_2 capture with Vicron limestone using a close-coupled precalciner -- chromium refractory, long version 10-5

10-4 SO_2 capture with Vicron limestone using a close-coupled precalciner -- chromium refractory, short version 10-6

A-1 Coal Feeder Calibration for Utah Coal. A-4

A-2 "Fuel Check" during the burner test series A-5

A-3 "Fuel check" during jet experiment series. A-6

A-4 Schematic of SWS sampling system A-9

A-5 SWS furnace analytical system. A-10

A-6 Phase discrimination probe A-12

A-7 Suction pyrometer tip construction A-15

A-8 Suction flow rate calibration for suction pyrometer. A-16

A-9 Relative accuracy of heating value determinations. . A-18

A-10 Relative accuracy of coal sulfur A-19

LIST OF TABLES

Table Page

2-1 Characteristics of the SWS 2-3

2-2 Analyses of Fuels. 2-5

2-3 Characteristics of Sorbent Vicron 45-3 2-6

2-4 Measurement Format for Low-NO_x Internally-Staged Burner Tests 2-22

2-5 Measurement Format for Sorbent Injection Tests . . . 2-28

3-1 Results of Secondary Air Distribution Variations with HV1 Burner. 3-2

3-2 Results of Secondary Air Swirl Variations with HV1 Burner 3-4

3-3 Effect of Burner Adjustments on NO_x Emissions for Axial Swirlers with LV1 Burner 3-13

3-4 Effect of Burner Adjustments on NO_x Emissions for Splitter Nozzles with LV1 Burner 3-18

3-5 Effect of Burner Adjustments on NO_x Emissions for Dense Phase Nozzles with LV1 Burner. 3-23

3-6 Effect of Burner Adjustments on NO_x Emissions for 15° Axial Swirler with HV2 Burner. 3-29

3-7 Effect of Burner Adjustments on NO_x Emissions for T-15° Splitter with HV2 Burner 3-34

3-8 Effect of Burner Adjustments on NO_x Emissions for 30° Axial Swirler in Dense Phase Coal Nozzle with HV2 Burner. 3-39

3-9 Effect of Burner Adjustments on NO_x Emissions for 30° Cone Spreader in Dense Phase Coal Nozzle with HV2 Burner 3-44

4-1 Low-NO_x Burner Conditions for Sorbent Injection Screening: LV1 Burner 4-14

7-1 Physical and Chemical Properties of Sorbents 7-3

7-2 Test Matrix for Preliminary Jet Experiment 7-8

7-3 Axisymmetric Jet Experiment Test Matrix. 7-12

LIST OF TABLES (continued)

Table Page

7-4 Test Matrix for Heating Rate Experiments 7-14

7-5 Test Matrix for Cross-Flow Sorbent Jets. 7-22

7-6 Test Matrix for Close-Coupled Precalciner. 7-25

7-7 Measurement Format for Sorbent Injection Tests . . . 7-27

8-1 Results of Co-Flow Double Concentric Sorbent Jet Injection Tests: Uniform Flow Testing 8-21

9-1 SO_2 Capture Results for 2-Inch Jets. 9-11

9-2 Peak Sorbent Temperatures Measured During Jet Temperature Surveys. 9-20

9-3 Summary of Jet Sulfur Capture Predictions: Effect of Jet Velocity on SO_2 Capture. 9-29

9-4 Sorbent Surface Areas Measured at Furnace Exit for Different Jet Configurations 9-34

10-1 Sorbent Surface Areas Generated with Close-Coupled Precalciner 10-8

A-1 Program Objectives for Measurement Precision Accuracy and Completeness A-2

A-2 SWS Venturi Flowmeter Calibrations A-8

A-3 Continuous Gas Analyzers A-11

A-4 Instrument Performance Tests Summary A-14

A-5 Solids Analysis Inter-Laboratory Comparison. A-20

A-6 Summary of Quality Assurance Procedures A-21

METRIC CONVERSION FACTORS

Although it is EPA's policy to use metric units in its documents, non-metric units have been used in this report consistent with common practice in the furnace design field. Readers more accustomed to the metric system may use the following factors to convert to that system.

Non-Metric	Times	Yields metric
degrees Fahrenheit (°F)	5/9 (°F - 32)	degrees Centigrade (°C)
inch (in.)	2.54	centimeter (cm)
foot (ft)	0.305	meter (m)
foot per second (ft/s)	0.305	meter per second (m/s)
10^6 British thermal units per hour (10^6 Btu/hr)	0.293	megawatts (MW) thermal
cubic feet per minute (ft^3/min)	0.47	liters per second (L/s)

EXECUTIVE SUMMARY

The Limestone Injection/Multistage Burner (LIMB) program is designed to develop technology which can achieve moderate (50-60%) reductions in both SO_2 and NO_x from electric utility boilers, through the use of calcium-based SO_2 sorbents (such as limestone) and staged burners. LIMB technology is intended to be relatively easy to retrofit into existing boilers as part of an acid rain control strategy.

In the study covered in this report, alternative coal burner designs are tested which attempt to achieve fuel/air staging internal to the burner (i.e., avoiding the external tertiary air ports present in commercial low-NO_x staged burners). An internally staged low-NO_x burner should be much simpler to retrofit into existing boilers. A variety of internally-staged burner designs were tested in the 10 million Btu/hr Small Watertube Simulator (SWS) experimental furnace, with Vicron limestone (10 microns mass mean) injected at various locations through the burner throat or through ports near the burner. This testing is described in Sections 1 through 5 of this report.

This study then focussed upon an investigation of sorbent jet aerodynamics, in an effort to define sorbent jet parameters which could improve sorbent reactivity (and SO_2 removal performance) by controlling peak temperatures seen by the sorbent, and by controlling sorbent heating rate. Since injection near the burner should provide the best sorbent dispersion and the longest sorbent residence time in the furnace, initial jet aerodynamics testing addressed double concentric (co-axial) jets, where an annular air jet surrounds the sorbent jet. Such double concentric jets offer the best potential for enabling near-burner injection, since the annular air sheath would be expected to best protect the sorbent from high near-burner temperatures which could cause sintering.

The double concentric jet testing in the SWS with Vicron limestone is described in Section 8 of this report.

The jet aerodynamics testing in the SWS then addressed smaller, generally single-pipe jets, at conditions representative of upper-furnace sorbent injection, remote from the burners. The single-pipe jets permitted a more effective study of sorbent heating rate as a means to improve reactivity. The small-jet testing of upper-furnace injection, which considered five different calcium-based sorbents, is described in Section 9.

The final part of the SWS effort involved testing of a precalciner close-coupled to the SWS. The objective was to determine whether sorbent could be calcined under controlled conditions at a high heating rate in order to develop high reactivity, and then immediately injected into the furnace before the surface area decayed. The precalcination testing with Vicron limestone is described in Section 10.

This project continued with testing of upper-furnace sorbent injection in the 100 million Btu/hr Large Watertube Simulator furnace (LWS), operating with an internally-staged coal burner. The LWS testing is described in a separate report.

E.1 Low-NO_x Internally-Staged Burners

Two coal-fired burners were tested. One of these burners (referred to as HV2) was a high-velocity, intense-mixing coal burner (secondary air velocity about 190 ft/sec), designed to produce short, compact flames, typical of pre-NSPS burners. The testing of this burner was intended to represent the case where there is no flexibility in an existing boiler to increase the burner throat diameter in order to reduce velocity. The second burner tested was a low-velocity burner (secondary air velocity about 80 ft/sec), representing the case where there is flexibility to increase the burner throat diameter during retrofit. The main modifications to achieve internal staging in each burner included various different coal nozzles, and secondary air baffles intended to deflect the air stream away from the burner, to achieve staging.

The NO_x-related objective of this testing was to determine whether internal staging could achieve 50-60% reduction in the 500-750 ppm NO_x levels characteristic of pre-NSPS coal burners. With the low-velocity burner, NO_x emissions with the various coal nozzles were between 300 and 500 ppm (dry, corrected to 0% O_2), as shown in Figure E-1. Thus, if the existing boiler provides the flexibility to increase the burner throat diameter, it would appear that the NO_x objective could be met. But with the high-velocity burner, as also shown in Figure E-1, coal nozzle modifications which resulted in acceptable flames gave NO_x emissions of 650-850 ppm; this level reflects no reduction in comparison with typical pre-NSPS burners. Thus, where there is not flexibility for throat enlargement, nozzle modifications alone are not sufficient to meet the objective. However, as shown in Figure E-2, the inclusion of secondary air baffles did reduce the high-velocity burner NO_x emissions to 400-550 ppm, approaching the objective. For all of the results summarized here, the burner configuration gave stable flames, with CO emissions below 60 ppm.

The ability to achieve high levels of SO_2 reduction with near-burner sorbent injection was tested with internally-staged burners, injecting Vicron limestone with the primary air/coal, with the secondary air, and through outboard ports. Some of the data are shown in Figure E-3. Reductions for the different burners (low- or high-velocity) and for the different injection locations were typically no greater than about 20-30% at a Ca/S molar ratio of 2. The injection location (through the throat or through outboard ports) did not appear significant when burning SO_2-doped natural

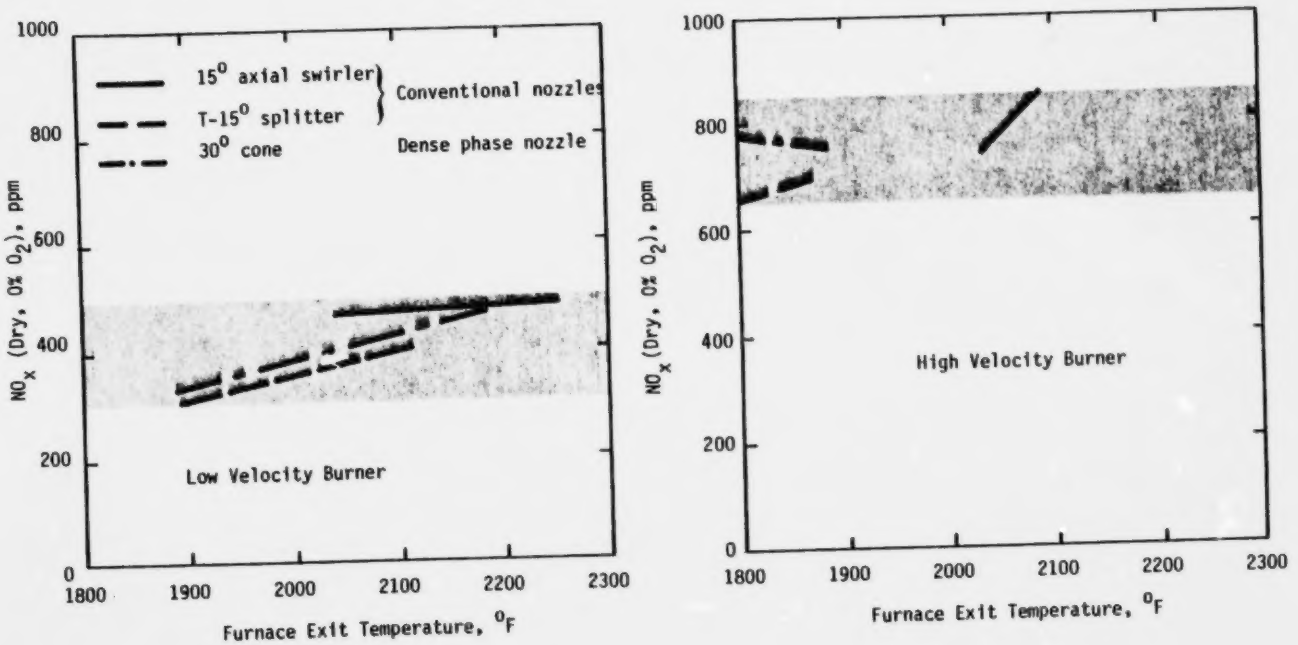

Figure E-1. Summary of NO_x emissions for low-NO_x coal nozzles tested with low velocity and high velocity burners.

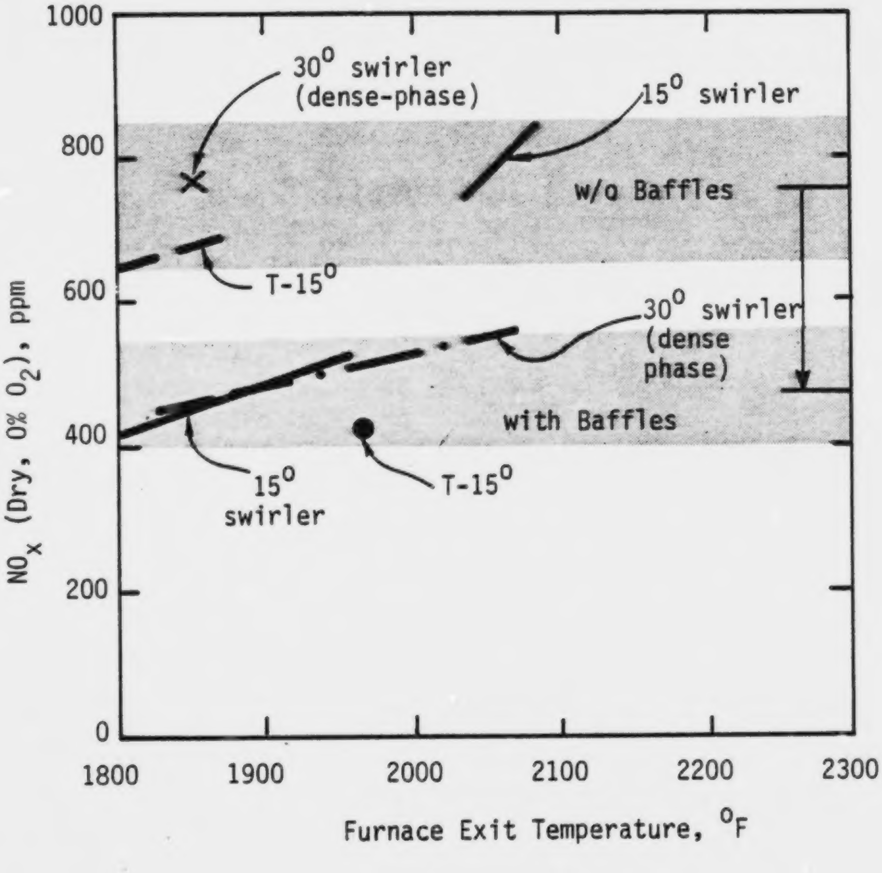

Figure E-2. NO_x Reductions achieved by secondary air baffles with high velocity burner.

HV1 Burner: 8% ISA, 32% MSA, 60% OSA: Maximum Swirl
Natural Gas Doped with SO_2
Vicron 45-3

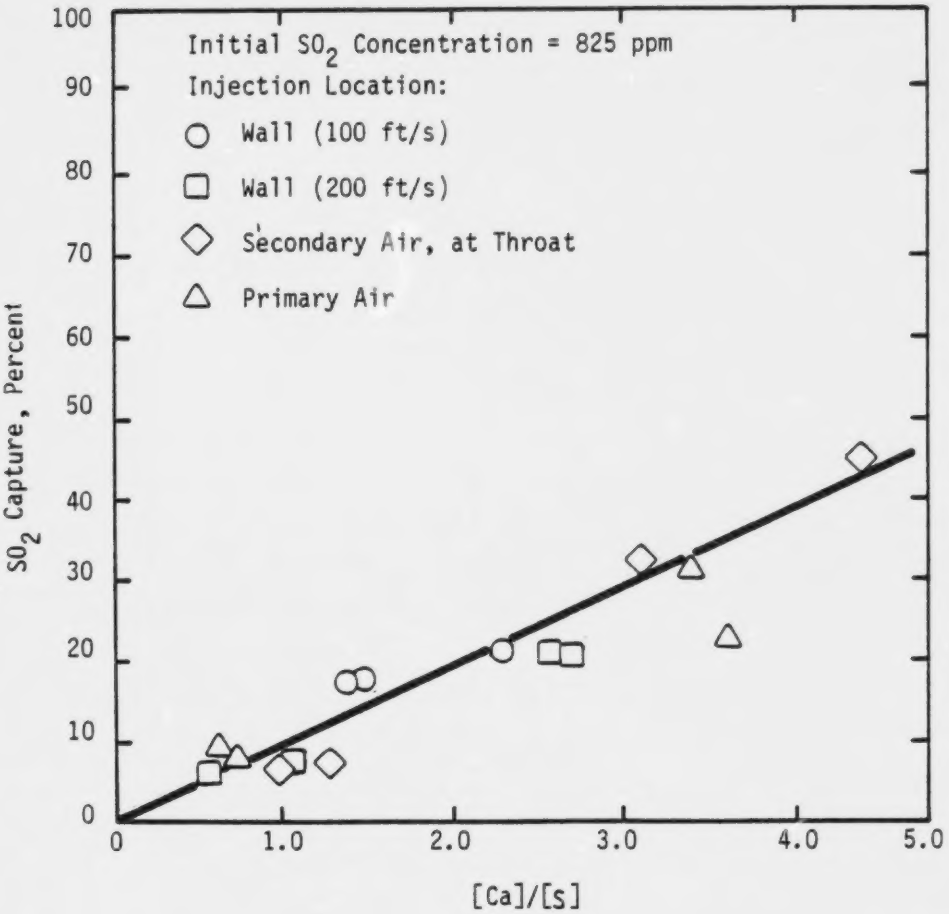

Figure E-3. SO_2 capture with Vicron 45-3 sorbent in HV1 burner (Natural gas flames) -- effect of injection location.

gas (where thermal deactivation in the near-burner environment is the primary concern). However, with coal flames (where coal ash deactivation as well as thermal effects might be important), the outboard ports consistently provided greater removals than did through-burner injection. In view of the relatively limited SO_2 removals, it was concluded that sorbent reactivity would be limited for all near-burner injection locations, unless sorbent jets could be designed to protect the sorbent from thermal and ash effects.

E.2 Sorbent Jet Investigations - Double Concentric Jets

The first phase of the sorbent jet investigations addressed relatively large double concentric jets, which, it was hoped, might provide the necessary protection of the sorbent to permit injection near the burner. In this testing, the variables studied included the diameter of the annular air jet, and the velocities of the annular air jet and the inner sorbent jet. SO_2 reductions typically ranged between 28 and 38% at Ca/S = 2. However, these large jets introduced such a large mass of air that they significantly reduced the background temperature of the SWS furnace; this thermal effect dramatically affected the peak temperature and the time/temperature history seen by the sorbent, in a manner unique to the SWS experimental system. As a result, it is not possible to assess from these results how effectively double concentric jets might in fact protect the sorbent in a large-scale boiler. Because of the impact of the jets on SWS operating conditions, these tests showed no consistent effect of jet parameters (e.g., jet velocities) on capture performance.

E.3 Sorbent Jet Investigations - Small Jets

The small sorbent jets tested were primarily 2-inch (or 1-inch) diameter single-pipe jets, without the annular air jet present in double concentric jets. The small jets were tested at conditions (temperatures) representative of injection into the upper furnace, remote from the burners. These small jets gave higher and better-controlled sorbent heating rates, permitting a better study of heating rate effects on sorbent activation. The test matrix for these tests was designed to permit separation of the effects of sorbent peak temperature and heating rate. Peak sorbent temperature was controlled by adjusting the SWS background temperature. Heating rate was controlled by adjusting the jet velocity, as well as the background temperature; a doubling of the velocity doubles the heating rate, all other factors being equal.

The effect of peak sorbent temperature for five different calcium-based sorbents at constant heating rate is shown in Figure E-4. As expected, the SO_2 capture for all of the sorbents tested was found to be sensitive to peak temperature, with the higher-reactivity sorbents showing the greater sensitivity. Maximum SO_2 capture was found with peak sorbent temperatures in the range of 2250 to 2350 °F. (Heating Rate 1 in the figure corresponds to a calculated 15,000 F°/sec, while Heating Rate 2 is a calculated 34,000 F°/sec.) As in other studies, pressure-hydrated dolomitic lime ("Type S" in Figure E-4) and pulverized dolomite were found to be the most reactive of the sorbents tested; calcitic limes which had been hydrated at atmospheric pressure (Colton and Longview) had somewhat lower reactivity; and pulverized limestone (Vicron, 10 microns mass mean) had the lowest reactivity.

At constant peak sorbent temperature, the effect of (calculated) heating rate was not consistent over the full range of temperatures tested. But at the temperatures producing maximum capture (2250-2350 °F), the higher heating rate consistently produced higher SO_2 removals. As an example, results with Vicron limestone at the two jet velocities (heating rates), at different peak temperatures, are shown in Figure E-5. Sulfation modelling studies indicate that this increase in capture cannot be explained solely

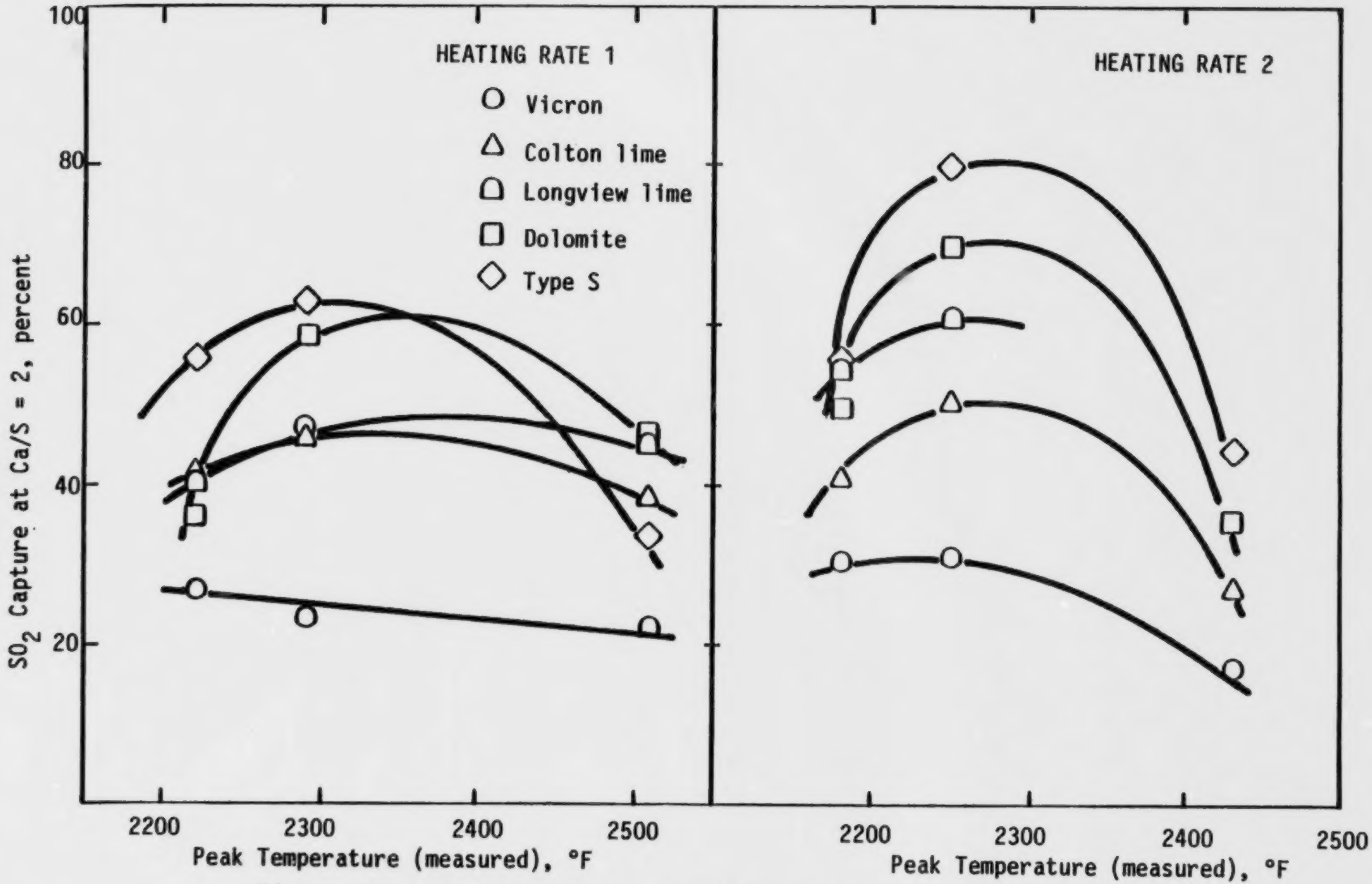

Figure E-4. Effect of peak sorbent temperature on SO_2 capture at different sorbent initial heating rates.

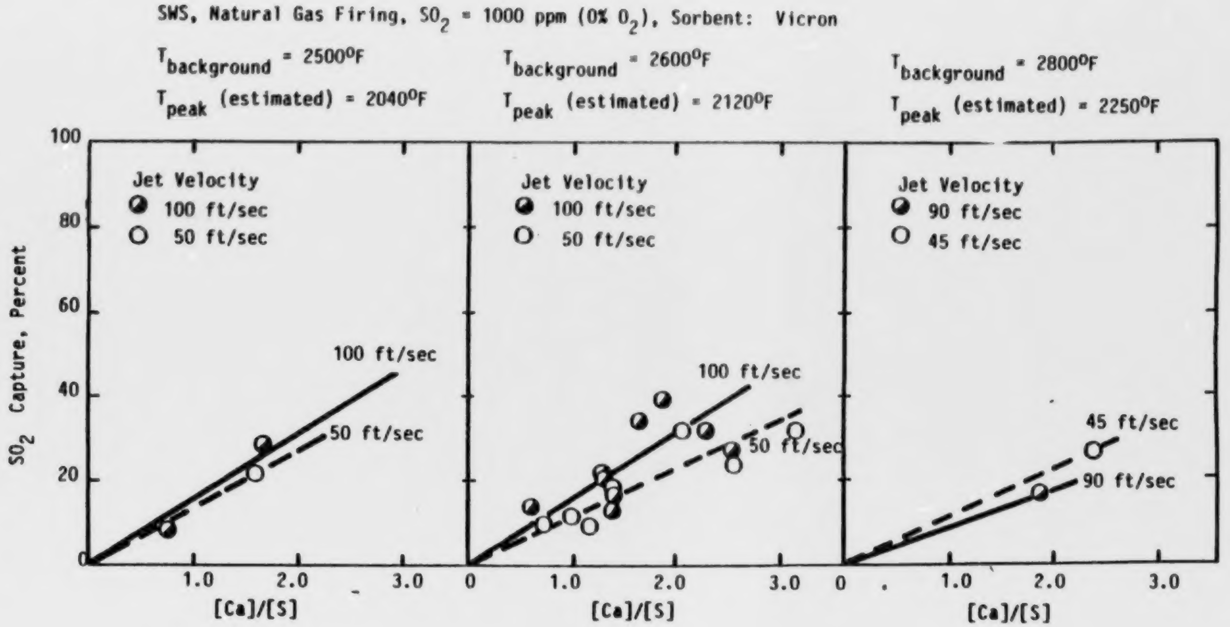

Figure E-5. SO_2 capture with Vicron sorbent injected through a 2-inch single-pipe jet -- heating rate studies.

on the basis of the different time/temperature histories experienced by the sorbent in the different tests; thus, the differences in heating rate might in fact have been playing a role.

Sorbent samples were taken at the furnace exit for surface area analysis, to determine if in fact the higher heating rates were generating higher surface areas. These test were made with no SO_2 doping of the natural gas being burned in the SWS, so that no area loss would be occurring due to the sulfation reaction. The results of these measurements are summarized in Figure E-6. As expected, the surface areas tend to decrease with increasing peak temperature. But there was no observable influence of heating rate on the final surface area of sorbent at the furnace exit. This suggests that, if heating rates did create different areas early in the jet, these differences were gone by the time the sorbent reached the furnace exit.

E.3 Testing of a Close-Coupled Precalciner

A calcination vessel was installed near the SWS, to test the concept of whether a highly-active sorbent could be generated by controlled, high-heating-rate precalcination of the sorbent, followed by immediate injection of the calcined material into a furnace before the surface area could decay. Four different versions of the precalciner were used to study the effects of calciner temperature and residence time, and the possible influence of chromium in the calciner refractory as a reactivity promoter. The SO_2 capture results did not show any improvement with use of the calciner, compared to the case where the sorbent was allowed to bypass the calciner, except in one case. Surface area measurements on sorbent taken from both the jet issuing into the SWS, and the SWS exit, showed that the sorbent was only partially calcined in the precalciner, with final calcination being completed in the furnace. Surface area at the end of the furnace was the same with or without the precalciner.

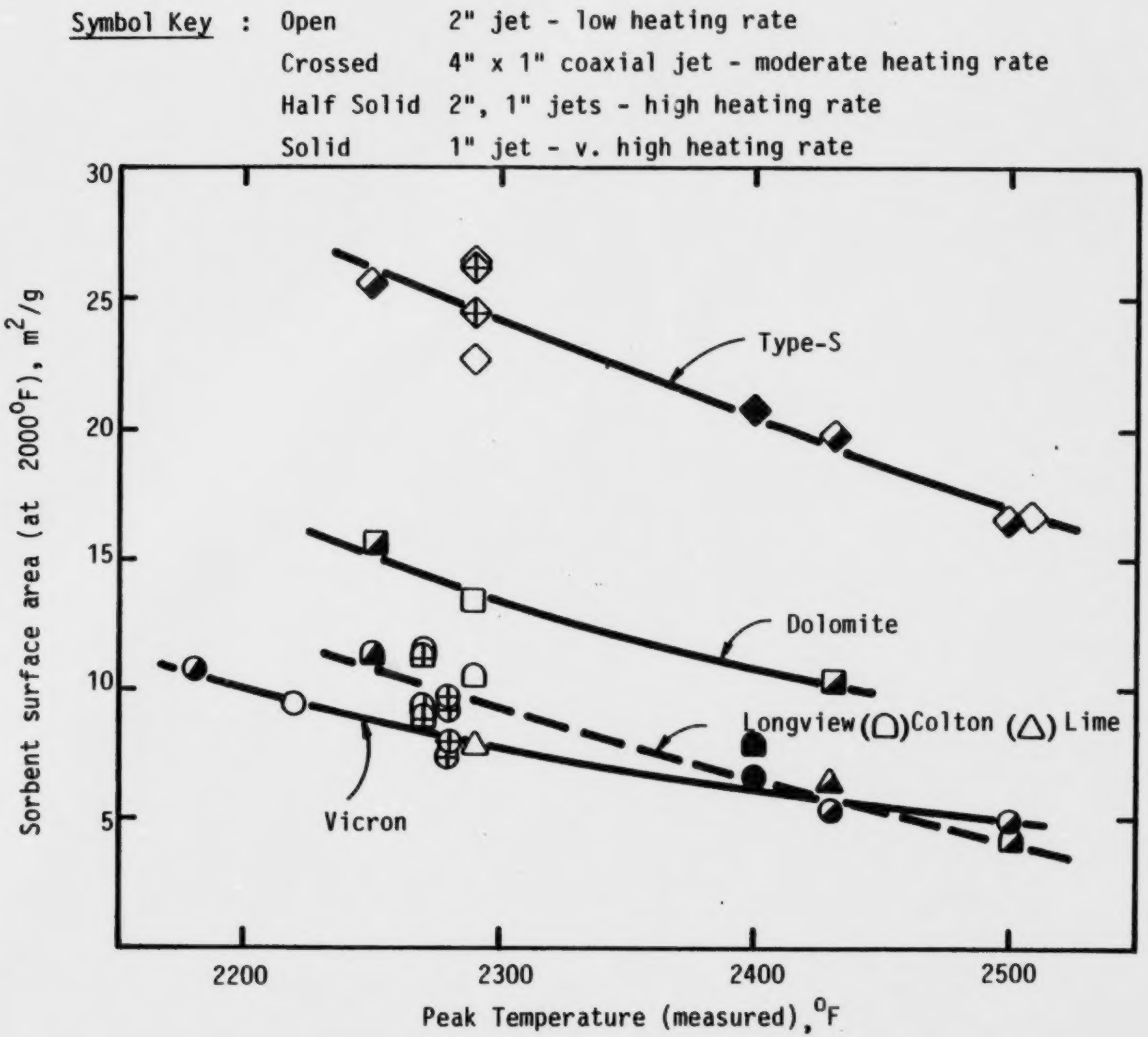

Figure E-6. Effect of peak temperature and heating rate on sorbent surface area.

1.0 INTRODUCTION - INTERNALLY-STAGED BURNERS

Coal-burning electric utility boilers contribute about 75 percent of the SO_2 emissions, and about 20 percent of the NO_x emissions, which are released to the atmosphere in the United States. These two pollutants are major precursors to acid rain. Significant levels of these pollutants can be emitted from coal fired boilers which were installed prior to the promulgation of EPA's initial New Source Performance Standards (NSPS) for large boilers in 1971. One potential component of an acid rain control strategy could be the application of some level of control to such pre-NSPS boilers.

Limestone Injection/Multistage Burners (LIMB) is a technology being investigated to achieve simultaneous SO_x and NO_x control for existing coal-fired utility boilers. The process envisions the use of calcium-based sorbents to achieve intermediate levels of SO_2 removal (50-60 percent), and staged burners for 50-60 percent NO_x reduction (relative to uncontrolled pre-NSPS burners). A major reason for interest in this process is its envisioned ability to be retrofit into existing boilers with minimum capital and space requirements.

Some low-NO_x staged wall burners which have been tested involve the use of outboard tertiary air ports--external to the burner throat--in order to achieve air staging. In some cases, such external ports could prove difficult to retrofit into an existing boiler originally designed for a pre-NSPS burner; additional tube bends would be required to accommodate the ports (of potential concern when the boiler is top-supported), and the ports could interfere with buckstays, windbox trusses and other structural constraints surrounding the original burners. An objective of the current study was to investigate wall burner design approaches which could effectively achieve air and/or fuel staging without external ports--i.e., by modifications internal to the burner, in a manner which would facilitate retrofit. In this report, burners with such modifications are referred to as internally-staged burners.

The sulfur capture performance of a calcium-based sorbent is largely dictated by the surface area (the reactivity) it develops upon calcination (along with its residence time at sulfation temperatures). Another objective of this study was to investigate how design parameters for the sorbent jets--jet velocity, jet diameter, jet "location" (background temperature) and jet configuration (single versus double concentric jets)--might influence the development of surface area and reactivity.

To accomplish these objectives, testing was conducted on a 2.9 MWt (10 x 10^6 Btu/hr) pilot-scale experimental furnace referred to as the Small Watertube Simulator (SWS). This furnace is a horizontal cylinder, partially refractory lined, which can be fired from one end with coal, oil or gaseous fuel.

For the investigation of internally-staged burner design approaches, the modified coal burner to be tested was mounted at the firing end of the furnace. The internal staging modifications tested included: modifications to the secondary air channels (including the use of dual channels, and of conical baffles); and modifications to the coal nozzles (including the use of various swirlers and splitters, and including dense-phase nozzles utilizing primary air/coal feed ratios about one-tenth that normally used). The testing addressed burner configurations having a high secondary air velocity (about 58 m/sec, or 190 ft/sec, representative of the velocities in pre-NSPS burners), and also a configuration having a low velocity (24 m/sec, or 80 ft/sec). From a retrofit standpoint, the high-velocity case represents the situation where the host boiler offers no flexibility for enlarging the throat of the modified burner in order to reduce secondary air velocity; the low-velocity case represents the situation where the host boiler offers maximum flexibility. The testing of the burners focused on NO_x emissions, combustion performance and flame stability. As part of this effort, limestone was injected at several locations through and near the internally-staged burner, in order to test the effectiveness of burner zone injection (and thus the potential for combined low-NO_x/low-SO_x burners).

For the study of sorbent jet parameters, a uniform flame gas flow field in the SWS was established using a series of gas-fired burners at the firing end. The gas fuel was usually doped with sulfur in order to permit observation of the sulfur capture performance. The jet to be tested was mounted through the firing wall (co-flowing jet) or through the side of the furnace (crossflow jet). Variables included jet diameter, jet velocity, jet configuration and background temperature, with the peak temperatures seen by the sorbent particles being representative, for the most part, of those in the upper part of a utility furnace (i.e., injection remote from the burner zone, in the sulfation temperature region of 950-1230°C or 1750-2250°F). Testing generally focused on the sulfur capture capability of the sorbent under the various jet conditions, as a measure of its reactivity (and reflecting its time-temperature history). One specific objective of the sorbent jet experiments was to determine whether sorbent heating rate, as well as peak temperature, influenced the reactivity developed by the sorbent during calcination.

1.1 Considerations in Low-NO_x Burner Design

Two basic approaches can be utilized in reducing NO_x emissions from fossil-fuel-fired burners: air staging and fuel staging. These two approaches are represented in Figure 1-1. In air staging, NO_x emissions are reduced by reducing the rate at which the fuel and combustion air mix, so that as much fuel as possible reacts under conditions which, overall, are oxygen deficient. Under these conditions, nitrogen radicals formed during the combustion process are less likely to react with oxygen to form NO_x; also, peak temperatures are generally reduced (reflecting a concomitant reduction in combustion intensity), reducing both the kinetics and the equilibrium for NO_x formation. In fuel staging, the products of combustion (including NO_x) are exposed to a fuel-rich zone, where NO_x is reduced. Fuel staging is often considered on a more global scale--i.e., the reburning process, where a reducing zone is created in the furnace, above the burner zone, while the burner zone itself is oxygen-rich overall. However, fuel staging can also be effected within the burner zone, through suitable selection of burner design and operating conditions. Figure 1-2

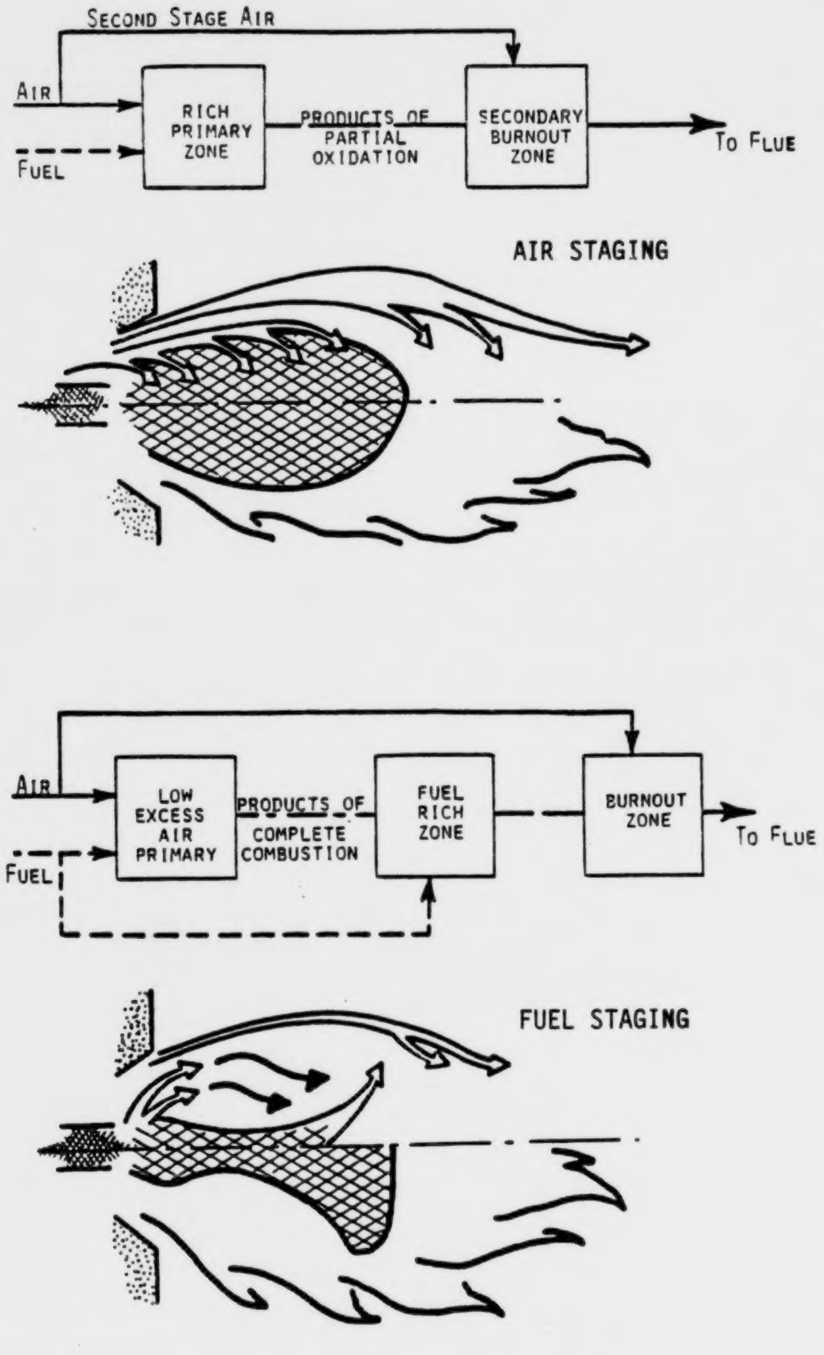
SECOND STAGE AIR
AIR
FUEL
RICH PRIMARY ZONE
PRODUCTS OF PARTIAL OXIDATION
SECONDARY BURNOUT ZONE
TO FLUE
AIR STAGING
AIR
FUEL
LOW EXCESS AIR PRIMARY
PRODUCTS OF COMPLETE COMBUSTION
FUEL RICH ZONE
BURNOUT ZONE
TO FLUE
FUEL STAGING

Figure 1-1. Air and fuel staging.

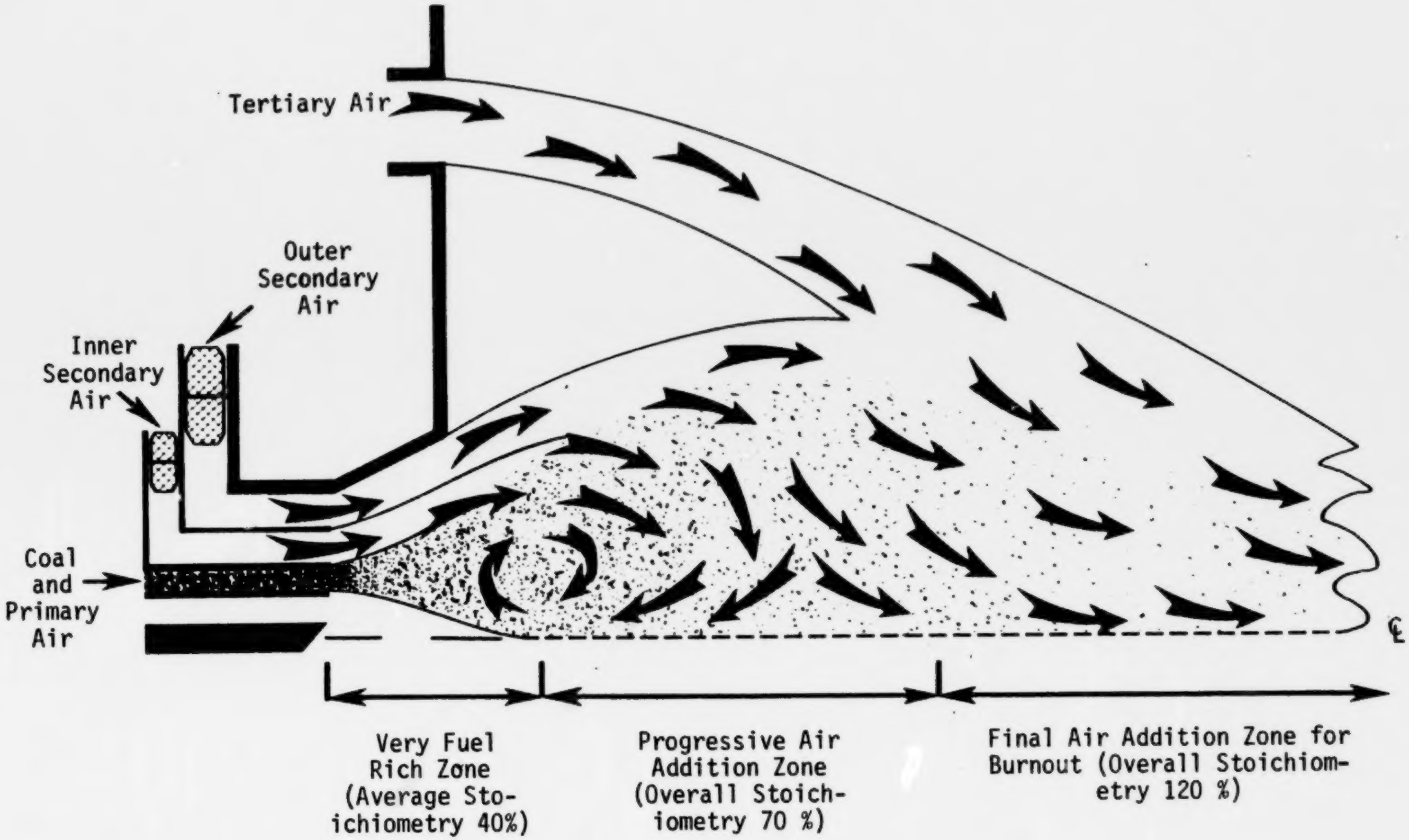
Tertiary Air
Outer Secondary Air
Inner Secondary Air
Coal and Primary Air
℄
Very Fuel Rich Zone (Average Stoichiometry 40%)
Progressive Air Addition Zone (Overall Stoichiometry 70 %)
Final Air Addition Zone for Burnout (Overall Stoichiometry 120 %)

Figure 1-2. Air staging effects with a distributed mixing burner utilizing external tertiary air ports.

schematically illustrates the air-staging effects achieved by a low-NO_x distributed mixing burner utilizing external tertiary air ports.

One objective of the current study was to explore burner design and operating modifications which could accomplish air and/or fuel staging solely by means of adjustments internal to the original burner--i.e., internal staging. In order to satisfy the requirement that this technology be suitable for retrofit into existing boilers--i.e., for modifying existing burners--any internal staging modifications would have to satisfy a number of constraints imposed by the particular existing unit being modified. Key constraints include the following.

1. The modified burner must physically fit into the space available. For example, increases in throat diameter (relative to the original burner) will be determined by the site-specific flexibility for adding or relocating tube bends, or for removing refractory around the throat and quarl region. Retrofit burner components within the existing windbox must not interfere with the structural members or impede air flow through the windbox.

2. The modified burner must be compatible with the existing ancillary equipment. For example: the pressure drop through the burner must be consistent with fan and ducting capabilities; the primary air/coal mass ratios must be within the capabilities of the existing coal mills and exhaustors; the burner must be compatible with the existing burner control systems and with the coal ducting arrangement; and flue gas recirculation should not be utilized unless provided for in the original equipment.

3. The modified burner must be compatible with the furnace. That is, the heat release rate must be consistent with the cooled surface area available in the burner belt. also, flame length (and diameter) must be consistent with furnace dimensions.

4. The modified burner must provide acceptable combustion performance (e.g., acceptable flame stability, combustion efficiency and turndown capability).

A variety of possible burner modifications were considered which offered potential for achieving the desired internal staging within the retrofit constraints listed above. The various options are listed below. The intent was to select from this list, for inclusion in this study, those modifications which appeared to be the most promising for providing reduced NO_x emissions.

1. Larger burners (i.e., increased throat diameter for the same thermal input). This approach reduces throat velocity, reducing the rate of air and fuel mixing and thus effecting air staging.

2. Reduced throat velocity (at constant burner throat diameter). This approach reduces the rate of air and fuel mixing, as in 1 above, but would require de-rating of the burner. Thus, this approach would not generally be preferred.

3. Reduced quarl burners. The quarl may be formed from refractory surrounding the burner proper, which then increases in diameter on the furnace side of the throat in order to create the quarl. In such cases, it can be possible to increase burner diameter by removing some of the surrounding "excess" refractory, thus permitting a reduction in throat velocity. This approach has the effect of reducing the length of the quarl. The quarl is intended primarily to aid in flame stabilization, and a significant reduction in quarl length might need to be accompanied by adjustments to various burner settings in order to keep the flame attached.

4. Divided registers for the secondary air (i.e., two or more annular secondary air channels, each with its own register and swirl control). Divided registers provide an added degree of flexibility

in controlling the distribution of secondary air mass, velocity and swirl at the burner throat. This approach can be used to slow the rate of mixing of air and fuel, while still controlling flame stability, thus effecting air staging.

5. Burner inserts on secondary air channels. An insert could typically be conical baffle mounted on the lip of the sleeve separating the inner and outer secondary air channels in divided register burners. Such a baffle would have the effect of diverting the secondary air in the outer channel away from the near flame, thus delaying its mixing with the fuel and achieving further air staging. See Figure 1-3.

6. Coal nozzle modifications. This approach includes modifications to the central axial pipe through which coal and primary air are injected into the burner throat. See Figure 1-4. One such modification could include the placement of an insert--or adjustment of the existing insert--at the throat end of the coal pipe. One type of insert (which is used in some existing burners) is an axial swirler which adds a degree of swirl to the injected coal; modifying the swirler to reduce the amount of swirl, by reducing the vane angle or repositioning the insert within the coal pipe, would reduce the rate of fuel/air mixing, providing an added degree of air staging. Another type of insert would be a splitter or separator, for dividing the coal stream into separate regions; if designed properly, this type of insert could provide a degree of fuel staging. Another modification that could be made to the coal nozzle in some cases could be the relocation of any ancillary equipment (such as igniter, oil start-up nozzles or flame scanners) which might be occupying space in the center of the coal pipe. Such relocation would allow the coal pipe to be made smaller, thus effectively increasing the annular area available for secondary air flow and hence reducing air velocity.

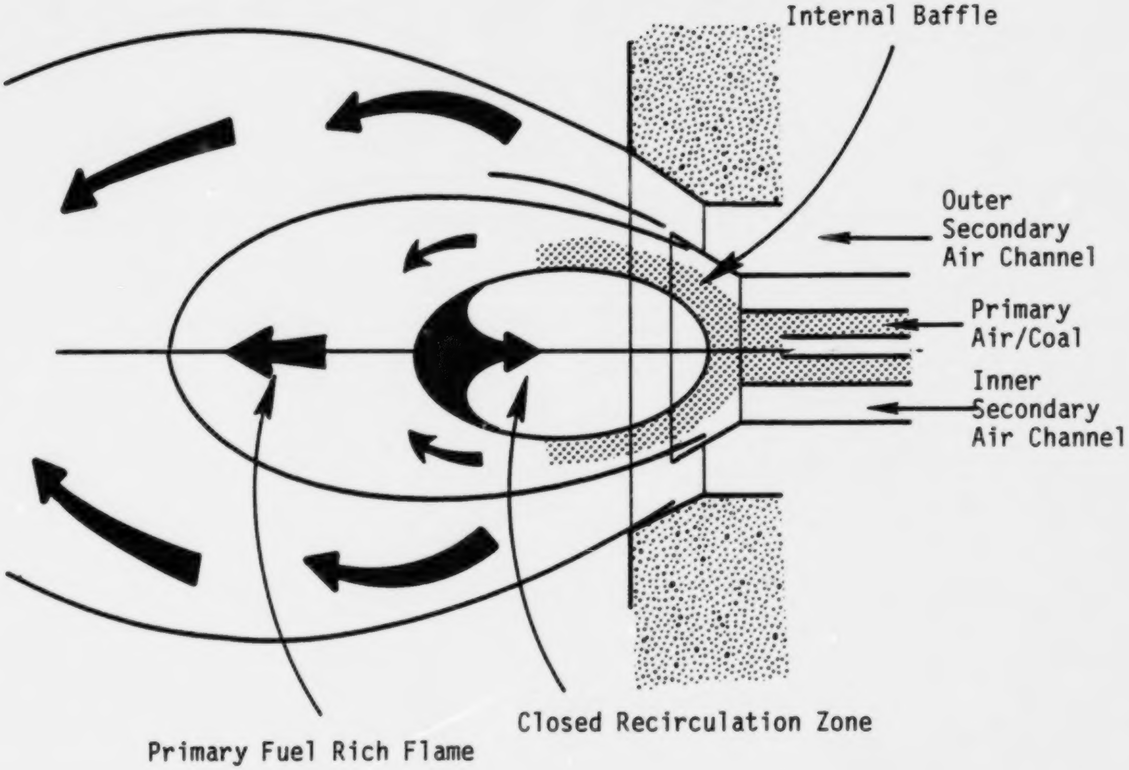
Internal Baffle
Outer Secondary Air Channel
Primary Air/Coal
Inner Secondary Air Channel
Closed Recirculation Zone
Primary Fuel Rich Flame

Figure 1-3. An internal conical baffle between inner and outer secondary air channels of a divided register burner.

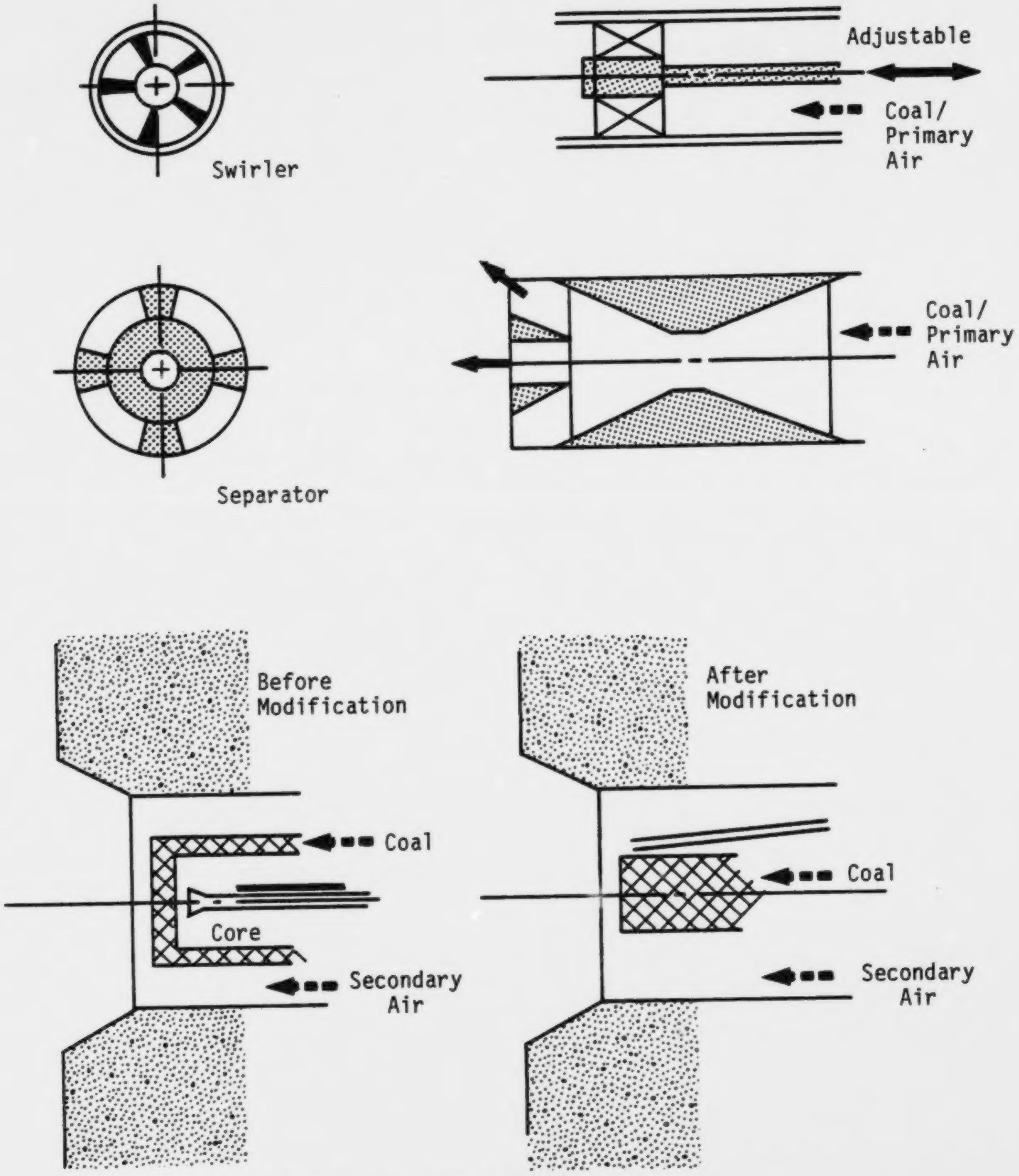
Swirler
Adjustable
Coal/
Primary
Air
Separator
Coal/
Primary
Air
Before
Modification
Coal
Core
Secondary
Air
After
Modification
Coal
Secondary
Air

Reduced coal pipe diameter

Figure 1-4. Alternative approaches for coal nozzle modifications.

7. Multiple fuel injectors. This approach would envision injecting only a portion of the coal through the main coal pipe, with the remainder being injected through separate injectors located around the periphery of the throat (either within or outside the throat). This approach could potentially effect a degree of fuel staging. However, a number of design and operating difficulties would have to be overcome with such an approach.

8. Dense-phase coal transport. A typical bituminous coal is normally injected with about 2 pounds of primary air per pound of coal. It is technically possible to pneumatically transport the coal with perhaps only one-tenth that amount of primary air. Utilization of the much lower primary air flow would aid NO_x reduction in two ways: a) it would reduce the amount of air present in the initial fuel-rich combustion zone; and b) it would permit a significant reduction in the size of the coal pipe, increasing the annular space available for secondary air flow and reducing velocity. such low primary air flows might not be compatible with the air requirements of some existing coal mills.

9. Coal size distribution changes. Changes in the coal size distribution--together with a suitable splitter/separator in the coal nozzle--could potentially aid in providing some fuel staging, if the grind provides an appropriate mix of fine and coarse coal particles. With a separator such as that shown in Figure 1-4, the venturi preceding the splitter aerodynamically causes the larger coal particles to concentrate in the center of the fuel jet while the finer particles divert outwards. The fine particles might then tend to burn close to the burner exit, while the central coarse coal stream might penetrate this flame to produce a fuel-rich zone downstream.

10. Flue gas recirculation. Flue gas recirculation (FGR) can reduce the "thermal NO" component of NO_x emissions through the reduction of peak flame temperature. If injected through discrete passages

between the coal and secondary air streams, it could also serve to separate the streams and delay fuel/air mixing. However, FGR may not be practical for retrofit burner modifications unless the furnace being modified was equipped with FGR originally; addition of FGR capability to a boiler not originally designed for it could be expensive, and would change the pattern of heat absorption within the boiler (requiring a boiler with the flexibility to cope with such a change). Also, to the extent that FGR functions by reducing peak flame temperature, its effectiveness would be limited to the thermal NO_x component; NO_x resulting from fuel nitrogen (the major contributor to NO_x from coal-fired systems) is not sensitive to temperature, and hence would not be affected by any FGR-created temperature reduction.

Based upon consideration of the alternative internal staging approaches discussed above, several of these approaches were selected for experimental investigation in this study. The selection was made considering the potential of the approach for NO_x reduction, and the relative ease of commercial applicability. The modifications selected for study were as follows:

Larger burners. The two baseline burners used in this testing had a throat diameter of about 9 inches and operated at high secondary air velocity (190 ft/sec), representative of the velocities found in pre-NSPS burners. Attempts in this study to reduce NO_x emissions at these high velocities represented the retrofit case where the existing boiler would offer no flexibility for enlarging the burner throat as a means for reducing velocity. For comparison, testing was also performed on a low-velocity burner, where the throat was enlarged to 12 3/4 inches in order to reduce secondary air velocity to 80 ft/sec at constant burner thermal input. This lower velocity is representative of modern low-NO_x burners, and--in retrofit applications--represents the case where the existing boiler offers maximum flexibility for enlarging the burner throat, through additional tube bends or removal of refractory around the existing burner, and through a forgiving arrangement of the existing windbox.

Divided registers. All burners tested utilized multiple secondary air channels with independently variable swirl. One of the two high-velocity burners, and the low-velocity burner, employed two channels; the second high-velocity burner had three channels. Variables studied included the distribution of air among the channels, and the degree of swirl in each channel.

Burner inserts. Conical baffles were tested on the lip of the sleeve between the inner and outer secondary air channels of the two-channel high-velocity burner. Baffles of two length-to-diameter ratios were tested.

Coal nozzle modifications. Axial swirlers of different vane angles were tested; also tested were two types of splitters. In addition, alternative nozzles were tested in conjunction with dense-phase transport, listed below. Variables studied included the position of the swirler or splitter within the coal pipe, and the position of the coal pipe relative to the burner throat.

Dense-phase coal transport. Tests were conducted, with both the high- and low-velocity burners, in which the coal nozzle utilized 0.2 lb of primary air per pound of coal. Three types of coal nozzles, and the option of secondary air baffles, were tested in conjunction with dense-phase transport.

The specific burner designs used to test these various modifications are described in detail in Section 2.2.

1.2 Considerations in Sorbent Injection Testing

The SO_2 removal performance achieved by injection of a calcium-based sorbent into a coal-fired boiler will be determined by three factors:

1. the reactivity of the sorbent after calcination;
2. the effectiveness with which the sorbent is dispersed in the combustion gases; and

3. the residence time of the sorbent in the temperature region (approximately 1750 to 2250°F) where the temperature is sufficiently high to yield reasonable sulfation reaction kinetics, but sufficiently low to reduce the impacts of sintering and $CaSO_4$ decomposition.

The reactivity of a given sorbent will depend upon: the conditions under which it is calcined upon injection (in particular, the peak temperature to which it is exposed); and any effects of coal ash minerals (the coal ash might either reduce or enhance sorbent reactivity).

In most cases, the reactivity of the sorbent appears to be directly related to its total surface area (including both external area and internal pore area), as measured by the Brunauer-Emmett-Teller (B.E.T.) technique. A high surface area suggests that much of the calcium is accessible for reaction with SO_2, and hence that the sorbent is more reactive. Surface area and reactivity tend to decay as the sulfation reaction proceeds, for two reasons: a) sorbent molecules will expand as CaO converts to physically larger $CaSO_4$, plugging micropores and thus blocking off internal surface area; and b) thermal sintering (growth of CaO grains), which would also plug micropores. Sorbent parameters which could influence the retention of surface area as reaction proceeds are: pore size distribution (with larger pores being more resistant to plugging); and sorbent particle size (with smaller particles having a greater proportion of their area present as external area, not subject to pore plugging).

Peak temperature is a key variable in determining the initial reactivity of the calcined sorbent. Upon injection, the raw sorbent will begin to calcine, creating surface area as the CO_2 evolves; however, in parallel with the calcination, sintering will occur, tending to reduce surface area. The net effect of these two competing processes is that the initial surface area of the raw sorbent (generally less than 1 m^2/g) increases to some maximum value (as the calcination/surface area development phenomenon predominates), then drops off (typically to less than 10 m^2/g) as the sintering phenomenon begins to predominate. Higher temperatures increase the sintering rate, and hence would reduce the height of the surface area peak, as well as the ultimate surface area.

In view of the above consideration, the sorbent injection component of the low-NO_x burner portion of the SWS testing had the following objective: To determine whether the internally-staged burner modifications which effectively reduce NO_x emissions might also provide an environment which would simultaneously permit effective SO_2 control when sorbent is injected through or near the burner.

Concerning this objective, the ability to inject sorbent in the vicinity of the flame zone offers a number of potential advantages: a) it assures effective dispersion; and b) it provides maximum sorbent residence time at sulfation temperatures. However, in past studies, sorbent injection near the burner has generally resulted in poor sorbent reactivity, because the high flame temperatures cause sintering, and hence low surface area. Coal ash in the flame zone might also contribute to deactivation. The question here is whether the internal staging modifications tested in this study might moderate peak temperature, or permit shielding of the sorbent particles from the peak temperatures and ash effects. If so, the modified burner could serve as a combined low NO_x/low SO_x unit. Accordingly, for selected promising low NO_x conditions, a limestone was injected at alternative locations in the SWS: with the primary air/coal stream; through the outer secondary air channel; and through separate injection ports through the furnace wall around the burner. Sulfur capture performance was measured as a means of assessing the effectiveness of near-burner limestone injection.

This testing of near-burner injection around the internally-staged burners in the SWS is described in Section 4 of this report. Additional sorbent studies in the SWS -- including studies of sorbent jet parameters as a means of achieving good sorbent dispersion and activation -- are discussed in Sections 6 through 11 of this report. (Studies of double concentric jets, of most interest for possible near-burner sorbent injection, are discussed in Section 8; testing with single-pipe sorbent jets, focussing on upper-furnace injection remote from the burners, is discussed in Sections 9 and 10.) Finally, sorbent injection testing remote from the burners in a larger experimental furnace (the 100 x 10^6 Btu/hr Large Watertube Simulator, or LWS) is described in a separate volume.

2.0 EQUIPMENT, MATERIALS AND TEST MATRICES

The tests discussed in this part of the report fall into two categories:

- Tests with internally-staged burners, investigating the NO_x reduction potential of a variety of burner designs and operating modifications.

- Sorbent injection tests with internally-staged burners to evaluate SO_2 removal capabilities under low-NO_x conditions, when sorbent is injected through or near the burners.

In this section, the experimental systems, fuels and sorbents are described, along with the test matrices for the NO_x and SO_x tests.

2.1 Experimental Furnace, Fuels and Sorbents

The experiments reported here were carried out in the Small Watertube Simulator (SWS) furnace. This is a partially refractory-lined, water-jacketed cylindrical furnace which is primarily used for testing pilot scale burners up to firing rates of 10×10^6 Btu/hr. The furnace and the auxiliary equipment are shown in Figure 2-1, and key furnace characteristics are listed in Table 2-1. The facility consists of coal and air feed systems, the furnace, and the particulate removal system. The heat content of the flue gases is used to preheat the combustion air supplied to the burner. The air flow rates are measured by calibrated venturi flow meters. The coal and sorbent feed rates are measured by screw type feeders. The SWS can also be fired on natural gas and fuel oil, as necessary; gas flow rates are measured with a laminar flow element; whereas oil flow rates were measured with a calibrated rotameter. The details of the SWS furnace measurement systems are given in Appendix A, summarizing the quality assurance activities.

In the experiments covered in this report, three types of fuels were used. For the sorbent jet tests and some of the high-velocity internally-staged burner tests (HV1), natural gas was employed. The gas was obtained

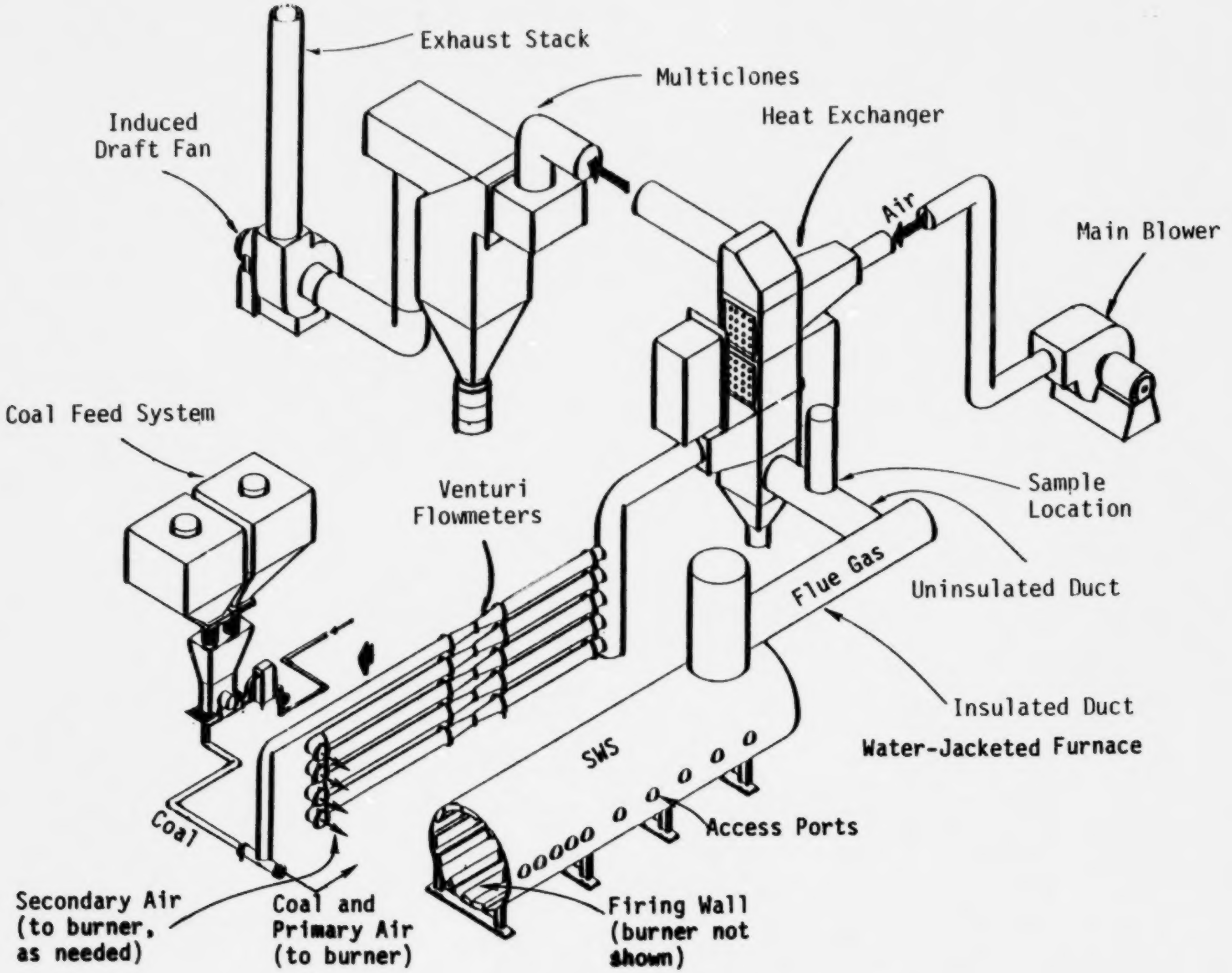

Exhaust Stack
Multiclones
Induced Draft Fan
Heat Exchanger
Air
Main Blower
Coal Feed System
Venturi Flowmeters
Sample Location
Flue Gas
Uninsulated Duct
Insulated Duct
Water-Jacketed Furnace
SWS
Coal
Access Ports
Secondary Air (to burner, as needed)
Coal and Primary Air (to burner)
Firing Wall (burner not shown)

Figure 2-1. Component parts of SWS furnace and exhaust system.

TABLE 2-1. CHARACTERISTICS OF THE SWS

Parameter	Value
Shape	Cylinder
Diameter	6 ft
Length	17 ft
Refractory Insulation	50% of interior surface
Firing Rate	10×10^6 Btu/hr
Volumetric Heat Release	20,000 Btu/hr/ft^3
Heat Release per Cooled Surface	60,000 Btu/hr/ft^2
Exit Temperature (Typical)	1800°F to 2200°F
Cooling	Recirculating Water Jacket

directly from the Southern California Gas Company mains without processing. For most of the internally-staged burner tests (HV2 and LV1), the fuel was bituminous coal from Utah. This coal was preground to 70 percent by mass less than 200 mesh (74 micron, mean size). For a few tests (with the HV1 burner), a No. 2 distillate oil was burned. The fuel analyses are shown in Table 2-2.

The sorbent used for the SO_x tests was Vicron 45-3, a pulverized limestone, produced by Pfizer Co. A typical analysis of the sorbent, along with its size distribution, is given in Table 2-3.

2.2 Burner Configurations for Internally-Staged Burner Tests

Three basic burner configurations were utilized in the testing of internal staging modifications for NO_x reduction. Two of these configurations (referred to as HV1 and HV2) operated at high secondary air velocity (190 ft/sec), representing the retrofit case where the original pre-NSPS burner does not provide flexibility for any enlargement of the throat to enable velocity reduction. One configuration (referred to as LV1) operated at low velocity (80 ft/sec), representing the retrofit case where the original burner provides significant flexibility for throat enlargement. Within each basic configuration, a variety of burner design and operating variables were tested. Each burner was rated at 10×10^6 Btu/hr.

2.2.1 HV1 Burner

The first configuration tested was the high-velocity HV1 burner, the dimensions of which are shown in Figure 2-2. A distinguishing feature of this configuration is a divided register providing three separate secondary air channels, each permitting independent control of air flow rate and degree of air swirl. The intent of this configuration was to permit maximum control over secondary air. Much of the testing with this configuration consisted of burner stability tests using natural gas as the fuel; the commercial gas nozzle used for this testing is shown in Figure 2-3. (During gas-fired tests, the central coal pipe depicted in Figure 2-2 was replaced by the gas

TABLE 2-2. ANALYSES OF FUELS

	Natural Gas*	No. 2 Fuel Oil**	Utah Coal***	
			As Received	Dry
Carbon (%)	72.77	86.76	67.42	69.61
Hydrogen (%)	23.04	12.65	5.02	5.18
Nitrogen (%)	1.94 (as N_2)	0.036	1.38	1.42
Sulfur (%)	-	0.41	.67	.69
Oxygen (%) (by difference)	0.59	0.144	12.71	13.12
Moisture (%)	-	-	3.14	-
Ash (%)	-	-	9.67	9.98
Higher Heating Value Btu/lb	21,088	19,290	-	13,066

*Analysis from So. California Gas Co.

**Analysis from Truesdail Laboratories, Inc.

***Elemental analysis at EER; HHV from Hazen Research

TABLE 2-3. CHARACTERISTICS OF SORBENT VICRON 45-3

	Characteristics	$CaCO_3$
Physical Properties	Mean Size (μm)	9.8
	Density (gm/cm^3)	2.7
Chemical Analysis (Percent by Wt)	Ca	39.2
	Al	0.02
	Si	0.09
	Fe	0.06
	Na	0.007
	Mg	0.33
	K	0.01
	Cr	0.006

- Small throat diameter (no enlargement possible).
- High secondary air velocity (190 ft/s).
- Axial coal nozzles (swirlers, splitters, dense phase).
- Shallow quarl
  L/D = 0.25.

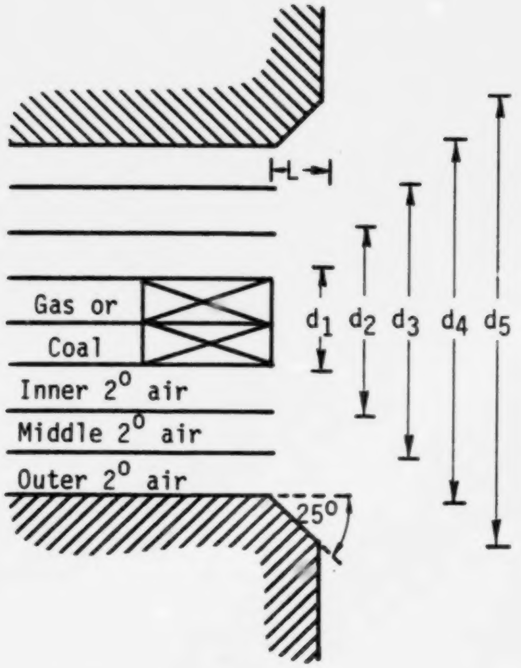
L
Gas or
Coal
Inner 2° air
Middle 2° air
Outer 2° air
25°
d_1
d_2
d_3
d_4
d_5

Throat Dimensions (In.)

	I.D.	O.D.
d_1	4.25	4.5
d_2	6.1	6.6
d_3	7.7	8.0
d_4	9.0	
d_5	11.25	
L	2.5	

Figure 2-2. High velocity burner with three secondary air channels (HV1).

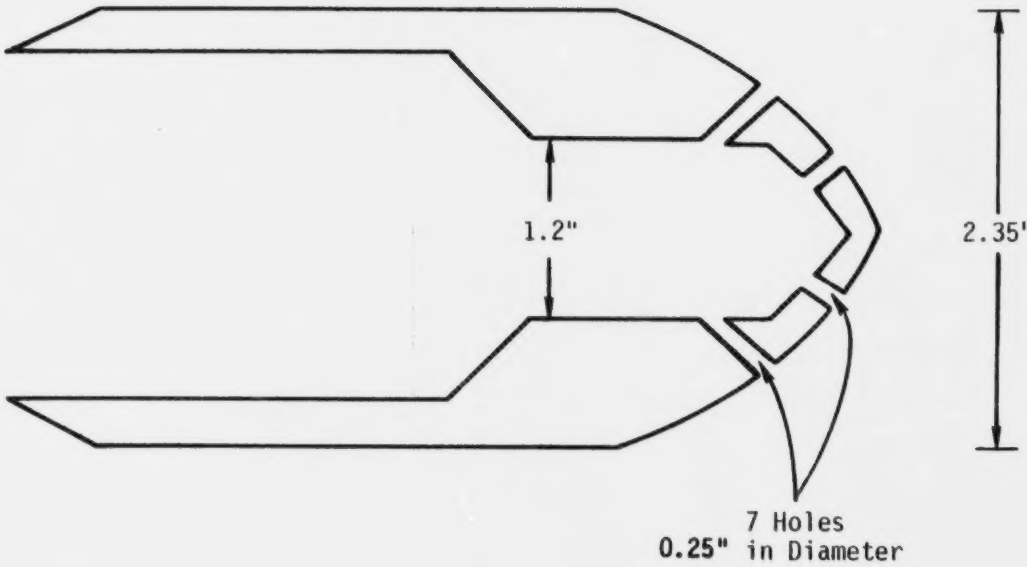
1.2"
2.35"
7 Holes
0.25" in Diameter

Figure 2-3. Peabody gas nozzle used in HV 1 testing.

nozzle.) During tests with Utah coal, axial coal swirlers of the type shown in Figure 2-4 were inserted within the coal pipe (as schematically represented in Figure 2-2). Two different vane angles were tested with this swirler configuration: 15° off the axial, providing a relatively more limited degree of coal swirl; and 45° off the axial, providing a much greater degree of swirl. The testing with this configuration focused on the distribution of the secondary air, and of the degree of swirl, among the three channels; testing with coal addressed the effect of swirler vane angle.

No extensive burner modification and optimization tests were carried out with the HV1 burner because the burner provided stable flames over only a narrow range of operating conditions. The primary problem appeared to be that the secondary air channels were so narrow (only 1/2 to 3/4 inches wide) that representative secondary air swirl patterns could not be established. In a full-scale burner (possibly ten times the size of the pilot burner tested here), this problem might not be so severe.

2.2.2 LV1 Burner

The second burner configuration tested was the low-velocity LV1 burner, the dimensions for which are presented in Figure 2-5. This configuration included a divided register with two secondary air channels, avoiding the stability difficulties encountered with the three-channel HV1 burner. The secondary air velocity was decreased by enlarging the LV1 throat diameter to 12.75 inches (compared to 9.0 inches for HV1).

Several coal nozzle modifications were tested with the LV1 burner. With conventional coal transport (2 lb primary air per lb of coal), the nozzles tested included:

- an axial swirler, of the type shown in Figure 2-4, inserted within the coal pipe. The vane angles used were:
  - 15° off the axial
  - 30°

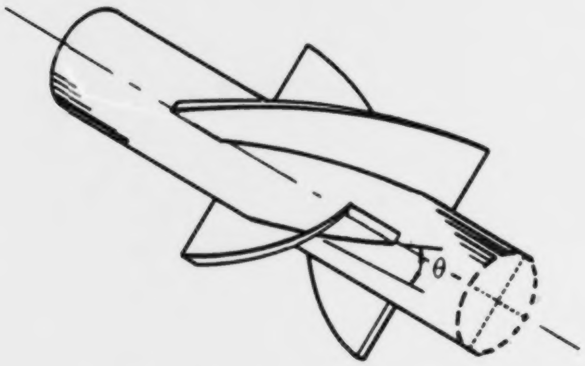

θ = Blade Angle

Figure 2-4. Sketch of an axial vane swirler.

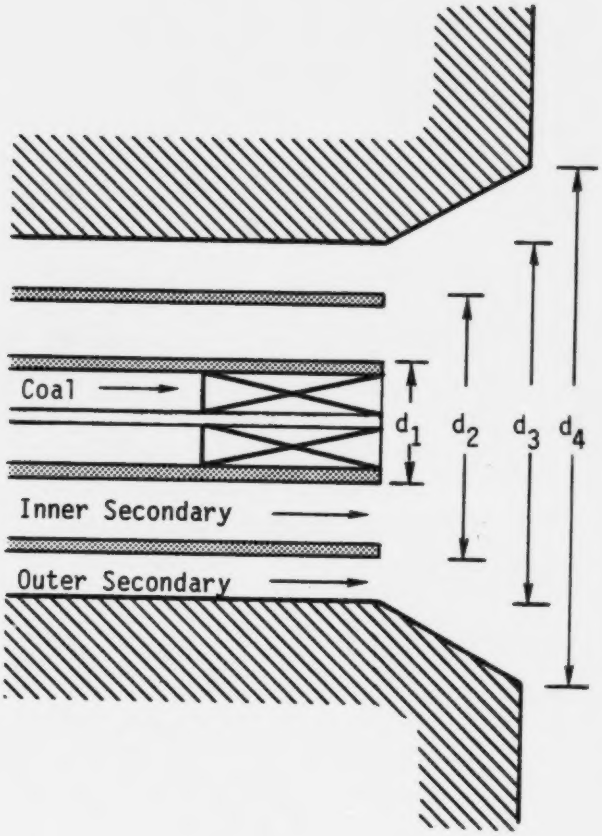
Coal
Inner Secondary
Outer Secondary
d_1
d_2
d_3
d_4

- o Large throat diameter
- o Low secondary air velocity
  - 80 ft/sec (conventional coal transport)
  - 70 ft/sec (dense-phase coal transport)
- o Coal nozzles:
  - swirlers
  - splitters
  - dense-phase transport
- o Coal nozzle (primary air) velocity
  - 65-70 ft/sec (conv.)
  - 50-60 ft/sec (dense)
- o Deep quarl (L/D = 0.65)

Throat Dimensions (In.)

		I.D.	O.D.
Dense Phase	d_1	1.61	1.90
Conventional	d_1	4.25	4.50
Conventional & Dense Phase	d_2	9.25	10.0
	d_3	12.75	-
	d_4	20.6	-

Figure 2-5. Low velocity burner (LV1).

  - 45° (with normal vane length)
  - 45° (with reduced vane length, in an effort to reduce the solidity of the vane ring and hence the angle of spread of the coal stream.

- splitters of the two types shown in Figure 2-6, inserted within the coal pipe, intended to divide the coal stream into four initially fuel-rich flames. The 3T splitter illustrated in the figure was designed to block a greater fraction of the coal pipe, and hence to produce higher-velocity coal streams, compared to the T splitter. The splitter angles tested included:

  - a T splitter with the exit ramps inclined at 15° relative to the axis, providing a relatively more limited degree of divergence between the four coal jets

  - a T splitter with the exit ramps inclined at 30°, providing relatively greater divergence

  - a 3T splitter with a 15° incline

  - a 3T splitter with a 30° incline.

Testing was also conducted using dense-phase coal transport (0.2 lb air/lb coal). Three nozzles were tested with the dense-phase transport pipe; these are depicted in Figure 2-7:

- a commercial spray nozzle, typically used with liquids, mounted on the end of the coal pipe. This nozzle was tested with an without an internal "spinner" device intended to impart swirl to the exiting stream.

- a 30° cone inserted essentially within the coal pipe.

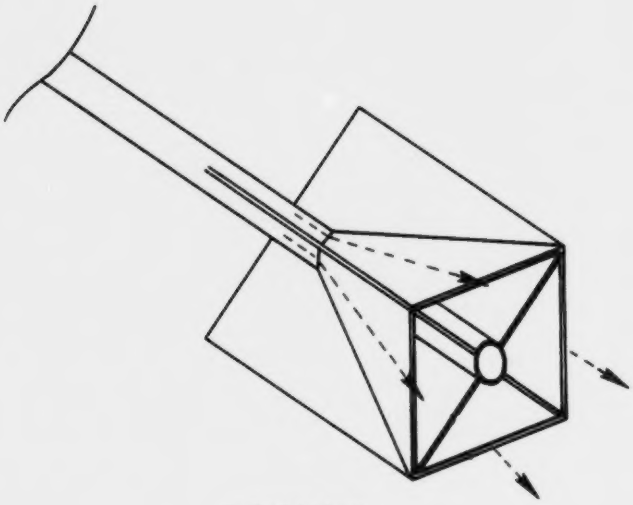

T-Splitter

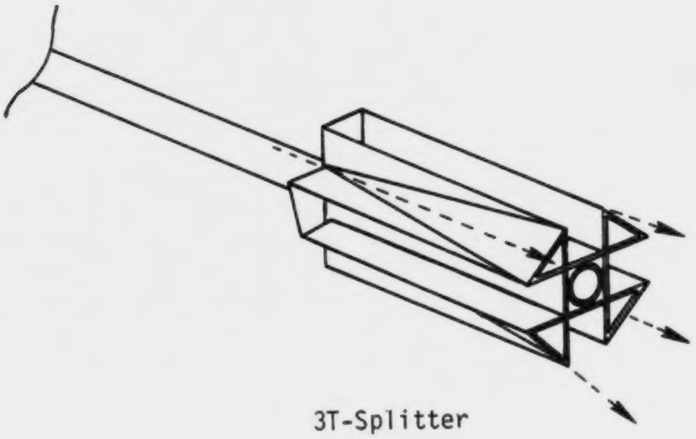

3T-Splitter

Figure 2-6. Sketch of divergent splitters.

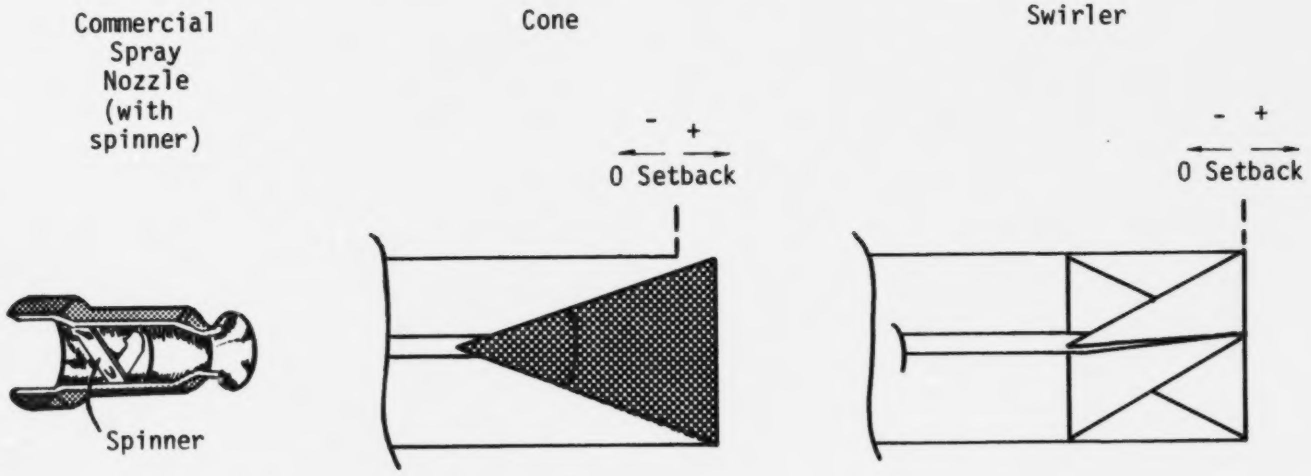
Commercial Spray Nozzle (with spinner)
Spinner
Cone
- +
0 Setback
Swirler
- +
0 Setback

Dense phase based on primary air-to-coal ratio of .2

Figure 2-7. Sketch of dense phase coal nozzles.

- an axial swirler with a 30o vane angle, inserted within the coal pipe.

The coal nozzles tested on the LV1 burner configuration, as described above, are summarized in Figure 2-8.

The operating variables addressed during the testing with each coal nozzle in the LV1 configuration, are shown schematically in Figure 2-9. These variables include:

- air distribution between the two secondary air channels
- swirl for each of the two secondary air channels
- overall excess air
- coal nozzle setback (the coal pipe could be retracted back into, or projected out through, the burner throat, by several inches)
- coal spreader setback (the swirler, spreader and cone inserts could be retracted into, or projected out through, the coal pipe, be several inches).

2.2.3 HV2 Burner

The final burner configuration tested was a second high-velocity unit (HV2), illustrated in Figure 2-10. This configuration had a throat diameter of 8.75 inches, approximately the same as the HV1 burner, and thus had the same 190 ft/sec secondary air velocity; however, HV2 had only two (relatively wider) secondary air channels, rather than three narrow channels, greatly reducing the difficulties with flame stability experienced with HV1.

The coal nozzle modifications tested on the HV2 burner were those which provided the lowest NO_x emissions with the LV1 burner:

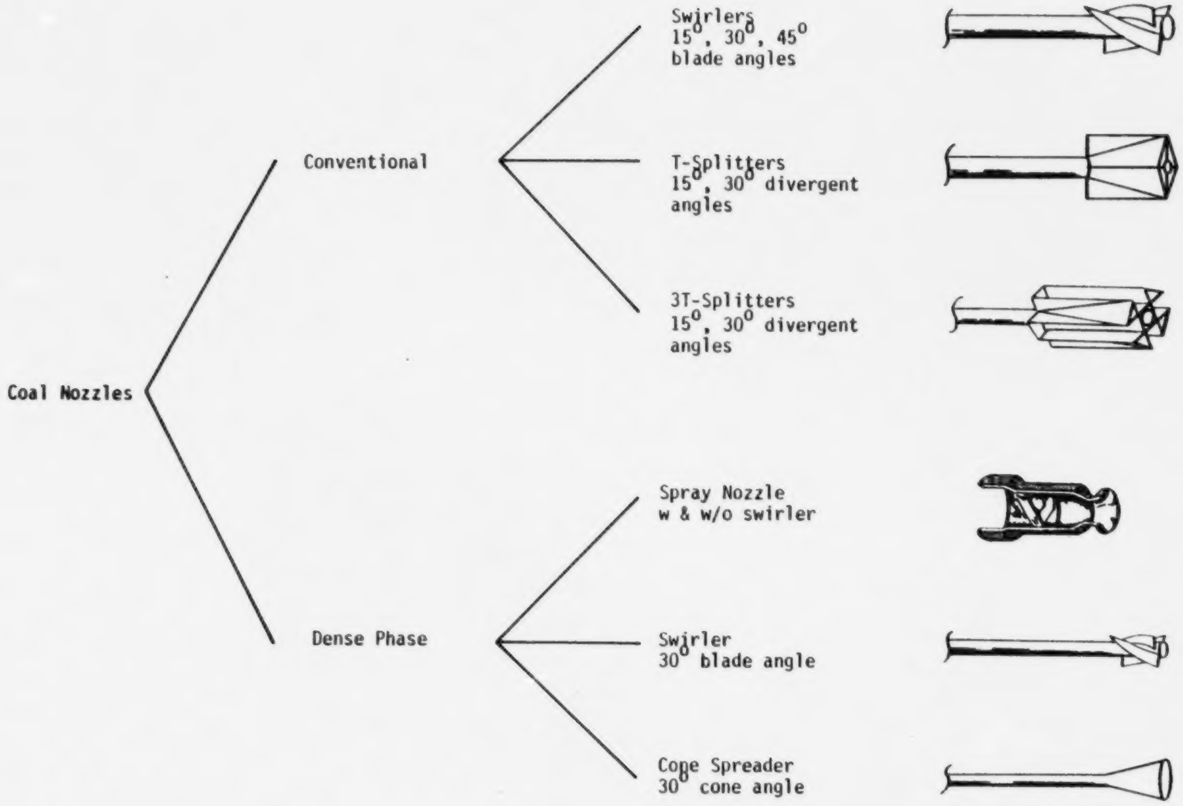
Coal Nozzles
Conventional
Dense Phase
Swirlers
15°, 30°, 45°
blade angles
T-Splitters
15°, 30° divergent
angles
3T-Splitters
15°, 30° divergent
angles
Spray Nozzle
w & w/o swirler
Swirler
30° blade angle
Cone Spreader
30° cone angle

Figure 2-8. Coal splitters/spreaders tested for LV1 burner.

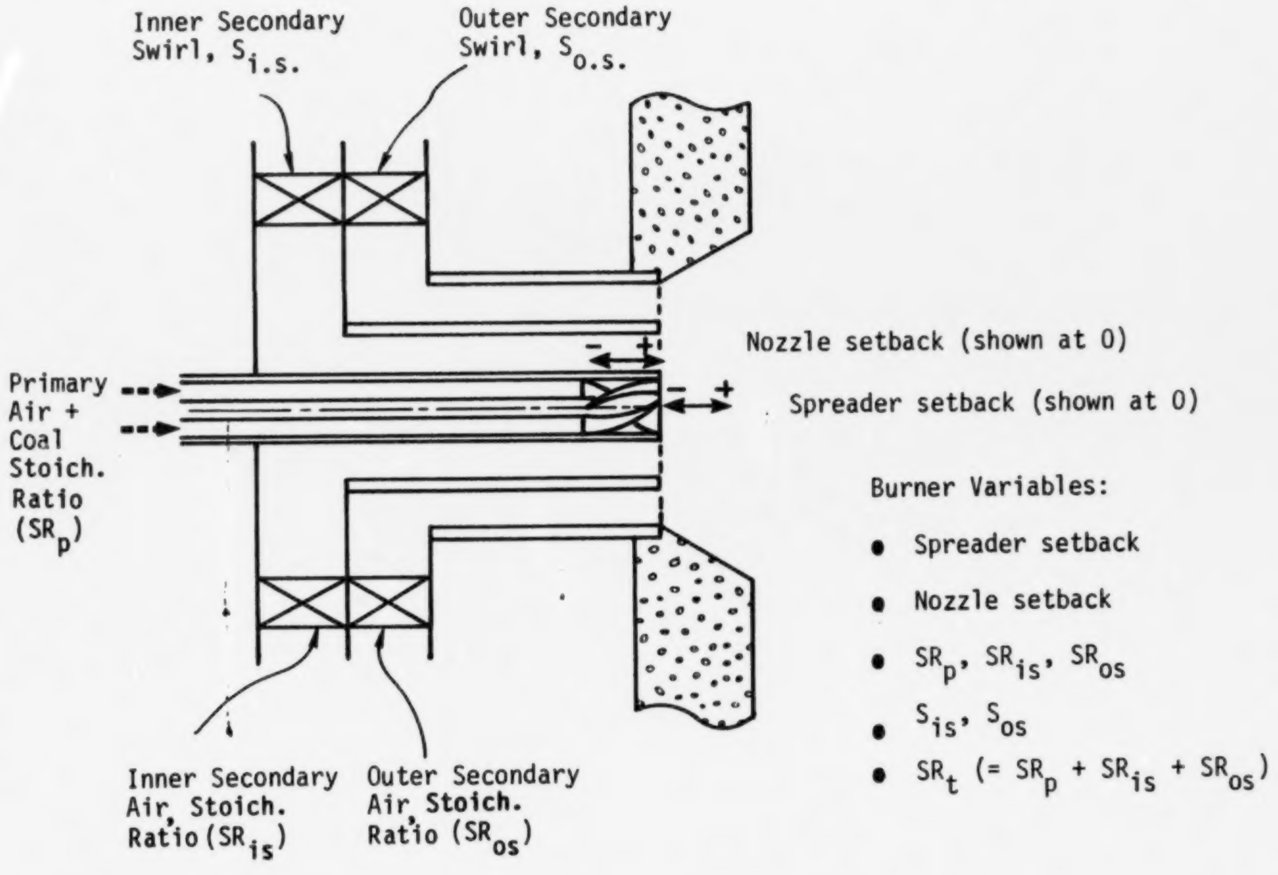
Inner Secondary Swirl, $S_{i.s.}$
Outer Secondary Swirl, $S_{o.s.}$
Primary Air + Coal Stoich. Ratio (SR_p)
Nozzle setback (shown at 0)
Spreader setback (shown at 0)
–
+
Inner Secondary Air, Stoich. Ratio (SR_{is})
Outer Secondary Air, Stoich. Ratio (SR_{os})

Burner Variables:

- Spreader setback
- Nozzle setback
- SR_p, SR_{is}, SR_{os}
- S_{is}, S_{os}
- SR_t (= SR_p + SR_{is} + SR_{os})

Figure 2-9. Burner operating parameters investigated on the LV1 and HV2 burner configurations.

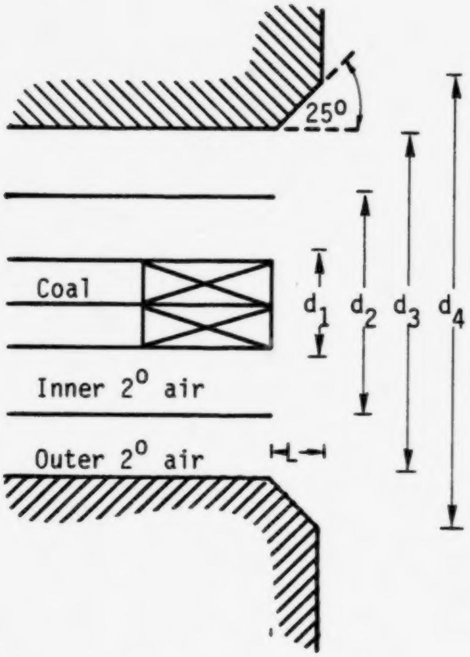
25°
Coal
Inner 2° air
Outer 2° air
L
d_1
d_2
d_3
d_4

- Small throat diameter (no enlargement possible)
- High secondary air velocity
  - 190 ft/sec (conventional coal transport)
  - 145 ft/sec (dense-phase)
- Axial coal nozzles (swirlers, splitters, dense-phase)
- Shallow quarl (L/D = 0.25)

Throat Dimensions (In.)

	I.D.	O.D.
d_1	4.25	4.5
d_2	7.75	8.0
d_3	8.75	
d_4	11.25	
L	2.5	

Figure 2-10. High velocity burner with two secondary air channels (HV2).

- an axial swirler, with a 15° vane angle, inserted into the coal pipe for conventional transport (2 lb air/lb coal)

- a T splitter, with a 15° incline on the exit ramp, inserted into the conventional coal pipe

- a 30° axial swirler inserted into a dense-phase coal pipe

- a 30° cone spreader inserted into a dense-phase coal pipe.

Each of these four coal nozzle modifications was tested with and without conical baffles on the lip of the sleeve separating the inner and outer secondary air channels (see Figure 2-11). These baffles were intended to divert the outer secondary air away from the near flame. Two different baffles were tested, representing two different cone angles (expressed here as L/D, the axial length of the baffle lip divided by the diameter of the baffle outlet); L/D values investigated here were 0.22 (representing relatively less diversion of the outer secondary air) and 0.13 (representing relatively greater diversion). The coal nozzles and air baffles tested on the HV2 burner are summarized schematically in Figure 2-12.

The operating variables tested with each coal nozzle and air baffle arrangement in the HV2 configuration are the same as those shown previously in Figure 2-9, except that air baffle position is now an additional variable. The baffle could be retracted into the burner throat, or extended out towards the furnace (essentially lengthening the air channel sleeve).

2.2.4 Measurements for Internally-Staged Burner Tests

The measurements conducted during the testing of the three internally-staged burner configurations are summarized in Table 2-4. Measurements associated with the control variables which were adjusted are part of this testing ("input" measurements) are listed on the left side of the table; measurements of the response (output) variables are on the right.

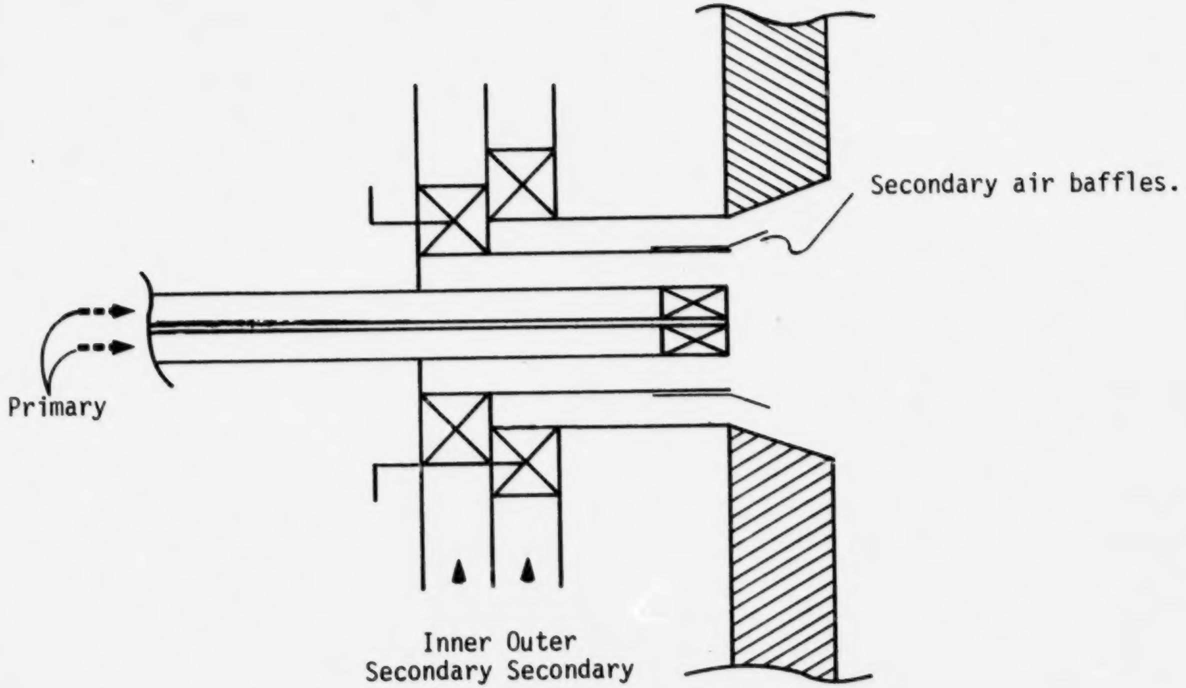
Secondary air baffles.
Primary
Inner Outer
Secondary Secondary

Figure 2-11. Secondary air baffle installed in the HV2 burner configuration.

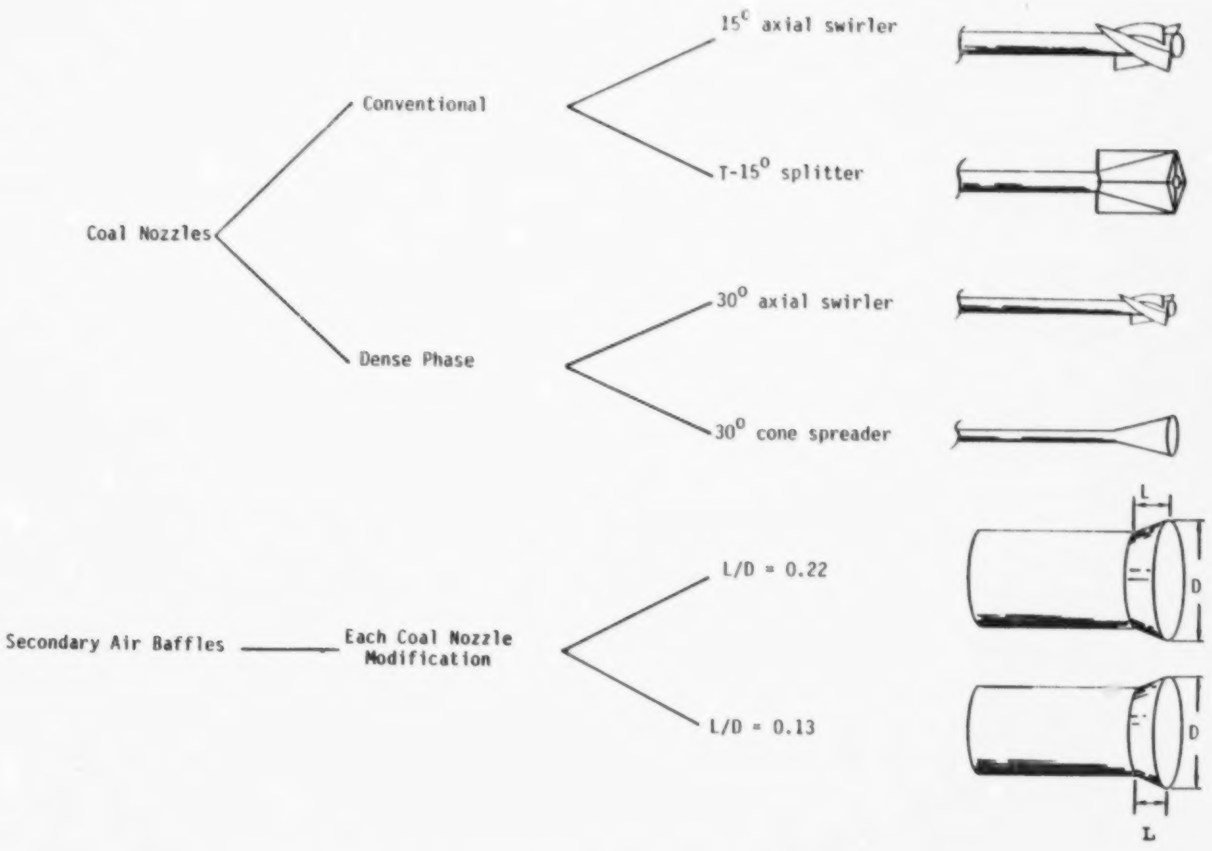
Coal Nozzles
Conventional
Dense Phase
15° axial swirler
T-15° splitter
30° axial swirler
30° cone spreader
Secondary Air Baffles
Each Coal Nozzle Modification
L/D = 0.22
L/D = 0.13
L
D
D
L

Figure 2-12. Burner modifications tested during HV2 burner tests.

TABLE 2-4. MEASUREMENT FORMAT FOR LOW-NO_x INTERNALLY-STAGED BURNER TESTS

Inputs			Outputs		
Parameter	Method	Record	Parameter	Method	Record
Routine			Routine		
Burner Settings	Manual	Manual	Flame Characteristics	Manual Observation	Manual
Air Flow Rates	Venturis	Computer	Combustion Products O_2	Beckman--Paramagnetic	
Air Temperature	Thermocouples	Computer	CO_2	Anarad-NDIR	Computer and Strip Chart Recorders
Fuel Flow Rate	Coal--Volumetric Feeder	Computer	NO/NO_x	TECO-Chemi-Luminescent	
	Oil--Rotometer		Furnace Pressures	Magnehelics	Manual
	N. Gas--Laminar Flow Element and Calculation from Fuel Composition, Air Flow & Excess O_2		Stack Temperatures	Thermocouples	Computer
Detailed			Detailed		
Coal Composition	Ultimate and Proximate Analysis (ASTM)		Fly Ash Carbon Content (Carbon Balance)	Grab Sample and Ultimate Analysis	

The response variables measured routinely as the primary indicators of burner performance were:

- measures of combustion performance, including visual observation of flame shape and stability, and analysis of CO, CO_2 and O_2 in the stack gas

- measures of NO_x reduction, including flue gas NO/NO_x.

Furnace pressures and stack temperatures were also measured. In a limited number of cases, the fly ash collected in the SWS multiclones was analyzed for carbon in order to permit a carbon balance (in conjunction with coal analysis and stack gas analysis).

The control variables have been discussed in the previous sections. Key burner operational settings were controlled manually: the degree of swirl in the individual secondary air channels, and the setbacks of the coal nozzle, coal spreader and secondary air baffle. Air distribution between the various air channels, and the overall excess air, were controlled/measured using venturi meters.

2.3 Experimental Arrangement for Sorbent Injection Testing

The sorbent injection testing had two objectives: to determine whether internal staging modifications for NO_x reduction would provide an environment suitable for near-burner sorbent injection; and to determine whether sorbent jet parameters could be adjusted to improve sorbent reactivity upon injection. All injection tests were performed with Vicron 45-3 limestone.

The sorbent injection system used in these tests is shown schematically in Figure 2-13. The system consists of a volumetric screw feeder which meters sorbent into the suction side of an air ejector supplied with air from the house air system. The air flow rate is monitored with an orifice meter located upstream of the ejector and corrected for the air leakage through the

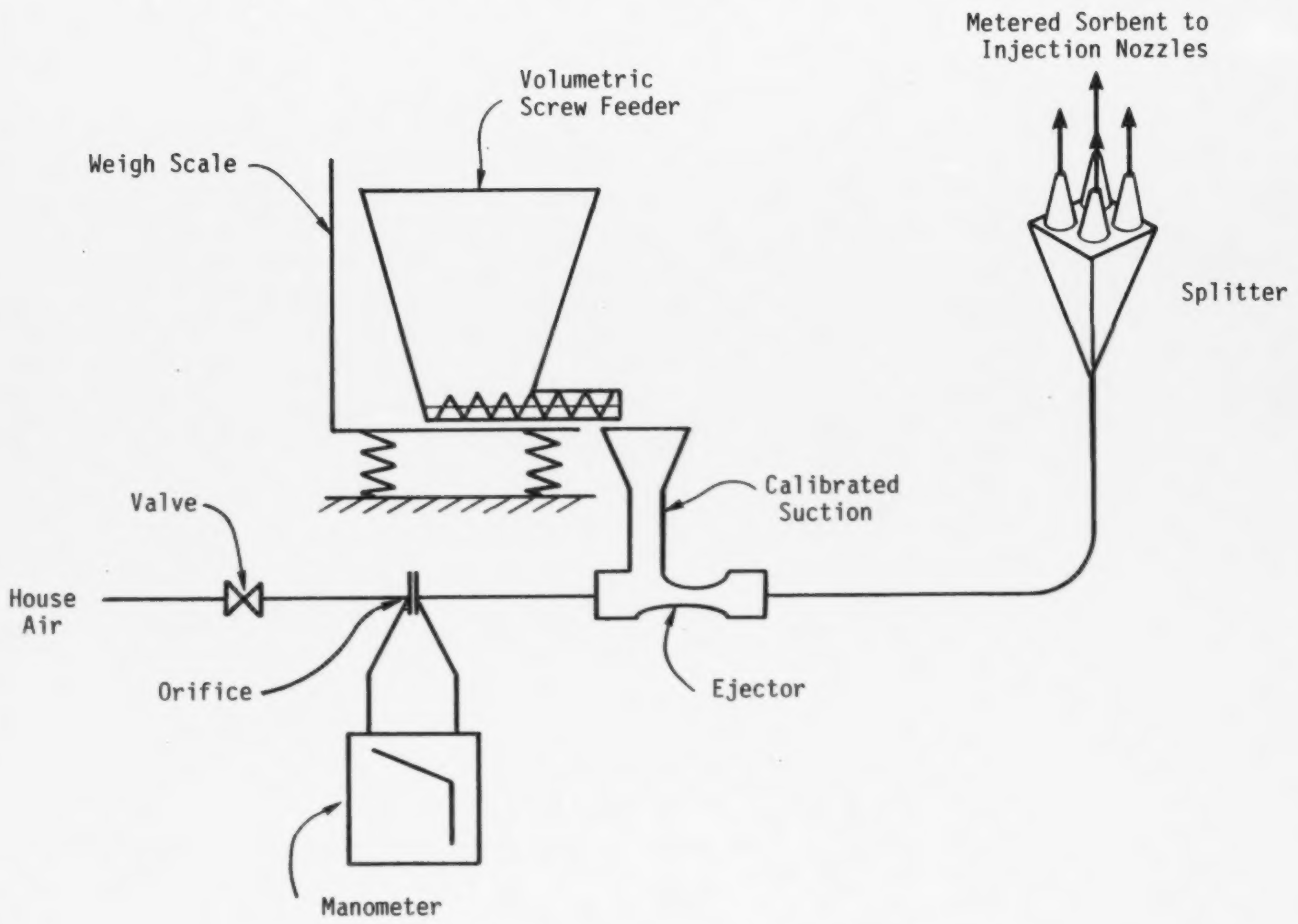
Metered Sorbent to
Injection Nozzles
Volumetric
Screw Feeder
Weigh Scale
Splitter
Calibrated
Suction
Valve
House
Air
Orifice
Ejector
Manometer

Figure 2-13. Schematic diagram of sorbent feed system.

suction inlet of the ejector. The bin feeder is supported on a weigh scale to provide a gravimetric measure of the sorbent feed rate.

Downstream of the ejector the sorbent stream can connect directly to a single sorbent injector or, if necessary, through a 2 or 4-way splitter to multiple injection points.

2.3.1 Sorbent Injection with Internally-Staged Burners

Sorbent injection tests were conducted with two of the internally staged burner configurations: with the HV1 configuration, burning either SO_2-doped natural gas or Utah coal; and with the LV1 configuration burning Utah coal. With each configuration, the specific burner conditions used for the injection tests were those which had provided the lowest NO_x emissions (or the best flame stability). In the case of the HV1 configuration, the injection tests were conducted with the 15° axial swirler coal nozzle, and with 60 percent of the secondary air in the outer channel with maximum swirl in the outer channel. In the case of LV1, the injection tests were conducted with the 15° T splitter coal nozzle, and with dense-phase coal transport (including both the 30° axial swirler and the 30° cone spreader).

For each burner configuration, alternative near-burner sorbent injection methods were investigated. The three methods tested with the HV1 burner are illustrated in Figure 2-14. Sorbent was injected: a) into the primary air/coal stream, within the coal pipe; b) through the outer secondary air channel; and c) through four outboard ports in the firing wall of the furnace, surrounding the burner throat. For outboard wall injection two different injection velocities were tested. With the LV1 configuration, only primary air injection and wall injection were tested, and only one wall injection velocity was considered. The wall injection was accomplished using four single jets (as distinguished from double concentric jets) in all cases.

Other variables adjusted during parts of this injection testing included sorbent feed rate, SO_2 concentration, furnace firing rate, and overall excess air.

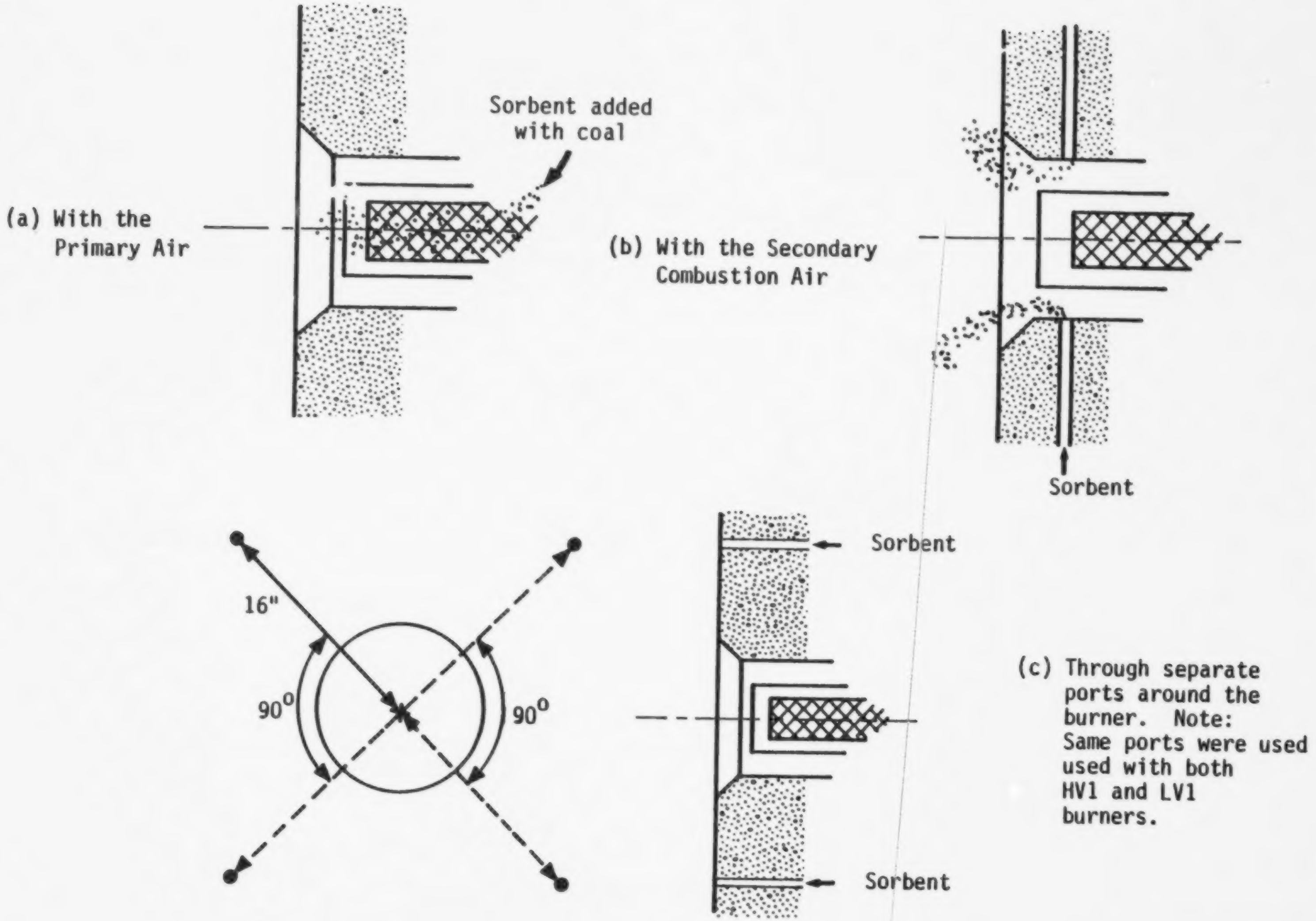

(a) With the Primary Air

(b) With the Secondary Combustion Air

(c) Through separate ports around the burner. Note: Same ports were used used with both HV1 and LV1 burners.

Sorbent added with coal
Sorbent
Sorbent
Sorbent
16"
90°
90°

Figure 2-14. Sorbent injection locations for tests with internally-staged burners.

2.3.2 Measurements for Sorbent Injection Tests

The measurements conducted during the sorbent injection testing with the internally-staged burners are summarized in Table 2-5. Measurements for control variables and responses were generally the same as those conducted for the burner tests and listed in Table 2-4. Key additional measurements relating to sorbent injection were the sorbent characteristics and sorbent injection parameters (sorbent flow, sorbent jet velocity) and the SO_2 concentration in the stack gas as the primary measure of sorbent performance.

TABLE 2-5. MEASUREMENT FORMAT FOR SORBENT INJECTION TESTS

Inputs		Outputs	
Parameter	Method	Parameter	Method
Routine		Routine	
Burner conditions --burner settings, fuel flows, air flows	Same as Table 2-4	Burner performance --combustion products in flue gas, NO/NO_x	Same as Table 2-4
Sorbent injection location	Manual	SO_2 in stack gas (primary measure of sorbent performance)	DuPont ultraviolet
		Furnace exit temperature	Type "S" suction pyrometer
		Sample point	Thermocouple
Detailed		Detailed	
Sorbent jet velocity	Venturi on air line to sorbent jet	Sorbent surface	B.E.T. analysis on extracted samples (nitrogen quench sampling probe)
Sorbent flow rate	Volumetric feeder	In-furnace temperature profiles	Type "S" suction pyrometer
Sorbent composition and size distribution	Manufacturers specifications and EER in-house sizing (Sedigraph)	Solids sulfur content (for sulfur balance)	Ultimate analysis grab sample

3.0 LOW-NO$_x$ INTERNALLY-STAGED BURNER TEST RESULTS

The NO$_x$ emissions produced by the flames from the three burner configurations described in Section 2.2 were evaluated. The tests with the HV1 burner involved burner stability tests with natural gas followed by NO$_x$ tests with Utah coal. Tests with the LV1 burner investigated the effect of coal nozzle modifications and burner adjustments on NO$_x$ emission levels. The burner modifications found to be most effective in reducing NO$_x$ emissions from the LV1 burner were selected for studies with the HV2 burner. Secondary air baffles were also tested with the HV2 burner to determine their effects on NO$_x$ emissions and flame stability.

In the presentation of NO$_x$ data, the furnace exit temperature is used as a key parameter. This is because the furnace exit temperatures during the tests increased with time and the NO$_x$ emission was sensitive to furnace temperature levels. This exit temperature variation was primarily due to the thermal inertia of the SWS furnace cooling system and due to ash deposition in the furnace, which changed the extent of the furnace heat extraction. This effect was most pronounced for coal firing with similar but smaller effects observed during oil and gas firing. In the following subsections, the results from each of the three burners are described.

3.1 High Velocity Burner 1 (HV1)

3.1.1 HV1 Tests with Natural Gas

The initial tests on the 190 ft/sec HV1 burner were aimed at characterizing flame stability and burner performance burning natural gas. The key variables investigated were the air distribution and the swirl distribution among the three secondary air passages. These three passages are referred to here as the inner (ISA), middle (MSA) and outer (OSA) secondary air passages.

The first variable adjusted was the air distribution. The results of the air distribution tests are summarized in Table 3-1. In these tests, the

TABLE 3-1. RESULTS OF SECONDARY AIR DISTRIBUTION VARIATIONS WITH HV1 BURNER (NATURAL GAS FLAMES)

- Tests were conducted with maximum secondary air swirl in each passage
- 20% overall excess air

Flame #	Secondary Air Distribution*			Flame Characteristics			NO_x(**)
	ISA	MSA	OSA	Attached to Quarl	Length ft	Blowoff	
NG-1	7	8	85	Yes	N/A	No	70
	↓	Increase	↓				
NG-2	8	32	60	Yes	13.0	No	68
	↓	Increase	↓				
NG-3	7	47	46	Yes	9.0	No	76
	Increase	Decrease	↓				
NG-4	20	35	45	Yes	7.5	No	71
	Decrease	Increase	Decrease				
NG-5	14	46	40	Yes	10.0	No	75
	Increase	Increase	Decrease				
	↓	↓	↓	No	N/A	No	47

* ISA = Inner Secondary Air

MSA = Middle Secondary Air

OSA = Outer Secondary Air

The secondary air distribution figures presented here are the percent of the total secondary air directed to each of the three passages.

(**) ppm dry, corrected to 0% O_2

swirl distribution was held constant (with maximum swirl in each of the three passages); the overall excess air was also constant at 20 percent, and primary air was constant at zero (i.e., all air flow was secondary air). In the first three test conditions shown in the table, OSA was decreased from a high value (85 percent of all secondary air through the outer channel in NG-1) to a moderate value, with MSA increasing correspondingly and ISA remaining constant. In the next two runs, OSA was held approximately constant at the moderate value, and the MSA and ISA were adjusted. Finally, after run NG-5, an attempt was made to reduce OSA further.

As indicated in the Table, stable flames, attached to the burner quarl, were maintained only so long as at least 40-45 percent of the total secondary air was channeled to the outer secondary air passage. Attempts to reduce the OSA below 40-45 percent resulted in flame blowoff. Decreasing the OSA from 85 percent to 46 percent resulted in some reduction in flame stability, as manifested by intermittent episodes of flame liftoff and reattachment. At a constant value of OSA (40-60 percent), tradeoff of secondary air between MSA and ISA had little effect on flame characteristics, except that biasing the air toward the inner channel tended to produce somewhat shorter flames, as would be expected based upon more rapid fuel/air mixing. For all of the stable flames, NO_x levels remained within the range of 68 to 76 ppm, irrespective of air distribution.

The second variable adjusted was the swirl distribution, the results from which testing are summarized in Table 3-2. For these tests, the secondary air distribution was held constant at values found to provide a stable, attached flame (8 percent ISA, 32 percent MSA, 60 percent OSA); again, total excess air was 20 percent and primary air was zero. The swirl distribution was varied using adjustable vanes in each secondary air passage which permitted the swirl in each passage to be controlled independently of the air flow rate. As shown in Table 3-2, variation of the swirl in the ISA and MSA channels had little visible effect on flame characteristics or on NO_x emissions, so long as maximum swirl was maintained in the outer channel. However, any reduction in the OSA swirl below maximum resulted in flame blowoff.

TABLE 3-2. RESULTS OF SECONDARY AIR SWIRL VARIATIONS WITH HV1 BURNER (NATURAL GAS FLAMES)

Secondary Air Distribution: 8% ISA, 32% MSA, 60% OSA

Flame #	Secondary Swirl Setting			Flame Characteristics			NO_x*
	ISA	MSA	OSA	Attached	Length (ft)	Blowoff	
NG-2	Max	Max	Max	Yes	13	No	76
NG-6	Zero	Max	Max	Yes	13	No	76
NG-7	Zero	Zero	Max	Yes	13	No	76
NG-8	Zero	Zero	<Max	No	-	Yes	-

*ppm dry, corrected to 0% O_2.

Burners operating at secondary air velocities as high as this (190 ft/sec) generally require moderate to high secondary air swirl numbers in order to achieve stability. The results in Table 3-2 suggest that the tangential component of the secondary air momentum--imparted by the swirl vanes--was being largely damped out by wall effects in the narrow secondary air channels. (The width of the three channels ranged from 0.35 to 0.8 inches.) In addition, some loss of tangential momentum might have been occurring within the movable swirl vanes themselves, due to the nature of their construction. As a result--even though the burner had been designed to achieve swirl numbers as high as 3, which is fairly high--the secondary air issuing through the burner throat probably did not retain sufficient swirl to provide stability over the desired range of burner conditions. The need to divert most of the secondary air to the outer passage, and to maintain maximum swirl in that passage, indicated that the flames were being stabilized by a combination of bluff-body stabilization as well as swirl stabilization.

It is possible that the 10 x 10^6 Btu/hr experimental scale available here is too small to permit a fair test of the three-channel concept which provides maximum control over secondary air. A full-scale wall burner (of perhaps 100 x 10^6 Btu/hr) would permit wider secondary air channels; such a large burner, with appropriately-designed registers and swirl vanes, might overcome the difficulties encountered here and enable effective application of the three-channel concept.

3.1.2 HV1 Tests with Utah Coal

A primary objective of the coal-fired tests on the HV1 burner was to establish an NO_x emissions baseline, against which NO_x data from the other burner configurations might be compared. Since it was apparent from the natural gas tests that the burner had narrow limits of stability, no extensive tests on coal were contemplated.

Initial coal testing was aimed at confirming the necessary distribution of secondary air among the three channels. In these tests, maximum swirl was maintained in each of the passages; overall excess air was 20 percent, and the primary air fed with the coal was 15 percent stoichiometric (i.e., the total secondary air was 105 percent stoichiometric). (The primary stoichiometric ratio (SR_p) had to be reduced to 0.15 from the originally-intended 0.20 in order to obtain a stable flame. The results from these air distribution tests with coal confirmed the natural gas results: when OSA was reduced below 40 percent of the total secondary air flow, the flame became detached from the quarl (although it did not totally blow off, as in the gas case); and as OSA was increased above 40 percent, the flame became longer and more stable. Effects on NO_x emissions were more pronounced in the coal case. In the natural gas case, where NO_x resulted entirely from thermal fixation of atmospheric nitrogen, the NO_x emissions had held fairly steady between 68 and 76 ppm over a wide range of air distributions. But in the coal case--where most of the NO_x results from fuel-bound nitrogen--an increase in OSA at the expense of ISA (changing from 12 percent ISA/44 percent MSA/44 percent OSA to 6 percent ISA/43 percent MSA/51 percent OSA) resulted in a reduction in NO_x emissions from 636 ppm to 542 ppm.

Coal combustion tests were then conducted with two different coal nozzles--specifically, with a 45° axial swirler inserted in the coal pipe, and with a 15° axial swirler. Some results are shown in Figure 3-1. For these coal nozzle tests, the air distribution between the secondary air channels was selected as a value which had shown good results in the initial coal tests (14 percent ISA/34 percent MSA/51 percent OSA, corresponding to stoichiometric ratios of 0.15 for the ISA, 0.36 for the MSA and 0.54 for the OSA). The setback of the coal nozzle in the Figure 4-1 tests was set at 0.0 inches (i.e., the coal pipe ended flush with the burner throat); the spreader setback was -3.0 inches (i.e., the axial swirlers were retracted 3 inches into the coal pipe). These coal nozzle settings had been found to give reasonable burner performance. The flames obtained at these burner conditions were approximately 4 to 5 feet long and 2 to 3 feet wide at their maximum width, and were stable and attached to the quarl. As discussed

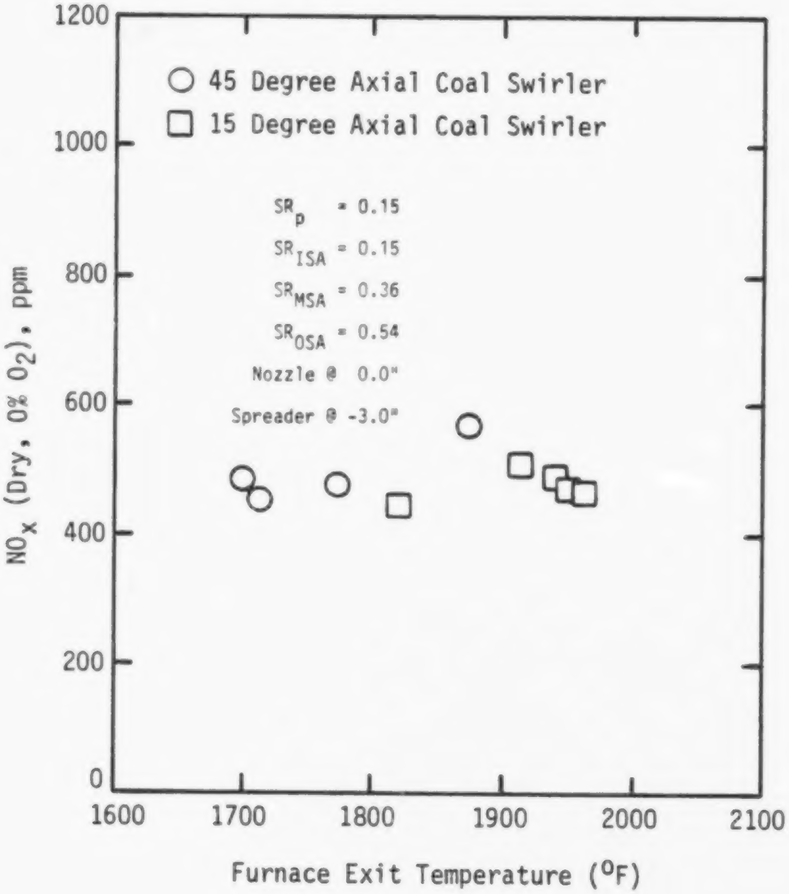

- Maximum swirl level in each of the secondary air passages
- Overall excess air 20%

Figure 3-1. NO_x emissions versus furnace exit temperature during coal combustion tests with HV1 burner.

previously, the NO_x emissions were plotted as a function of SWS exit temperature since the exit temperature unavoidably varied.

As apparent from the figure, NO_x emissions ranged between 400 and 600 ppm (dry, corrected to 0 percent O_2) at these burner conditions. These emissions are similar to data obtained by other investigators with internally-staged pilot-scale burners (1), and represent a reduction compared to the 650-850 ppm typical of full-scale uncontrolled pre-NSPS coal burners. There is no clear trend in emissions distinguishing the 45° coal swirler from the 15° swirler. However, flames generated by the 45° swirler tended to be wider, and to curl back onto the burner plate, damaging the plate. As a result, the remainder of the coal testing with this burner--including the sorbent injection tests described in Section 4.1--were conducted with the 15° swirler.

Because of the limited stability of the three-channel HV1 burner, substantial additional testing was not conducted to quantify the NO_x effects of coal nozzle design, secondary air and swirl distribution, excess air, coal nozzle setback and coal spreader setback. All further NO_x tests with internally-staged burners were conducted using two-channel configurations.

3.2 Low Velocity Burner 1 (LV1)

The LV1 burner configuration was tested to represent the retrofit case where an existing burner provides maximum flexibility for enlarging the throat and thus reducing secondary air velocity (to 80 ft/sec). The LV1 configuration utilized two secondary air passages. As discussed in Section 2.2.2, the LV1 testing considered several alternative coal nozzles, and adjustments to burner operating conditions (air distribution and swirl distribution between the secondary air channels, overall excess air, and the positioning of the coal nozzle and the nozzle insert). The types of coal nozzles tested included both conventional coal transport (approximately 2 lb primary air per lb of coal, representing a primary stoichiometric ratio of about 0.15 to 0.20) and also dense-phase transport (approximately 0.2 lb primary air/lb coal, representing a SR_p of 0.02 to 0.03). All tests were conducted burning Utah coal.

3.2.1 LV1 Tests with Conventional Coal Transport

The conventional coal transport alternatives tested included axial swirlers of several different vane angles inserted within the coal pipe, and several different splitter designs inserted into the coal pipe.

Four axial swirlers were tested with the LV1 burner: a 15° vane angle (imparting relatively less swirl to the coal); a 30° vane angle; a 45° vane angle (imparting a relatively higher degree of swirl; and a second 45° swirler having vanes of shorter length, in an effort to reduce the roping pattern created by the vanes of normal length. Figure 3-2 summarizes the NO_x results obtained with these four swirlers at the set of burner operating conditions defined as "baseline." Baseline operating conditions for the swirlers were: even distribution of the secondary air between the inner and outer channels; even distribution of the secondary air swirl between the two channels, with a moderate degree of swirl in each channel; a total excess air of 20 percent, with $SR_p = 0.15\text{-}0.20$; a nozzle setback of 0.0 inches (coal pipe ends flush with burner throat); and a spreader (axial swirler) setback of 0.0 inches (swirler insert ends flush with end of coal pipe). The NO_x results are intuitively reasonable: lowest emissions (around 450-500 ppm) were obtained with the 15° swirler, which produces the least swirl and hence the least rapid coal/air mixing; intermediate NO_x levels (around 550-750 ppm) were observed with the 30° swirler; and highest levels (600-750 ppm) were generated by the 45° swirlers, which produce the most rapid coal/air mixing. The short versus the normal vane length with the 45° swirlers does not appear to significantly influence NO_x. As discussed previously, NO_x emissions vary with furnace outlet temperature; for convenience in comparing results from different burners, future discussion will often refer to NO_x emissions at the $2000^\circ F$ exit temperature. In all cases with the axial swirler tests, CO emissions were between 35 and 65 ppm, which is felt to represent acceptable combustion performance.

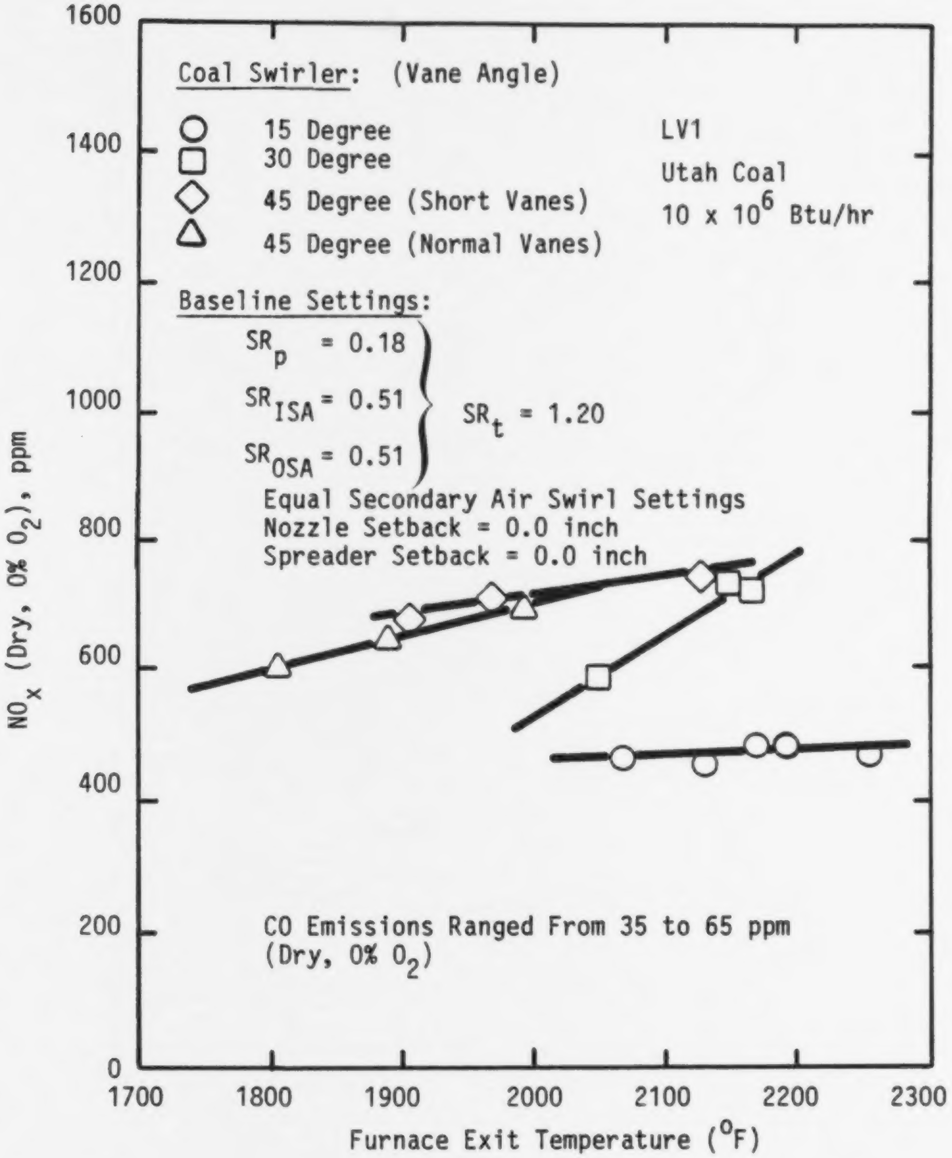

Figure 3-2. Summary of NO_x emissions at baseline burner settings for LV1 with axial vane coal swirlers.

Figure 3-3 depicts the approximate flame shapes and dimensions obtained with the four swirlers at baseline conditions. These diagrams represent the average boundaries of the flames; the actual boundaries, of course, showed some short-term fluctuations about these averages. Again, the results are intuitively reasonable: the 15° swirler gave a longer, narrower flame, consistent with slower coal/air mixing, while the 45° swirlers gave the shortest, widest flames, representing more rapid mixing.

Following the definition of the baseline NO_x emissions with the axial swirler coal nozzles, the key burner parameters were adjusted one at a time, in order to indicate how these various adjustments influenced emissions relative to the baseline. The results from this systematic adjustment of burner operating variables are summarized in Table 3-3. (It should be noted that the changes in NO_x emissions indicated for the individual adjustments would not necessarily be additive if multiple adjustments were implemented in combination.) The one adjustment which provided effective additional NO_x reduction was adjustment of the secondary air distribution between the two channels (which had been $SR_{ISA} = SR_{OSA} = 0.51$ at baseline conditions). Biasing the secondary air to the outer channel ($SR_{OSA} = 0.71$, $SR_{ISA} = 0.31$) reduced NO_x emissions by over 50 ppm for both the 15° and 30° swirlers, reflecting an apparent slowing of fuel/air mixing; such outer biasing did not reduce NO_x for the 45° swirlers, presumably because the wide and highly swirling coal jet from those swirlers achieved rapid mixing with the outer secondary air, negating any effect of outer biasing. For all swirlers, biasing the secondary air to the inner channel ($SR_{ISA} = 0.71$, $SR_{OSA} = 0.31$) resulted in increased NO_x, reflecting the anticipated increase in coal/air mixing.

The other adjustments illustrated in Table 3-3 had less consistent or pronounced effects with axial swirlers. The secondary air swirl distribution had been moderate inner/moderate outer at baseline conditions; adjustment to either high inner/low outer swirl or low inner/high outer swirl generally increased NO_x, if there was any NO_x effect, but this increase was generally small (except in cases where swirl reduction caused flame detachment). Extending or retracting either the coal pipe or the swirler insert sometimes

SWS Furnace Side View

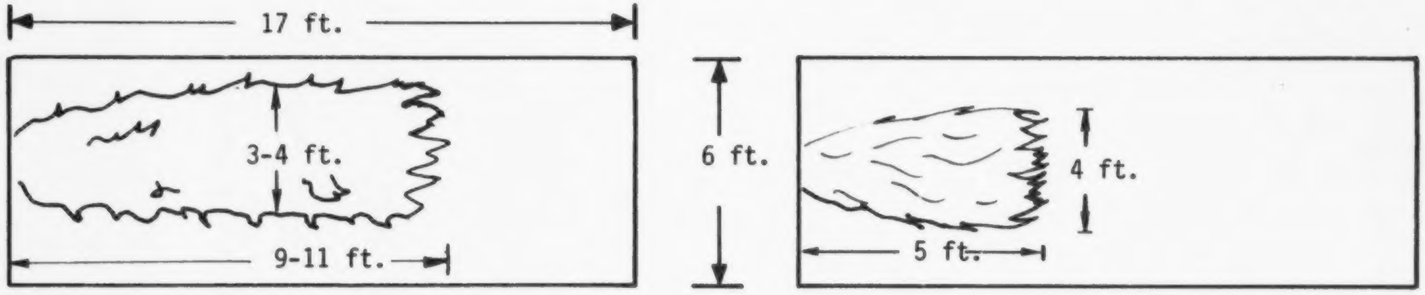

a) 15° axial swirler, Baseline Settings
NO_x = 490 ppm, CO = 60 ppm

b) 30° axial swirler, Baseline Settings
NO_x = 520 ppm, CO = 40 ppm

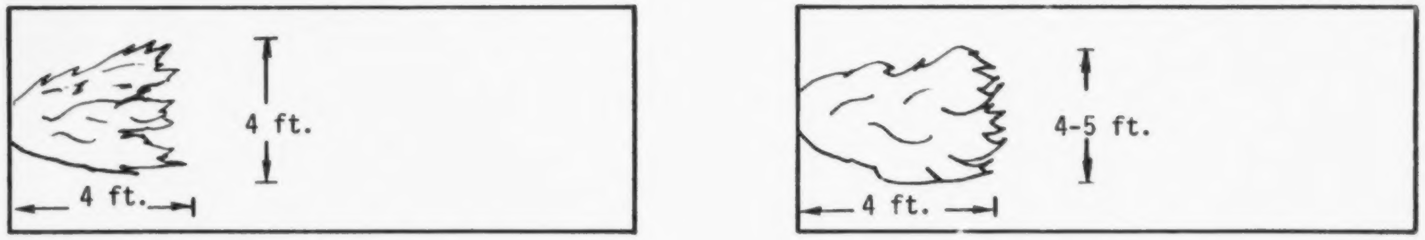

c) 45° axial swirler (short blades)
Baseline Settings
NO_x = 710 ppm, CO = 40 ppm

d) 45° axial swirler (normal blades)
Baseline Settings
NO_x = 680 ppm, CO = 60 ppm

Figure 3-3. Flame shapes for baseline flames with axial swirlers in LV1 burner (NO_x and CO emission values are dry and corrected to 0% O_2, at 2000°F furnace exit temperature).

TABLE 3-3. EFFECT OF BURNER ADJUSTMENTS ON NO_x EMISSIONS FOR AXIAL SWIRLERS WITH LV1 BURNER

		Axial Swirler Coal Nozzles			
	Variables	15 Deg	30 Deg	45 Deg (Short)	45 Deg (Normal)
Effect of Variables on NO_x Emissions	Spreader Setback:				
	Into Furnace (+4")	No Change	No Change	Decreased NO_x by ~90 ppm	Increased NO_x by ~100 ppm
	Out of Furnace (-4")	Increased NO_x ~50 ppm	No Change	No Change	Increased NO_x by ~100 ppm
	Nozzle Setback:				
	Into Furnace (+4")	Increased NO_x	No Change	No Change	N.A.*
	Out of Furnace (-4")	Increased NO_x	No Change	Increased NO_x by ~300 ppm	
	Air Distribution:				
	Biased to Inner Secondary ($SR_{ISA} = 0.71$, $SR_{OSA} = 0.31$)	Increased NO_x by ~20 ppm	Increased NO_x by ~80 ppm	Increased NO_x by ~50 ppm	Increased NO_x by ~100 ppm
	Biased to Outer Secondary ($SR_{ISA} = 0.31$, $SR_{OSA} = 0.71$)	Decreased NO_x by ~50 ppm	Decreased NOx by ~100 ppm	No Change	No Change
	Air Swirl Distribution:				
	Biased to Inner Secondary (high inner, low outer)	Increased NO_x by ~330 ppm	No Change	Increased NO_x by ~20 ppm	Increased NO_x by ~300 ppm
	Biased to Outer Secondary (low inner, high outer)	Increased NO_x by ~50 ppm	No Change	No Change	Increased NO_x by ~50 ppm
Burner Baseline NO_x Emissions (2000°F (Dry, 0% O_2)		475 ppm	500 ppm	700 ppm	675 ppm

*N.A. = Not Attempted

Note: The changes in NO_x emissions shown for individual adjustments would not necessarily be additive if multiple adjustments were implemented in combination.

increased NO_x, sometimes had no effect, and in only one instance (4-inch retraction of 45° short-vane swirler into coal pipe)appeared to decrease NO_x.

The second type of coal nozzle tested with conventional coal transport in the LV1 burner configuration involved the use of divergent coal splitters as inserts within the coal pipe. Two types of splitters were used, as described in Section 2.2.2: one referred to as the "T" splitter, the other (producing a higher coal jet velocity) referred to as the "3T" splitter. For each type of splitter, both a 15° and a 30° incline were tested, resulting in a total of four splitter type/incline angle combinations. Figure 3-4 summarizes the NO_x emissions from these four splitters at baseline conditions. Baseline conditions with the splitters were essentially the same as for the axial swirlers in Figure 3-2, with one exception: the baseline spreader position was +2.5 inches rather than 0.0 inches (i.e., the splitter insert was extended 2.5 inches out of the coal pipe).

The approximate flame shapes and dimensions obtained with the four splitters at baseline conditions are depicted in Figure 3-5. The lowest NO_x emissions (320-380 ppm) were observed with the T-15 splitter; as shown in Figure 3-5, this splitter yielded the longest, thinnest flame among the four splitters, indicating that the small divergence angle and the relatively lower coal velocity were resulting in slower coal/air mixing. (The T-15 splitter provided lower emissions than even the 15° axial swirler, despite the fact that the 15° swirler generated even longer flames, as shown in Figure 3-3.) The other three splitters tended to result in discrete flame fingers, since the increased incline angle and/or increased coal jet velocities undoubtedly were resulting in more distinctly separated coal streams emerging from the splitter. It had been hoped that such discrete fingers might reduce NO_x, through breakup of the single large flame into multiple, less intense flames; perhaps also, the separated combustion zones might provide some degree of fuel staging. However, NO_x emissions from these other splitters were higher than with the T-15 flame, suggesting that the effects of more rapid coal/air mixing caused by these fingers--as evidenced by the overall shorter and wider flames relative to T-15--outweighed the potential effects of flame splitting and fuel staging. The T-30 splitter

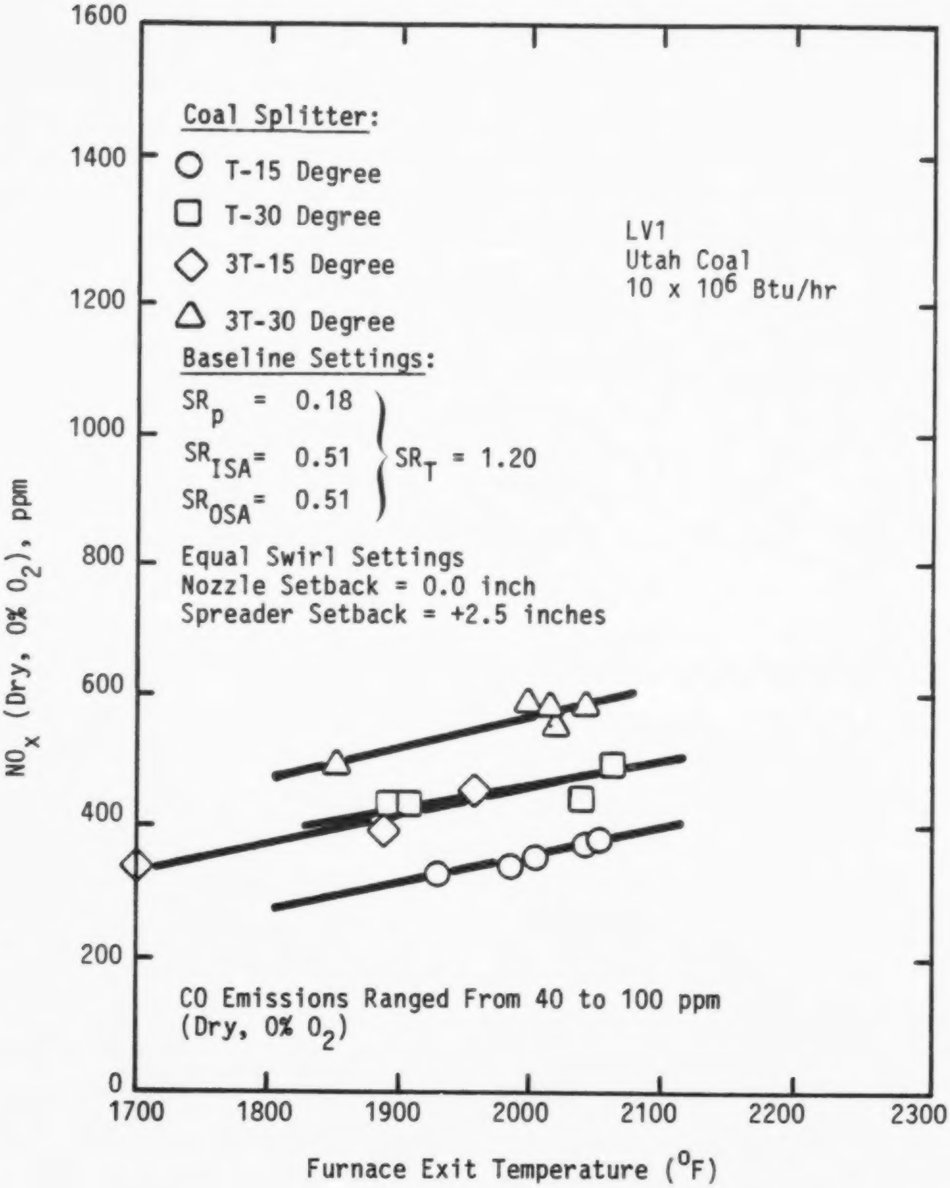

Figure 3-4. Summary of NO_x emissions at baseline burner settings for LVI with divergent splitter nozzles.

SWS Furnace Side View

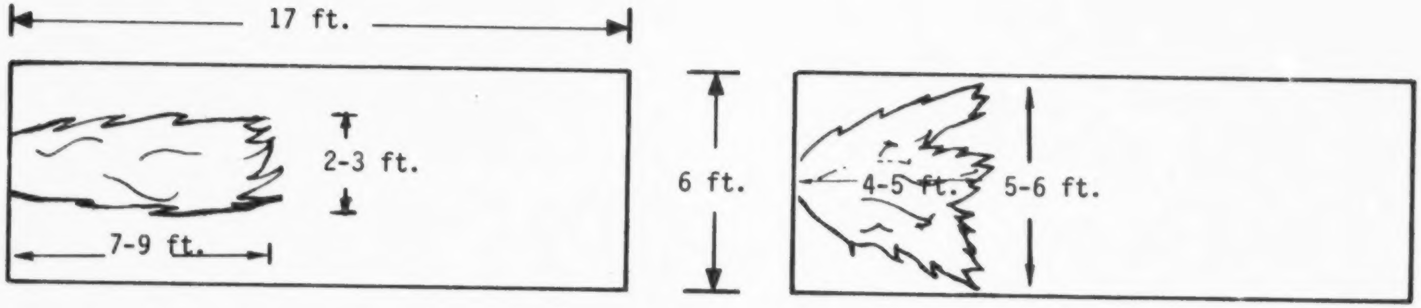

a) T-15° splitter, Baseline Settings
NO_x = 350 ppm, CO = 75 ppm

b) T-30° splitter, Baseline Settings
NO_x = 450 ppm, CO = 60 ppm

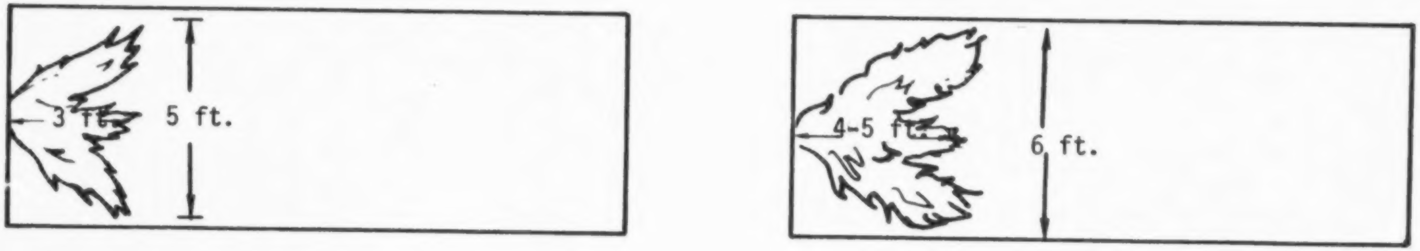

c) 3T-15° splitter, Baseline Settings
NO_x = 450 ppm, CO = 95 ppm

d) 3T-30° splitter, Baseline Settings
NO_x = 580 ppm, CO = 50 ppm

Figure 3-5. Flame shapes for baseline flames with T and 3T splitters in LV1 burner (NO_x and CO emissions values are dry and corrected to 0% O_2, at 2000°F furnace exit temperature).

gave NO_x emissions roughly 100 ppm higher than T-15 (with more rapid mixing presumably resulting from the larger angle). The 3T-15 splitter also gave emissions about 100 ppm higher, with the higher coal velocity presumably giving more rapid mixing. And the 3T-30 splitter, with both a larger angle and a higher coal velocity, produced the highest NO_x of all the splitters, 580 ppm at 2000°F exit. It is noted, though, that with the exception of the 3T-30 splitter, the splitters yielded lower NO_x (350-450 ppm at 2000°F exit) than the best of the swirlers (the 15° swirler, which produced 490 ppm). Carbon monoxide emissions with the swirlers ranged from 40 to 100 ppm, representing generally acceptable combustion performance.

Following the definition of the baseline NO_x emissions with the coal splitters, a parametric study was conducted varying the key burner variables. The results from this systematic adjustment of burner operating variables are summarized in Table 3-4. For all splitters except the 3T-15, biasing the secondary air to the outer channel (from the baseline of $SR_{ISA} = SR_{OSA} = 0.51$ to $SR_{ISA} = 0.31$, $SR_{OSA} = 0.71$), thus slowing coal/air mixing, reduced NO_x emissions (by about 100 ppm in the T-15 case, by perhaps 40 ppm with the other splitters). Decreasing the total excess air with the T-15 splitter (from 20 percent to 10 percent) reduced NO_x by about 100 ppm, although there was a concurrent increase in CO emission to over 100 ppm. (Operation at 10 percent excess air might not be commercially practical, because of reduced combustion efficiency and increased risk of localized reducing conditions and slagging.) On the other hand, biasing the secondary air to the inner channel ($SR_{ISA} = 0.71$, $SR_{OSA} = 0.31$) increased emissions for all splitters (by about 70 to 130 ppm). Biasing the secondary air swirl to the inner channel (from moderate inner/moderate outer to high inner/low outer) increased emissions, generally by about 25 to 50 ppm. Retracting the coal pipe 6 inches back into the burner throat appeared to increase NO_x from the 3T splitters by 40 to 60 ppm. Other adjustments had effects which varied from splitter to splitter.

In summary, with conventional coal transport, the divergent coal splitter nozzles generally tended to lower NO_x than the axial swirler nozzles. Nozzles which resulted in less rapid coal/air mixing (lower swirler vane angles, splitter diverging angles or coal velocities) formed

TABLE 3-4. EFFECT OF BURNER ADJUSTMENTS ON NO_x EMISSIONS FOR SPLITTER NOZZLES WITH LV1 BURNER

		Divergent Splitter Coal Nozzles			
	Variables	T-15	T-30	3T-15	3T-30
Effect of Variables on NO_x Emissions	Splitter Setback:				
	Into Furnace (+4")	Decreased NO_x by ~80 ppm	No Change	Increased NO_x by ~180 ppm	Increased NO_x by ~60 ppm
	Out of Furnace (-4")	No Change	Increased NO_x by ~20 ppm	N.A.	N.A.
	Nozzle Setback:				
	Into Furnace (+6")	No Change	No Change	Decreased NO_x by ~20 ppm	No Change
	Out of Furnace (-6")	Increased NO_x by ~50 ppm	No Change	Increased NO_x by ~60 ppm	Increased NO_x by ~40 ppm
	Air Distribution:				
	Biased to Inner Secondary (SR_{ISA} = 0.71, SR_{OSA} = 0.31)	Increased NO_x by ~80 ppm	Increased NO_x by ~130 ppm	Increased NO_x by ~70 ppm	Increased NO_x by ~90 ppm
	Biased to Outer Secondary (SR_{ISA} = 0.31, SR_{OSA} = 0.71)	Decreased NO_x by ~120 ppm	Decreased NO_x by ~20 ppm	No Change	Decreased NO_x by ~50 ppm
	Air Swirl Distribution:				
	Biased to Inner Secondary (high inner, low outer)	Increased NO_x by ~20 ppm	Increased NO_x by ~80 ppm	No Change	Increased NO_x by ~40 ppm
	Biased to Outer Secondary (low inner, high outer)	Increased NO_x by ~20 ppm	No Change	No Change	Decreased NO_x by ~70 ppm
	Excess Air:				
	Decreased (to 10%)	Decreased NO_x by ~100 ppm	N.A.	N.A.	N.A.
Burner Baseline NO_x Emissions @ 2000° (Dry, 0% O_2)		350 ppm	450 ppm	450 ppm	580 ppm

*N.A. = Not Attempted

Note: The changes in NO_x emissions shown for individual adjustments would not necessarily be additive if multiple adjustments were implemented in combination.

less NO_x than those which created more rapid mixing. Adjustments to burner operating variables which slowed mixing (in particular, biasing the secondary air toward the outer channel) reduced NO_x. Except for the 45° axial swirlers, the conventional nozzles in this low-velocity (enlarged throat) burner resulted in NO_x emissions about 25-50 percent below the 650-850 ppm typical of uncontrolled high-velocity pre-NSPS coal burners.

3.2.2 LV1 Tests with Dense-Phase Coal Transport

Dense-phase coal transport offers the potential for reducing NO_x emissions through two mechanisms: 1) by reducing the diameter of the central coal pipe, thus increasing the annular space available for secondary air flow and hence reducing secondary air velocity (from 80 ft/sec to 70 ft/sec in the LV1 case); and b) by significantly reducing the amount of air available in the near flame (reducing SR_p from about 0.18 to about 0.02). Both of these mechanisms reduce the rate of coal/air mixing, and increase the amount of coal devolatilized under reducing conditions. One potential commercial problem with dense-phase transport is that the reduced air flow/increased solids loading could increase the risk of plugging.

As discussed in Section 2.2.2, three types of coal nozzles were tested with the dense-phase coal pipe: a commercial spray nozzle (typically used with liquids), with and without an internal "spinner" device; a 30° cone; and an axial swirler with a 30° vane angle. Figure 3-6 summarizes the NO_x results obtained with the dense-phase nozzles at the conditions defined as baseline. The baseline conditions are similar to those with the conventional transport burners, although there are a few differences: there was even distribution of the secondary air between the inner and outer channels, as before, except now $SR_{ISA} = SR_{OSA} = 0.59$ rather than 0.51 due to the lower value of SR_p in the dense-phase case; there was an even (moderate) distribution of secondary air swirl between the two channels; total excess air was 20 percent; nozzle setback was 0.0 inches; and spreader setback was +1.0 inch (i.e., the cone or axial swirler inserts were extended one inch out of the coal pipe). The approximate shapes and dimensions of the dense-phase flames at baseline conditions are illustrated in Figure 3-7. The commercial

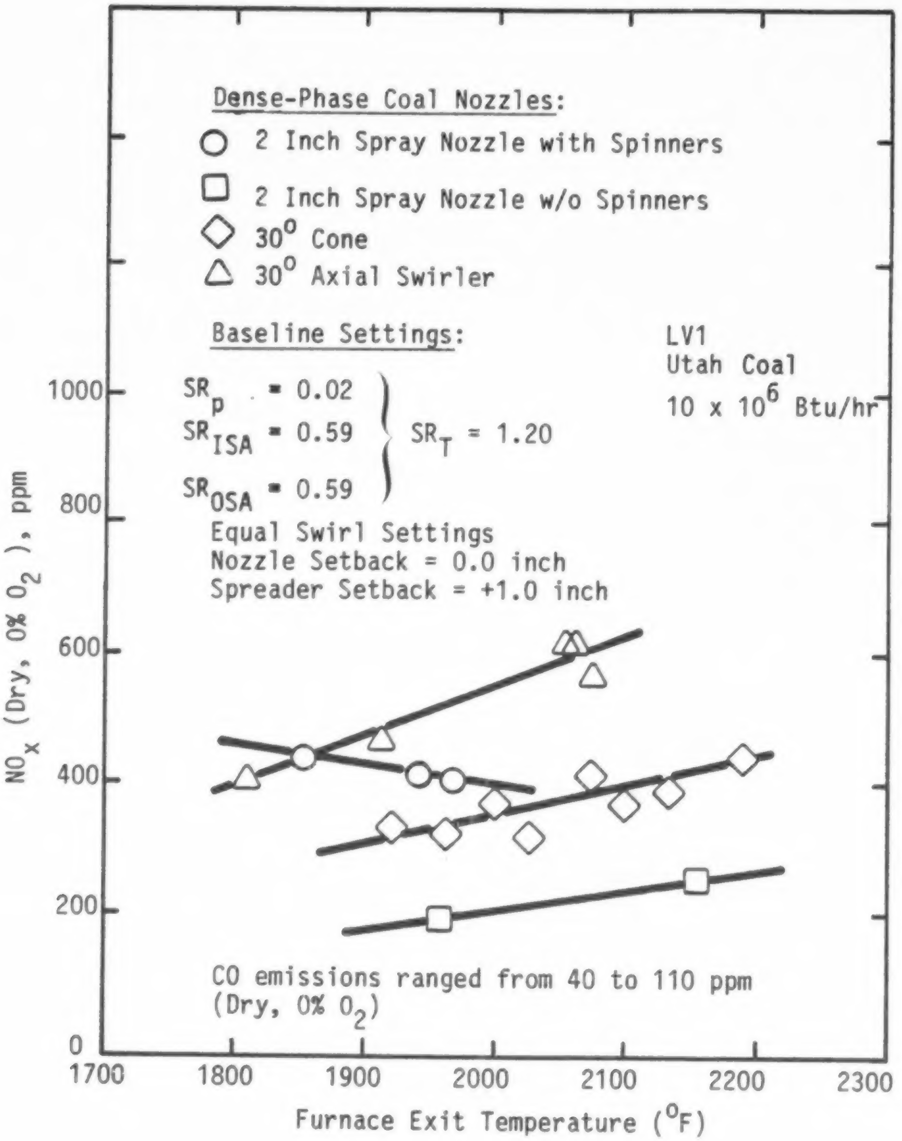

Figure 3-6. Summary of NO_x emission at baseline burner settings for LV1 with dense phase nozzles.

SWS Furnace Side View

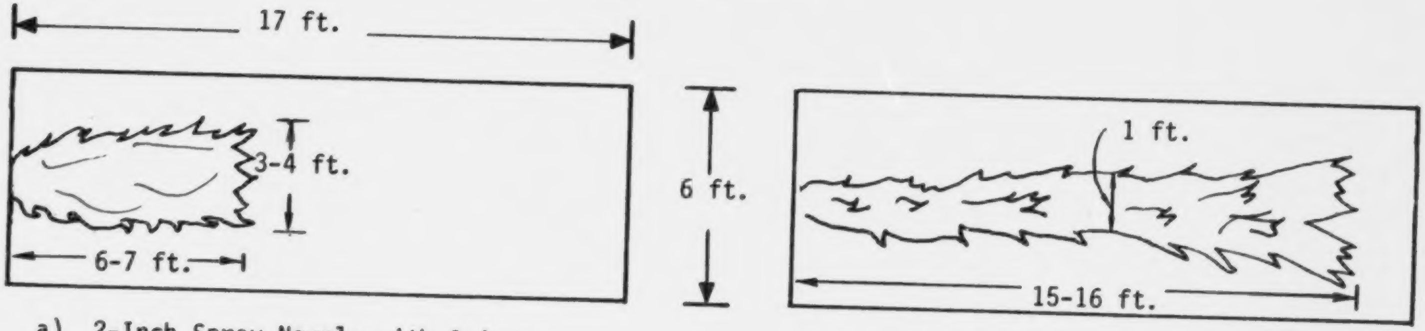

a) 2-Inch Spray Nozzle with Spinner Baseline Settings, NO_x = 400 ppm CO = 60 ppm

b) 2-Inch Spray Nozzle without Spinner Baseline Settings, NO_x = 200 ppm CO = 60 ppm

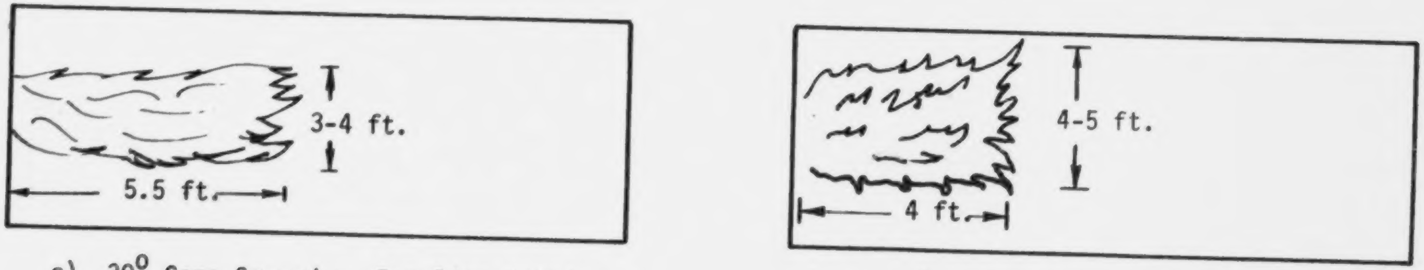

c) 30^0 Cone Spreader, Baseline Settings NO_x = 350 ppm, CO = 60 ppm

d) 30^0 axial Swirler, Baseline Settings NO_x = 550 ppm, CO = 45 ppm

Figure 3-7. Flame shapes for baseline flames with dense phase coal nozzles in LV1 burner (NO_x and CO emission values are dry and corrected to 0% O_2 at 2000^0F exit temperature).

spray nozzle with the spinner insert often did not provide uniform coal feed; with the low air-to-coal ratio, the spinner often caused in plugging and high back pressure in the coal feed lines. When uniform coal feed was sustained long enough to permit data collection, the spray nozzle/spinner resulted in NO_x emissions between 400 and 430 ppm. With the spinner removed, the commercial spray nozzle avoided back-pressure problems, but at the same time it imparted very little swirl to the exiting coal; this, together with the low SR_p, resulted in very slow coal/air mixing and thus produced very narrow flames (see Figure 3-7b). The NO_x emissions were correspondingly quite low (around 200 ppm, the lowest of any coal burner tested in this program), but the flame length would not be acceptable for practical retrofit applications since it would suggest likely impingement against the back wall of an existing furnace. Also, for the spray nozzle (either with or without the spinner), the carbon content of the fly ash was high, suggesting reduced combustion efficiency relative to the other burners; whereas the other coal burners typically resulted in less than 1 percent carbon in the ash, the dense-phase spray nozzles resulted in about 3 percent. The dense-phase nozzle with the cone spreader resulted in NO_x emissions of about 350 ppm, with flames of reasonable shape. The 30° axial swirler yielded shorter, wider flames (representing faster mixing), and NO_x emissions (about 550 ppm) were consequently the highest among the dense-phase nozzles. With the exception of the spray nozzle with the spinner, the operability of the dense-phase burners was satisfactory.

Following the definition of the baseline NO_x emissions with the dense-phase nozzles, a parametric study was conducted to determine how variation of key burner operating conditions changed emissions relative to the baseline. The results of this parametric study are presented in Table 3-5. The results are generally consistent with expectations, and with the conventional transport results. Biasing the secondary air toward the outer channel generally decreased NO_x by over 100 ppm (except in the atypical case of the spray nozzle without the spinner). Biasing the swirl of the secondary air toward the outer channel also reduced NO_x by 25 to over 100 ppm in some cases. For both the air and swirl biasing, the NO_x reductions presumably resulted from delayed coal/air mixing. Conversely, biasing the secondary air or the secondary air swirl to the inner channel generally tended to increase

TABLE 3-5. EFFECT OF BURNER ADJUSTMENTS ON NO_x EMISSIONS FOR DENSE PHASE NOZZLES WITH LV1 BURNER

		Dense Phase Coal Nozzles			
	Variables	30° Axial Swirler	30° Cone Spreader	Commercial Spray Nozzle with Spinner	Commercial Nozzle w/o Spinner
Effect of Variables on NO_x Emissions	Spreader Setback:				
	Into Furnace (+)	N.A.*	No Change	N.A.	N.A.
	Out of Furnace (-)	N.A.	N.A.	N.A.	N.A.
	Nozzle Setback:				
	Into Furnace (+2.0")	Decreased NO_x by ~140 ppm	Decreased NO_x by ~20 ppm	Decreased NO_x by ~20 ppm	No Change
	Out of Furnace (-2.0")	N.A.	Increased NO_x by ~30 ppm	Decreased NO_x by ~20 ppm	No Change
	Air Distribution:				
	Biased to Inner Secondary SR_{ISA} = .71, SR_{OSA} = .31	N.A.	No Change	Increased NO_x by ~150 ppm	Increased NO_x by ~60 ppm
	Biased to Outer Secondary SR_{ISA} = 0.31, SR_{OSA} = 0.71	Decreased NO_x by ~170 ppm	Decreased NO_x by ~100 ppm	Decreased NO_x by ~100 ppm	Increased NO_x by ~60 ppm
	Swirl:				
	Biased to Inner Secondary (high inner, low outer)	N.A.	Increased NO_x by ~130 ppm	Increased NOx by ~30 ppm	Increased NO_x by ~20 ppm
	Biased to Outer Secondary (low inner, high outer)	Decreased NO_x by ~150 ppm	No Change	N.A.	N.A.
	Excess Air:				
	Decreased (to 10%)	Decreased No_x	Decreased NO_x by ~150 ppm	N.A.	N.A.
Burner Baseline NO_x Emissions @ 2000°F (Dry, 0% O_2)		550 ppm	350 ppm	400 ppm	200 ppm

*N.A. = Not Attempted

Note: The changes in NO_x emissions shown for individual adjustments would not necessarily be additive if multiple adjustments were implemented in combination.

NO_x by increasing the mixing rate. Decreasing overall excess air from 20 percent to 10 percent reduced NO_x (e.g., to a level of 200 ppm with the cone spreader), but such low excess air levels might not be suitable for commercial application. Extending the coal pipe out through the burner throat also generally reduced NO_x.

In summary, the use of dense-phase coal transport with a cone spreader in a low-velocity (enlarged throat) LV1 burner provided stable flames with NO_x emissions of about 350 ppm. This NO_x level is at the low end of the range achieved with the conventional coal nozzles in the LV1 burner (350-710 ppm); the emission is comparable to that achieved with the T-15 splitter in the conventional transport. The 350 ppm with the dense-phase cone nozzle in the low-velocity burner represents approximately a 50 percent NO_x reduction compared to the 650-850 ppm typical of uncontrolled high-velocity pre-NSPS burners. Dense-phase transport with a 30° axial swirler produced NO_x emissions (550 ppm) in the middle of the range observed with conventional transport (about the same as the level seen with a conventional 30° axial swirler). The commercial spray nozzle did not provide suitable coal flames with dense-phase transport. As expected, burner operating adjustments which slowed coal/air mixing reduced NO_x.

3.3 High-Velocity Burner 2 (HV2)

The HV2 burner configuration was tested to represent the retrofit case where an existing burner provides no flexibility for enlarging the throat, so that secondary air velocity must remain at high pre-NSPS levels (190 ft/sec). The HV2 configuration utilized two secondary air passages, avoiding many of the operability difficulties encountered with the HV1 burner. As discussed in Section 2.2.3, the HV2 testing considered the alternative coal nozzles found to offer the greatest NO_x reduction potential during the LV1 testing (including two conventional transport nozzles and two dense-phase nozzles). Parametric adjustments to burner operating conditions were also tested. In addition, two alternative secondary air baffle configurations were investigated, to determine their effectiveness for reducing NO_x by directing the outer secondary air away from the near flame. Utah coal was burned during all tests.

3.3.1 HV2 Tests with Conventional Coal Transport

The conventional coal transport alternatives tested included the 15° axial swirler and the T-15 splitter, which produced the lowest NO_x emissions among the conventional swirlers and splitters (respectively) tested with LV1. Each of these two conventional coal nozzles were investigated without any secondary air baffle, and also with each of two alternative conical baffles positioned on the lip of the sleeve separating the inner and outer secondary air channels. One of the two baffles was designed with an L/D of 0.22, the other had an L/D of 0.13. See Section 2.2.3.

Figure 3-8 summarizes the NO_x emissions obtained with the 15° swirler in the HV2 burner at the burner conditions defined as being "baseline." The figure includes data with no secondary air baffle, and with each of the alternative baffles. For the case with no baffle, the baseline conditions--which are identified in the figure--involve a biasing of the secondary air toward the outer channel ($SR_{OSA} = 0.71$), because the range of burner settings which gave stable flames for this burner was very narrow and these baseline conditions were needed to achieve an acceptable flame. For both the cases with and without baffles, a fairly high baseline nozzle setback of -5.0 inches was used (representing retraction of the coal pipe five inches from the burner throat), to give acceptable flame stability. Results from the low-velocity LV1 burner with the same 15° axial swirler coal nozzle (and with no baffles), taken from Figure 3-2, are shown in Figure 3-8 for comparison. As evident from the figure, emissions from the HV2 burner without baffle ranged between 750 and 850 ppm (extrapolating to approximately 700 ppm at 2000°F exit); these emissions are comparable to those observed in uncontrolled high velocity pre-NSPS burners, and are much higher than the 490-500 ppm observed with the 15° swirler in the LV1 burner. This comparison suggests the extent of the benefit that throat enlargement/velocity reduction can provide, although the comparison is hindered somewhat by the differences in baseline burner conditions for the HV2/no baffle case versus the LV1 case. The

HV2, 15^{o} Axial Swirler Coal Nozzle
10 x 10^{6} Btu/hr, Utah Coal

Baseline Settings:

	w/o Baffle	w/Baffle
SR_p	0.14	0.16
SR_{ISA}	0.35	0.51
SR_{OSA}	0.71	0.53
Swirl Settings	Equal	Equal
Spreader Setback	-5.0"	-5.0"
Nozzle Setback	-1.0"	-1.0"
Baffle Setback	0.0"	0.0"

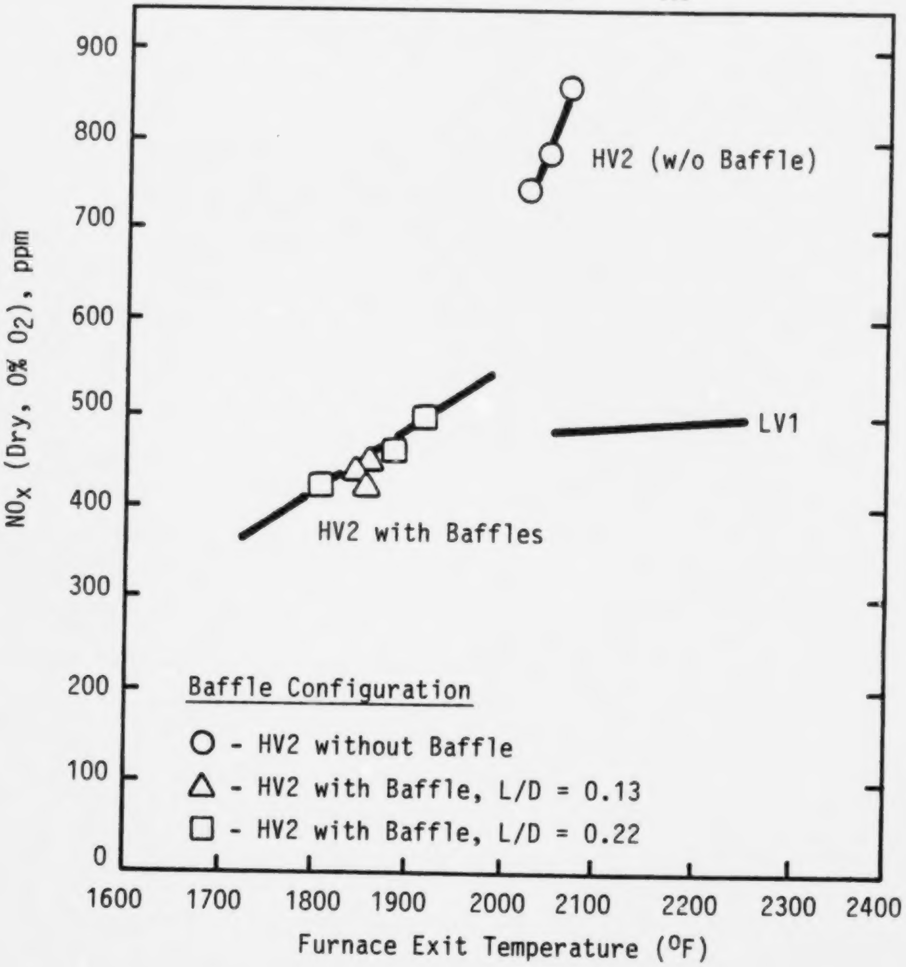

Figure 3-8. Summary of NO$_x$ emissions at baseline burner settings for HV2 with 15 degree axial swirler (with and without baffles). LV1 results with 15^{o} swirler shown for comparison.

inclusion of secondary air baffles in the HV2 burner significantly reduced emissions, down to 400 to 500 ppm, extrapolating to about 550 ppm at 2000°F exit (a level only about 60 ppm high than that observed with the LV1 burner at 2000°F exit). Both baffles resulted in similar NO_x emissions, probably because the aerodynamic effect of these two baffles on the flow was similar. It would thus appear that baffles might be a viable approach for achieving NO_x reductions (about 40 percent reduction in this instance) in burners where velocity reductions are not possible. Emissions of CO in all baseline cases were in the range of 60 to 70 ppm, representing reasonable combustion performance.

The approximate flame shapes and dimensions for the HV2/15° swirler flames at baseline conditions are illustrated in Figure 3-9; again, the LV1/15° swirler case is also shown for comparison. The HV2 case with no baffles gives a flame at least 2 feet shorter than its LV1 counterpart, reflecting the more rapid mixing which yields the higher NO_x at the higher velocity. The longer HV2 baffle (L/D = 0.22, Figure 3-9c) produced a distinctly shorter, wider flame compared to LV1, which would normally be associated with higher NO_x; in this case, NO_x emissions were 60 ppm higher (at 2000°F exit) with the HV2 flame. The shorter HV2 baffle (L/D = 0.13) gave a flame similar in dimensions to the LV1 flame, but with a standoff of up to 4 inches off the quarl; standoffs are often associated with increased NO_x, due to air being sucked into the base of the flame, and here again, NO_x emissions were about 60 ppm higher with HV2 at 2000°F exit.

Following the definition of the HV2 baseline NO_x emissions with the 15° swirler, a parametric study was conducted adjusting the various key burner operating parameters. The results are summarized in Table 3-6, with and without the secondary air baffles. The HV2 burner had a more limited operating range compared to the LV1, and some of the HV2 adjustment accordingly resulted in unstable flames. Biasing of the secondary air to the outer channel resulted in improved flame stability and reduced NO_x in all cases (in the case of no baffle, outer channel biasing was in fact necessary to assure a stable flame). Decreasing overall excess air also consistently resulted in reduced NO_x, as would be expected, although low-excess-air (5

SWS Furnace Side View

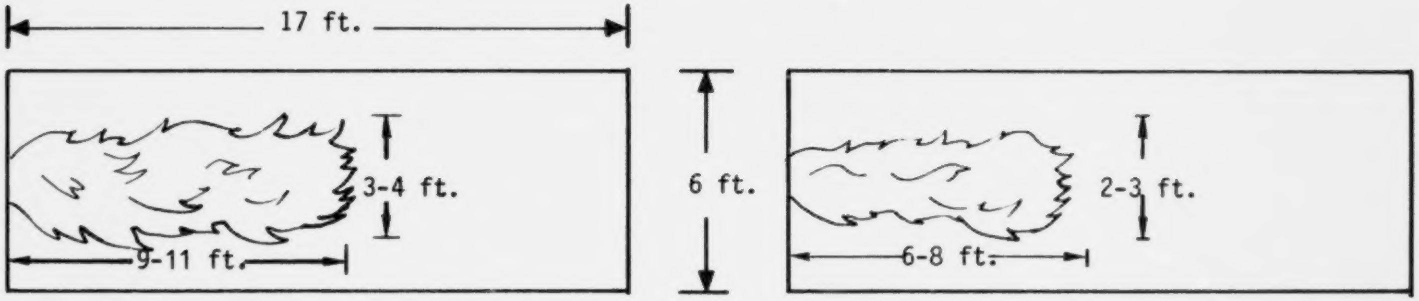

a) LV1 Burner, Baseline Settings
NO_x = 490 ppm, CO = 60 ppm

b) HV2 Burner, Baseline Settings
NO_x = 700 ppm, CO - 62 ppm

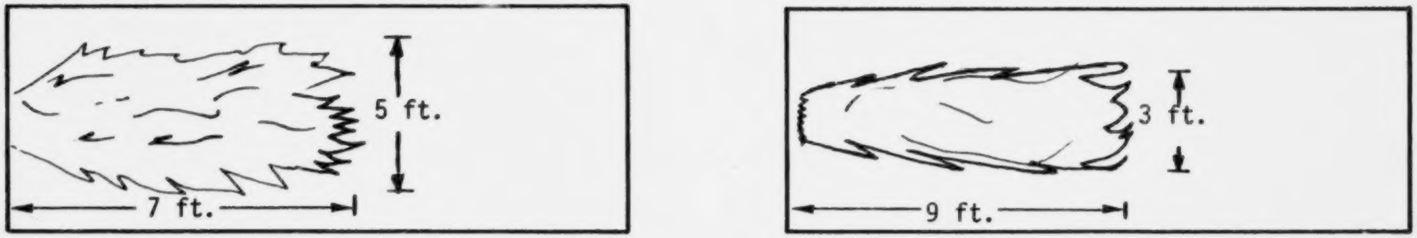

c) HV2 Burner, with Baffle L/D = 0.22
NO_x = 550 ppm, CO = 60 ppm

d) HV2 Burner, with Baffle L/D = 0.13
NO_x = 550 ppm, CO = 66 ppm
(0-4" standoff)

Figure 3-9. Comparison of baseline flame shapes for LV1 and HV2 burners with 15^o axial swirler (NO_x and CO emissions values are dry and corrected to 0% O_2, at 2000^oF furnace exit temperature).

TABLE 3-6. EFFECT OF BURNER ADJUSTMENTS ON NO_x EMISSIONS FOR 15° AXIAL SWIRLER WITH HV2 BURNER

		15° Axial Swirler Coal Nozzle		
	Variables	Without Baffle	Baffle L/D = 0.22	Baffle L/D = 0.13
Effect of Variables on NO_x Emissions	Swirler:			
	Into Furnace	N.A.	Increased by ~50 ppm	No Change
	Out of Furnace	N.A.	Decreased by ~150 ppm	Decreased by ~50 ppm
	Nozzle Setback:			
	Into Furnace	Increased by ~50 ppm	N.A.	Decreased by ~20 ppm
	Out of Furnace	Increased by ~120 ppm	N.A.	Increased by ~30 ppm
	Air Distribution:			
	Biased to Inner Secondary	Unstable Flame	Unstable Flame	Unstable Flame
	Biased to Outer Secondary	*	Decreased by ~20 ppm	Decreased by ~30 ppm
	Swirl:			
	Decreased Inner Secondary	No Significant Change	Unstable Flame	Increased by ~50 ppm
	Decreased Outer Secondary	No Significant Change	Unstable Flame	No Significant Change
	Excess Air:			
	Decreased (to $SR_T = 1.05$)	Decreased by ~150 ppm	Decreased by ~130 ppm	Decreased by ~250 ppm
	Baffle Position:			
	In	N.A.	Decreased by ~50 ppm	Unstable Flame
	Out	N.A.	N.A.	N.A.
Baseline NO_x Emissions		700 ppm	550 ppm	550 ppm

*Baseline already involves bias to outer secondary

Note: The changes in NO_x emissions shown for individual adjustments would not necessarily be additive if multiple adjustments were implemented in combination.

percent excess) might not always be a viable commercial operating approach. Biasing secondary air toward the inner channel always yielded unstable flames, reflecting some of the same difficulties encountered with the HV1 burner (which also required significant air in the outer channel for flame stability). Other burner adjustments yielded mixed effects for the three baffle configurations.

The second type of conventional coal nozzle tested with the HV2 burner configuration was the T-15 splitter. Figure 3-10 summarizes the baseline NO_x emissions for this coal nozzle, with and without secondary air baffles. The LV1 results with the T-15 splitter (and with no baffles), taken from Figure 3-4, are shown for comparison. Baseline conditions are defined on Figure 3-10. Without baffles, this burner produced between 600 and 700 ppm NO_x (extrapolating to about 750 ppm at 2000° SWS exit temperature). This NO_x level is similar to that with the 15° swirler in the HV2 configuration, and is about 400 ppm higher than the levels observed in the LV1 burner with the T-15 splitter; this level is also within the range observed from uncontrolled pre-NSPS burners. In testing with the longer baffle (L/D = 0.22), NO_x levels were reduced to about 600 ppm. This level represents a reduction of about 150 ppm compared to the case with no baffle, and thus confirms the possible air staging benefits achievable with baffles. A similar degree of reduction (from about 700 to about 550 ppm at 2000°F exit) had been observed with the axial swirler in Figure 3-8. In testing with the short baffle (L/D = 0.13), the one data point in Figure 3-10 suggests substantial additional NO_x reduction achievable with this baffle to a concentration of 436 ppm, representing a reduction of about 300 ppm, or about 40 percent, compared to the case with no baffle). With this more steeply-angled baffle, the emissions from the HV2 burner appear to have been reduced to a level less than 100 ppm higher than the 350 ppm achieved with the low-velocity LV1 burner with the T-15 splitter; the T-15 splitter had produced the lowest NO_x emissions of any of the LV1 coal nozzles, including the dense-phase nozzles. The limited data with the steep baffle prevent confirmation of these promising results, so that replication of these tests would be desirable. It would appear that secondary air baffles warrant further consideration for NO_x reduction in high velocity burners.

HV2, T-15 Splitter Coal Nozzle
10 x 10^6 Btu/hr, Utah Coal

Baseline Settings:

	w/o Baffle	w/Baffle
SR_p	0.14	0.14
SR_{ISA}	0.53	0.53
SR_{OSA}	0.53	0.53
Swirl Settings	Equal	Equal
Spreader Setback	+1.0"	+1.0"
Nozzle Setback	0.0"	-2.0"
Baffle Setback	-	+1.0"

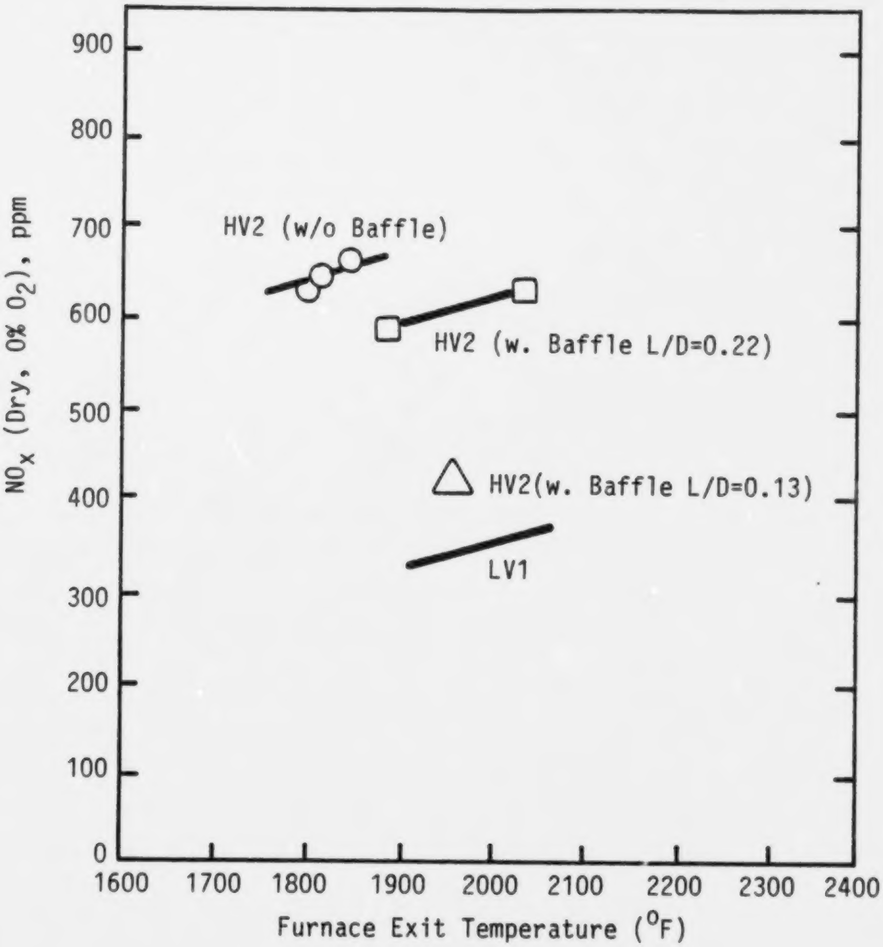

Figure 3-10. Summary of NO_x emissions at baseline burner settings for HV2 with T-15° splitter (with and without baffles). LV1 results for T-15° splitter shown for comparison.

In all baseline tests with the T-15 splitter, CO emissions were between 50 and 75 ppm, reflecting reasonable combustion performance.

The approximate shapes and dimensions for the HV2/T-15 splitter flames at baseline conditions are shown in Figure 3-11, with the LV1/T-15 splitter flame also illustrated for comparison. Compared to the LV1 flame, the HV2 flame with no secondary air baffle was distinctly shorter (but about the same width), reflecting the more intense combustion which produces the elevated NO_x emissions. The HV2 flame with the baffle having L/D = 0.22 produced a flame of about the same length as the no-baffle case, but wider (and with a 1- to 2-inch standoff); the reduced NO_x with this baffle, relative to no baffle, suggests that, at a given flame length and thermal output, an increase in flame width (i.e., an increase in flame volume) can indicate a reduced combustion intensity and reduced NO_x. The flame with the 0.13 baffle was longer than the flame with the 0.22 baffle, and was about the same width (again with a standoff), indicating a further increase in flame volume which could be a partial explanation for the significantly reduced NO_x with this baffle design.

Following the definition of the HV2 baseline NO_x emissions with the T-15 splitter, a parametric study was conducted varying burner operating parameters. The results are summarized in Table 3-7, with and without baffles. As indicated, few of the burner adjustments that were tested resulted in decreases in NO_x; a number of the adjustments produced increased emissions, or resulted in an unstable flame.

In summary, with conventional coal transport in the HV2 burner configuration, NO_x emission levels without secondary air baffles were high, comparable to uncontrolled pre-NSPS burners, for each of the two coal nozzles tested. In all cases, NO_x was reduced (by between 15 and 40 percent) through the use of either of the two secondary air baffles that were considered; in one case (the T-15 splitter coal nozzle with the more steeply-angled baffle), NO_x levels with the HV2 burner were reduced to only about 100 ppm above the lowest of the NO_x emissions obtained under the best conditions with the low-velocity LV1 burner. Thus, secondary air baffles might be a potential

SWS furnace side view

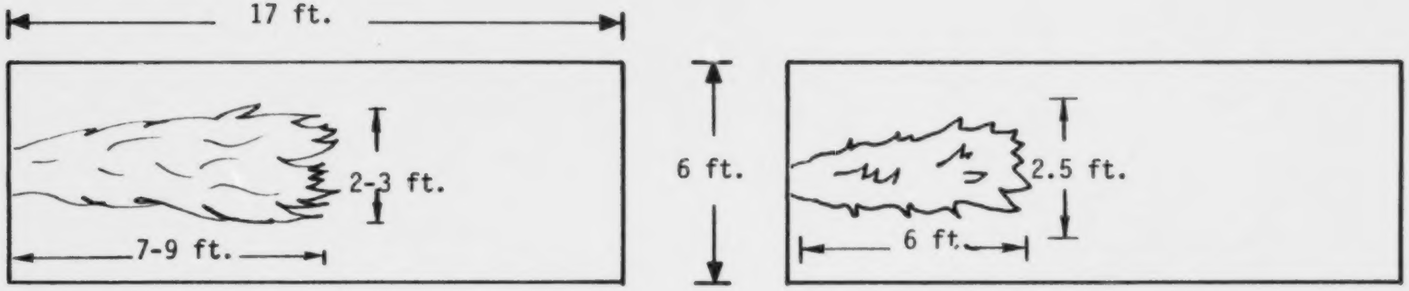

a) LV1 Burner, Baseline Settings
NO_x = 350 ppm, CO = 75 ppm

b) HV2 Burner, Baseline Settings
NO_x = 700 ppm, CO = 58 ppm

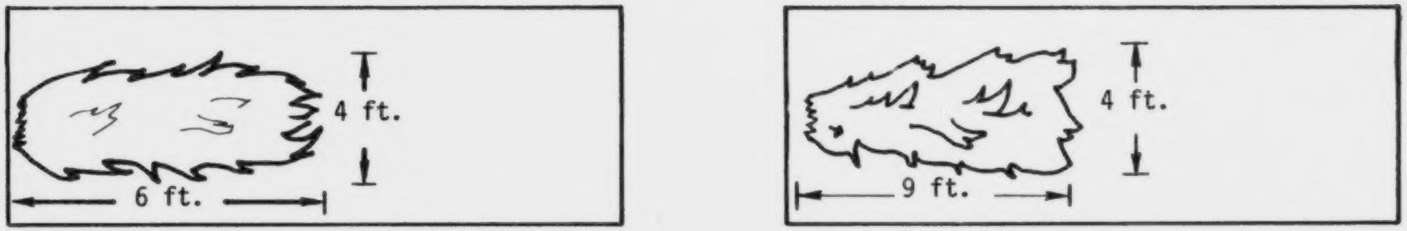

c) HV2 Burner, with baffle L/D = 0.22
NO_x = 630 ppm, CO = 57 ppm
(1" - 2" standoff)

d) HV2 Burner, with Baffle L/D = 0.13
NO_x = 440 ppm, CO = 55 ppm
(0 - 1" standoff)

Figure 3-11. Comparison of baseline flame shapes for LV1 and HV2 flames with T-15^{o} splitter (NO_X and CO emissions values are dry and corrected to 0% O_2 at 2000^{o}F furnace exit temperature).

TABLE 3-7. EFFECT OF BURNER ADJUSTMENTS ON NO_x EMISSIONS FOR T-15^o SPLITTER WITH HV2 BURNER

		T-15^o Divergent Splitter Coal Nozzle		
	Variables	Without Baffles	Baffle L/D = 0.22	Baffle L/D = 0.13
Effect of Variables on NO_x Emissions	Spreader Setback:			
	Into Furnace	Decreased by ~20 ppm	Unstable Flame	Unstable Flame
	Out of Furnace	Decreased by ~30 ppm	Unstable Flame	Unstable Flame
	Nozzle Setback:			
	Into Furnace	N.A.	Unstable Flame	Increased
	Out of Furnace	Decreased by ~15 ppm	Unstable Flame	Unstable Flame
	Air Distribution:			
	Biased Air to Inner Secondary	Increased by ~60 ppm	Increased by ~80 ppm	Unstable Flame
	Biased Air to Outer Secondary	Increased by ~30 ppm	Increased by ~50 ppm	No Significant Change
	Swirl:			
	Decreased Inner Secondary	Unstable Flame	Unstable Flame	Unstable Flame
	Decreased Outer Secondary	No Significant Change	Unstable Flame	Unstable Flame
	Excess Air:			
	Decreased	N.A.	N.A.	N.A.
	Baffle Position:			
	In		N.A.	Unstable Flame
	Out		No Significant Change	Unstable Flame
Baseline NO_x Emissions		700 ppm	630 ppm	440 ppm

*N.A. - Not Attempted

Note: The changes in NO_x emissions shown for individual adjustments would not necessarily be additive if multiple adjustments were implemented in combination.

internal staging approach in retrofit cases where throat enlargement/velocity reduction are not possible. The high-velocity HV2 burner design tested here had a more limited stable operating range, compared to the LV1 burner. This limited range might have been due to the relatively limited degree of coal swirl imparted by the coal nozzles tested, or to the particular construction of this experimental burner. In general, use of secondary air baffles improved flame stability.

3.3.2 HV2 Tests with Dense-Phase Coal Transport

Two types of coal nozzles were tested on the HV2 burner in conjunction with dense-phase coal transport: A 30° axial swirler, and a 30° cone spreader. These were the two nozzles which provided the best results during dense-phase testing with the LV1 configuration. Each of the dense-phase nozzles was tested without any secondary air baffle, and also with each of the two baffle designs addressed previously (having L/D values of 0.22 and 0.13). The reduction in central coal pipe diameter, made possible by dense-phase coal transport, reduce the secondary air velocity of the HV2 burner from 190 ft/sec to 145 ft/sec.

Baseline results from the dense-phase nozzle with the 30° axial swirler insert are presented in Figure 3-12, with and without baffles. In all cases,the data points in the figure represent the results with the HV2 burner, while the heavy solid line represents the results shown previously for the dense-phase 30° swirler nozzle in the LV1 burner. The baseline conditions, indicated on the figure, are generally the same for each of the three cases shown. As discussed previously, the low SR_p of 0.02 is the characteristic of dense-phase transport. As evident from the figure, NO_x levels with the dense-phase swirler without the baffle were about 800 ppm, roughly 400 ppm higher than observed with the same coal nozzle in the low-velocity LV1 burner (without a baffle); this difference underscores the role of velocity reduction in reducing NO_x. Surprisingly, the 800 ppm is also comparable to (perhaps even slightly higher than) the levels observed with conventional coal transport in the HV2 configuration (see Figures 3-8 and 3-10); thus, in the high-velocity case, switching to dense-phase transport

HV2, Dense-Phase 30^{o} Axial Swirler
10 x 10^{6} Btu, Utah Coal

Baseline Settings:

	w/o Baffle	Baffle L/D = 0.22	Baffle L/D = 0.13
SR_p	0.02	0.02	0.02
SR_{ISA}	0.59	0.59	0.59
SR_{OSA}	0.59	0.59	0.59
Swirl Settings	Equal	Equal	Equal
Nozzle Setback	0.0"	0.0"	0.0"
Swirler Setback	-4.0"	-4.0"	-2.0"
Baffle Setback	N/A	+1.0"	0.0"

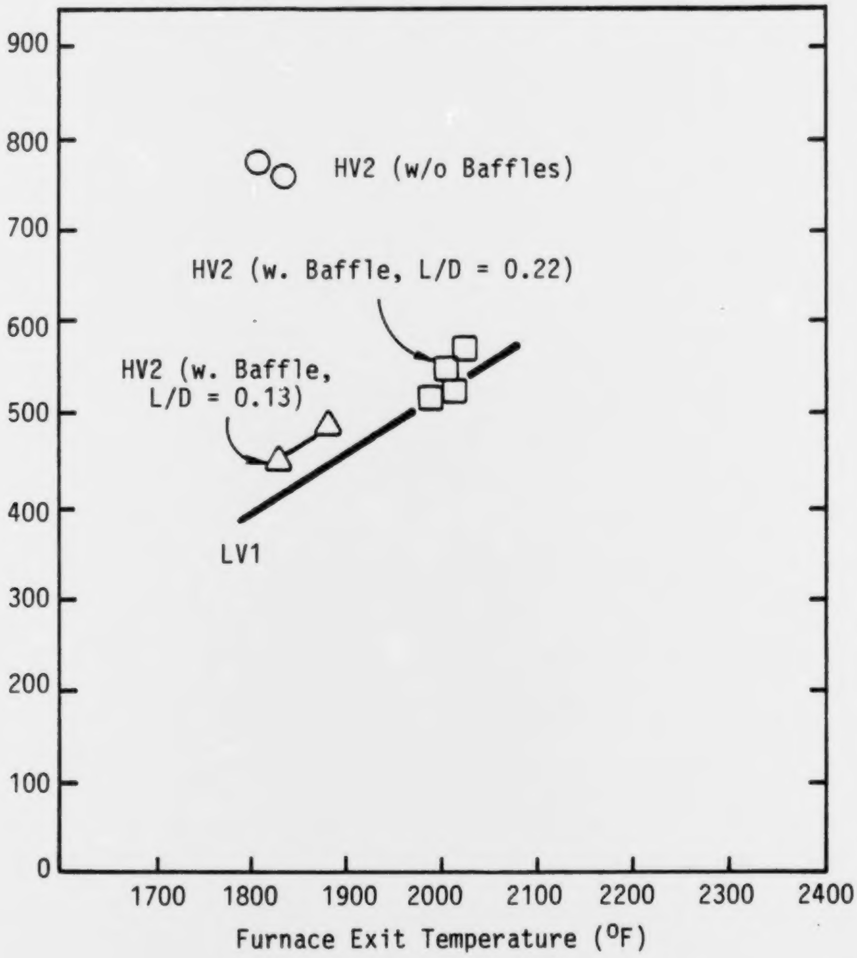

Figure 3-12. Summary of NO_x emissions at baseline burner settings for HV2 with swirler (with and without baffle). LV1 results with dense-phase swirler shown for comparison.

does not by itself appear to offer any NO_x advantage. (In the LV1 configuration, dense-phase operation had yielded NO_x levels at the low end of the range observed for conventional transport.) Both of the secondary air baffles substantially reduced NO_x by about 40 percent, to roughly 525 ppm at 2000°F furnace exit. This level is comparable to that achieved with the LV1 burner with this dense-phase coal nozzle. Both of the conventional transport nozzles with the HV2 burner had also shown substantial NO_x reductions with baffles, but in neither of the conventional cases had the baffles given the full degree of NO_x reduction that had been achieved by reducing air velocity to LV1 levels. The 525 ppm seen with this dense-phase nozzle with baffles is comparable to the levels seen with the conventional swirler with baffles in the HV2 burner, confirming the earlier indication that dense-phase operation does not yield significant additional NO_x reductions in the high-velocity case. Emissions of CO were between 45 and 60 ppm during these baseline tests, indicating acceptable combustion efficiency.

The approximate flame dimensions and shapes for the dense-phase/30° swirler nozzle in the HV2 burner are illustrated in Figure 3-13, along with the flame from the LV1 configuration with the same coal nozzle. As would be expected, the two arrangements with baffles produced longer flames than the no-baffle case, reflecting slower mixing. But surprisingly, the shortest flame--which would intuitively be expected to be associated with higher NO_x--was produced by the LV1 burner, which had low NO_x.

Following the baseline definition with the dense-phase swirler, a parametric study was conducted, as summarized in Table 3-8. Only decreased excess air consistently provided further NO_x reductions. Other burner adjustments gave mixed results, or no significant change. A number of adjustments resulted in unstable flames.

The second dense-phase coal nozzle tested with the HV2 burner utilized the 30° cone spreader. The baseline results for this nozzle are presented in Figure 3-14, with and without secondary air baffles, with the LV1 curve for this same nozzle also shown for comparison. All flames obtained with the HV2/dense cone configuration were basically unstable; attempts were made to

SWS Furnace Side View

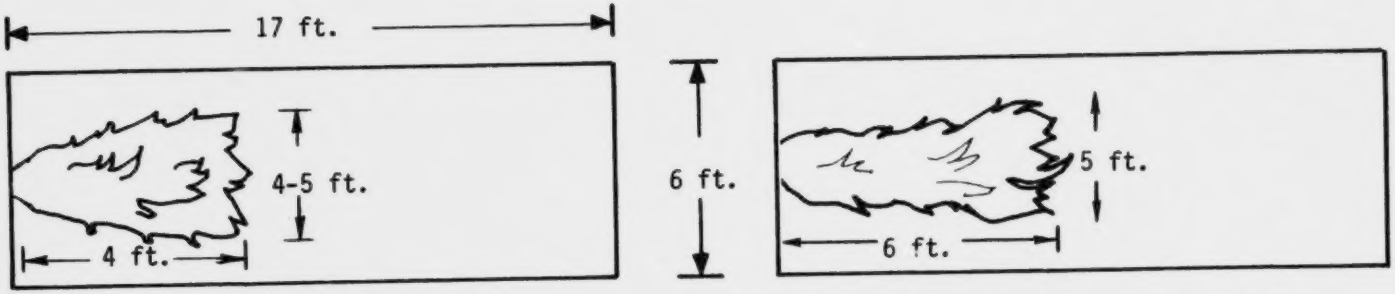

a) LV1 Burner, Baseline Settings
NO_x = 550 ppm, CO = 45 ppm

b) HV1 Burner, Baseline Settings
NO_x = 800 ppm, CO = 57 ppm

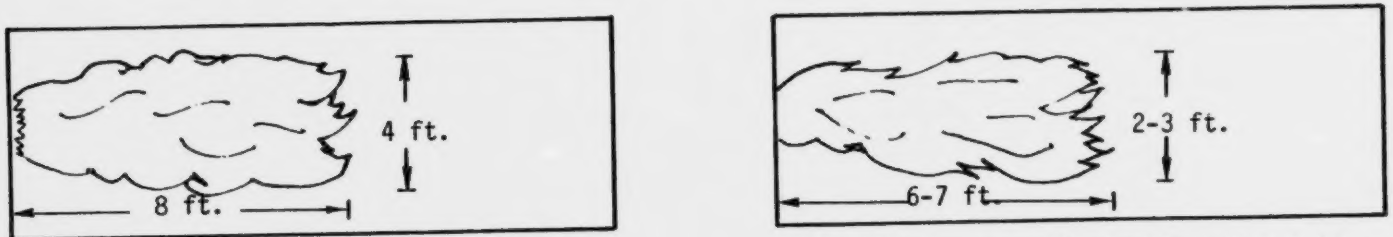

c) HV2 Burner, with baffle L/D = 0.22
NO_x = 520 ppm, CO = 60 ppm
(Assymmetric flame, 0-1" standoff)

d) HV2 Burner, with baffle L/D = 0.13
NO_x = 550 ppm, CO - 60 ppm
(Assymmetric flame)

Figure 3-13. Comparison of baseline flame shapes for LV1 and HV2 burners with 30° axial swirler in dense phase and nozzle.

TABLE 3-8. EFFECT OF BURNER ADJUSTMENTS ON NO_x EMISSIONS FOR 30^o AXIAL SWIRLER IN DENSE PHASE COAL NOZZLE WITH HV2 BURNER

		30^o Axial Swirler Dense Phase Coal Nozzle		
	Variables	Without Baffle	Baffle L/D = 0.22	Baffle L/D = 0.13
Effect of Variables on NO_x Emissions	Spreader Setback:			
	Into Furnace	Unstable Flame	N.A.	N.A.
	Out of Furnace	N.A.	N.A.	N.A.
	Nozzle Setback:			
	Into Furnace	Unstable Flame	Decreased by ~20 ppm	Decreased by ~20 ppm
	Out of Furnace	Decreased by ~280 ppm	Increased by ~250 ppm	Increased by ~20 ppm
	Air Distribution:			
	Biased Air to Outer Secondary	Increased by ~20 ppm	Increased by ~20 ppm	No Significant Change
	Biased Air to Inner Secondary	Unstable Flame	N.A.	N.A.
	Swirl:			
	Decreased Inner Secondary	Unstable Flame	Increased by ~550 ppm	Increased by ~480 ppm
	Decreased Outer Secondary	N.A.	Increased by ~40 ppm	Increased by ~90 ppm
	Excess Air:			
	Decreased to SR_T = 1.05	Decreased by ~200 ppm	Decreased by ~200 ppm	Decreased by~200 ppm
	Baffle Position:			
	In (+)	--	N.A.	Unstable Flame
	Out (-)	--	N.A.	N.A.
Baseline NO_x Emissions		850 ppm	520 ppm	550 ppm

HV2, Dense-Phase 30° Cone

10×10^6 Btu/hr, Utah Coal

Baseline Settings:

	w/o Baffle	Baffle L/D = 0.22	Baffle L/D = 0.13
SR_p	0.02	0.02	0.02
SR_{ISA}	0.59	0.59	0.59
SR_{OSA}	0.59	0.59	0.59
Spreader Setback	+0.75	+0.75"	-0.75"
Nozzle Setback	-2.0"	-2.0"	-6.0"
Baffle Setback	-	+1.0"	+1.0"

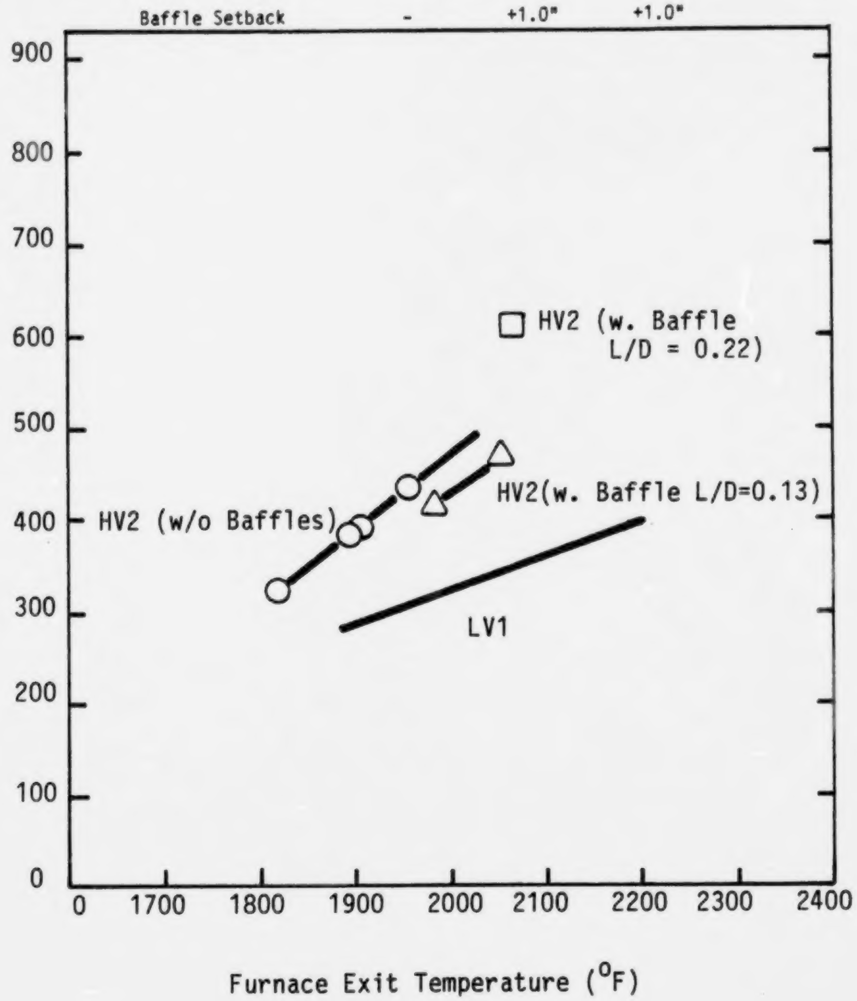

Figure 3-14. Summary of NO_x emissions at baseline burner settings for HV2 with dense phase 30° cone spreader (with and without baffle). LV1 results with dense-phase cone shown for comparison.

stabilize the flames through suitable selection of burner operating conditions, but no reliably stable flame was achieved under any of the conditions. The results shown in Figure 3-14 represent emissions during periods when the flame operated with adequate stability for a sufficient duration to produce reasonably consistent data. Interestingly, the NO_x emissions from this nozzle without baffles--about 300-450 ppm, extrapolating to about 470 ppm at 2000°F exit--were the lowest from any of the HV2 nozzles without baffles, the only HV2/no baffle configuration to yield NO_x levels below the range of typical high-velocity pre-NSPS coal burners. At 2000°F exit, the HV2/dense cone without baffles produced NO_x only about 150 ppm higher than the low-velocity LV1 burner with the same nozzle (which had yielded the lowest NO_x of all the practical LV1 nozzles). With the secondary air baffle having L/D = 0.13, NO_x from the HV2/dense cone was apparently reduced slightly, by about 50 ppm. The NO_x concentration with the 0.13 baffle--420 ppm--represents the lowest NO_x level achieved with any of the HV2 test configurations. With the baffle having L/D = 0.22, one data point suggests NO_x was increased to over 600 ppm, the only instance in any of the HV2 testing where baffles appeared to increase NO_x; presumably this atypical result was a consequence of the inherent instability of this particular burner/nozzle configuration. Actually, this apparent NO_x increase with the 0.22 baffle results because the emissions with no baffle were unusually low; the actual emission levels with the 0.22 baffle (607 ppm) were within the range (525-625 ppm) observed with the 0.22 baffle with the other coal nozzles tested in the HV2 burner.

The approximate baseline flame shapes and dimensions for the HV2/dense cone configuration are illustrated in Figure 3-15. Due to instabilities, these shapes often fluctuated. Without baffles, the HV2/dense cone produced a flame, on the average, that was somewhat longer, and often wider, than the other HV2/no baffle flames; this could be one explanation for the reduced NO_x levels in this case. With each of the two baffles, the flames were notably longer than the no-baffle case, and. with the 0.13 baffle, considerably wider as well; such longer flames would normally be expected to be associated with reduced NO_x, and the lack of any significant NO_x reductions with baffles is probably due to the unstable nature of these flames.

SWS Furnace Side View

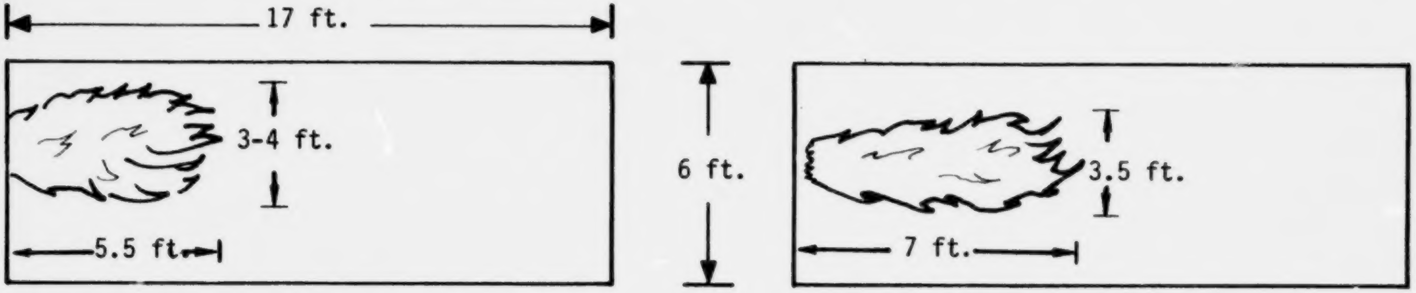

a) LV1 Burner, Baseline Settings
NO_x = 350 ppm, CO = 60 ppm

b) HV2 Burner, Baseline Settings
NO_x = 470 ppm, CO = 57 ppm
(unstable)

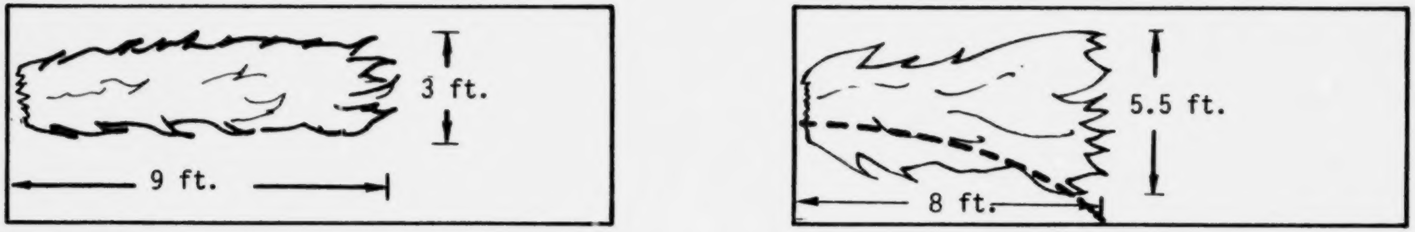

c) HV2 Burner, with baffle L/D_o = 0.22
NO_x = 560 ppm (Texit = 2050°F),
CO = 55 ppm (unstable, slightly
assymmetric flame)

d) HV2 Burner, with baffle L/D - 0.13
NO_x = 420 ppm, CO = 59 ppm
(unstable, flame fluctuates to
the dotted line shown)

Figure 3-15. Comparison of baseline flame shapes for LV1 and HV2 burner with 30° cone spreader in dense phase coal nozzle (NO_x and CO emissions values are dry and corrected to 0% O_2 at 2000°F furnace exit temperature).

The results of the parametric study--as the HV2/dense cone operating conditions were varied from the baseline conditions--are summarized in Table 3-9. Since the flames even at the baseline conditions were not consistently stable, variations from the baseline in most cases resulted in unstable flames.

In summary, with the HV2 burner configuration, dense-phase coal transport did not appear to offer any significant reductions in NO_x emissions relative to conventional support. Dense-phase operation reduced flame stability, especially in the case of the cone spreader coal nozzle, although perhaps that difficulty might be reduced with hardware design different from that tested here. As in the case of conventional transport in the HV2 burner, secondary air baffles were generally necessary (at least in the dense-phase/axial swirler case) to provide NO_x levels significantly below those of high-velocity pre-NSPS coal burners.

3.4 Summary of NO_x Results from Internally-Staged Burners

Figure 3-16 summarizes the baseline NO_x levels observed with the three lowest-NO_x coal nozzles providing acceptable flame characteristics on both the low-velocity LV1 and the high-velocity HV2 burner configurations (without secondary air baffles). With the LV1 burner, NO_x emissions ranged between 300 and 500 ppm, reflecting the air and fuel staging benefits resulting from the low secondary air velocity, the dual secondary air registers and the coal nozzle designs. On the other hand, with the HV2 burner, emissions were between 650 and 850 ppm, levels representative of uncontrolled high-velocity pre-NSPS coal burners. Since the HV2 burner utilized divided secondary air registers and coal nozzle designs similar to the LV1 case, it is apparent that the roughly 50 percent NO_x reduction achieved with LV1 (relative to the uncontrolled pre-NSPS burner) was primarily the result of the velocity reduction. Such velocity reductions in retrofit applications will depend upon the flexibility for enlargement of the throat of the original burner, and will probably not be readily feasible in many cases.

TABLE 3-9. EFFECT OF BURNER ADJUSTMENTS ON NO_x EMISSIONS FOR 30° CONE SPREADER IN DENSE PHASE COAL NOZZLE WITH HV2 BURNER

		30° Cone Spreader Dense Phase Coal Nozzle		
	Variables	Without Baffles	Baffle L/D = 0.22	Baffle L/D = 0.13
Effect of Variables on NO_x Emissions	Spreader Setback:			
	Into Furnace	Unstable Flame	Unstable Flame	Unstable Flame
	Out of Furnace	N.A.	N.A.	N.A.
	Nozzle Setback:			
	Into Furnace	No Significant Change	No Significant Change	Unstable Flame
	Out of Furnace	No Significant Change	Increased by ~30 ppm	N.A.
	Air Distribution:			
	Biased Air to Inner Secondary	Unstable Flame	Unstable Flame	Unstable Flame
	Biased Air to Outer Secondary	Increased by ~40 ppm	Decreased by ~100 ppm	Decreased by ~50 ppm
	Swirl:			
	Decreased Inner	Unstable Flame	Unstable Flame	Unstable Flame
	Decreased Outer	Unstable Flame	N.A.	Unstable Flame
Baseline NO_x Emissions		470 ppm	610 ppm	420 ppm

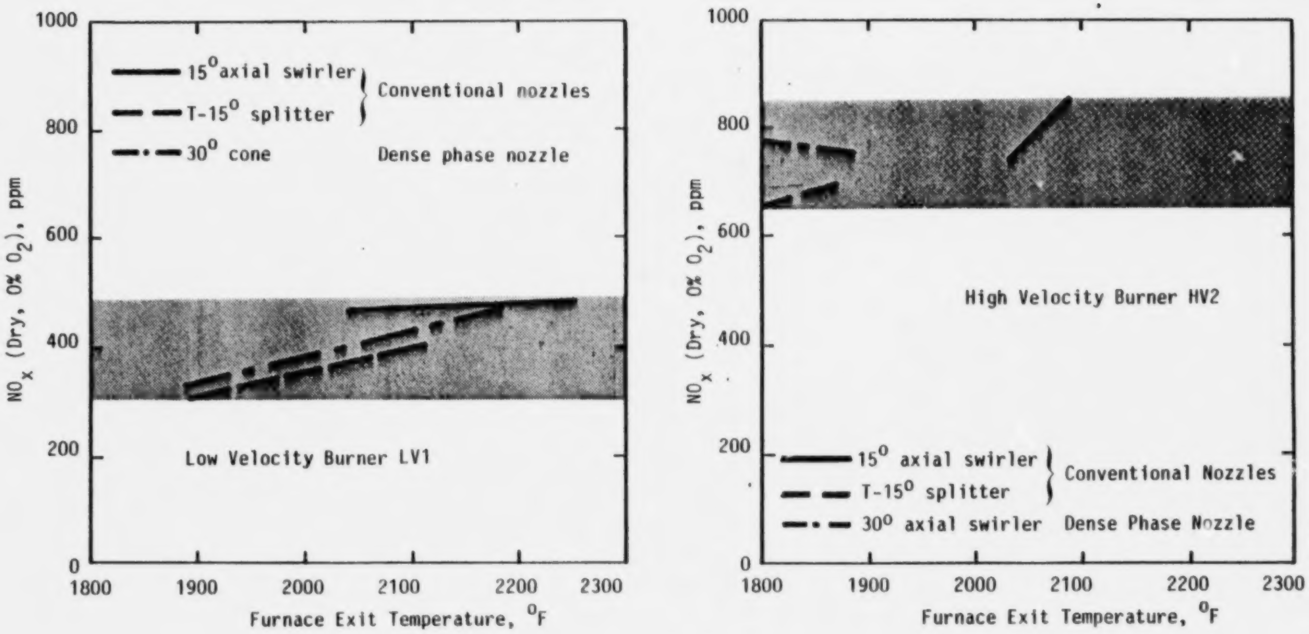

Figure 3-16. Summary of baseline NO_x emissions for low-NO_x coal nozzles tested with low velocity and high velocity burners (without secondary air baffles).

Figure 3-17 summarizes the NO_x levels obtained with the high-velocity HV2 burner through the use of baffles to divert outward the secondary air in the outer channel. Two bands are presented in the figure: a band representing the data without baffles, taken from the right-hand graph in Figure 3-16; and a band showing the data with the same coal nozzles but with the secondary air baffles. As indicated, baffles reduced the NO_x emissions from 650-850 ppm to 400-550 ppm, representing a reduction of up to 40 percent in individual cases. The baffles also improved flame stability. Thus, in retrofit cases where throat enlargement is not possible, a comparable NO_x reduction might be achieved using baffles.

The formation of NO_x in practical flames is determined to a large extent by mixing processes in the flame (i.e., the rate of fuel/air mixing) and the bulk thermal environment in the furnace (i.e., the thermal input to the flame and the heat extraction characteristics of the furnace). A preliminary attempt was made to correlate the NO_x results presented in Sections 3.2 and 3.3, by means of alternative mathematical expressions addressing mixing and thermal characteristics.

One simplified method for quantifying the mixing rate is to consider the dimensions of the flame. In this case, the ratio of the flame length L to the flame width D was utilized. A large L/D ratio--that is, a long and narrow flame--would presumably suggest slow fuel/air mixing, whereas a small ratio (a short, wide flame) would suggest rapid mixing, at a constant thermal input and thermal environment. The results of this analysis are presented in Figure 3-18, where NO_x is plotted against flame L/D for all of the LV1 data which were obtained with furnace exit temperatures near 2000°F, representing a relatively comparable furnace environment. Also shown in the figure are several points for stable flames from the HV2 burner with 2000°F exit. In each case the NO_x data has been corrected to an exit temperature of 2000°F. As apparent from the figure there does appear to be a clear trend toward reduced NO_x levels at increased values of L/D with the LV1 burner data, as would be anticipated. Emissions tend to rise sharply as L/D is reduced below about 2. The correlation with the LV1 data appears to be dependent upon the coal nozzle, with the data from the conventional transport/axial swirler case

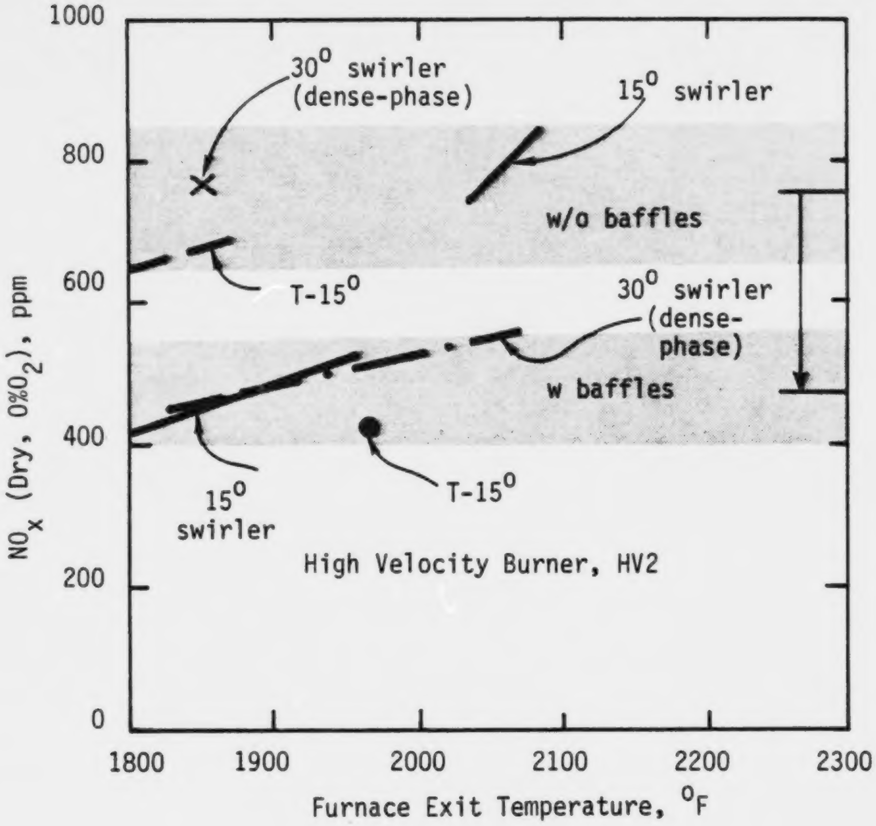

Figure 3-17. NO_x reductions achieved by secondary air baffles with HV2 burner.

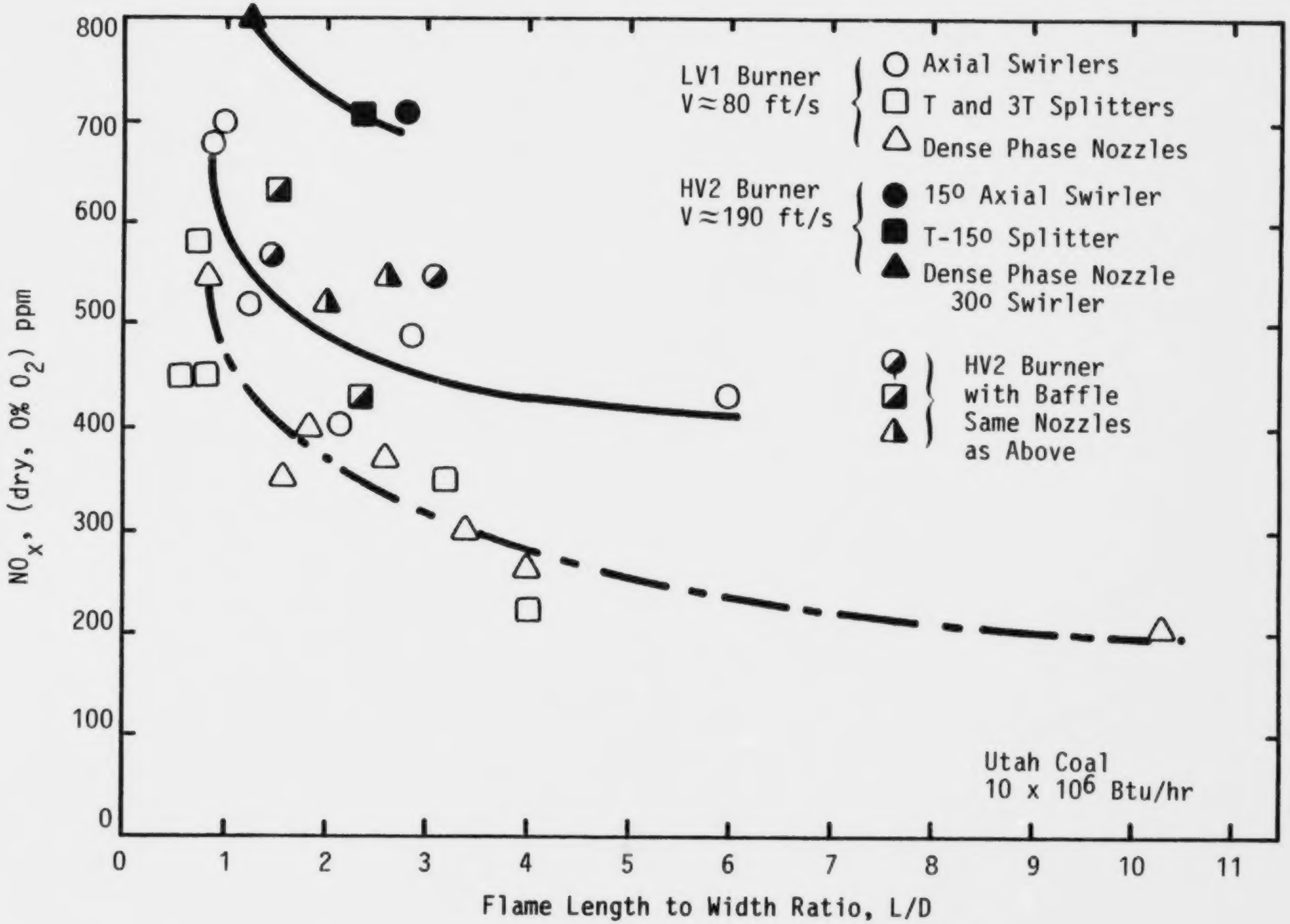

Figure 3-18. Correlation of NO_x emissions with flame shape factor (2000°F furnace exit temperature).

defining a curve higher than that defined by the conventional/splitters and the dense-phase nozzles. This variation between nozzle types suggests that the mixing parameters influencing NO_x production cannot be expressed totally in terms of flame L/D. The data from the HV2 burner generally lie above the LV1 curves and also show a dependence on the fuel nozzle/air baffle arrangement, confirming that mixing rate and NO_x production are not totally defined by flame shape alone.

A somewhat more sophisticated attempt to correlate the NO_x emissions from the LV1 burner was made based upon an approach reported previously by Payne et al. (2). This approach considers not only flame shape (in this case, flame volume), but also thermal conditions (heat input and heat extraction) and the entrainment characteristics of the flame. This approach had been developed based upon data from many different oil-fired burners in a variety of furnaces. Since the bulk entrainment characteristics (defined by the Thring-Newby parameter) are constant for constant burner velocity and diameter, the correlation attempted for the LV1 data accounted only for flame shape and thermal characteristics. The correlating parameter used was $Q/V_f \cdot H_e$, where Q is the gross heat input in megawatts, V_f is the observed flame volume and H_e is the heat entracted in the furnace in megawatts. The results of the correlation are presented in Figure 3-19. The correlation appears to work well for the LV1 data although, again, there are distinct curves for the different coal nozzles. For a given value of $Q/V_f\ H_e$, the conventional axial swirlers produce higher NO_x than the conventional splitters, which in turn produce higher NO_x than the dense-phase nozzles. Because of the smaller size of the coal pipe, burners with dense phase nozzles had reduced secondary air velocities. The lower NO_x production achieved with these coal nozzles probably results partly from changes in mixing brought about by reduced secondary air velocity and partly from altered air/coal distribution with the dense-phase injectors. This difference between nozzles indicates a need for another parameter in the abscissa which takes into account differences in near-burner mixing as a result of coal nozzle design.

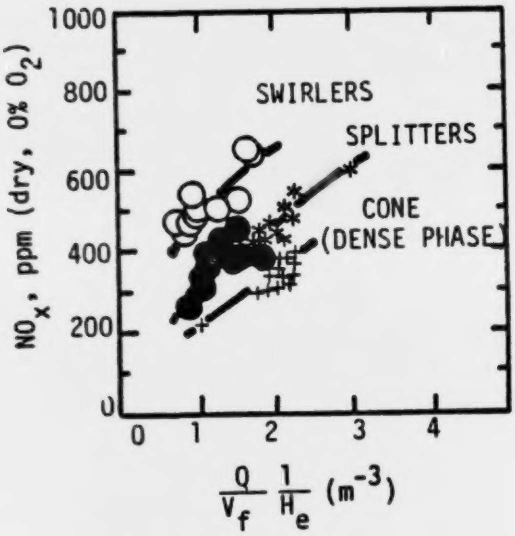

Figure 3-19. Correlation of LV1 NO_x emissions using parameter accounting for flame volume and thermal characteristics.

4.0 SORBENT INJECTION WITH INTERNALLY-STAGED LOW-NO_x BURNERS

The sorbent injection testing with the internally-staged burners in the SWS experimental furnace was intended to determine whether internal staging modifications for NO_x reductions would provide an environment suitable to permit sorbent injection through or near the burner, avoiding sorbent deactivation by high temperatures and/or by coal ash. Sorbent injection through or near the burner -- if possible without unacceptable sorbent deactivation -- would facilitate effective sorbent dispersion across the boiler cross-section, and could provide longer sorbent residence times, compared to injection in the upper furnace remote from the burners.

Testing to evaluate thermal deactivation alone (in the absence of coal ash) was conducted using natural gas as the fuel, doped with SO_2. The parameters studied in these gas-fired screening tests included: injection location (in or near the burner); injection velocity; SO_2 concentration; and thermal environment (burner load). This gas-fired testing was conducted using the HV1 burner in the SWS furnace.

Testing to evaluate the combined effects of thermal and ash deactivation was conducted burning Utah coal, using both the HV1 and the LV1 burner configurations.

The sorbent injection testing was conducted with the fuel nozzles and burner operating conditions which had been found in the prior testing to yield the best NO_x results. The sorbent in all cases was Vicron 45-3 limestone.

4.1 Natural Gas Flames Doped with SO_2

The high-velocity burner (HV1) was used for the tests with natural gas. It was fitted with the gas nozzle shown in Figure 2-

3, and had the air register settings which gave stable flames and minimum NO_x levels as determined in Section 3.1.1. The secondary air distribution was 8 percent to inner (ISA), 32 percent to middle (MSA), and 60 percent to outer (OSA) secondary air passages. Each secondary air swirler was set to maximum.

The key parameters varied during these tests included: sorbent injection location; sorbent injection velocity; initial SO_2 concentration; and burner heat load.

4.1.1 Effect of Injection Location

Sorbent was injected through three locations, as shown in Figure 2-14 (repeated here as Figure 4-1): external to the burner, through four 1-inch i.d. jets surrounding the burner exit, on the firing wall of the SWS furnace; through the burner throat with the secondary air; and with the primary air stream. Air was used as the carrier gas during injection through the external wall ports. It was expected that injection at these different locations would subject the sorbent to different overall thermal histories, thus possibly causing differences in sorbent reactivity and SO_2 capture.

Figure 4-2 shows SO_2 removal versus calcium-to-sulfur molar ratio (Ca/S) for sorbent injection at each of the locations during the gas-fired testing, including high- and low-velocity injection through the ports external to the burner. As shown in Figure 4-2, SO_2 removal was approximately the same regardless of sorbent injection location, ranging from 15 to 20 percent at Ca/S = 2.0. This relatively low level of SO_2 capture in the absence of coal ash suggests that the sorbent was being overheated by mixing into the flame in a region where temperatures were still too high. To the extent that the low captures were in fact due to thermal deactivation of the sorbent, it is apparent that none of the near-burner injection location alternatives avoided this deactivation.

(a) With the
Primary Air

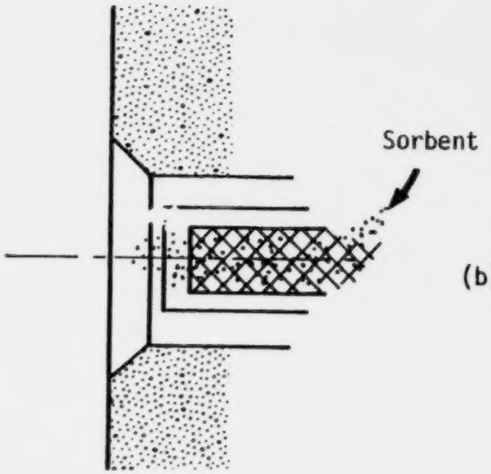

(b) With the Secondary
Combustion Air

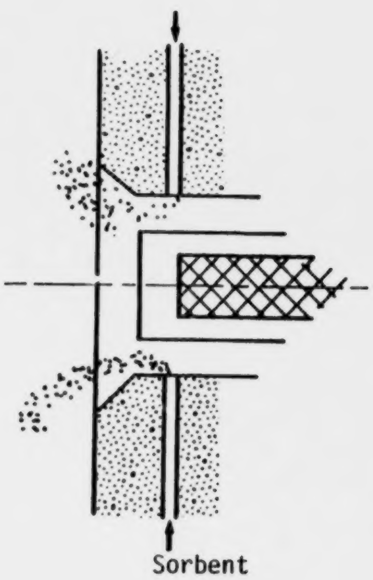

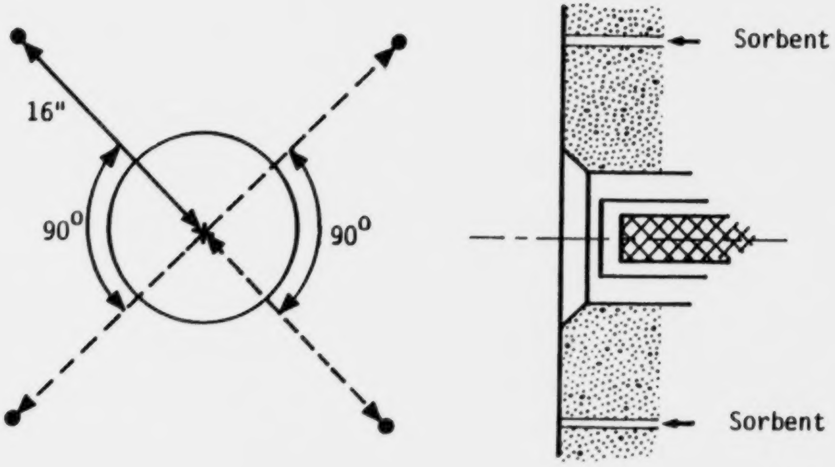
16"
90⁰
90⁰
Sorbent
Sorbent

(c) Through separate
ports around the
burner. Note:
Same ports were used
used with both
HV1 and LV1
burners.

Figure 4-1. Sorbent Injection Locations for Low-NO_x burners.

HV1 Burner, Load = 10 x 10^6 Btu/hr
Burner conditions: 8% ISA, 32% MSA, 60% OSA
Fuel: Natural gas doped with SO_2
Sorbent: Vicron 45-3
Initial SO_2 concentration: 825 ppm
Furnace exit temperature: 2030 °F

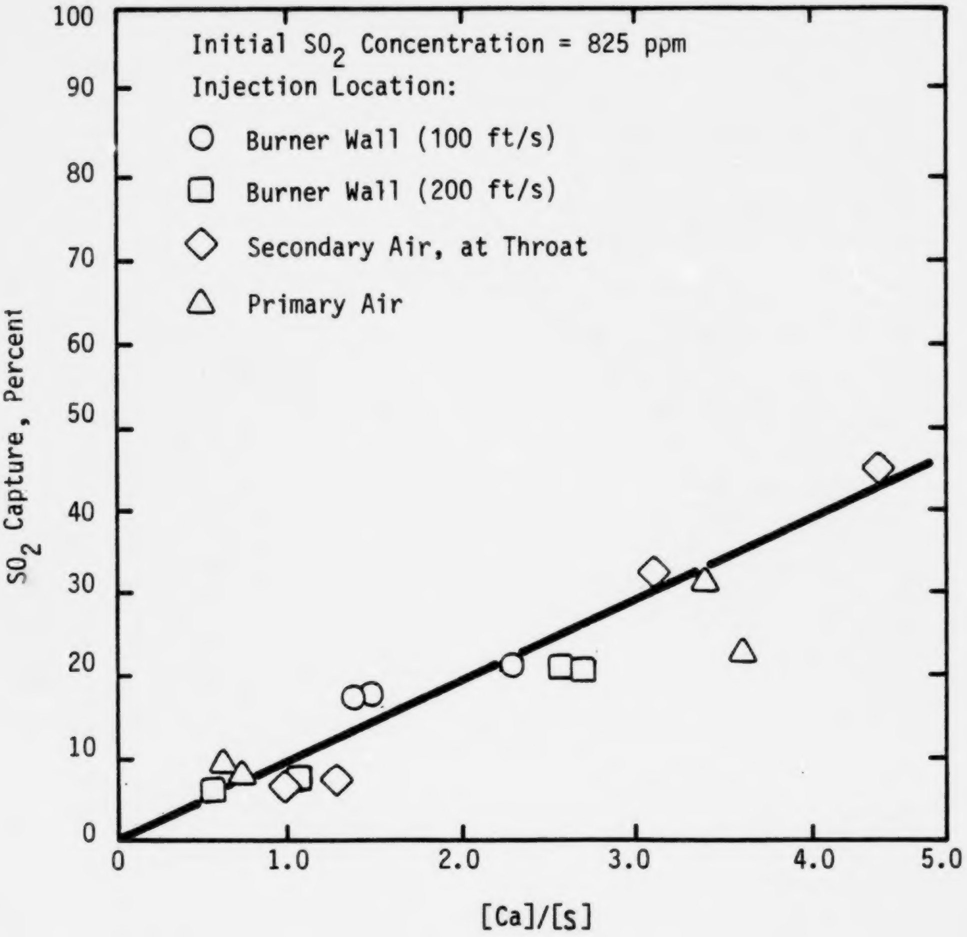

Figure 4-2. SO_2 capture in HV1 burner (doped natural gas flame) -- effect of sorbent injection location.

The low-NO_x characteristics of the HV1 burner did not provide any apparent significant benefits for sulfur capture with the sorbent injection locations tested here.

4.1.2 Effect of Injection Velocity (Wall Injection)

Increased sorbent injection velocity should proportionately increase the sorbent heating rate upon injection into the furnace, and thus possibly could influence sorbent reactivity. Increasing velocity will not significantly influence the peak temperatures that the sorbent sees. At a given distance "d" from the injection point, a higher-velocity jet will have entrained proportionately more background gases, and hence will be at the same temperature as a lower-velocity jet; thus, increased jet velocity (at constant jet diameter) cannot "punch" the sorbent through the flame zone into a cooler region of the furnace. But the higher-velocity jet will raise the sorbent to the peak temperature more quickly by reaching distance "d" faster.

Sorbent injection velocity through the ports in the burner wall was varied in the SWS by varying the flow rate of the sorbent carrier air. Sulfur capture at injection velocities of 100 ft/sec and 200 ft/sec is shown in Figure 4-3 as a function of Ca/S ratio, for two different initial SO_2 concentrations. Although there is scatter in the data, neither injection velocity nor initial SO_2 concentration appeared to have a significant effect on sulfur capture. As before, capture was about 20 percent at Ca/S = 2.0.

Sorbent reactivity continues to be low, perhaps because the sorbent is continuing to see unacceptably high peak temperatures at either injection velocity. Any possible impacts of sorbent heating rate are being masked by the low overall sorbent reactivity.

HV1 Burner, Load = 10 x 10^6 Btu/hr
Fuel: Natural gas doped with SO_2
Sorbent: Vicron 45-3
Injection location: Wall ports
Furnace exit temperature: 2030 °F

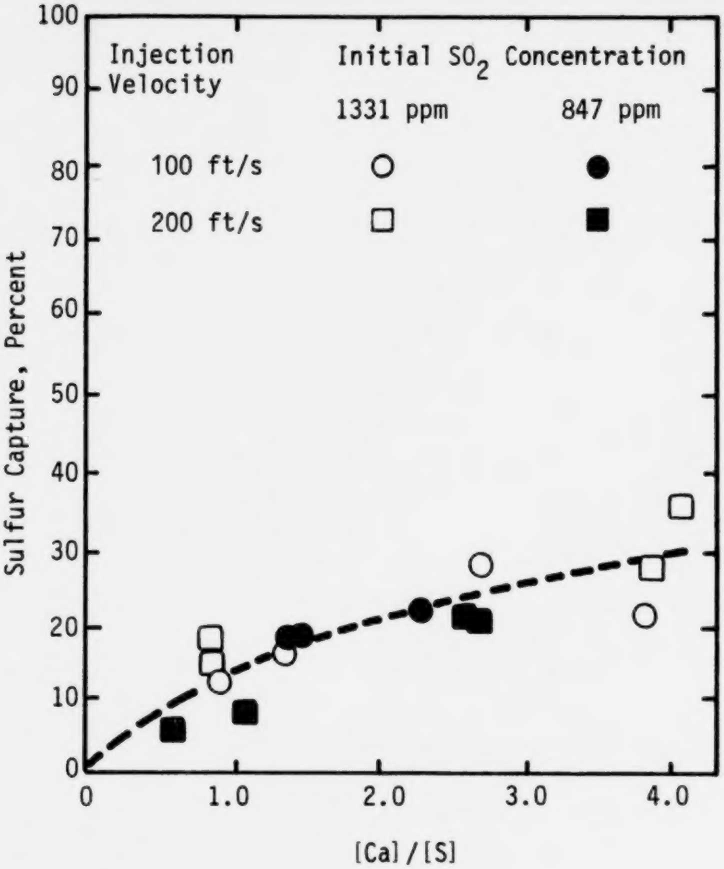

Figure 4-3. SO_2 capture in HV1 burner (doped natural gas flame) -- effect of sorbent injection velocity.

4.1.3 Effect of Burner Load (Wall Injection)

The SO_2 capture at burner loads of 10×10^6 Btu/hr (full load on the SWS) and 5×10^6 Btu/hr (half load) is compared in Figure 4-4. In these tests, Vicron was injected through the wall ports at a velocity of 100 ft/sec. Two levels of initial SO_2 concentration were tested at each burner load. Figure 4-4 shows that sulfur capture increased when the load decreased.

These effects can be explained by considering the key factors which affect the capture of sulfur by calcium-based sorbents, and evaluating the influence of furnace parameters and injection conditions. The key factors which affect sulfur capture are:

o Sorbent reactivity. Experimental work shows that the surface area developed by the sorbent during calcination (a key determinant of reactivity) depends mainly on the peak particle temperature. Exposure to higher temperatures would reduce the amount of generated sorbent surface area. Lower furnace temperatures in the SWS resulting form operation at reduced load would be likely to result in higher sorbent reactivity.

o Residence time at temperature. The degree of sulfation of a sorbent of given reactivity depends upon its residence time in the temperature range between about 1750 and 2250 °F (the "sulfation window"). The upper temperature results from equilibrium constraints, whereas the lower limit is due to kinetic limitations. Operation of the SWS at half load (i.e., at 5×10^6 Btu/hr) somewhat decreased particle residence time in the sulfation temperature window.

Figure 4-5 presents the gas temperature profiles along the SWS furnace axis for the two load conditions. While not necessarily reflecting the exact time-temperature history experienced by the

HV1 Burner
Fuel: Natural gas doped with SO_2
Sorbent: Vicron 45-3
Injection location: Wall ports
Furnace exit temp: 2030 °F (10 x 10^6 Btu/hr)
1380 °F (5 x 10^6 Btu/hr)

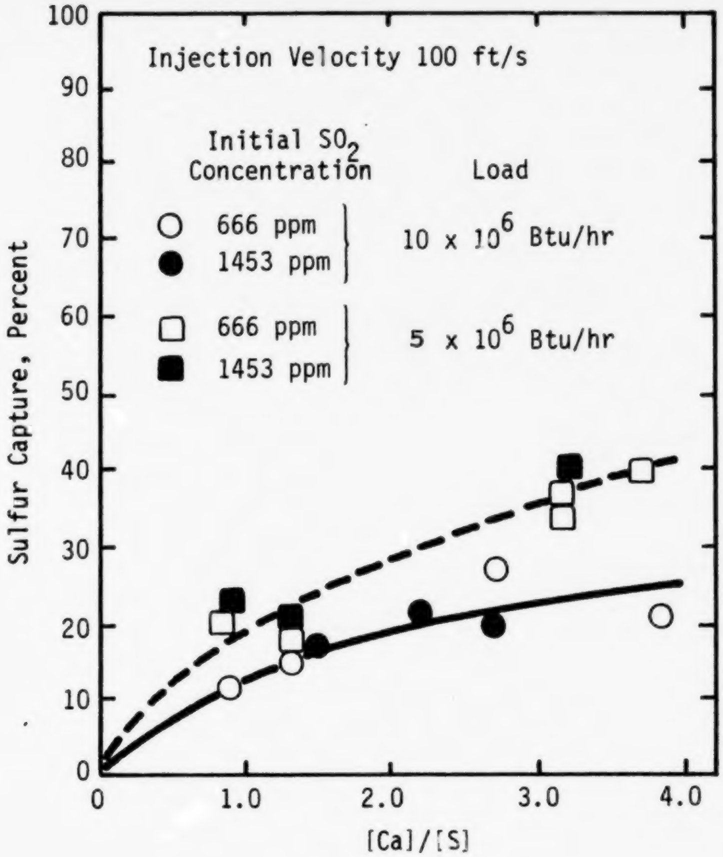

Figure 4-4. SO_2 capture in HV1 burner (doped natural gas flame) -- effect of burner load.

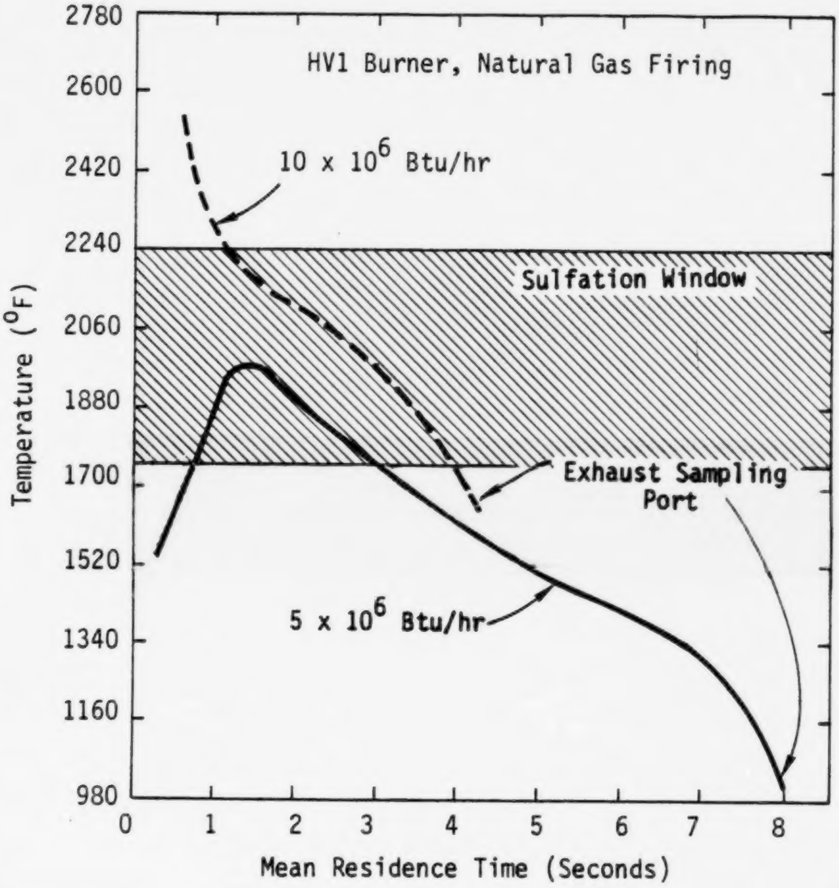

Figure 4-5. Mean time-temperature profiles on axis of the SWS furnace at full load and half load.

individual sorbent particles (e.g., while not accounting for the near-jet mixing effects), these axis profiles suggest at least generally the mean temperature history of the sorbent. Marked on the curves are: the points on each profile where the gases are exiting the 17-foot-long furnace (the "furnace exit temperature"); and the point in the SWS exhaust ducting where the gaseous sample is extracted for SO_2 analysis. As evident from the figure, the peak temperature seen in the half-load case is several hundred degrees below that in the full-load case, suggesting potentially higher reactivities (less thermal sintering) at half load. The residence time between 2250 and 1750 °F is actually somewhat longer for the full-load case -- about 2.5 seconds, compared to about 2.0 seconds at half load, both of which times are relatively long compared to full-scale boiler profiles. Apparently the reduced sintering in the half-load case more than compensates for the lost half-second of residence time. (The half-load case also provides the sorbent with an additional 5 seconds of residence time in the temperature region 1750-1000 °F; while sulfation kinetics are not rapid at these lower temperatures, the residence time is relatively long, so that some additional sulfur capture could occur.)

4.1.4 Effect of Initial SO_2 Concentration

The tests on the effects of injection velocity and of reduced load operation with wall injection were conducted at 2 levels of initial SO_2 concentration (i.e., of SO_2 level in the natural gas). The results given in Figures 4-3 and 4-4 show that sulfur capture was not significantly affected by the initial SO_2 concentration. Theoretical considerations and bench-scale experimental data indicate that there is a slight influence of SO_2 concentration on overall sulfur capture. But apparently, other factors masked this effect in these tests.

4.2 Coal Flames

Sorbent injection tests were conducted while firing Utah coal in both the HV1 and LV1 burners. With Utah coal, the baseline SO_2 level in the SWS gases without limestone (i.e., the "initial SO_2 concentration") was typically 660-685 ppm (corrected to 0% O_2).

4.2.1 HV1 Burner

The burner settings used for these tests were the same as those used for the natural gas firing tests (Section 4.1), with the exception that the 15° axial swirler coal nozzle was used. Sorbent was injected through the front (firing) wall jets at a velocity of 200 ft/sec, or mixed with the primary air and coal. Sulfur capture for these tests is shown in Figure 4-6. Also shown in this figure is the mean line for SO_2 removal for natural gas firing at the same burner load (10×10^6 Btu/hr), taken from Figure 4-2. An effect of injection location on capture is seen with the coal; with gas, SO_2 capture had not varied with injection location.

Sulfur capture with injection of the sorbent through wall jets was slightly higher with coal than with natural gas, giving 25-30 percent capture at Ca/S of 2.0, compared with 15-20 percent with gas. This suggests that the sorbent developed higher reactivity, possibly because it was not exposed to such high temperatures as a result of lower flame temperatures and slower development of combustion with coal firing. Another possibility is that sorbent reactivity was promoted by certain minerals present in the coal ash under these particular conditions. Residence times in the sulfation window were similar for both the gas and coal flames, so that residence time would not appear to be the explanation.

Capture was significantly lower when the sorbent was injected with the primary air and coal, only 10-15 percent at Ca/S = 2.0. Since no effect of sorbent injection location was observed with the

HV1 Burner, Load 10 x 10^6 Btu/hr
Coal Nozzle: 15° vane swirler, setback -3 inch
Fuel: Utah coal
Sorbent: Vicron 45-3
Furnace exit temp.: 1873-1980 °F (avg. 1953 °F)

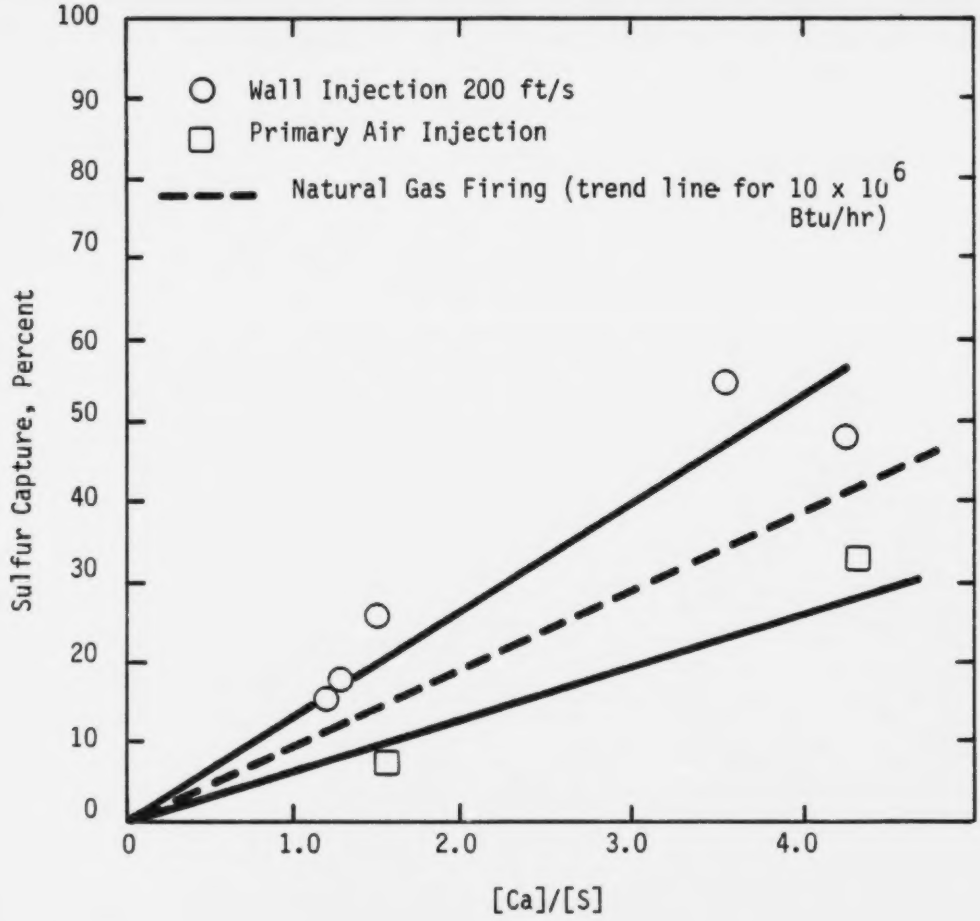

Figure 4-6. SO_2 capture in HV1 burner (Utah coal flame) -- effect of sorbent injection location and of fuel type.

natural gas flames, the lower capture with primary injection with coal could have been caused by lower sorbent reactivity as a result of interaction between ash and sorbent in the high-temperature region of the flame. However, other differences (e.g., initial particle heating and mixing history, etc.) between the natural gas and coal flames might also have affected the sorbent activation.

Thus with coal, as with gas, the HV1 internally-staged burner did not in this case appear to avoid the sorbent deactivation which has been experienced in other near-burner injection studies. It is of interest to note that the coal tests gave higher SO_2 captures than the gas tests for wall injection, and that primary air injection gave significantly reduced captures in the coal case but showed no differences from wall injection in the gas case. If in fact coal ash interactions are responsible for these differences between the coal and gas results, these observations suggest that the coal ash minerals can result in a net improvement in sorbent reactivity if the sorbent and ash come into contact in somewhat cooler regions away from the near flame; however, if they contact in the near flame, the net effect is one of deactivation, possibly because different ash minerals or different interaction mechanisms predominate.

4.2.2 LV1 Burner

The sorbent injection test matrix for the LV1 burner (firing Utah coal) is presented in Table 4-1, together with the sulfur capture results obtained at each test condition (Ca/S = 2). Injection tests were conducted with the three coal nozzles found to produce the lowest NO_x: the T-15 splitter (conventional transport), and the 30° axial swirler and 30° cone with dense-phase transport. Sorbent was injected either through the wall ports (at 248 ft/sec), or with the coal/primary air. The overall excess air was also varied, between 10 and 20 percent.

TABLE 4-1. LOW-NO_x BURNER CONDITIONS FOR SORBENT INJECTION SCREENING: LV1 BURNER

Conditions for Sorbent Injection Screening						
			Temperature ^oF			
Spreader	SR_T	NO_x ppm Dry 0% O_2	Furnace Exit	Sample Point	Injection Location	Percent Capture (@ Ca:S = 2.0)
T-15 deg	1.2	260	2110	1710	Wall	28
T-15 deg	1.2	232	2030	1670	Primary	31
T-15 deg	1.1	200	2160	1770	Wall	20
T-15 deg	1.1	260	2200	1810	Primary	10
Dense Phase 30^o Axial Swirler	1.2	335	1910	1570	Wall	48
Dense Phase 30^o Cone	1.2	246	2050	1720	Wall	33
Dense Phase 30^o Cone	1.1	248	2240	1820	Wall	21%

The results of the LV1 injection tests are plotted in Figure 4-7. The best removals (33-48 percent at Ca/S = 2) were obtained with the two dense-phase nozzles at SR_T = 1.20 with wall injection. This effectiveness with the dense-phase nozzles might be due to the tendency of these nozzles to retain the coal closer to the burner axis for a longer time after injection, thus effectively staging the combustion and possibly lowering the peak temperatures experienced by the sorbent injected around the periphery of the narrow flame. Also, due to the nature of these nozzles and of the experimental system, the tests with these nozzles involved lower bulk gas temperatures in the SWS; as discussed later, these reduced bulk temperatures had some impact on sulfur capture. Figure 4-7 also suggests that -- unlike the results with the HV1 burner/15° swirler presented in Figure 4-6 -- the LV1/T-15 splitter configuration did not appear to show a significant difference in sulfur capture between wall injection and primary air sorbent injection at an SR_T of 1.20; for both sorbent injection locations, removal was about 28-31 percent at Ca/S = 2.0, similar to the capture seen with wall injection on the HV1 burner with Utah coal. However, at SR_T = 1.10 with the T-15 splitter, sulfur captures dropped relative to SR_T = 1.20, and a significant difference in captures between the two injection locations appeared. Sulfur captures also fell with the dense-phase cone spreader nozzle when SR_T was reduced. Part of the reason for the reduced capture at low SR_T is that, at the reduced stoichiometry (reduced air flow), bulk gas temperatures in the furnace were increased, probably increasing sintering of the sorbent.

The variations in sulfur capture with the variables discussed above were at least in part due to the bulk temperature environments created in the SWS by the various nozzles and excess air conditions. This is demonstrated in Figure 4-8, where the sulfur captures from the seven conditions in Table 4-1 are plotted

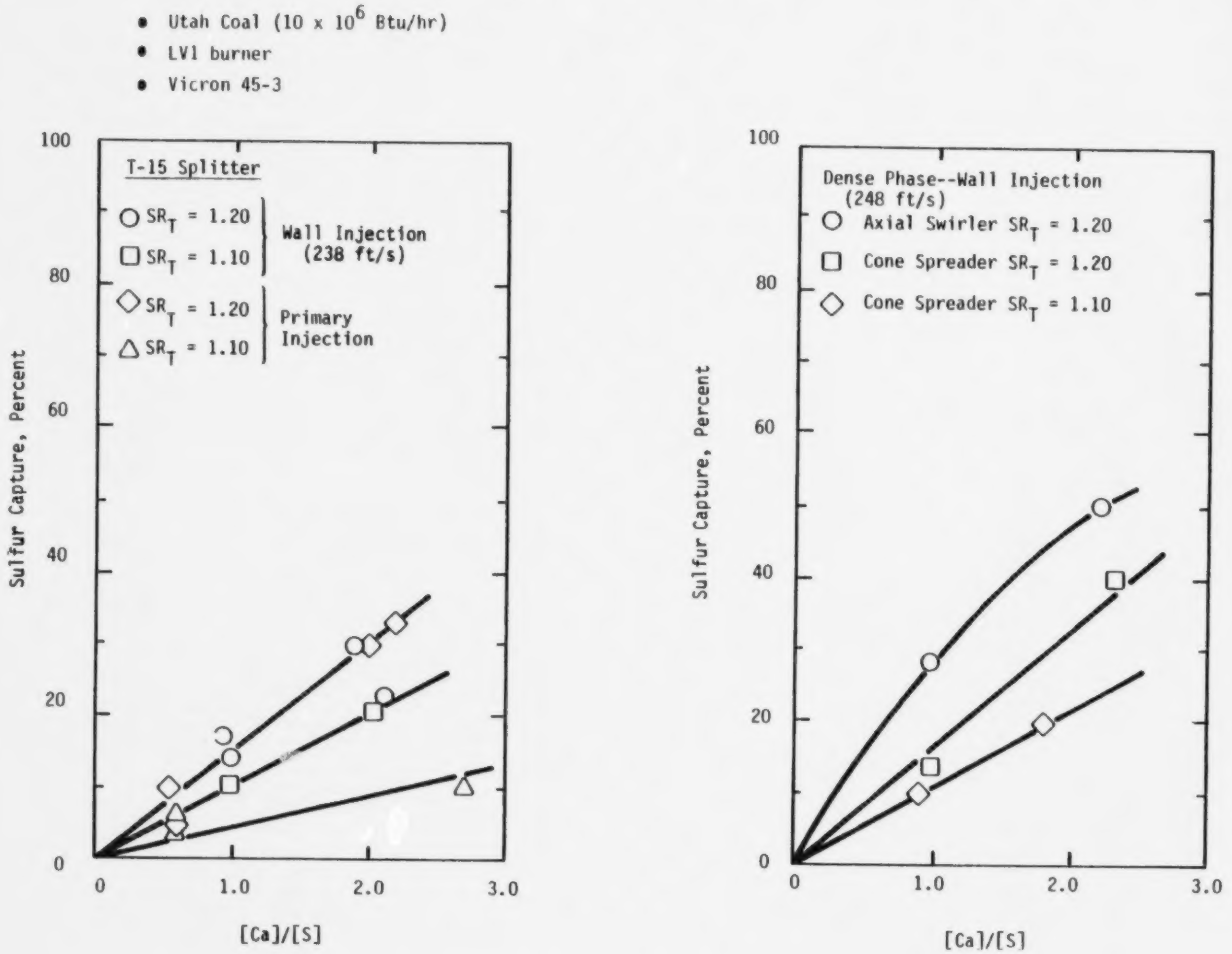

Figure 4-7. SO_2 capture results with low-NO_x burner conditions

LV1 Burner, Load = 10 x 10^6 Btu/hr
Fuel: Utah coal
Sorbent: Vicron 45-3
Ca/S = 2.0

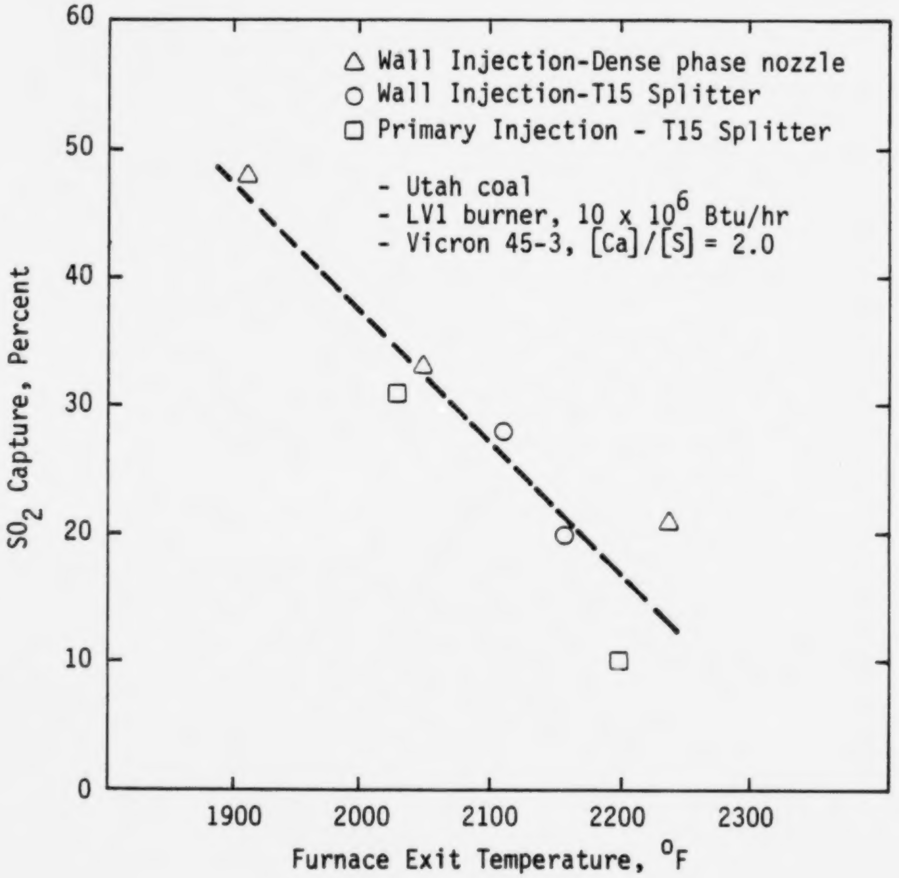

Figure 4-8. SO_2 capture in LV1 burner as a function of SWS furnace exit temperature, with Vicron 45-3 at Ca/S = 2.0.

against the furnace exit temperature (as a representative of the furnace time-temperature history for each condition). As shown in the figure, the data correlate fairly well. For example, the three lowest, right-hand data points are the three conditions involving low excess air (SR_T = 1.10); with less excess air to cool the system, the furnace temperatures were higher and the sulfur capture lower, possibly due to thermal deactivation of the sorbent. The highest, left-hand data point is the condition involving the dense axial swirler at SR_T = 1.20; this best removal corresponds to the lowest exit temperature tested. Not all of the variation can be explained as being due to bulk temperature effects: for example, the removal with primary injection through the T-15 splitter at SR_T = 1.10 (the lowest point in the figure) is well below the correlation line, suggesting that perhaps near-flame sorbent-ash interaction effects might have played a role. In addition, factors such as flame shape, mixing pattern and near-flame temperature distributions undoubtedly also contributed to variations between the individual conditions. However, it appears clear that the bulk temperature profile is perhaps the most important single correlating parameter in these tests. To the extent that bulk temperature effects are an inherent property of the burner condition which would be reproduced in full-scale operation -- e.g., increased bulk temperatures at reduced excess air -- then the results here could be used to evaluate sorbent injection approaches for that burner condition. However, in some cases, the bulk temperature effects here might be an artifact of the experimental system, in which case the comparisons apparent from these data might have to be adjusted in evaluating effects on full-scale systems. An example of such an experimental artifact is the thermal inertia of the SWS cooling water system; for a given set of burner operating conditions, the bulk temperature in the furnace could be somewhat higher or lower, depending upon how long the SWS had been in operation and thus the temperature of the circulating cooling water.

4.3 Potential for Sulfur Capture with Near-Burner Sorbent Injection

The near-burner sorbent injection tests with the HV1 and LV1 internally-staged coal burners operating under low-NO_x conditions, gave relatively poor sulfur captures at acceptable calcium-to-sulfur ratios. SO_2 removal at Ca/S = 2.0 ranged from about 10 percent up to a maximum of about 50 percent (the highest removal being achieved with the low-velocity burner with a dense-phase coal nozzle). The factor which appeared to have the largest influence on SO_2 removal was the bulk temperature level in the furnace, with high temperatures sharply reducing sulfur capture levels. This suggests that, during these tests, sorbent reactivity might have been limited by exposure of the sorbent particles to high temperatures when injected at near-burner locations. These results indicate that it could be difficult to meet SO_2 capture objectives (50 percent SO_2 removal at Ca/S = 2.0) if the sorbent were injected near the burner. Even in cases where acceptable captures are obtained with near-burner injection, these systems are likely to be sensitive to changes in operating conditions, because of the effect that changes in burner settings or boiler operating conditions can have on the size and temperature of the flame region. Thus, there is always a risk with these systems that capture effectiveness could be adversely affected by practical boiler operating requirements.

Based upon these results, and other similar results from bench-scale, larger pilot-scale and field tests, efforts to improve sorbent performance are now being directed towards sorbent injection in the upper regions of the furnace, remote from the burners. In the upper furnace, gas temperatures are lower and more predictable, and peak temperatures experienced by the sorbent particles can be better controlled to give optimum sorbent reactivity. The most practical method of sorbent injection is typically by way of sorbent jets, using either air or flue gas as a carrier medium. Jet injection allows adequate penetration and dispersion of the sorbent in the upper furnace regions. With jet injection, the possibility also exists to control the thermal history of the sorbent, and hence sorbent reactivity, by appropriately selecting the exact injection location (injection temperature), and by adjustment of jet parameters influencing the heating rates and furnace gas entrainment into the jet.

Thus, efforts under this project were re-directed towards investigating sorbent injection techniques under well-controlled experimental conditions focussing on upper-furnace jet injection, away from the burners. Initial jet experiments in the 10 x 10^6 Btu/hr SWS are described in Sections 6 through 8 which follow in this report. Upper-furnace sorbent injection studies in the 100 x 10^6 Btu/hr Large Watertube Simulator (LWS) furnace are discussed in the separate report on the second phase of this project.

5.0 CONCLUSIONS FROM INTERNALLY-STAGED BURNER TESTS

The investigations described here were aimed at development of a burner and sorbent injection system for simultaneous NO_x and SO_x control for existing coal-fired utility boilers. NO_x control was to be achieved by staged combustion, with SO_x control by injection of calcium-based sorbents. A key constraint was the need to limit the size of the burners so that they could be retrofitted into the walls of pre-NSPS boilers with minimal modification. Thus, only limited scope was available for reducing burner velocities, and staging had to be achieved internally through adjustment of the internal burner passages, by adjustment of air mass flow and swirl, distribution and by use of different types of coal nozzles.

Similarly, sorbent injection methods were limited to near-burner injection locations--either with the coal or the secondary air, or through small ports in the burner wall around the burner opening.

Two general types of burners were tested: high velocity types which would be necessary if the retrofit application offered no potential for increase in burner size; and low velocity types where the retrofit application offered a certain amount of flexibility for increasing the size of the retrofit burner.

The results of the NO_x testing showed that the low velocity burner was capable of achieving significant reductions of NO_x, producing about 400 ppm (dry, 0% O_2) compared to baseline pre-NSPS burner emissions of about 800 ppm. In comparison, the high velocity burner initially produced NO_x emissions close to pre-NSPS baseline levels, showing the limited potential for NO_x reduction if air-fuel mixing cannot be controlled to produce adequate staging. Since the high and low velocity burners had essentially the same geometrical arrangement of secondary air passages and used the same coal nozzles, the approximately 50 percent NO_x reduction achieved with the low velocity burner is primarily a result of the velocity reduction. Such velocity reductions in retrofit applications will depend upon the flexibility for enlargement of the throat of the original burner and may not be possible in many cases.

The investigation of the high velocity burner with the secondary air baffles showed that substantial NO_x reductions could be obtained with the addition of these baffles. The secondary air baffles are conical extensions to the pipe separating the inner and outer secondary air flows which serve to deflect the outer secondary air away from the base of the flame, thus achieving a greater degree of air staging. With these baffles in place the high velocity burner achieved NO_x emissions in the range of 400-500 ppm (dry, 0% O_2) compared to emissions without the baffles in the range 650-850 ppm. The baffles also improved flame stability. Thus, for retrofit applications where throat enlargement was not possible, the use of secondary air baffles offers the potential for NO_x reductions comparable to those that can be achieved with reduced velocity internally staged burners.

The investigations of different types of coal injector nozzles showed that the nozzle type has a clear influence on the NO_x emission characteristics of the burner. The axial swirlers tended to spread the coal out into the surrounding air stream, promoting mixing and generating higher NO_x levels. The T-splitters and cone spreaders apparently minimized the spread of the coal and hence produced a greater staging effect with correspondingly lower NO_x emissions. The dense-phase nozzles tested showed variable results. Dense phase nozzles were expected to improve NO_x reduction in two ways: they used a minimum amount of primary air thus reducing air/fuel stoichiometry in the primary combustion zone; and they minimize the size of the primary coal pipe, thus, allowing a reduction in secondary air velocity. Generally the dense phase coal injectors did not show any clear advantage over the more conventional coal nozzles. For any given burner type, the best of the conventional coal nozzles gave equal or better NO_x reduction than the dense-phase nozzles.

An important observation of these tests was the apparent relationship between flame geometry and NO_x emission. NO_x formation in practical flames is determined to a large extent by the mixing processes between fuel and air in the flame. Staged combustion implies a reduction in the overall rate of fuel/air mixing and an increase in flame size or change in its shape. Several methods of characterizing this effect were tried here. The first correlated NO_x emissions against flame length to width ratio, showing that NO_x was reduced as flame length/width ratio increased. The second method correlated NO_x with a parameter that took account of flame volume and heat extraction from the flame. This showed good correlations for each of the different classes of burner. These correlations suggest that flame shape or volume is an important factor influencing overall NO_x emissions, with low-NO_x emissions being associated with longer or larger volume flames. This may impose a practical limit to NO_x reduction in retrofit situations in pre-NSPS boilers where furnaces are relatively small and limit the increase in flame volume needed to obtain low NO_x emissions.

The near-burner sorbent injection tests with the internally-staged coal-burners operating under low-NO_x conditions, gave relatively poor capture of SO_2 at acceptable calcium to sulfur ratios. SO_2 removal at Ca/S = 2.0 ranged from about 10 percent up to a maximum of about 50 percent for the low velocity burner with a dense-phase coal nozzle. The factor which appeared to have the greatest influence on capture was temperature, with lower furnace temperatures yielding higher captures. This suggests that the poor sulfur capture was caused by loss of sorbent reactivity due to sorbent overheating. Thus, near-burner sorbent injection appears to have limited potential for SO_2 capture in high temperature situations such as pre-NSPS burners or with these low-NO_x internally staged burners for retrofit into pre-NSPS boilers. Although near-burner injection is desirable for achieving good mixing of sorbent with the combustion products, thermal deactivation of the sorbent seems unavoidable, because the sorbent is exposed to high temperatures. With coal flames, there is also the possibility of sorbent de-activation through interaction with mineral matter at high temperatures. Sorbent injection remote from the burner region appears to be a more attractive prospect, particularly for highly reactive sorbents whose reactivity appears to be sensitive particle overheating.

6.0 INTRODUCTION - SORBENT JET AERODYNAMICS

The study of sorbent injection with the internally-staged burner showed relatively poor SO_2 capture for near-burner injection locations, which was considered to be caused by sorbent being exposed to high temperatures as it was drawn into the flame. However, higher SO_2 captures have been observed with sorbent injection with the tertiary air in Distributed Mixing (DMB) Burners. The DMB has lower velocities than the internally-staged burner and produces slower mixing between air and fuel, resulting in larger, but lower temperature flames. The sorbent was injected along the axis of the tertiary air ports in a double-concentric jet configuration. The tests conducted included varying the sorbent injection velocity, which showed that increasing the sorbent velocity resulting in increased SO_2 capture. Thus, it was seen that the aerodynamic characteristics of the injection jets could have a significant influence on overall sulfur capture, either by altering sorbent heating rates and thermal history or dispersion and mixing patterns. The work in this part of the program was conducted with the objective of determining whether sorbent jet parameters could be adjusted to improve sorbent reactivity and overall SO_2 reduction.

The overall removal of SO_2 by injection of calcium-based sorbents into a coal-fired boiler under the LIMB process depends on three main factors:

1. the reactivity of the sorbent

2. the effectiveness of dispersion of the sorbent over the combustion gases, i.e. the coverage of the combustion gases

3. the residence time of the sorbent in the temperature region where sulfation can proceed. This sulfation "temperature window" is in the range of approximately 2250°F down to 1750°F, where the temperature is sufficiently high to yield reasonable sulfation reaction kinetics but sufficiently low to reduce the impacts of sorbent sintering and $CaSO_4$ decomposition.

The reactivity of the sorbent is a key factor in the overall performance of any LIMB system and can be strongly influenced by the temperature history of the sorbent particles. As sorbent is injected into the combustion gases, it is heated and calcines to CaO. This process produces porous particles having a large specific surface area and hence a large number of active sites for reaction of CaO with SO_2 to produce $CaSO_4$. Although other factors may influence sorbent reactivity, the reactivity seems to be directly related to its total surface area (including external area and internal pore area). In parallel with the development of surface area, thermal sintering (growth of CaO grains) will occur, at a rate that increases with temperature. Heating sorbent particles to high temperatures can lead to loss of reactivity through loss of available surface area due to sintering. The competing effects of temperature on development of reactivity on one hand and the rate of sulfation on the other lead to a relationship between SO_2 capture and peak sorbent temperature that shows a maximum capture for peak temperatures close to 2250°F.

Although peak sorbent temperature is a key variable influencing sorbent reactivity, another possible influence could be the sorbent heating rate. The rate of heating would influence the calcination rate and it is plausible that the rate at which CO_2 is evolved during calcination could influence the development of the pore structure in the sorbent particles and thus the resultant surface area. Hence, useful gains in SO_2 capture might be obtained by optimizing the particle heating rate within the constraints of peak particle temperature and available residence time in the sulfation window.

The main method of injecting calcium-based sorbent into combustion gases has been as a dilute suspension of particles in turbulent air jets. The turbulent jets spread into and entrain the surrounding gases, thus mixing the sorbent with the combustion gases and providing the dispersion necessary for adequate coverage of the flue gas with sorbent. The jet mixing process also generates the major part of the heating up of the sorbent particles. As the jets entrain hot furnace gas, the mean jet temperature rises and the sorbent particle temperature increases through transfer of heat by conduction and convection.

Jet parameters can influence sorbent activation in two ways. First, the jets can be used to protect the sorbent particles from regions of high temperature (or of potentially deactivating coal ash), through proper selection of jet mass or jet configuration. This is of particular value for near-burner injection. Second, jet parameters can be adjusted to vary the sorbent heating rate.

The jet parameters most likely to protect the sorbent from peak temperatures and from coal ash are: increased jet diameter; and the use of double concentric, or co-axial, jets (where a simple sorbent jet is surrounded by a larger annular air jet). With increased jet diameter at a given jet velocity, there is an increased mass of (relatively cool) carrier gas, so that the temperature of the jet rises more slowly due to sensible heat considerations, and the concentration of entrained coal ash from the background gases is diluted. With double concentric/co-axial jets, a protective sheath consisting of a high mass of relatively cool air surrounds the sorbent jet, similarly slowing the temperature rise and reducing the ash concentration in the sorbent jet. Perhaps if such jets are designed properly in near-burner injection cases, they could transport the sorbent beyond the immediate flame zone -- to a point where the background temperature is lower and the ash properties less a threat to activity -- before the sorbent reached background conditions.

Based upon the limited available results mentioned earlier, it appeared that increased sorbent heating rate in the jet (at a given peak sorbent temperature) might increase reactivity. The jet parameters most likely to increase heating rate are: increased jet velocity; decreased jet diameter (i.e., reduced jet mass flow at a given velocity); and single-pipe jet configuration vs. double concentric jet. All of those factors result in more rapid mixing of the jet with background gases. Increased background temperature will also increase heating rate. For near-burner sorbent injection, jet design to increase heating rate would have to be balanced with the primary need to protect the sorbent from high peak temperatures; temperature protection suggests larger-diameter jets and double concentric jets, which tend to reduce the heating rate. For upper-furnace injection, remote from the burners, smaller, single-pipe jets can be considered, since these give the fastest heating rate. However, even in the upper furnace, large or double concentric jets might sometimes be considered, since these will: a) provide temperature protection to sorbents which are particularly temperature-sensitive even at upper-furnace temperatures; and b) provide better sorbent dispersion across the furnace cross-section, by virtue of their greater mass. Double concentric jets also offer potential for additional control over heating rate through adjustments to the relative velocities (momentums) of the central and annular jets.

Of course, the designer of an injection system will not have total flexibility in selecting heating rate, any more than he would have total flexibility in selecting peak temperature. Of the variables that influence heating rate, jet velocity and diameter (i.e., jet momentum) will be determined in part by the desire to achieve proper sorbent penetration and dispersion in the boiler; background temperature will be dictated in part by the desire to maximize sorbent residence time in the sulfation temperature window. Thus, although there are considerations other than heating rate which will guide the selection of these key variables, an understanding of heating rate effects could help assure optimal design of the sorbent injection system.

The sorbent jet portion of this program on the SWS were conducted to investigate the influence of jet injection parameters on sorbent reactivity under relatively well-defined flow and thermal conditions. The parameters that were varied (in particular, jet diameter and velocity, and background temperature) were selected in an effort to control peak sorbent temperature and sorbent heating rate. This portion of the program consisted of three basic elements:

1. Initial testing of a double concentric jet in a non-uniform flow field, injecting near a coal- or oil-fired externally-staged burner (see Sections 7.2.1 and 8.1). This testing simulated sorbent injection through the tertiary air ports of an externally-staged burner, and was intended as a rapid test of whether double concentric jets could indeed provide the necessary thermal protection of the sorbent, or any beneficial heating rate effects, during near-burner injection.

2. Testing of (primarily) double concentric jets in a uniform bulk gas flow field. Most of this testing was conducted with a centrally-located jet surrounded by gas-fired burners, injecting sorbent in the direction of the flow field, i.e., in co-flow (see Sections 7.2.2 and 8.2). A limited amount of the testing was carried out in the uniform gas-fired flow field with the jets in cross-flow rather than co-flow (Sections 7.2.3 and 8.3).

3. Testing with a variety of sorbents using (primarily) single-pipe jets in co-flow in the uniform gas-fired flow field, with the injection conditions representative of upper-furnace injection, remote from the burners. The smaller, single-pipe jets permitted higher heating rates, and a better control of the heating rates, enabling a better-defined study of peak temperature and heating rate effects than was possible in 2 above (Sections 7.2.2 and 9.0). As one part of this testing, an experimental calciner was investigated, closely coupled to the SWS, precalcining sorbent at high heating rates immediately before injection into the SWS through a single-pipe jet (Section 10).

The initial testing (1 above) was conducted with a coal or oil flame on the axis of the furnace, and a parallel sorbent jet below the axis. This non-symmetrical arrangement simulated the injection of sorbent through the outboard tertiary air ports of an externally-staged distributed mixing burner. The sorbent was introduced through a small-diameter jet along the axis of the tertiary air jet. These tests turned out to be of limited value because of the confinement of the experimental furnace; the jet was close to the SWS wall, impacting its dispersion, and it was so close to the burner that the sorbent jet tended to rapidly become engulfed into the flame.

To overcome the flame engulfment problem, a new experimental configuration was developed, with a single sorbent jet issuing along the axis of the furnace from the end (firing) wall, and with a ring of six gas burners on the firing wall. With this arrangement, the jets issued into a relatively uniform flow of hot gas with a controlled background temperature, producing better-defined sorbent thermal histories. This is the configuration used for 2 and 3 above. Both large-diameter double concentric jets and small-diameter single-pipe jets were studied, with jet velocity, jet diameter and background temperature being varied to provide independent variation of sorbent heating rate and particle temperature history. A limited number of tests were conducted with jets injected from the side wall of the furnace to simulate more closely the cross-flow injection representative of jets in the upper furnace region.

An alternative way of generating very high sorbent heating rates would be to use a close-coupled high-temperature sorbent precalciner. In this concept, the sorbent is injected into the precalciner chamber and allowed to remain for only a short residence time before being rapidly cooled (by the addition of air or flue gas) at the precalciner exit. The precalcined sorbent is then immediately injected into the furnace at the beginning of the sulfation temperature window, before the freshly-generated sorbent surface area has had an opportunity to decay. Very brief exposure of the raw sorbent to high temperatures in the precalciner could create a high particle heating rate, and if the particles were removed quickly, overheating of the sorbent might be avoided. With this concept, it might be possible to produce highly-reactive sorbent particles using a precalciner considerably reduced in size (less than 1 second residence time) compared with low-temperature precalciners typically used in the lime industry (1300 °F with 90 minutes residence time). To test this concept, experiments were conducted using a high-temperature precalciner close-coupled to the injection jet along the axis of the SWS furnace. Testing was concentrated on determining the performance of the precalciner with variations in temperature and residence time for two different refractory types. The refractory types tested were a high-alumina type and a chromium type, because it was thought that chromium might act as an enhancer to produce higher-reactivity sorbent.

This sorbent jet aerodynamics and precalciner testing is described in Sections 7 through 11.

These experiments on sorbent jets focused on the effect of heating rate and of peak temperature on sorbent activation. Sulfur capture performance (and, in some cases, sorbent surface areas) were measured as indicators of the effect of heating rate and temperature on sorbent reactivity.

7.0 EQUIPMENT, MATERIALS AND TEST MATRICES FOR STUDIES OF SORBENT JET AERODYNAMICS

The tests discussed in this part of the report were all conducted in the SWS furnace, using coal, oil or gas as fuel, depending on the experimental configuration, as described below. The test configurations fall into three categories:

- tests with double-concentric sorbent jets in a non-axisymmetric configuration, with the SWS fired by oil.
- tests with both double-concentric and single-pipe jets in an axisymmetric configuration, with the SWS fired by gas. This category also included tests where the sorbent was first passed through a close-coupled precalciner.
- tests with sorbent injection jets from the side wall of the furnace, i.e., jets in cross-flow.

In this section, the experimental systems, fuels and sorbents are described, along with the test matrices for the tests.

7.1 Experimental Furnace, Fuels and Sorbents

The experiments were all conducted in the Small Watertube Simulator (SWS). This furnace is fully described in Section 2.1, apart from specific changes for these experiments which are described below. The fuels used were natural gas, No. 2 fuel oil and Utah coal, which are also described in Section 2.2 (see Table 2-2). The primary sorbent used in most of the testing was a pulverized limestone (Vicron 45-3). However, in the heating rate series of experiments with small sorbent jets (see Section 9), several additional sorbents were also tested: a pulverized dolomite, referred to as D3002; two calcitic limes, hydrated at atmospheric pressure (Colton Lime and Longview Lime); and a dolomitic lime hydrated at elevated pressure (Genstar S-type). The physical and chemical properties of these sorbents are given in

Table 7-1. Typical particle size distributions for these sorbents are given in Figures 7-1 and 7-2. Figure 7-1 shows Vicron and D3002 dolomite as having similar particle size distributions, with a median particle size of about 10 microns. The pressure hydrate (labelled PHDL in the figure) is very much finer, having a median particle size of about 1.5 micron, almost an order of magnitude smaller. The two atmospheric hydrates, shown in Figure 7-2, are similar in size and intermediate between the pulverized stones and the pressure hydrate, having median particle sizes around 4 microns.

7.2 Sorbent Jet Experiments

For the jet experiments, it was desired to arrange the SWS such that the experimental jet would be issuing into a uniform bulk flow field. A uniform flow would permit the effects of controlled variation of jet parameters to be seen without interferences from irregular flow patterns which might influence mixing and particle heating rate in some undefinable manner.

7.2.1 Non-Symmetric Jet Arrangement

A preliminary set of experiments was conducted using a large coal- or oil-fired burner on the axis of the SWS with a double concentric sorbent jet to one side, as shown in Figure 7-3. This arrangement did not provide a uniform flow field for the jet, but simulated the configuration where the tertiary air ports of the DMB burner were used for sorbent injection. It was utilized as a relatively simple, rapid approach for obtaining preliminary screening of jet parameter effects for a double concentric jet. In this arrangement, the bulk flow field was created by the LV1 burner mounted in the center of the firing wall. This burner was fired on either Utah coal or SO_2-doped No. 2 fuel oil. The only jet configuration tested was the double concentric configuration

TABLE 7-1. PHYSICAL AND CHEMICAL PROPERTIES OF SORBENTS

Sorbent	Vicron	Colton Hydrate	Longview Hydrate	Dolomite	Genstar Dolomitic Hydrate(s)
Petrographic Character	Calcite	Hydrated Lime	Hydrated Lime	Dolomite	Pressure Hydrated Dolomitic Lime
Composition	$CaCO_3$	$Ca(OH)_2$	$Ca(OH)_2$	$CaCO_3$ $MgCO_3$	$Ca(OH)_2$ $Mg(OH)_2$
Mean Size (μm)	9.8	4.0	3.9	11.8	1.4
Density (g/cm^3)	2.7	2.3	2.3	2.9	2.3
Chemical Composition (%)					
Ca	39.2	51.4	51.6	24.8	30.3
Al	0.002	0.21	0.18	0.04	0.26
Si	0.09	3.30	0.66	0.16	0.13
Fe	0.06	0.10	0.27	0.09	0.07
Na	0.007	0.007	--	0.007	--
Mg	0.33	0.25	0.97	11.3	16.0
K	0.01	0.05	0.04	0.008	--

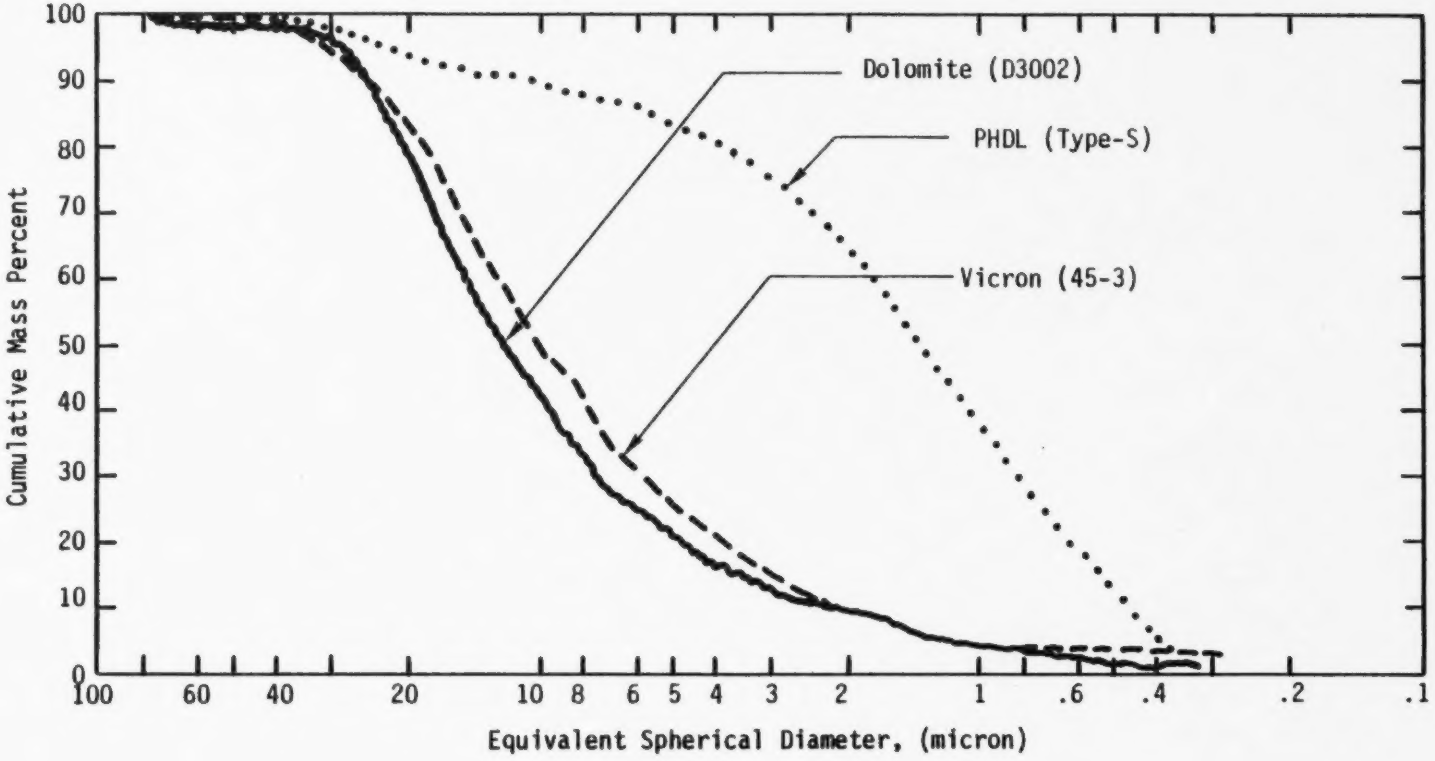

Figure 7-1. Sorbent particle size distributions.

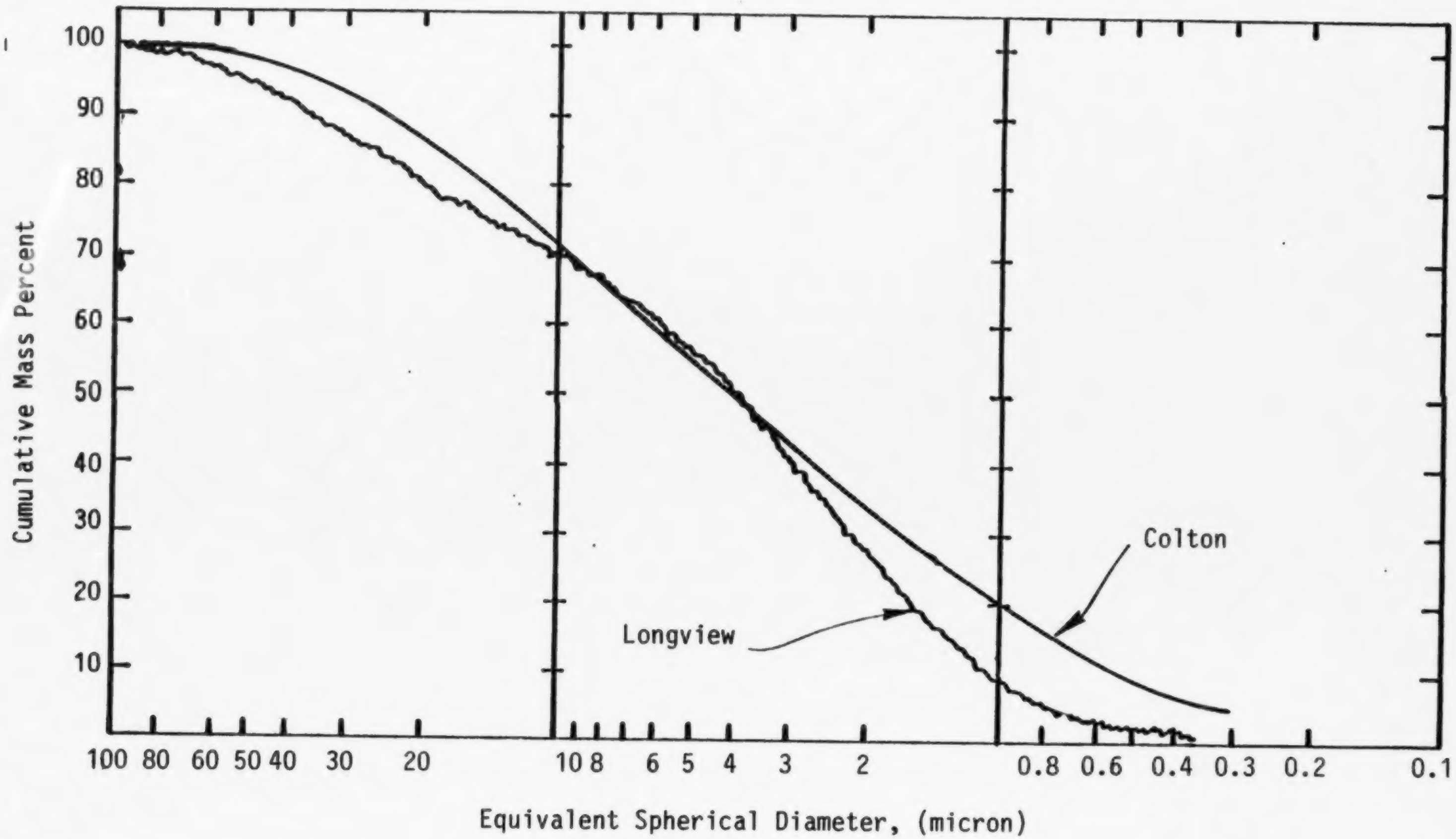

Figure 7-2. Commercial hydrate particle size distributions.

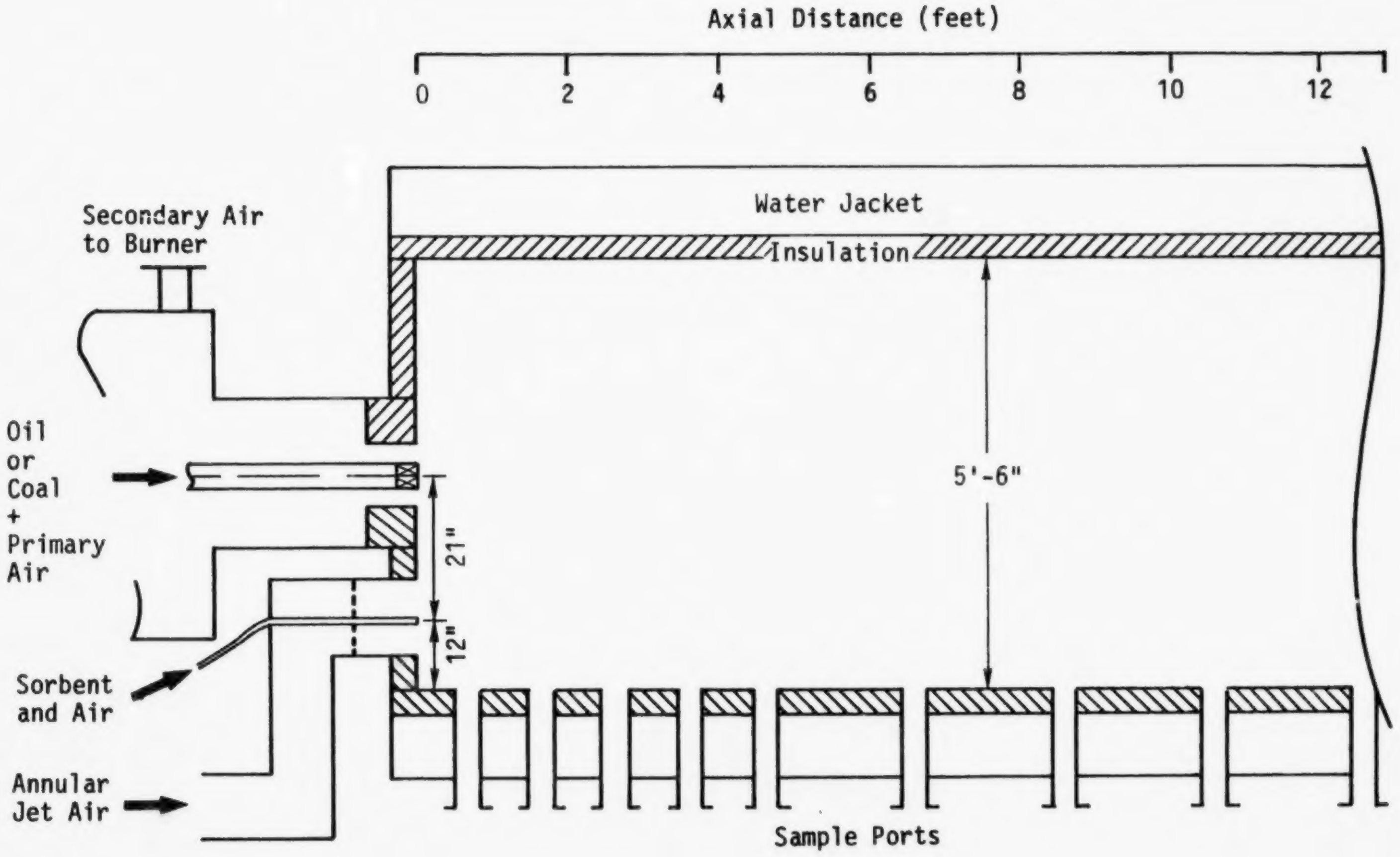
Axial Distance (feet)
0
2
4
6
8
10
12
Water Jacket
Insulation
Secondary Air to Burner
Oil or Coal + Primary Air
21"
12"
5'-6"
Sorbent and Air
Annular Jet Air
Sample Ports

Figure 7-3. SWS configuration for preliminary jet experiment.

with a central 1-inch diameter sorbent jet being surrounded by either a 10-inch or a 12-inch air jet, located flush with the firing wall between the burner and the side wall. This arrangement resulted in a non-uniform flow field for the jet because the single large burner created its own distinct flow patterns in the furnace, and because the proximity of the sorbent jet to the furnace side exposed the jet to distortions caused by wall effects. (The jet centerline was 12 inches from the wall). The experimental matrix for the testing in this configuration is shown in Table 7-2; the primary variables adjusted were the diameter of the annular air jet, the individual velocities of the sorbent jet and the annular jet, and the ratio of these two velocities.

7.2.2 Symmetric Co-Flowing Jet Arrangement

The second SWS arrangement for the sorbent jet experiments was designed to produce a more uniform background gas environment with the jet centered on the axis of the SWS (axi-symmetric), subjecting the jet to a more uniform flow field.

The SWS arrangement utilized for these experiments is shown in Figure 7-4. In this arrangement, a uniform background gas flow was created by a series of six gas burners (generally burning SO_2-doped natural gas) mounted radially around the firing wall. The sorbent jet was located in the center of the firing wall, minimizing wall effects. Where the jet configuration was double concentric, the jet was pushed into the furnace (as shown in Figure 7-4) such that the concentric jet pipe extended 3 feet inside the furnace; this reduced the extent to which the jet would be exposed to any flow irregularities in the immediate vicinity of the gas burners. For the single-pipe jets, initial testing was conducted with the jet nozzle flush with the burner face, because the extended nozzle would not have been adequately cooled and would have been destroyed. However, the majority of the single-pipe jet

TABLE 7-2. TEST MATRIX FOR PRELIMINARY JET EXPERIMENT (NON-UNIFORM FLOW FIELD)

Fuel	Annular Air Jet				Sorbent Jet (1" I.D.)		λ*
	Diameter (Inside)	SCFM	Temp (°F)	Velocity (ft/s)	SCFM	Velocity (ft/s)	
No. 2 Oil + SO_2	12 inch	990	480	41	27 45 11	82 138 33	.5 .3 1.25
		495	480	20	5.5 11 40	16 33 125	1.26 .63 .17
		2000	445	79	22 42	66 131	1.2 .6
	10 inch	990	517	59	11 20 38	33 59 115	1.8 1.0 .5
		560	480	33	11 22	33 66	1.0 .5
Utah Coal	10 inch	990	480	59	5.5	16	3.6
					20	59	1.0
					38	115	.5

*λ Velocity ratio, annular jet to sorbent jet

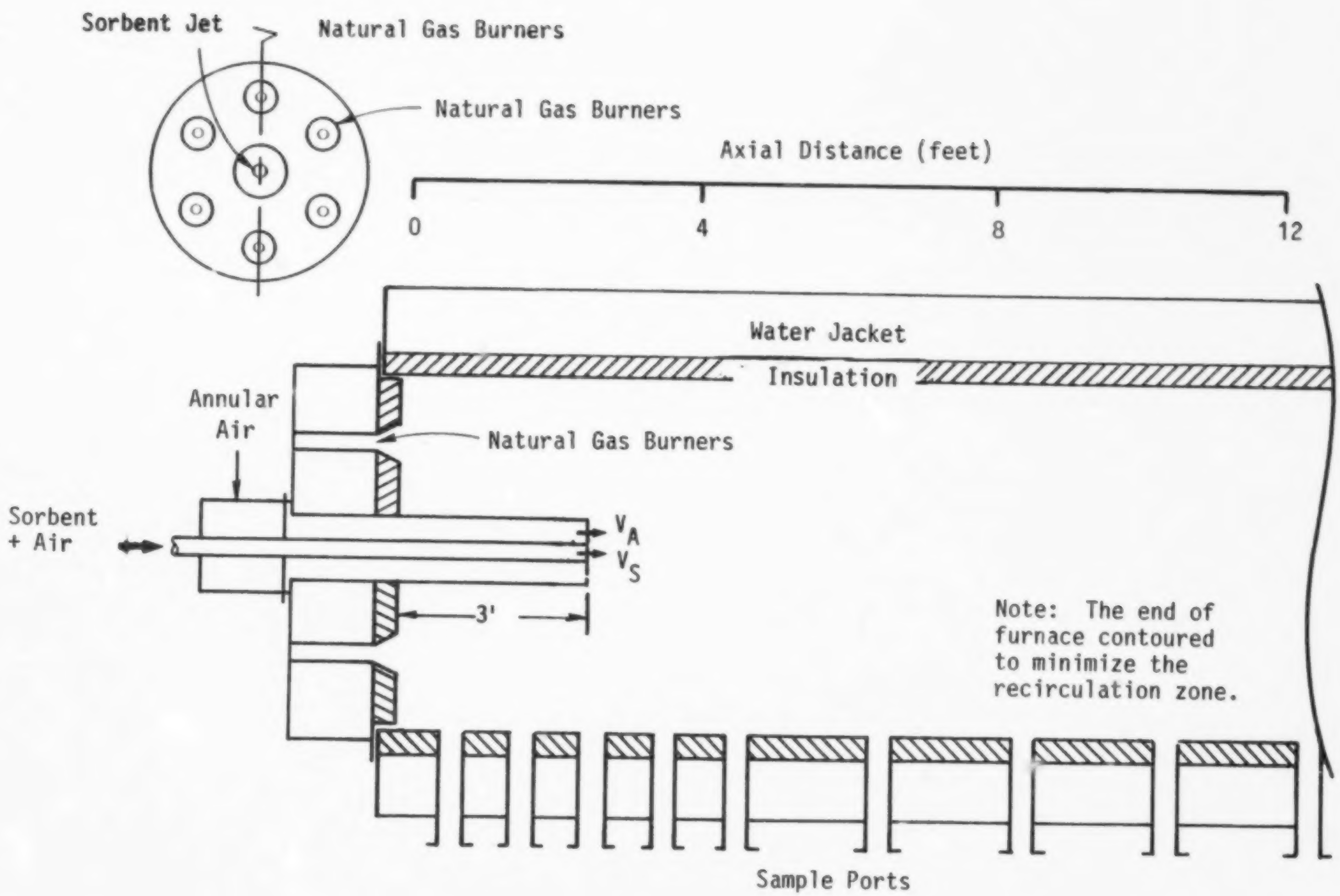
Sorbent Jet
Natural Gas Burners
Natural Gas Burners
Axial Distance (feet)
0
4
8
12
Water Jacket
Insulation
Annular Air
Natural Gas Burners
Sorbent + Air
V_A
V_S
3'
Note: The end of furnace contoured to minimize the recirculation zone.
Sample Ports

Figure 7-4. SWS configuration for double-concentric jet experiments with uniform bulk gas flow field.

testing was conducted with the pipe extended and insulated with refractory, as shown in Figure 7-5. Another important consideration was the need to avoid heating the sorbent in the injection pipe before it exited the nozzle into the furnace gases. The double concentric jets tested all used a 1 inch i.d. central sorbent jet; the diameter of the annular outer air jet varied between 4 and 12 inches o.d. The single-pipe jets tested were either 1 inch or 2 inches diameter; in combination with different background temperatures and jet velocities, this allowed sorbent heating rate and peak sorbent temperature to be varied separately.

One feature of the SWS is that a recirculation zone is created at the rear end of the furnace, where the bulk flow must make a 90° upward turn into the exhaust duct. This zone is particularly pronounced with the double concentric jets, because of the large mass of air introduced with these large jets. While this recirculation zone would not have a significant impact on the near-jet phenomena which were of interest in this study, it makes difficult the estimation of particle residence time in the furnace, a parameter often needed in the interpretation of the jet results. Accordingly, efforts were made during the single-pipe jet heating rate experiments to reduce the extent of this zone by adding refractory to contour the end of the furnace to provide a smooth transition for the furnace gas into the exhaust duct.

The experimental matrix for the co-flowing jet arrangement is shown in Table 7-3. The variables adjusted included jet configuration (double concentric vs. single-pipe jets), diameter of the sorbent jet and the annular air jet, velocity of the sorbent jet (V_S) and annular air jet (V_A), background temperature (T_B), and the presence or absence of coal ash (Test No. 5). Test Nos. 1 through 6 focussed on double concentric jets (with the SWS in the configuration depicted in Figure 7-4), and are referred to as the "clean jet" series of experiments. The results of these six tests are

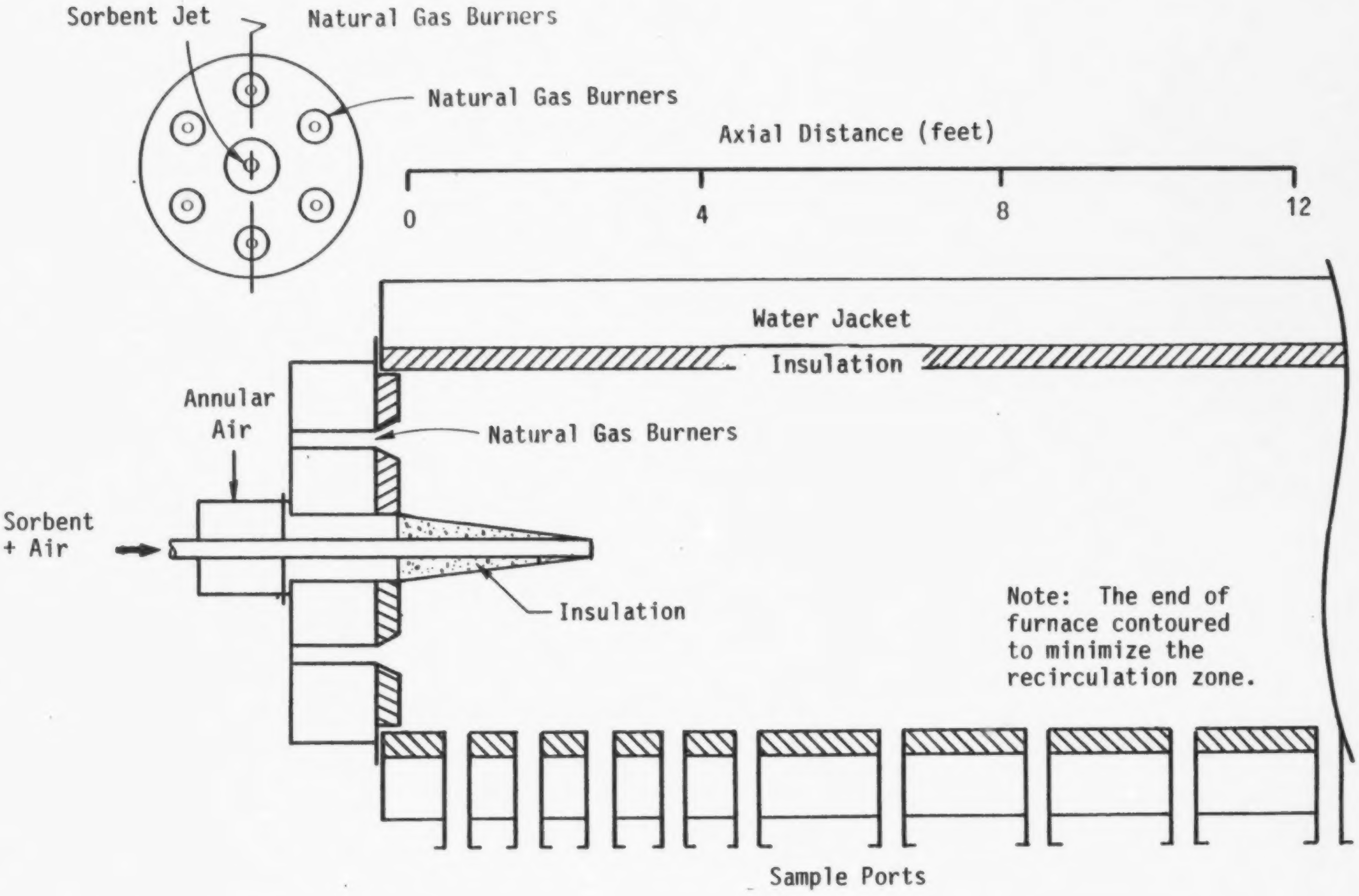
Sorbent Jet
Natural Gas Burners
Natural Gas Burners
Axial Distance (feet)
0
4
8
12
Water Jacket
Insulation
Annular
Air
Natural Gas Burners
Sorbent
+ Air
Insulation
Note: The end of
furnace contoured
to minimize the
recirculation zone.
Sample Ports

Figure 7-5. SWS configuration for single jet experiments with uniform bulk gas flow field.

TABLE 7-3. AXISYMMETRIC JET EXPERIMENT TEST MATRIX

Test Number	1	2	3	4	5	6	7	8	9
Test Fuel	Natural Gas + SO_2	Natural Gas + SO_2	Natural Gas +SO_2	Natural Gas +SO_2	Natural Gas +SO_2	Natural Gas +SO_2	Natural Gas +SO_2	Natural Gas +SO2	Natural Gas +SO_2
Air Jet Diameter D_A (in)	12	10	6	-	10 & 6	6	-	-	4
Air Jet Velocity V_A (ft/s)	30	30,60	30,60	-	30,60	30,60	-	-	60,100
Injection Method	Coaxial Jets	Coaxial Jets	Coaxial Jets	Single Dense Jet	Coaxial Jets	Coaxial Jets	Single Dense Jet	Single Dense Jet	Coaxial Jet
Sorbent Diameter d_S (in)	1	1	1	1	1	1	2	1	1
Sorbent Velocity V_S (ft/s)	50,100	50,100	50,100	25,50,100	50,100	100	45,50 90,100	50,100	60,100,150
Ca/S Ratio	1.0 2.0	1.0 2.0	1.0 2.0	1.0 2.0	1.0 2.0	1.0,2.0	1.0-3.0	1.0-3.0	1.0-3.0
Background Temperature T_B (^{0}F)	2200 2600	2200 2600	2200 2600	2200 2600 2800	2200 2600	2200 2600 2800	2500 2600 2800	2600	2600
Special Measure-ments	Temp. Profiles			Temp. Profiles		Surface Area	Surface Area, Temp. Profiles	Surface Area, Temp. Profiles	Temp. Profiles
Sorbent Type	Vicron	Vicron	Vicron	Vicron	Vicron	Vicron	Vicron Colton Lime Longview Lime Dolomite Type S	Vicron Longview Lime Type S	Vicron Longview Lime Type S

described in Section 8. Tests 7 and 8 were carried out with single-pipe jets, and were specifically designed to study sorbent heating rate effects on sorbent activation under injection jet conditions typical of upper-furnace injection; these tests were conducted with the SWS configuration depicted in Figure 7-5. The test matrix for Tests 7 and 8 is shown in greater detail in Table 7-4. These two tests, and Test 9, are described in Section 9.

The selection of jet diameters, jet velocities and background temperatures for Tests 7 and 8 was made with the objective of achieving a desired range of sorbent heating rates and peak sorbent temperatures. The jet diameters, velocities and background temperatures required to achieve the desired heating rates and peak temperatures were chosen on the basis of jet mixing calculations, using the free-jet entrainment equation of Ricou and Spalding (3). In using the Ricou and Spalding equation, account was taken of the fact that the background temperature T_B is not constant in the SWS, but is falling with axial distance from the firing wall due to heat losses to the furnace walls. From previous experiments in the SWS, this temperature decay rate was estimated to be 45 to 50 F°/ft. Figure 7-6 shows the calculated variation of jet/sorbent temperature with distance into the SWS with an initial background temperature T_B of 2600 °F, for the 1- and 2-inch single-pipe jets used in Tests 7 and 8. Because smaller jets mix faster than larger jets at the same velocity, the peak temperatures reached by the 1-inch jet occur earlier (and, because of the falling-temperature environment, are thus higher) than with the 2-inch jet. It is important to note that the peak temperatures reached by the jets can be higher than the local background temperature, because the jet has entrained background gases at higher temperatures closer to the firing wall. The peak temperatures in the 1- and 2-inch jets are different by 130 F°.

TABLE 7-4. TEST MATRIX FOR HEATING RATE EXPERIMENTS

Peak Temperature °F	2040		2100-2140		2250			
Heating Rate	Baseline	2xBaseline	Baseline	2xBaseline	Baseline	2xBaseline	2xBaseline	4xBaseline
Jet Diameter, in	2	2	2	2	2	2	1	1
Jet Velocity, ft/sec	50	100	50	100	45	90	50	100
Background Temp. °F	2500	2500	2600	2600	2800	2800	2600	2600

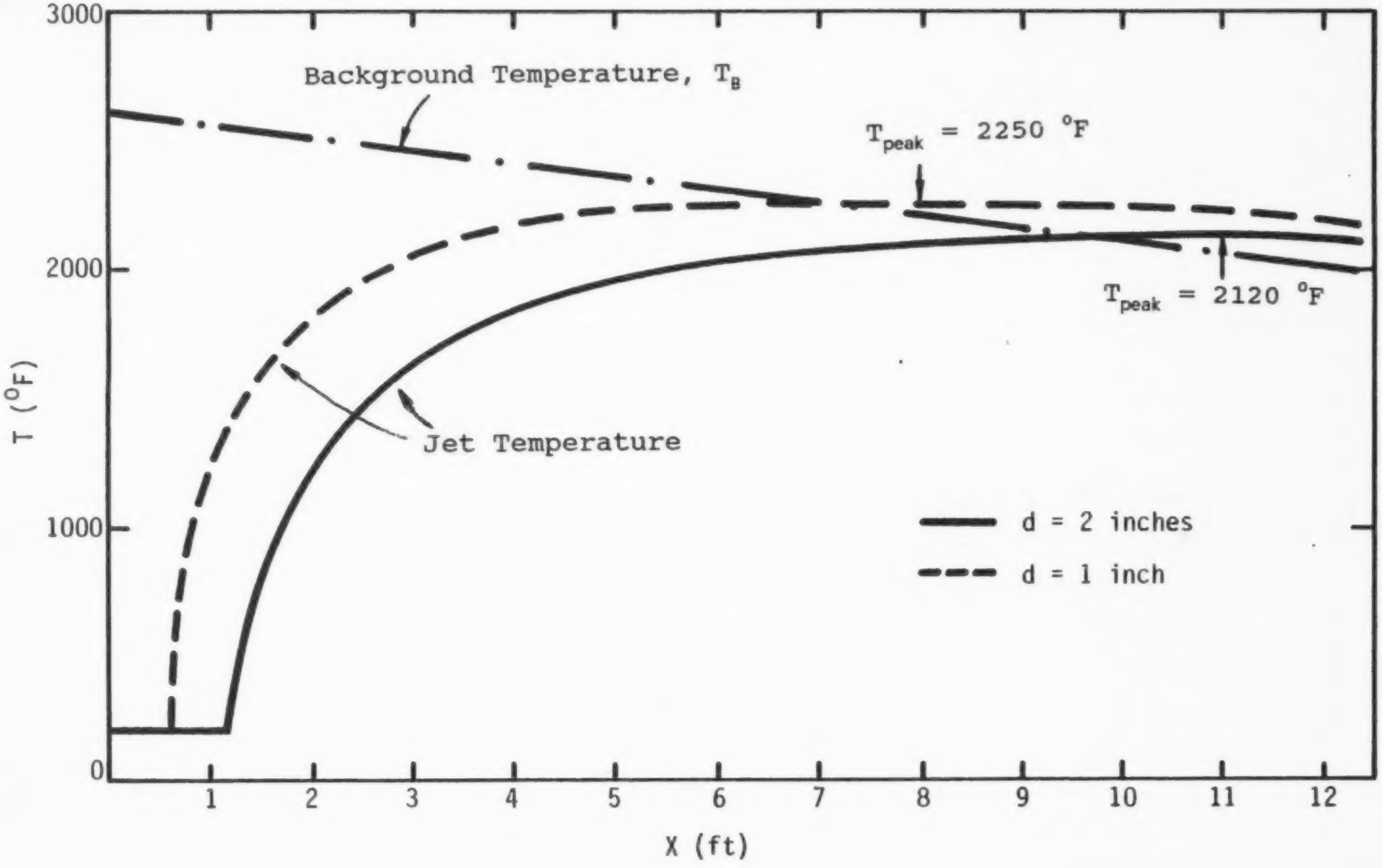

Figure 7-6. Calculated mean jet bulk temperatures as a function of time for 1-inch and 2-inch diameter single-pipe jets in an environment with falling background temperature T_B (initial T_B = 2600 °F) -- used in design of jet heating rate Tests 7 and 8.

Bulk jet velocities were used to compute the average temperature histories in the jets for Tests 7 and 8, and to determine the velocity and background temperature conditions for the test matrix. Figure 7-7 shows the calculated bulk temperature histories for the 2-inch jets at nozzle velocities of 50 and 100 ft/sec, in a furnace with an initial background temperature of 2500 °F. The plot on the left is an expanded-scale version of the first 0.1 sec of the longer-term plot on the right. The jet reaches the same peak temperature of 2040 °F at each of the velocities; but, as seen in the plot on the left, the high-velocity jet has a higher heating rate. The effect of doubling the velocity is to double the heating rate. Similarly, Figure 7-8 shows the calculated temperature histories for both 1- and 2-inch jets at different velocities and background temperatures, for combinations that result in a similar peak sorbent temperature of 2250 °F. It can be seen that the bulk heating rate for the 1-inch-diameter, 50 ft/sec jet is very similar to that for a 2-inch-diameter, 90 ft/sec jet, in addition to the similarity in peak temperature. Figure 7-9 shows similar calculations for different 2-inch jets which have approximately the same heating rate, but which reach different peak temperatures (2040 and 2250 °F). It is apparent that, by judicious selection of jet conditions and background temperature, the experiment can be designed in a manner which should permit separation of the effects of the different variables.

7.2.3 Cross-Flow Jet Injection

In addition to the co-flow tests, limited testing was performed with jets in cross-flow. The SWS configuration for this testing is illustrated in Figure 7-10. A jet was inserted through one of the existing ports in the SWS side wall, five feet downstream from the firing wall. This setup permitted operation as a double concentric jet, with a 4-inch diameter outer annular air jet (3.5-inch i.d.) surrounding a 1-inch diameter sorbent jet. Alternative-

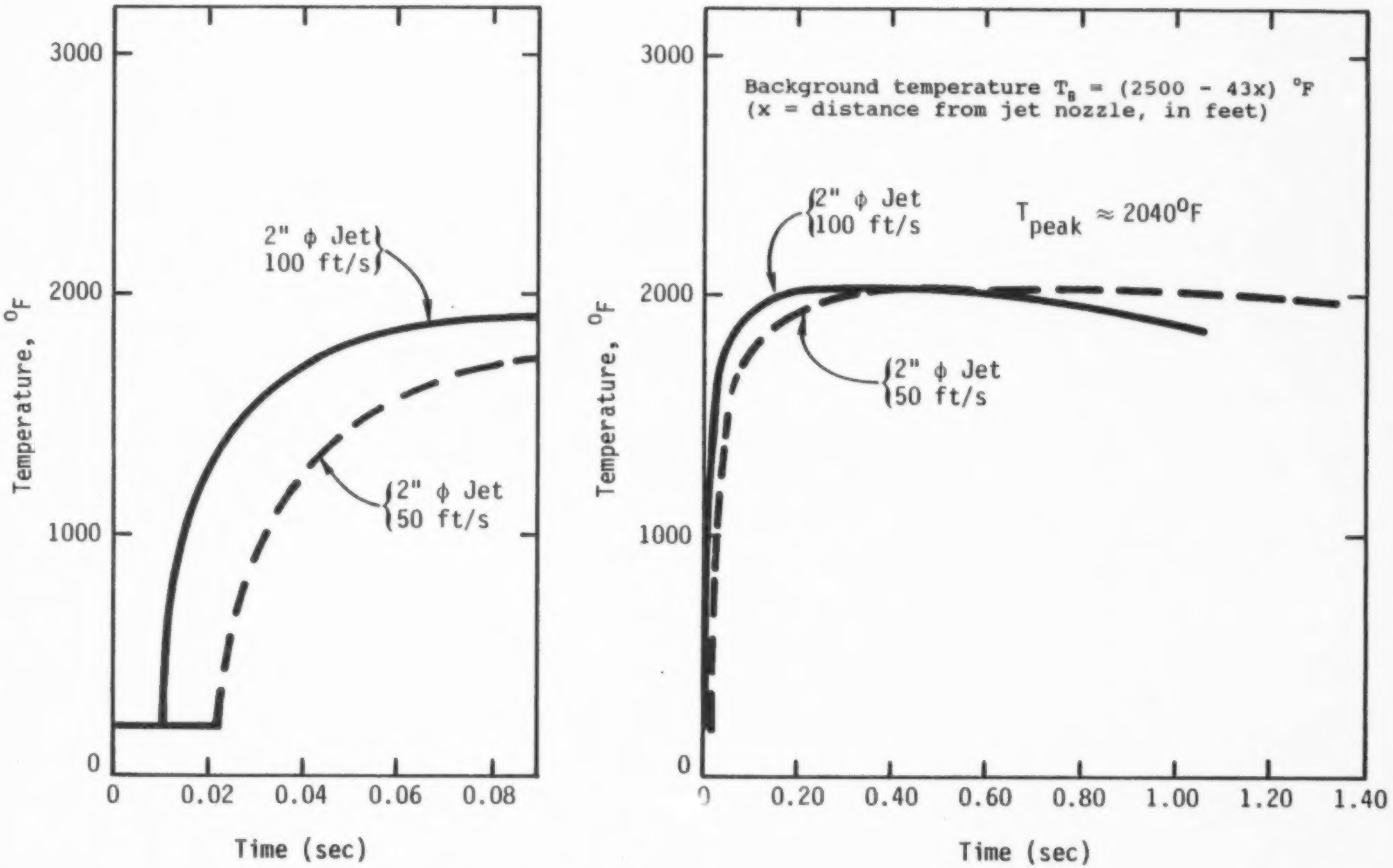

Figure 7-7. Calculated mean jet bulk temperatures as a function of time for 2-inch single-pipe jets at initial T_B = 2500 °F, for two values of jet velocity -- used in design of jet heating rate Tests 7 and 8.

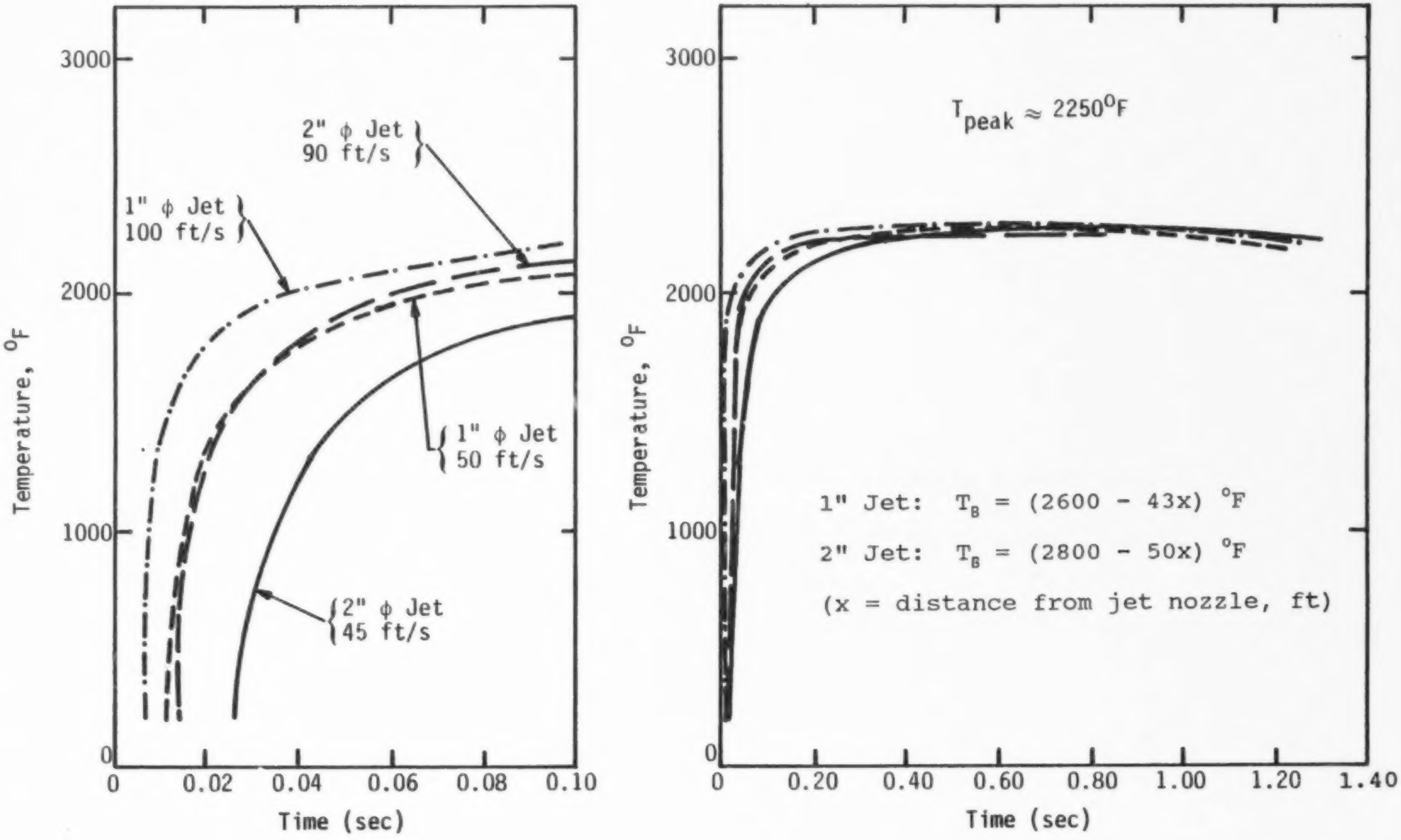

Figure 7-8. Calculated mean jet bulk temperature as a function of time for 1-inch and 2-inch single-pipe jets, for various jet velocities and background temperatures resulting in a peak sorbent temperature of about 2250 °F.

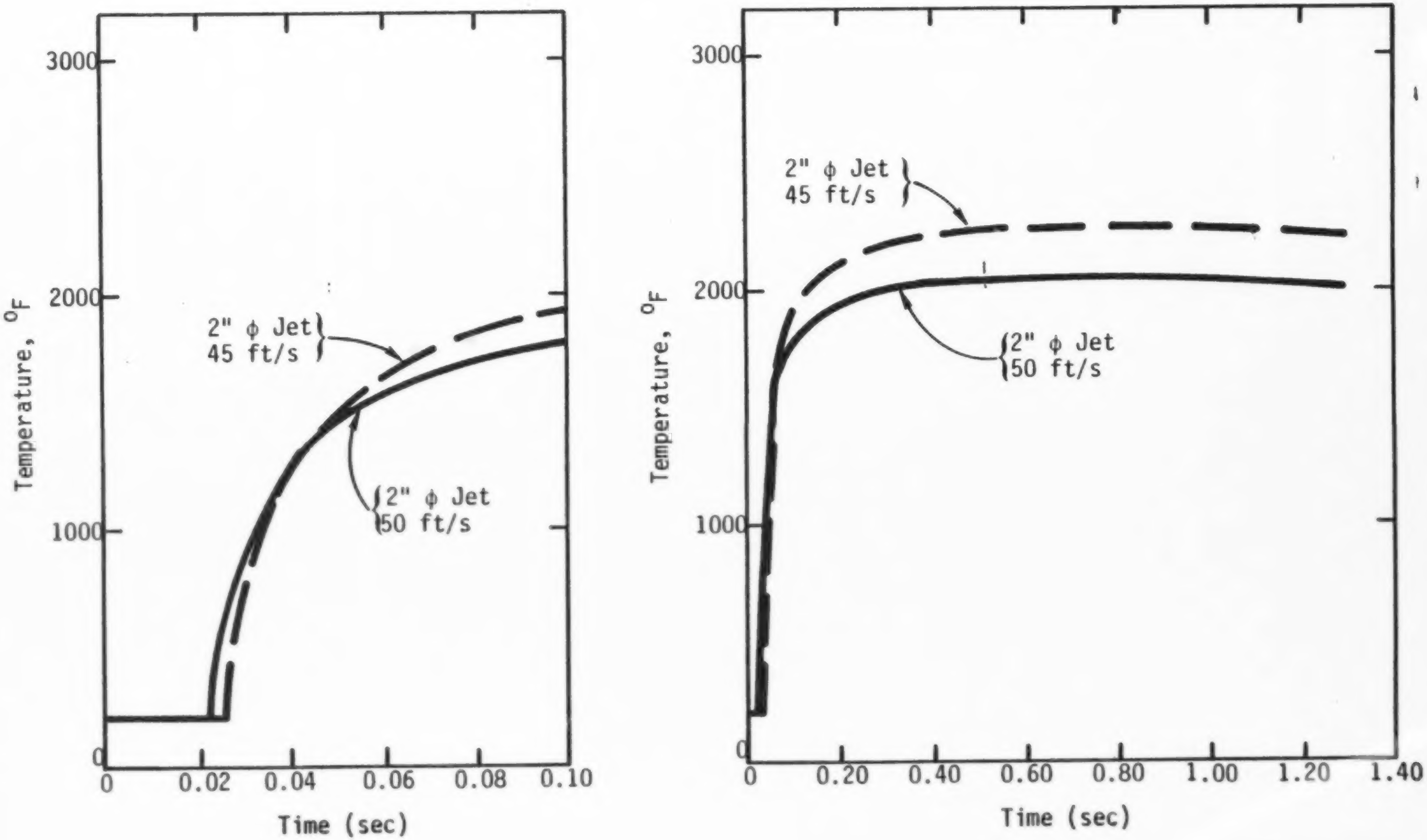

Figure 7-9. Calculated mean jet bulk temperature as a function of time for 2-inch single-pipe jets reaching peak sorbent temperatures of 2040 and 2250 °F at approximately the same heating rate -- used in design of heating rate Tests 7 & 8.

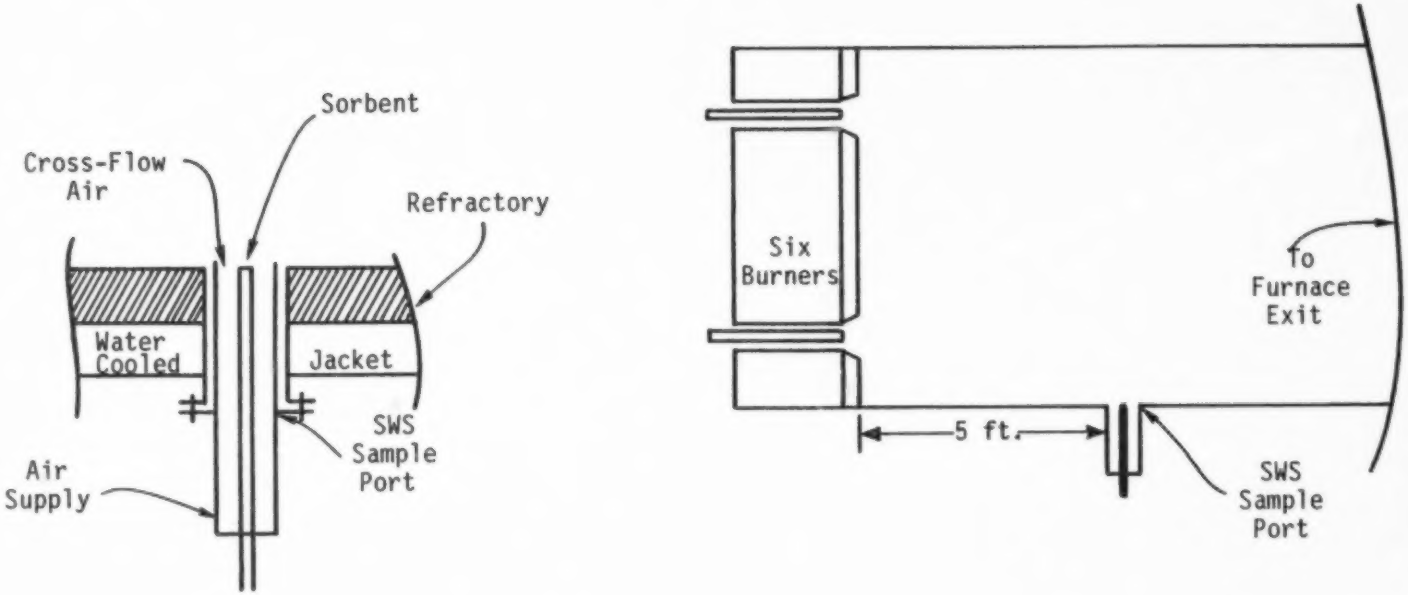
Sorbent
Cross-Flow Air
Refractory
Water Cooled
Jacket
SWS Sample Port
Air Supply
Six Burners
To Furnace Exit
5 ft.
SWS Sample Port

Figure 7-10. SWS arrangement for cross-flow sorbent injection into uniform gas flow field.

ly, the jet could be operated as a 1-inch single-pipe sorbent jet. The matrix for the cross-flow jet tests is given in Table 7-5. The variables included jet configuration, sorbent jet velocity, and annular air velocity.

7.3 Close-Coupled Precalciner

The purpose for the close-coupled precalciner was to provide a high-temperature environment where sorbent would be very rapidly heated (in an effort to improve reactivity with a very rapid heating rate caused by the high T_B). The precalcination would be followed by immediate quenching with dilution air in an effort to avoid sintering (i.e., to prevent the sorbent from seeing a high peak temperature close to the T_B in the calciner). A schematic diagram of the precalciner is shown in Figure 7-11. The unit consists of a cylindrical, refractory-lined chamber 12 inches inside diameter and 4 feet long. A swirl burner mounted on the left-hand end was fired with natural gas to produce a high-temperature environment inside the reactor. If necessary, the burner could be fired with oxygen-enriched air to increase temperature. The sorbent was fed into the calciner along a pipe on the centerline of the burner, thus passing directly through the center of the precalciner flame. At the exit from the calciner, additional quench and dilution air was introduced into the reactor through radial holes. The quenched sorbent then passed directly to the sorbent injector jet on the axis of the SWS furnace.

Four different versions of the precalciner were tested during these experiments. Two precalciners were built: one with high-alumina refractory (Greencast-94 from A. P. Green); the second with high-chromium refractory (Jade Pak-88-P from A. P. Green). Each of the calciners was made in two sections; one of these sections could be removed to reduce the length and thus reduce the residence time of the sorbent in the precalciner. All tests with the

TABLE 7-5. TEST MATRIX FOR CROSS-FLOW SORBENT JETS (UNIFORM FLOW FIELD)

Jet Configuration	Single Dense Jet	Co-Axial Jets
Test Fuel	Natural Gas + SO_2	Natural Gas + SO_2
Air Jet Diameter (in.)	-	3 1/2
Air Jet Velocity (ft/sec)	-	25, 50
Sorbent Jet Diameter (in.)	1	1
Sorbent Jet Velocity (ft/sec)	50	25, 50
Ca/S Ratio	1.0-3.0	1.0-3.0
Background Temperature (°F)	2200	2200

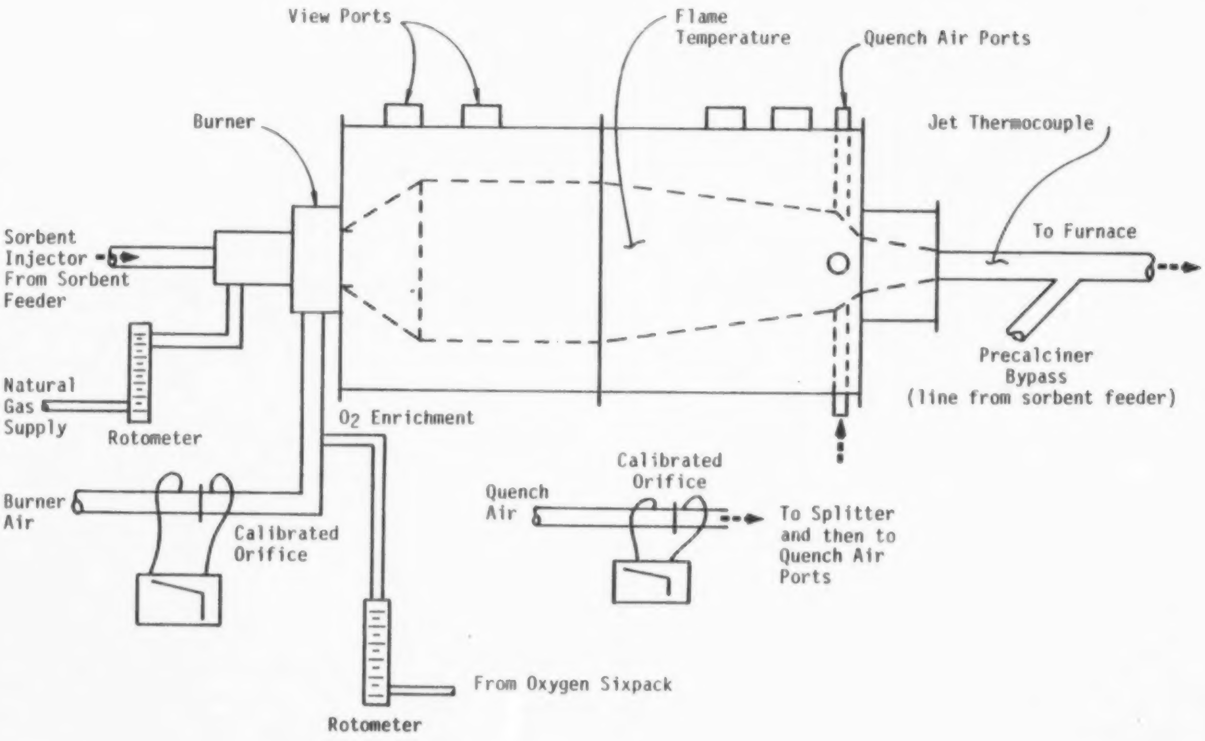
View Ports
Flame Temperature
Quench Air Ports
Burner
Jet Thermocouple
To Furnace
Sorbent Injector From Sorbent Feeder
Natural Gas Supply
Rotometer
Precalciner Bypass (line from sorbent feeder)
O_2 Enrichment
Calibrated Orifice
Quench Air
Burner Air
Calibrated Orifice
To Splitter and then to Quench Air Ports
From Oxygen Sixpack
Rotometer

Figure 7-11. Schematic for SWS precalciner.

precalciner were conducted with a 2-inch diameter jet injecting the sorbent from the calciner directly into the SWS, at a nominal jet velocity of 100 ft/sec. With these injection conditions, the mean residence time of the sorbent in the precalciner ranged from 0.2 to 1.0 seconds.

The test matrix for the precalciner studies in given in Table 7-6. The main parameters varied were: the precalciner refractory type and sorbent residence time (long vs. short precalciner); the precalciner temperature (flame temperature); and the calcium-to-sulfur mole ratio being fed to the SWS. Other variables were the SWS background temperature, and the temperature and velocity of the sorbent jet being fed to the SWS. It was intended to maintain the jet temperature at 1000 °F, the SWS background temperature at 2400 °F, and the jet velocity at 100 ft/sec. However, this proved to be impossible, because the precalciner added a variable amount of heat into the sorbent jet depending upon calciner operating conditions. The sorbent in all cases was Vicron limestone.

7.4 Measurements for Sorbent Jet Studies

For the most part, the degree of sorbent activation -- the prime result of interest in all of the injection tests -- was determined indirectly through measurements of SO_2 in the exhaust (i.e., the extent of sulfur capture). In a limited number of runs, solids samples were extracted from the SWS furnace for direct surface area analysis. For runs where surface area samples were extracted, the natural gas to the SWS burners was not doped with SO_2, so that the sorbent would not lose surface area due to the sulfation reaction. Also, in some cases, in-furnace temperature profiles were measured, since the time-temperature history of a sorbent (including true peak temperature) is key in determining its sulfur capture performance. A mathematical model for sulfur capture (relating sulfur capture to a number of variables,

TABLE 7-6. TEST MATRIX FOR CLOSE-COUPLED PRECALCINER

Precalciner	Regular Refractory		Chrome Refractory	
	Short	Long	Long	Short
Flame Temp °F	2950	2000 2600	2900 3000	2000 2500 2900
Jet Temp °F	1000	800-1100	1300-2000	1000-1300
Background Temp °F	2400	2300-2500	2300	2300
Nominal Residence Time, sec	0.22	0.75	0.5-1.0	0.25
Jet Velocity ft/s	150	90-120	150-200	150-200
Ca/S Molar Ratio	1.7-1.8	0.6-2.9	1.0-2.5	0.4-2.2
Special Measurements	Calciner Bypassed Surface Area	Calciner Bypassed	Calciner Bypassed Surface Area	Calciner Bypassed Surface Area

Jet Diameter: 2-inch
Sorbent Type: Vicron

including the initial sorbent reactivity and the time-temperature profile) was utilized to aid in interpreting the results. The measurements conducted on control (input) and response (output) variables during the sorbent injection testing are summarized in Table 7-7.

TABLE 7-7. MEASUREMENT FORMAT FOR SORBENT INJECTION TESTS

Inputs		Outputs	
Parameter	Method	Parameter	Method
Routine		Routine	
Burner conditions --burner settings, fuel flows, air flows	Same as Table 2-4	Burner performance --combustion products in flue gas, NO/NO_x	Same as Table 2-4
Sorbent injection location	Manual	SO_2 in stack gas (primary measure of sorbent performance)	DuPont ultraviolet
Background temperature and flow field (jet experiments)		Sorbent temperature history	
- Fuel flow rate to gas burner	Laminar flow element and calculation from fuel composition, air flow and excess O_2	- Background temperature in furnace measured adjacent to jet exit	Type "S" suction pyrometer
- Air flow rate to burners	Venturis	- Furnace stack temperature	Thermocouple
Detailed		Detailed	
Sorbent jet velocity	Venturi on air line to sorbent jet	Sorbent surface	B.E.T. analysis on extracted samples (nitrogen quench sampling probe)
Annular air jet velocity	Venturi on air line to annular jet		
Sorbent flow rate	Volumetric feeded	In-furnace temperature profiels	Type "S" suction pyrometer
Sorbent composition and size distribution	Manufacturers specifications and EER in-house sizing (Sedigraph)	Solids sulfur content (for sulfur balance)	Ultimate analysis grab sample

8.0 SORBENT INJECTION WITH LARGE DOUBLE CONCENTRIC JETS

The experiments discussed in this section focussed primarily on sorbent injection through double concentric (co-axial) jets -- i.e., jets in which the sorbent jet is surrounded by a larger annular air jet. As discussed in Section 6, double concentric jets are of particular interest as a means of thermally protecting sorbent which is injected in the high-temperature region near the burners. The double concentric jets tested here were relatively large, 6 to 12 inches in diameter. A limited amount of the testing discussed in this section (8.2.4) addresses 1-inch single-pipe sorbent jets (i.e., sorbent jets without a surrounding air jet).

Earlier testing on other projects showed that increased sorbent jet velocity could increase sulfur capture, when the sorbent jet was along the axis of the outboard tertiary air port in an externally-staged distributed mixing burner (DMB). This injection method represents a double concentric jet. It was believed that the tertiary air provided thermal shielding of the sorbent to protect it from overheating in the near-flame region, and that the changes in capture with sorbent jet velocity might be due to the changes caused in sorbent heating rate. This earlier DMB experience thus provided the impetus for testing the double concentric jet configuration in conjunction with this internally-staged burner project, and for this study of the ability to control sorbent heating rate using double concentric jets.

For a preliminary assessment of the double concentric jet concept in this study, brief tests were conducted injecting Vicron limestone into the SWS while operating with a 10 x 10^6 Btu/hr burner referred to as the V-10 burner. The V-10 burner was an externally-staged DMB, similar to the internally-staged LV1 burner in many respects (low secondary air velocity, dual secondary air registers), but including four external 12-inch i.d. tertiary air ports equally spaced around (outside) the burner quarl. One-inch diameter sorbent jets were installed along the axis of the four tertiary air ports, so that the tertiary air served as an annular sheath for the sorbent jet, as in the case of the earlier tests mentioned in the preceding paragraph. In these tests, 30 percent of stoichiometric air was being fed through the tertiary ports; 90 percent of stoichiometric air was fed as primary and secondary air through the burner throat, for a total stoichiometry of $SR_T = 1.2$. Under these conditions, the tertiary air velocity was 37 ft/sec. The sorbent jet velocity was varied between 50 and 200 ft/sec. In a few tests, only two of the four tertiary ports were used for sorbent, in order to check distribution effects. The results of the V-10 testing are presented in Figure 8-1. The results indicate that: a) at constant annular air velocity, capture increases with increasing velocity of the central sorbent jet (i.e., with more rapid mixing); and b) at the high sorbent velocity (200 ft/sec), captures are almost 50 percent at a Ca/S of 2, among the best that have been observed with Vicron. (The low furnace exit temperature might be playing a role in the high removal, reducing thermal deactivation). These results confirm that double concentric jets might indeed offer the potential for high captures and heating rate control during near-burner injection. Hence, it was decided that double concentric jets should receive attention during the sorbent jet experiments under this study.

8.1 Jet Experiments in Non-Axisymmetric Configuration

The initial, limited series of tests with double concentric jets was conducted with the SWS configuration shown in Figure 7-3, and the test matrix shown in Table 7-2. The one jet was located 21 inches below the SWS axis, below the axially-mounted LV1 burner burning coal or oil. The 1-inch sorbent jet was centered inside either a 10-inch or 12-inch annular air jet; the air jet sizes were selected as representative of the size of tertiary air ports on a full-scale (100×10^6 Btu/hr) DMB. The non-uniform flow field

V-10 Burner, Load = 10 x 10^6 Btu/hr
SR_T = 1.2, SR_{Burner} = 0.9
Fuel: Utah coal (baseline SO_2 level = 660-685 ppm @ 0% O_2)
Sorbent: Vicron 45-3
Furnace exit temperature: 1880-1940 °F (avg. = 1896 °F)

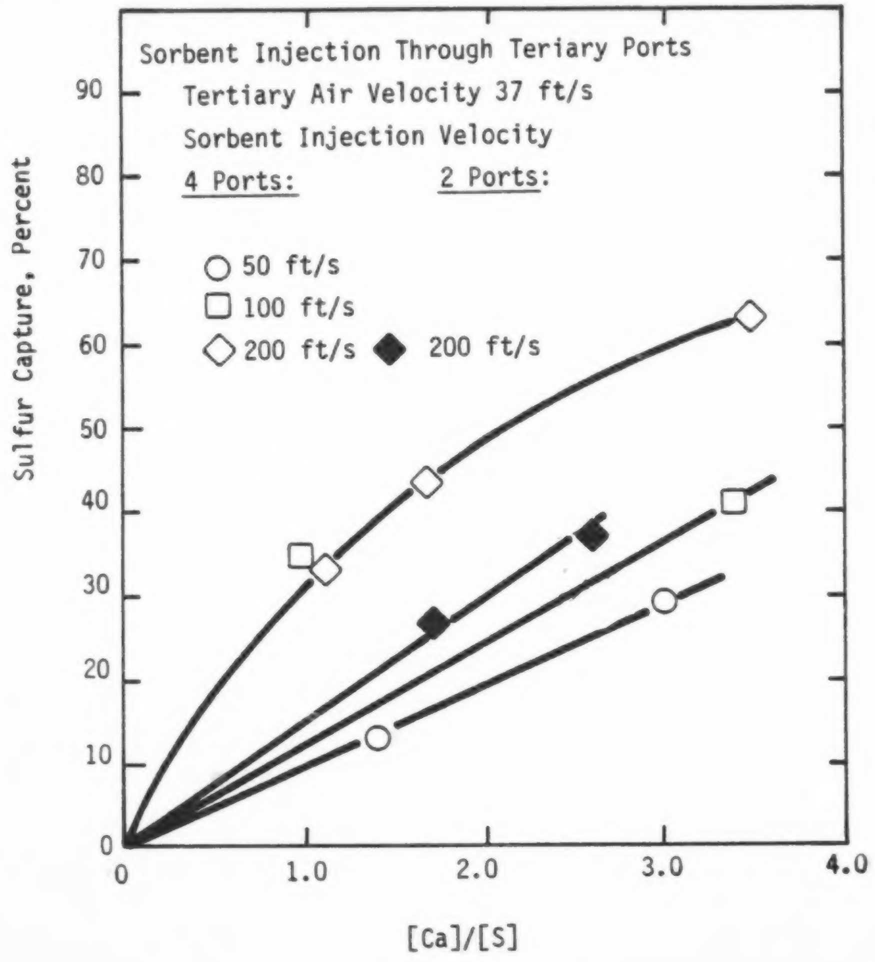

Figure 8-1. SO_2 capture with double concentric jets around V-10 externally-staged distributed mixing burner -- effect of sorbent injection velocity

created by this configuration was considered acceptable for this initial screening. The intent was to assess whether large changes in major variables (temperature, momentum, etc.) would significantly influence sorbent reactivity. The tests burning SO_2-doped #2 oil (yielding a baseline SO_2 emission of 800 ppm in the flue gas without limestone injection) were intended to assess performance in an ash-free environment. The tests with Utah coal (yielding a baseline SO_2 of 660-685 ppm without limestone) were conducted to assess ash effects. The sorbent reactivity was generally measured by the amount of SO_2 captured, although sorbent surface area was measured in some cases. Vicron 45-3 limestone was the sorbent utilized in all cases.

Results with the 12-inch annular air jet during operation burning oil are presented in Figure 8-2. In these tests, the actual central sorbent jet velocity was varied between 16 and 138 ft/sec, and the annular air jet velocity was varied between 20 and 80 ft/sec; the ratio of the air jet velocity to the sorbent jet velocity over this series of tests varied from 0.2 to 1.3. As apparent from the figure, all of the concentric jet velocity combinations yield essentially the same SO_2 capture performance: between 17 and 20 percent removal at a Ca/S of 2. Under these conditions, sorbent performance was insensitive to both sorbent velocity and annular air velocity.

Results with the 10-inch annular air jet during oil combustion are shown in Figure 8-3. With this jet, sorbent velocities were varied between 33 and 115 ft/sec, while annular air velocities were 33 and 60 ft/sec; the air-to-sorbent velocity ratio varied between 0.5 and 1.8. SO_2 captures are about the same as with the larger air jet, varying between 15 and 18 percent at Ca/S = 2. Again, sorbent performance seems insensitive to jet velocities (perhaps a slight increase with increased air velocity).

Load = 10 x 10^6 Btu/hr
Fuel: No. 2 oil doped with SO_2, baseline SO_2 in flue gas = 800 ppm (as measured)
Sorbent: Vicron 45-3

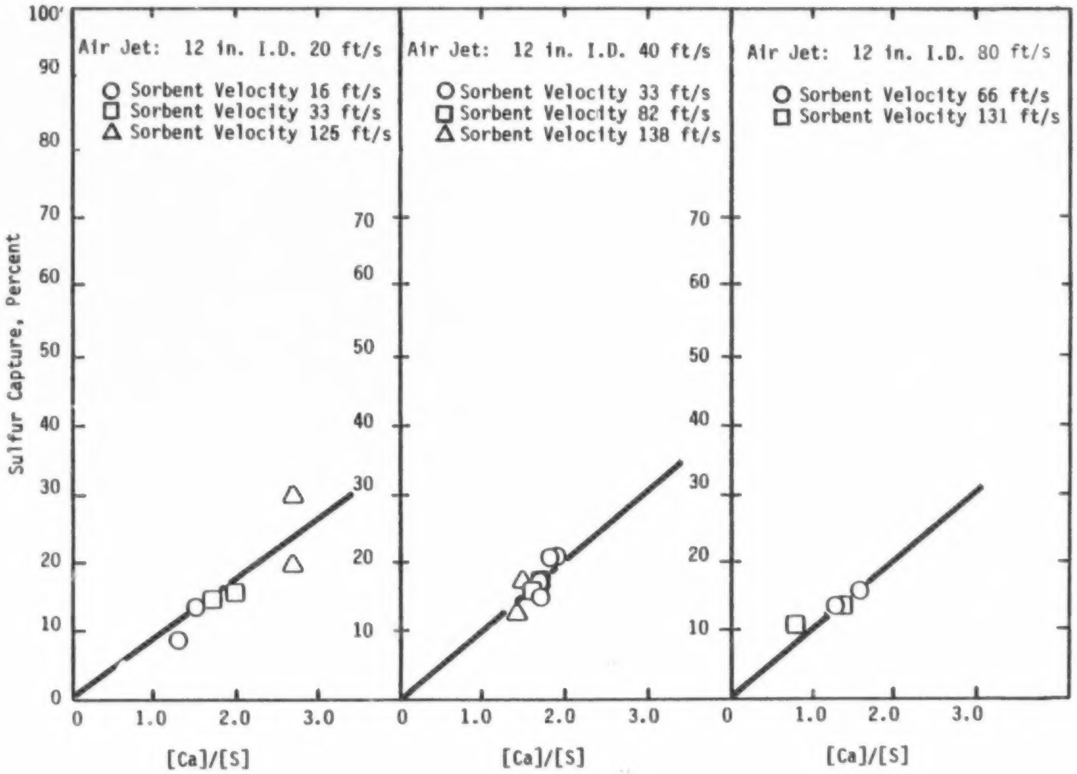

Figure 8-2. SO_2 capture with double concentric jets during preliminary (non-axisymmetric) testing -- effects of sorbent jet velocity and annular air jet velocity, with 12-inch air jet (oil firing).

Load = 10 x 10^6 Btu/hr
Fuel: No. 2 oil doped with SO_2, baseline SO_2 in flue gas = 800 ppm
Sorbent: Vicron 45-3

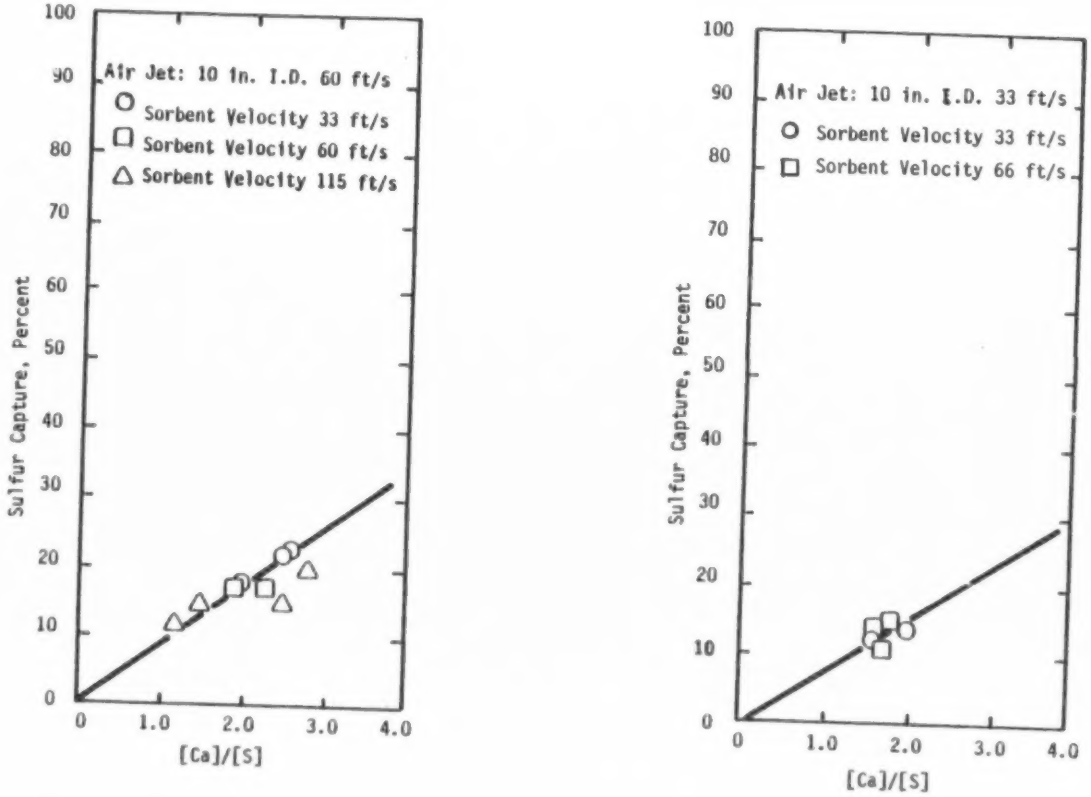

Figure 8-3. SO_2 capture with double concentric jets during preliminary (non-axisymmetric) testing -- effects of sorbent jet velocity and annular air jet velocity, with 10-inch air jet (oil firing).

During one of the tests with the 10-inch air jet (sorbent velocity 60 ft/sec, air velocity 60 ft/sec), SO_2 doping of the oil was stopped. This was done so that the calcined sorbent in the furnace would not lose surface area due to the sulfation reaction. Solids samples were extracted from the furnace with a nitrogen quench probe for direct measurement of in-situ calcine surface area. Samples were taken from inside the furnace (9 feet from the firing wall, approximately half the length of the SWS), and also from the flue gas ducting. Two separate samples drawn from within the furnace yielded surface areas of between 10 and 12 m^2/g. Samples taken from the stack had surface areas of 3 to 4 m^2/g, suggesting that much of the in-furnace area had sintered away during the several seconds of residence time between mid-furnace and the duct-work sampling port.

To understand the sorbent thermal history during the above run where surface areas were determined, radial temperature measurements were made across the SWS at various axial distances away from the firing wall. These measurements indicated that the center-line temperature of the sorbent jet appeared to reach a peak of 2100 to 2375 $^{\circ}F$ at about 8 feet into the SWS; this range in the temperature probably is the result of fluctuations in the jet trajectory/jet mixing or in the flame shape at the 8-foot point, or perhaps due to the difficulties in radially positioning the temperature probe precisely on the jet center-line. Background temperatures in the SWS (along the burner axis) appear to have been about 2900 $^{\circ}F$ at the 5- to 8-foot point, and to have been beginning to drop at greater distances, due to temperature losses through the SWS walls and due to the sensible heat effects of the large mass of (relatively cool) annular jet air. Possibly, due to the large amount of annular air in all of these runs, all of the jets tested were effective at protecting the sorbent from near-flame temperatures, and at reducing bulk background temperatures such that the sorbent did not see particularly high peak temperatures in any of the cases; this could explain the similarities in sulfur removal performance from run to run.

Following the testing with oil, described above, a few tests were run with the 10-inch annular air jet during combustion of Utah coal, in order to evaluate coal ash effects. A single annular air jet velocity of 33 ft/sec was used, and the sorbent jet velocity was varied between 16 and 115 ft/sec (an air-to-sorbent jet velocity ratio ranging between 0.3 and 2). The coal results are shown in Figure 8-4, together with the 10-inch jet results shown previously with oil firing. As in the case of the oil firing, the sorbent performance with coal firing appeared to be insensitive to variations in jet velocity. Thus, as in the oil case, the sorbent appears to be being equally well-protected from high flame temperatures (and from any coal ash deactivation) regardless of velocities, and equally activated despite any differences in heating rate. However, the surprising result is that there is a statistically significant improvement in sorbent performance with coal, compared to oil (25 percent removal at Ca/S = 2 with coal, versus 15-18 percent removal with oil). This improvement with coal could be due to the lower peak flame temperatures in the coal flame relative to the oil flame (thus potentially reducing the peak temperature seen by the sorbent). It could also be due to reactivity enhancement by minerals present in the coal ash.

These non-axisymmetric jet experiments with the LV1 burner showed no significant effect of double concentric jet velocities, unlike the earlier testing on the V-10 DMB which has suggested some effect. It is noted from Figure 8-1 that -- at the V-10 conditions similar to those used in these LV1 jet experiments (annular air velocity 33-37 ft/sec, sorbent jet velocity around 100 ft/sec or less, operation with Utah coal) -- SO_2 removals were fairly similar (25 percent removal at Ca/S = 2 in the LV1 jet experiments, 20-25 percent removal with the V-10). It was only with the 200 ft/sec

Load = 10 x 10^6 Btu/hr
Fuel: Utah coal (baseline SO_2 level = 660-685 ppm
corrected to 0% O_2, 475 ppm measured)
Sorbent: Vicron 45-3

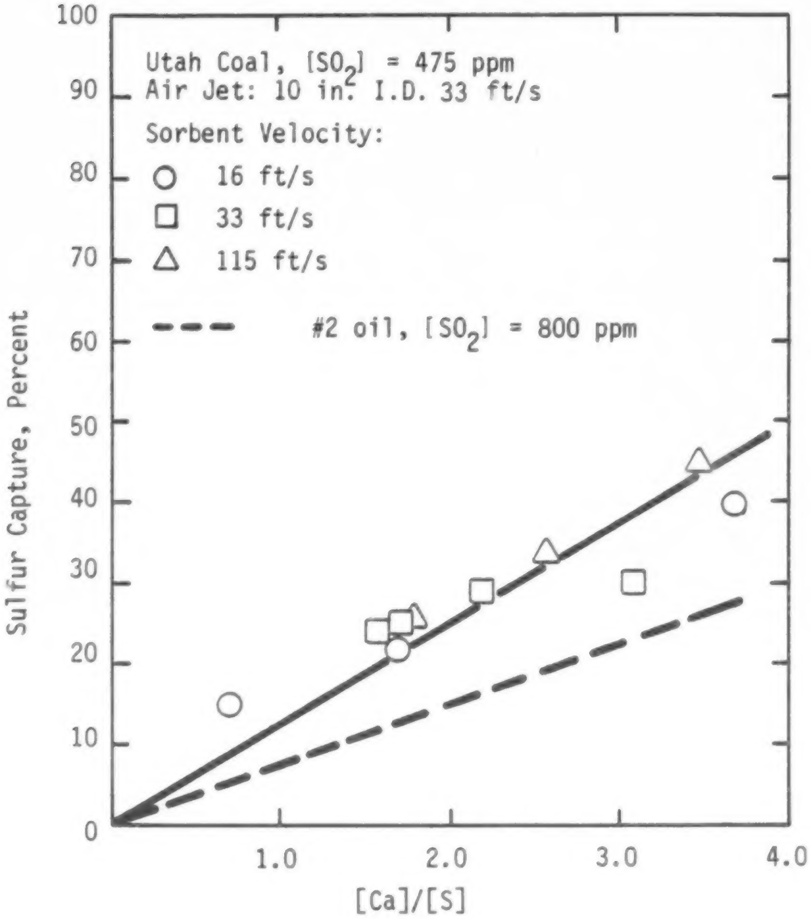

Figure 8-4. SO_2 capture with double concentric jets during preliminary (non-axisymmetric) testing -- effects of sorbent and annular air jet velocities, and effect of coal vs. oil, with 10-inch jet (coal firing)

sorbent jet velocity that the V-10 testing showed marked improvement in performance -- and sorbent velocities that high were not included in the LV1 jet experiment.

While these preliminary non-axisymmetric jet experiments provided a useful initial screening of double concentric jet parameters, they did not permit a "clean" assessment of the mixing patterns and heating rate in the jet. Normal entrainment of bulk gases into the jet was constrained both above and below: underneath the experimental jet was the furnace wall; and above the jet was the 10 x 10^6 Btu/hr burner which was creating its own distinct flow patterns in the furnace. In some cases, the flame from the burner could be seen to bend towards the air jet and engulf it. Clearly, this must have impacted the jet mixing processes and the sorbent heating rate in some undefinable manner. Accordingly, the subsequent jet experiments were conducted using an SWS configuration which provided a uniform bulk gas flow field, with an axisymmetric jet.

8.2 Jet Experiments with Axisymmetric Configuration

Following the preliminary screening of double concentric jets, the SWS was modified to provide the configuration illustrated in Figure 7-4. As discussed in Section 7.2.2, this configuration was intended to permit the jet to issue into the most uniform bulk flow field possible, so that jet mixing and particle heating rate would be governed by fundamental entrainment and heat transfer phenomena, and so that undefinable external irregularities would be minimized. For these reasons, this test series was referred to as the "clean jet" series.

The portion of the clean jet testing discussed in this section addressed primarily double concentric jets. (See the test matrix in Table 7-3; the primary single-pipe jet tests, Tests No. 7 and

8 in that table, are discussed in Section 9.) Emphasis here was placed on co-flowing jets (jets injected axially in the same direction as the bulk flow), since co-flowing jets provide the least complicated case for fundamental interpretation. More limited testing was performed in cross-flow; cross-flow jets are representative of what will likely often be employed in full-scale sorbent injection systems. Key variables in this testing were jet velocities, jet diameters, and background (bulk gas) temperatures. A primary objective of this testing was to determine whether heating rate influences sorbent reactivity. It was also desired to better understand the potential of double concentric jets.

The "background gas temperature" T_B cited here is defined as the temperature measured by a suction pyrometer 2 feet downstream from the jet exit and 1.75 feet from the jet center-line; the radial temperature profile at this axial location was uniform (± 20 F°). This background temperature was controlled by varying the stoichiometry and flowrate of the gas burners. The background temperature varied along the axial length of the furnace, for two reasons: 1) despite the fact that maximum insulation was used, the temperature fell with distance due to heat loss to the ambient; and 2) the jets themselves -- particularly the larger double concentric jets -- constituted a meaningful fraction of the total bulk gas flow, so that the cold jets could detectably reduce the bulk temperature as the jets and the bulk flow mixed. This axial temperature gradient varied from jet to jet, since the larger, higher-velocity jets introduced a greater amount of cold air than did the smaller, lower-velocity jets. As a result -- while the controlled "background temperatures" at the front of the furnace were varied between 2200 and 2800 °F -- the furnace exit temperatures varied between 1300 and 2400 °F.

Most tests were made using SO_2-doped natural gas as the burner fuel. In a few cases, coal was added to the gas flames in order to assess coal ash effects. The SO_2 loading in the natural gas yielded a baseline (no limestone) flue gas SO_2 concentration between 700 and 970 ppm as measured. The major output variable measured was SO_2 concentration in the flue gas (degree of sulfur capture), as an indication of sorbent reactivity. In a few cases, solid samples were extracted (while burning un-doped natural gas) for direct measurement of in-situ surface area and degree of calcination. The sorbent (in the tests described in Section 8) was Vicron 45-3 in all cases.

8.2.1 Double Concentric Jets in Co-Flow

In the testing of double concentric jets in co-flow, the annular air jet diameter was varied between 6 and 12 inches, the annular air velocity (V_A) between 30 and 60 ft/sec, the sorbent jet velocity (V_S) between 50 and 100 ft/sec, and the background temperature (T_B) between 2200 and 2800 $^{\circ}$F. The sorbent jet diameter was 1 inch in all cases. This testing includes Tests No. 1, 2, 3, 5 and 6 in Table 7-3.

The results with the 12-inch annular air jet are presented in Figure 8-5. (All tests with this jet diameter were performed at an annular air velocity of 30 ft/sec, since higher values of V_A with this large jet resulted in too great a jet mass flow for meaningful testing in the SWS. Even at 30 ft/sec, the mass flow of the jet -- 1.0 lb/sec -- was fairly large compared to the background gas flow -- 1.7 lb/sec -- thus exhibiting a substantial cooling effect on the furnace.) As observed in previous double concentric jet tests, sulfur capture in Figure 8-5 was insensitive to jet velocity; variations in V_S between 50 and 100 ft/sec did not significantly affect capture. However, background temperature did affect capture; removal was about 36 percent at Ca/S = 2 at a T_B of 2600 $^{\circ}$F, but only 20 percent at T_B = 2200 $^{\circ}$F. It would be suspected that this effect of T_B was a result of depressed temperatures in

Fuel: Natural gas + SO_2 (baseline SO_2 without sorbent = 653-739 ppm as measured)
Sorbent: Vicron 45-3
Furnace exit temperature: 1715 °F (T_B = 2600 °F)
1450 °F (T_B = 2200 °F)
Annular air jet: 12 inches (11.75 inch i.d.)
Annular air velocity V_A: 30 ft/sec

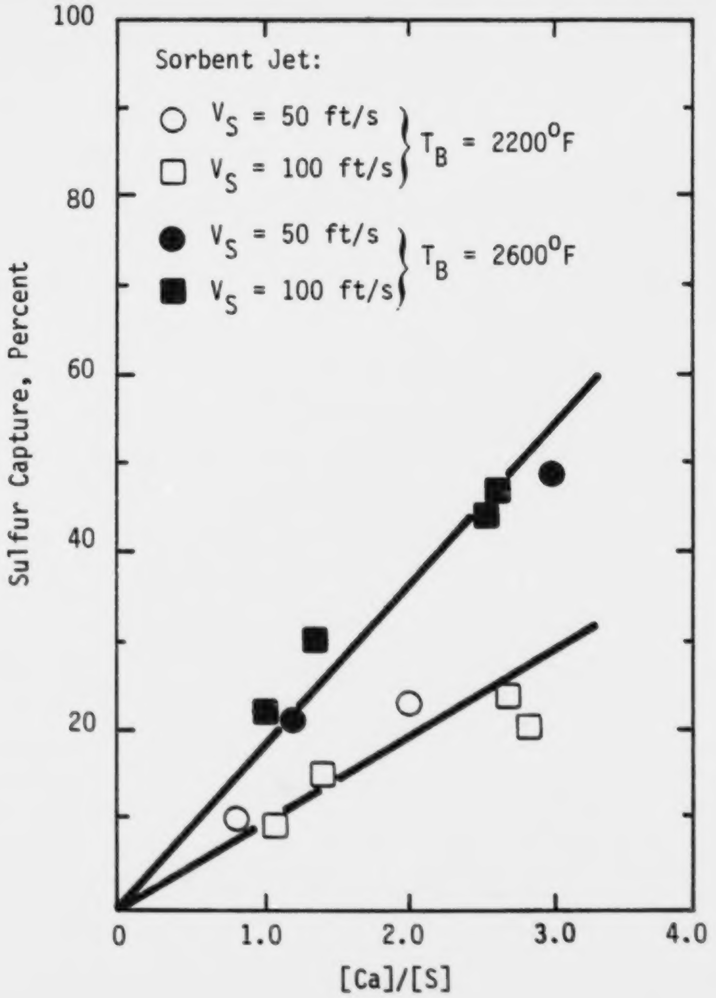

Figure 8-5. SO_2 capture with double concentric jets in uniform flow (axisymmetric) testing -- 12-inch annular air jet (co-flow).

the 2200 °F case. At T_B = 2600 °F with this jet, the furnace exit temperature was 1715 °F; at T_B = 2200 °F, the exit was only 1520 °F, due to the cooling effect of this large jet. It would be suspected that, in the 2200 °F case, the bulk of the sorbent might not have had much residence time in the sulfation window (2250 - 1750 °F), and might not even have become fully calcined.

The temperature measurements in the furnace for this jet confirm the suspicion that sorbent temperatures were depressed. Figure 8-6 shows -- in the upper pair of graphs -- the radial temperature profile at various axial distances along the 17-foot-long SWS. The lower pair of graphs shows these data in terms of jet center-line temperature as a function of axial distance. These data show that this large jet required almost the full length of the furnace to mix fully, and that the sorbent particles in the very center of the jet would have seen, as their peak temperature, the fairly low furnace exit temperature. Of course, the particles on the fringes of the jet would have experienced the somewhat higher upstream temperatures, accounting for much of the sulfur capture that was obtained. Thus, the performance difference between the two T_B levels in the case of the 12-inch annular jet was due to the fact that, at T_B = 2200 °F, many more of the particles spent most (or all) of their residence time at reduced temperatures where sulfation kinetics are relatively slow. The performance difference between the two T_B levels is therefore not the result of heating rate effects, but is an artifact of this experimental system.

The sulfur capture obtained at T_B = 2600 °F with this jet (36 percent at Ca/S = 2) was higher than the 20-25 percent capture seen with any of the jets during the preliminary tests (Section 8.1). This is probably because the temperatures seen by much of the sorbent with this jet at that T_B were sufficiently low to reduce sintering (relative to the runs in Section 8.1), but were also

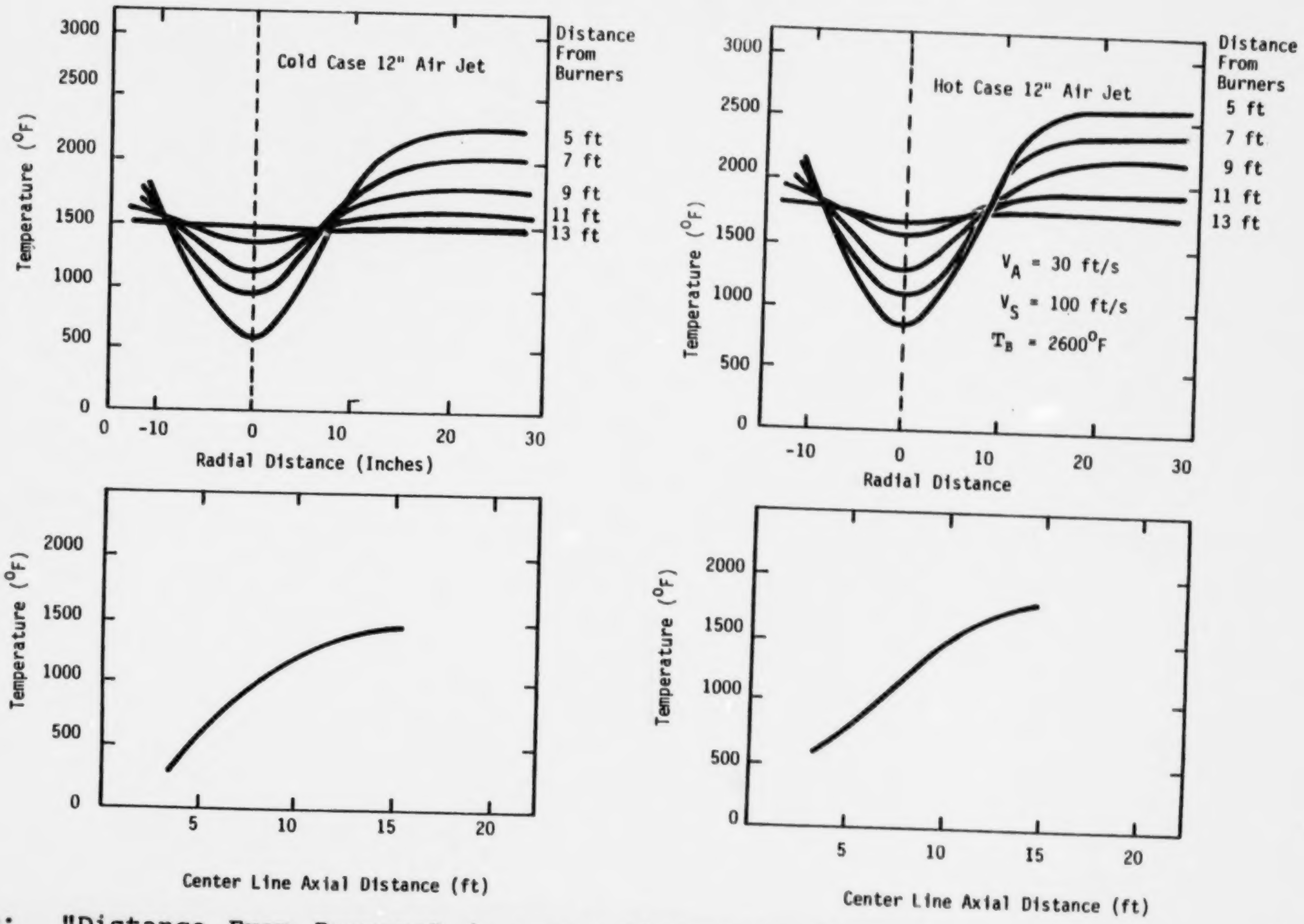

Note: "Distance From Burners" in upper figures is distance from SWS firing wall; "Center-Line Axial Distance" in lower figures is distance from end of sorbent jet (3 feet into SWS from firing wall).

Figure 8-6. Radial and axial temperature profiles for the 12-inch double concentric air jet

sufficiently high to give a high degree of calcination (activation) and reasonable sulfation kinetics.

The results for the 10-inch annular air jet are presented in Figure 8-7. At the lower annular air velocity (30 ft/sec), sorbent performance was insensitive to V_S (between V_S values of 50 and 100 ft/sec), as in the prior tests. But in this case, unlike the 12-inch air jet, performance also seems to be insensitive to T_B between 2200 and 2600 °F. In all cases at V_A = 30 ft/sec, sulfur capture with the 10-inch air jet (33 percent removal at Ca/S = 2) was comparable to that seen at the best conditions in the 12-inch jet. Furnace exit temperatures were 1540 °F in the case of T_B = 2200 °F, and 1920 °F in the case of T_B = 2600 °F at V_A = 30 ft/sec; therefore, it would seem that the sorbent in the low T_B case would have seen depressed temperatures, as it had with the 12-inch jet, and captures should again have been low at 2200 °F. The fact that captures with the 10-inch jet at low T_B were as high as they were with the high T_B suggests that, in the 10-inch case, more of the particles were experiencing peak temperatures greater than the furnace exit temperature, and longer residence time in the sulfation window, compared to the low-T_B 12-inch case. This would be consistent with the expectation that the 10-inch jet, being of lower mass at a given velocity, would mix with the bulk gases at a shorter distance into the SWS.

At the higher annular air velocity (60 ft/sec) with the 10-inch jet (the right-hand graph in Figure 8-7), the effects of T_B again become apparent. At the higher T_B (2400 °F in this case), removals were relatively high as before (33 percent capture at Ca/S = 2), and independent of V_S. But at low T_B (2200 °F), removals once more fell (to 13 percent at Ca/S = 2, insensitive to V_S), the lowest levels observed during the jet experiments. The furnace exit temperature in this case (V_A = 60 ft/sec, T_B = 2200 °F) was the lowest of any of the jet tests (1375 °F); clearly, the poor per-

Fuel: Natural gas + SO_2
Sorbent: Vicron 45-3

Air Jet: 10 inches (9.75 in. i.d.)
V_A = 30 ft/sec
Furnace exit temp: 1920 °F (T_B = 2600 °F)
1540 °F (T_B = 2200 °F)
Baseline SO_2 = 741-823 ppm as measured

Air Jet: 10 inches (9.75 in. i.d.)
V_A = 60 ft/sec
Furnace exit temp: 1690 °F (T_B = 2400 °F)
1375 °F (T_B = 2200 °F)
Baseline SO_2 = 582-630 ppm

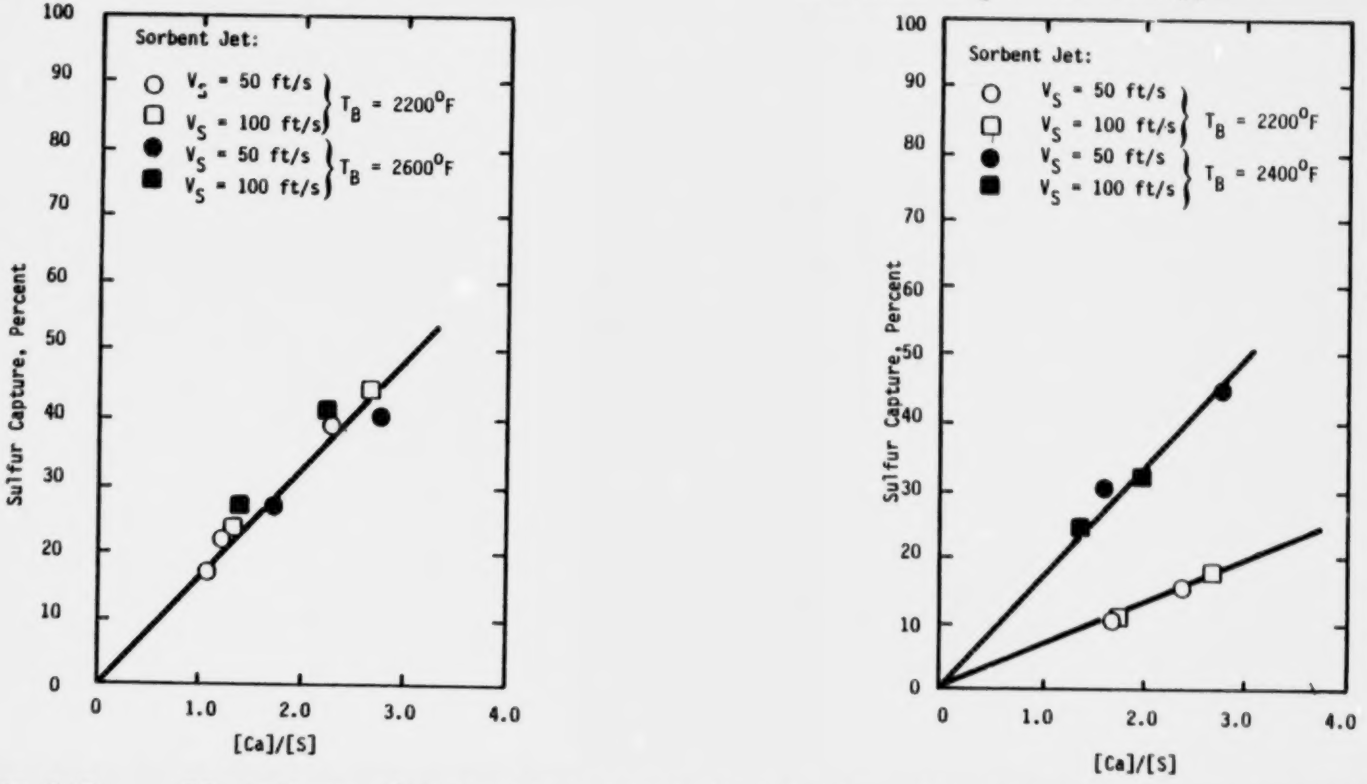

Figure 8-7. SO_2 capture with double concentric jets in uniform flow (axisymmetric) testing -- 10-inch annular air jet (co-flow).

formance was resulting because most of the sorbent was experiencing temperatures below the sulfation window. The large mass of cold air injected through the 10-inch high-velocity jet -- together with heat loss through the furnace walls -- significantly cooled the bulk flow. Again, we are seeing a furnace bulk temperature effect, not a sorbent heating rate effect.

The results for the 6-inch annular air jet -- the smallest of the air jets tested here -- are presented in Figure 8-8. While there was somewhat more scatter among the data from this jet, the data suggest a capture of 28 percent at Ca/S = 2 when V_A = 30 ft/sec (independent of V_S and T_B), and a capture of 38 percent at Ca/S = 2 when V_A = 60 ft/sec (again insensitive to V_S and T_B). (One run was also made at V_A = 30 ft/sec with a high background temperature, T_B > 2700 °F; at this condition, removal was very low, only 8 percent at Ca/S = 2.) With this relatively small jet, the cooling effects of the jet on the furnace were reduced, and depressed furnace exit temperatures were not a problem, even at high V_A and low T_B. The captures with the 6-inch jet at V_A = 60 ft/sec were comparable to (slightly higher than) those observed with the 10- and 12-inch jets where temperature depression was not a problem. However, the captures with the 6-inch jet at V_A = 30 ft/sec were somewhat lower. One reason for the reduced capture at V_A = 30 ft/sec could be that -- with the reduced furnace quenching effects of the smaller, low-velocity jet and with the expected dispersion of the sorbent particles into the bulk gas earlier in the furnace -- more of the sorbent particles in this jet experienced higher peak temperatures, and hence a slightly greater degree of sintering. That is, the problem might have shifted from being one where temperatures were too low, to one where temperatures were too high. This illustrates the balance that must be struck during design of a sorbent injection system.

Fuel: Natural gas + SO_2
Sorbent: Vicron 45-3

Air Jet: 6 inches (5.75 in. i.d.)
V_A = 30 ft/sec
Furnace exit temp: 1990 °F (T_B = 2600 °F)
1690 °F (T_B = 2200 °F)
Baseline SO_2 = 715-968 ppm as measured

Air Jet: 6 inches (5.75 in. i.d.)
V_A = 60 ft/sec
Furnace exit temp: 1895 °F (T_B = 2600 °F)
1595 °F (T_B = 2200 °F)
Baseline SO_2 = 828-909 ppm

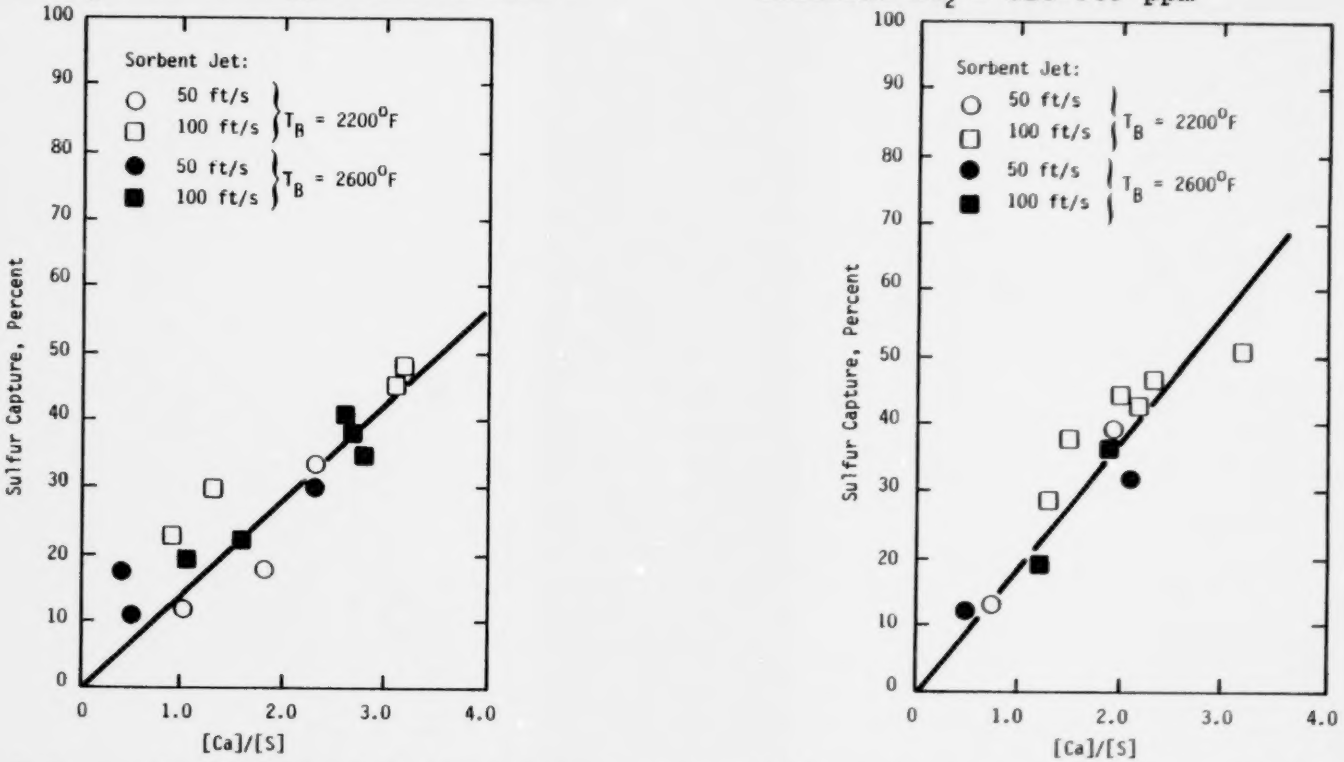

Figure 8-8. SO_2 capture with double concentric jets in uniform flow (axisymmetric) testing -- 6-inch annular air jet (co-flow).

The results from all of these co-flow double concentric jet experiments (for all three annular air jet diameters) are summarized in Table 8-1. Since bulk temperature in the furnace appeared to play an important role in determining sorbent performance, sulfur capture from each of these experiments (at Ca/S = 2) was plotted against furnace exit temperature (as one indicator of sorbent thermal history) to assess the nature of this correlation. The results are presented in Figure 8-9. As shown, for the two jet conditions with exit temperatures below 1500 °F, sulfur captures were distinctly reduced. However, at exit temperatures above 1500 °F, capture varied between 28 and 38 percent with no apparent correlation between capture and exit temperature. It is suspected that this data scatter above 1500 °F exit results because exit temperature by itself is not an adequate measure of sorbent thermal history in this system. Lower-velocity jets would result in more of the sorbent particles being dispersed into the bulk flow earlier in the furnace, where temperatures were higher; thus, for a given exit temperature, a lower-velocity jet would have exposed more of the sorbent to higher peak temperatures, and would have provided more residence time at temperatures above the exit temperature. At low temperatures, an increase in temperature (or in time at temperature) is desirable; however, above some value of temperature, further increases can reduce capture due to sintering. As determined earlier (in Figure 4-8), increases in furnace exit temperature above 1900 °F in Figure 8-9 would undoubtedly have shown capture begin to drop as the curve was extended to the right.

TABLE 8-1. RESULTS OF CO-FLOW DOUBLE CONCENTRIC JET INJECTION TESTS: UNIFORM FLOW TESTING (AXISYMMETRIC)

Jet Diameter Inch	Air Jet Velocity ft/s	Temperature °F		Percent Capture (@ Ca:S = 2.0)
		Background	Furnace Exit	
6	30	2200	1690	28
	60		1595	38
	30	2600	1990	28
	60		1895	38
10	30	2200	1540	33
	60		1375	13
	60	2400	1690	33
	30	2600	1920	33
12	30	2200	1450	19
	30	2600	1715	36

Fuel: Natural gas doped with SO_2

Sorbent jet velocity (V_s) does not have significant effect on percent capture.

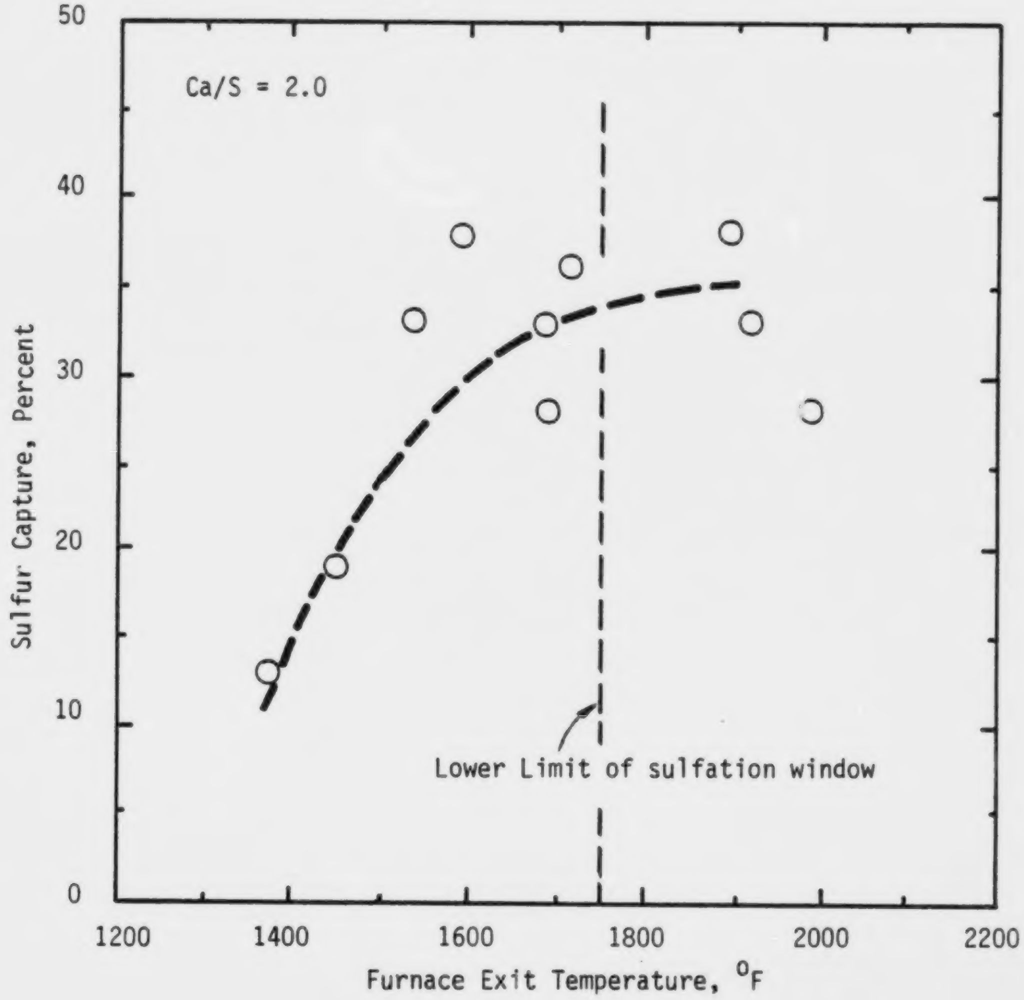

Figure 8-9. SO_2 capture as a function of furnace exit temperature for double concentric jet experiments.

8.2.2 Sorbent Surface Area and Calcium Utilization

In a part of the operation with the 6-inch annular air jet (Test No. 6 in Table 7-3), the exhaust SO_2 measurements were supplemented by more extensive sampling. Solids samples were extracted at various axial distances along the jet center-line to permit analysis for surface area, degree of calcination, and, in one run, degree of calcium conversion. Center-line temperature profiles were also measured. During this additional testing (except for the calcium conversion tests), the furnace was operating without SO_2 in the natural gas, so that surface area would not be reduced by the sulfation reaction.

These additional analyses were conducted with the 6-inch jet at both background temperatures (T_B = 2200 and 2600 $^{\circ}$F), for the case where V_A = 60 ft/sec and V_S = 100 ft/sec. Additional analyses were also conducted for the high-temperature run, where V_A = 30 ft/sec and T_B > 2700 $^{\circ}$F.

The results of the center-line surface area analyses are presented in Figure 8-10 for the three run conditions. The axial profiles of the degree of calcination and of the temperature along the center-line -- together with the calculated residence time from the end of the jet pipe -- are shown in Figure 8-11. As shown in Figure 8-10, the axial profile for the surface area (reactivity) development and decay varies distinctly depending upon run conditions. In the case of the 2200 $^{\circ}$F background temperature (and 1650 $^{\circ}$F exit temperature), the surface area develops relatively slowly, but reaches a fairly high ultimate value (about 23 m^2/g) by the time the sorbent exits the furnace. Referring to Figure 8-11, it is apparent that this area development was proceeding in the same pattern as the calcination, as would be expected. At the low center-line temperatures in this jet (1500-1600 $^{\circ}$F), there was roughly a 0.25-second delay time as the particle heated up and

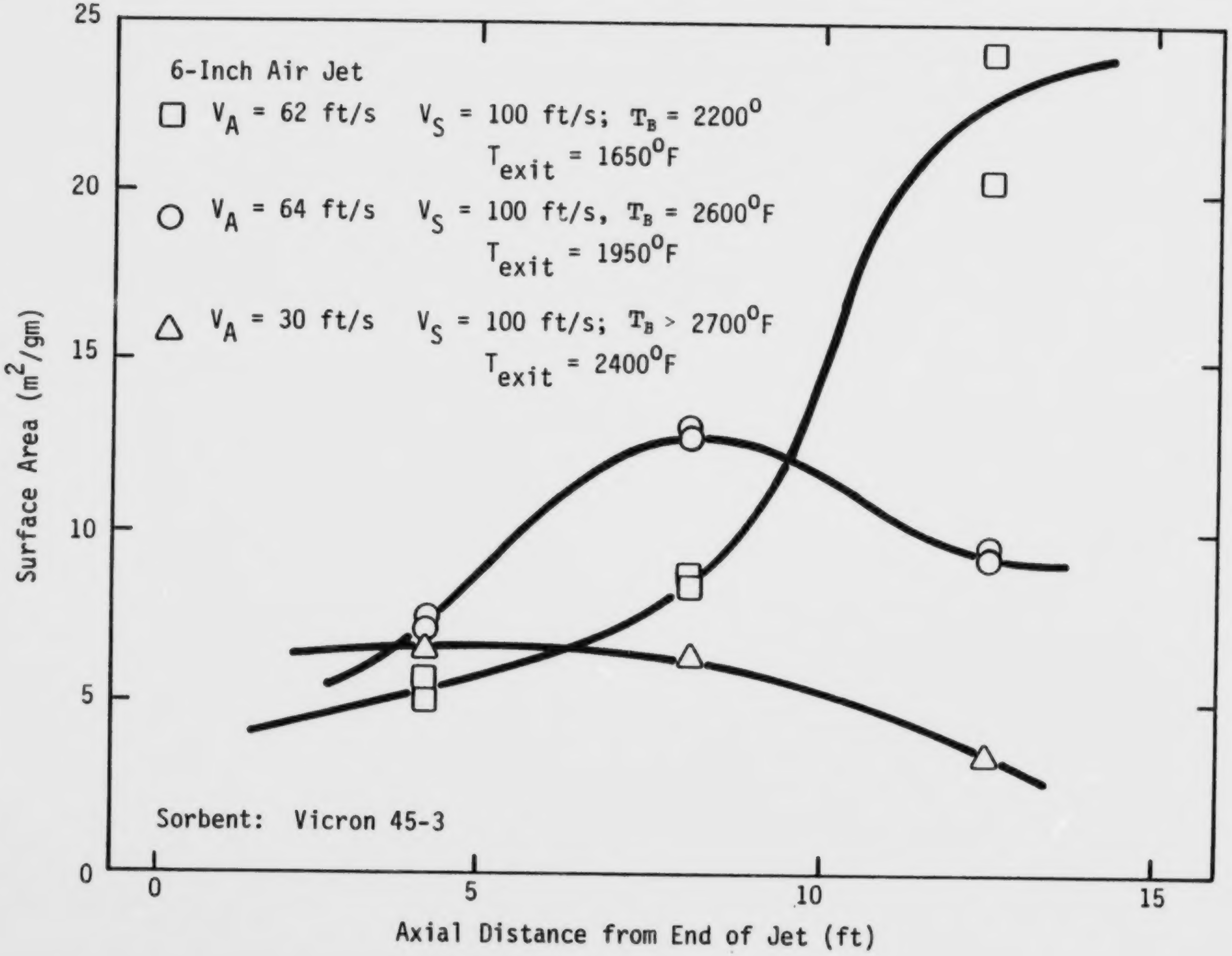

Figure 8-10. Sorbent surface area along the center-line of the 6-inch double concentric air jet (co-flow, uniform flow field)

6-inch annular air jet

□ $V_A = 62$ ft/sec, $V_S = 100$ ft/sec, $T_B = 2200$ °F

○ $V_A = 64$ ft/sec, $V_S = 100$ ft/sec, $T_B = 2600$ °F

△ $V_A = 30$ ft/sec, $V_S = 100$ ft/sec, $T_B > 2700$ °F

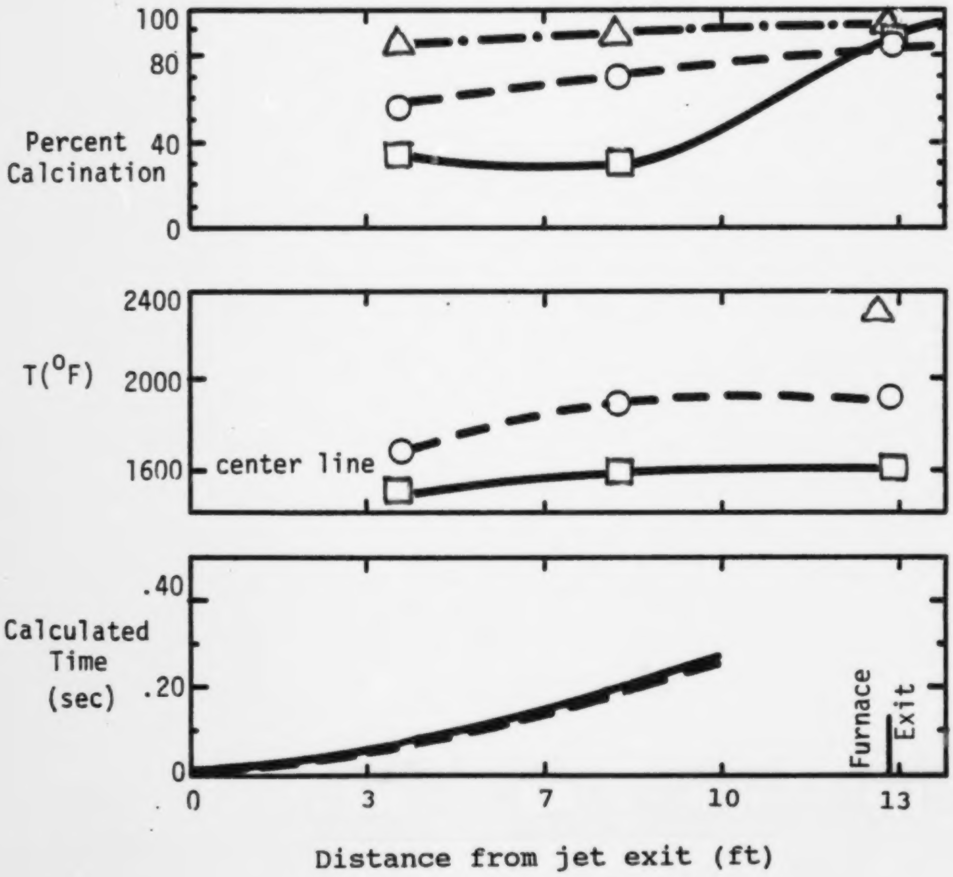

Figure 8-11. Profiles along the center-line of the 6-inch double concentric air jet

began calcining, and high levels of calcination (over 80 percent) and the highest surface areas were not achieved until near the end of the furnace. The temperatures in this run (somewhat below the sulfation window) apparently were high enough to yield adequate calcination kinetics, but low enough to reduce sintering. In the case of T_B = 2600 °F, surface area rose much more rapidly than in the lower-temperature case, to about 13 m^2/g after about 0.25 sec; calcination was about 70 percent complete at that point, much faster than in the previous case, explaining the more rapid formation of surface area. However, at the 1900 °F jet center-line temperature in this case, area then suffered a net decay after the first quarter-second, presumably due to sintering, falling to about 9 m^2/g by the furnace exit. Thus, the higher center-line temperature in the case of T_B = 2600 °F gave more rapid initial area development, but also more significant sintering loss. In the case of the highest background temperature (> 2700 °F), surface area was at its maximum within the first 100 msec (about 7 m^2/g), and it decayed through the remainder of the furnace (to about 3 m^2/g); the high temperature gave very rapid particle heat-up and calcination, but resulted in substantial sintering.

The calcium conversion profile was measured with the 6-inch jet at the 2200 °F background temperature. The utilization profile is presented in Figure 8-12; the surface area profile for these run conditions (taken from Figure 8-10) is also shown for comparison. As would be expected, conversion of the calcium to sulfate was relatively low during the first roughly 0.25 sec of residence time (the first 8 feet of furnace length). The degree of conversion then increased over the remainder of the furnace length, reflecting the increase in surface area, reaching about 20 percent measured sulfation at the furnace exit (and about 25 percent utilization at the sampling point in the downstream ducting). This is somewhat higher than the 19 percent utilization implied by the flue gas SO_2 measurements for this run, reflecting the type of discrepancy

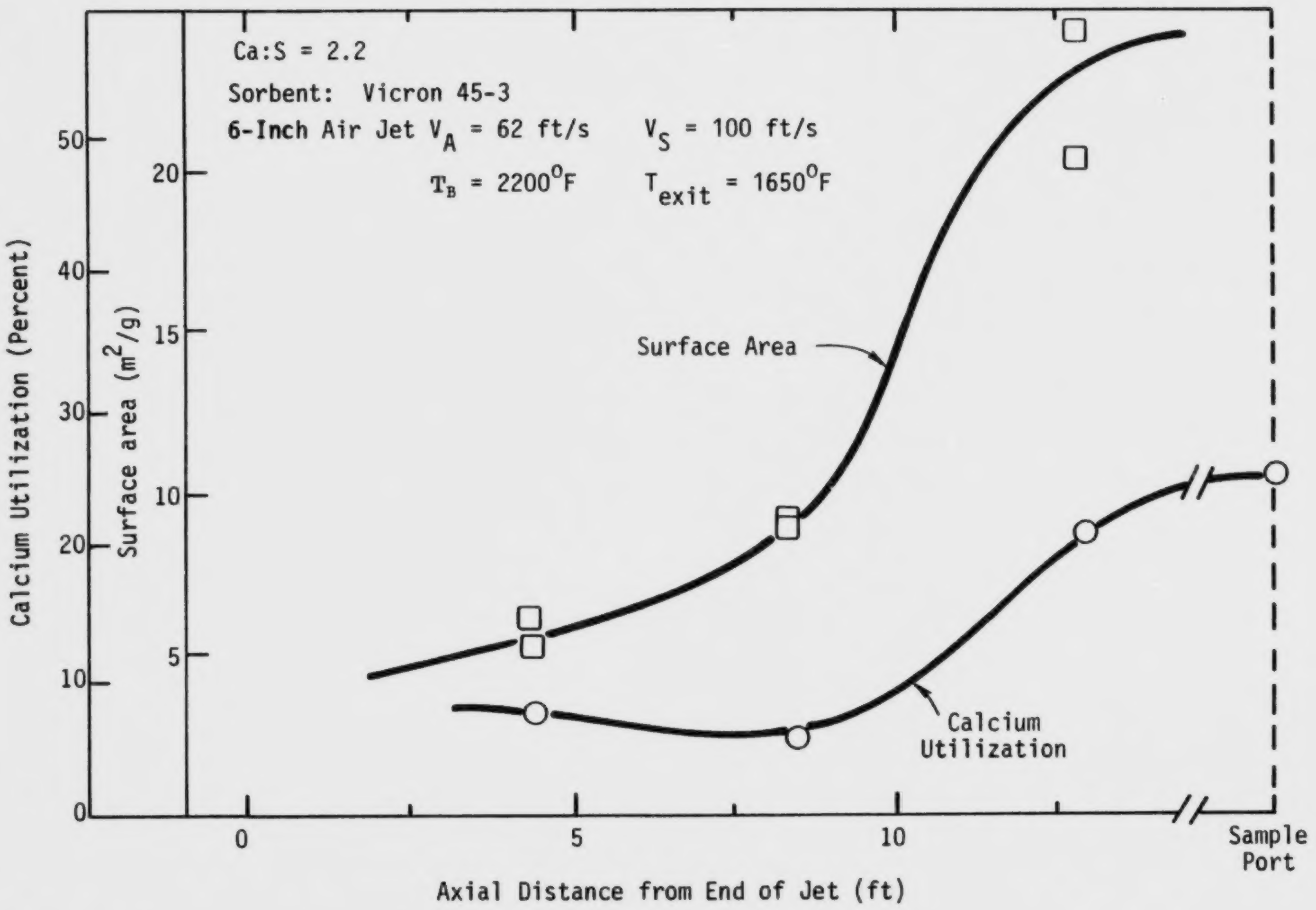

Figure 8-12. Calcium utilization and surface area along the center-line of the 6-inch double concentric jet

typically observed between flue gas SO_2 measurements and solids sulfation analyses.

To aid in the interpretation of the jet experiments where in-situ sorbent surface area was not measured, an attempt was considered to calculate the effective surface area. The calculation would be done by fitting the known sulfur removal, sorbent feed rate, and SWS time/temperature profile into an available mathematical model incorporating sorbent/SO_2 reaction kinetics; from this model fit, the effective sorbent reactivity (surface area) could be back-calculated. Unfortunately, this calculation was not possible. The SWS gases form a recirculation zone in the rear of the furnace, where they must turn 90° to enter the exhaust ducting; this zone is particularly pronounced with the large, high-mass double concentric jets. The residence time of the sorbent in this zone in unknown. Thus, the sorbent time/temperature history which would have to be fed into the model to permit the desired calculation is not known.

In an effort to assess where the sulfur capture was occurring in the SWS, tests with the 6-inch jet (at $V_A = 60$ ft/sec, $T_B = 2200$ °F) were conducted with the SO_2 being injected at different locations. The SO_2 injection locations were: through the burners with the natural gas, as usual; at a point on the center-line of the SWS 4 feet downstream of the firing wall; at a point 8 feet from the firing wall; and at a sample port near the furnace exit. The results showed that captures were about the same for all of the first three injection points (35 to 40 percent removal at Ca/S = 2). However, for SO_2 injection at the furnace exit, removals were much lower (21 percent at Ca/S = 2). These results suggest that -- at least for this smaller double concentric jet -- a substantial amount of capture occurs between the 8-foot point and the furnace exit; however, some potentially significant capture also occurs in the flue gas ducting downstream of the furnace (and perhaps in the recirculation zone). This split would probably have been different with the 10- and 12-inch jets, due to the lower temperatures at the furnace exit with these larger jets.

8.2.3 Effect of Ash Interaction

Sorbent deactivation by coal ash was briefly investigated in operation with the 10-inch and 6-inch jets (Test No. 5 in Table 7-3). In this testing, Utah coal was added to the natural gas flames in order to provide a concentration of coal ash. The results were compared to the case where the same jet conditions had been run without coal doping. The results are given in Figure 8-13. As shown, at none of the jet conditions tested did the coal ash cause any significant difference (either positive or negative) from sorbent performance obtained without ash. With the sheaths of air surrounding these sorbent jets, it is expected that -- by the time the ash and sorbent came into contact at some distance into the furnace -- the temperatures had cooled to the extent that deactivation or promotion did not occur.

8.2.4 Single-Pipe Sorbent Jets

While the testing reported in this section focussed on double concentric jets, a limited test series (Test No. 4 in Table 7-3) addressed single-pipe ("dense") sorbent jets without the surrounding sheath of annular air. Because of their smaller mass, single dense jets could provide a more rapid sorbent heating rate than the double concentric jets, and would avoid the cooling effect that caused low SWS exit temperatures in the double concentric testing.

For this initial brief single-pipe jet test series, the double concentric jet system shown in Figure 7-4 was replaced with a single 1-inch diameter pipe. Since this single pipe would not be protected from the furnace thermal environment by a high flow of annular air, the end of the pipe was located flush with the SWS

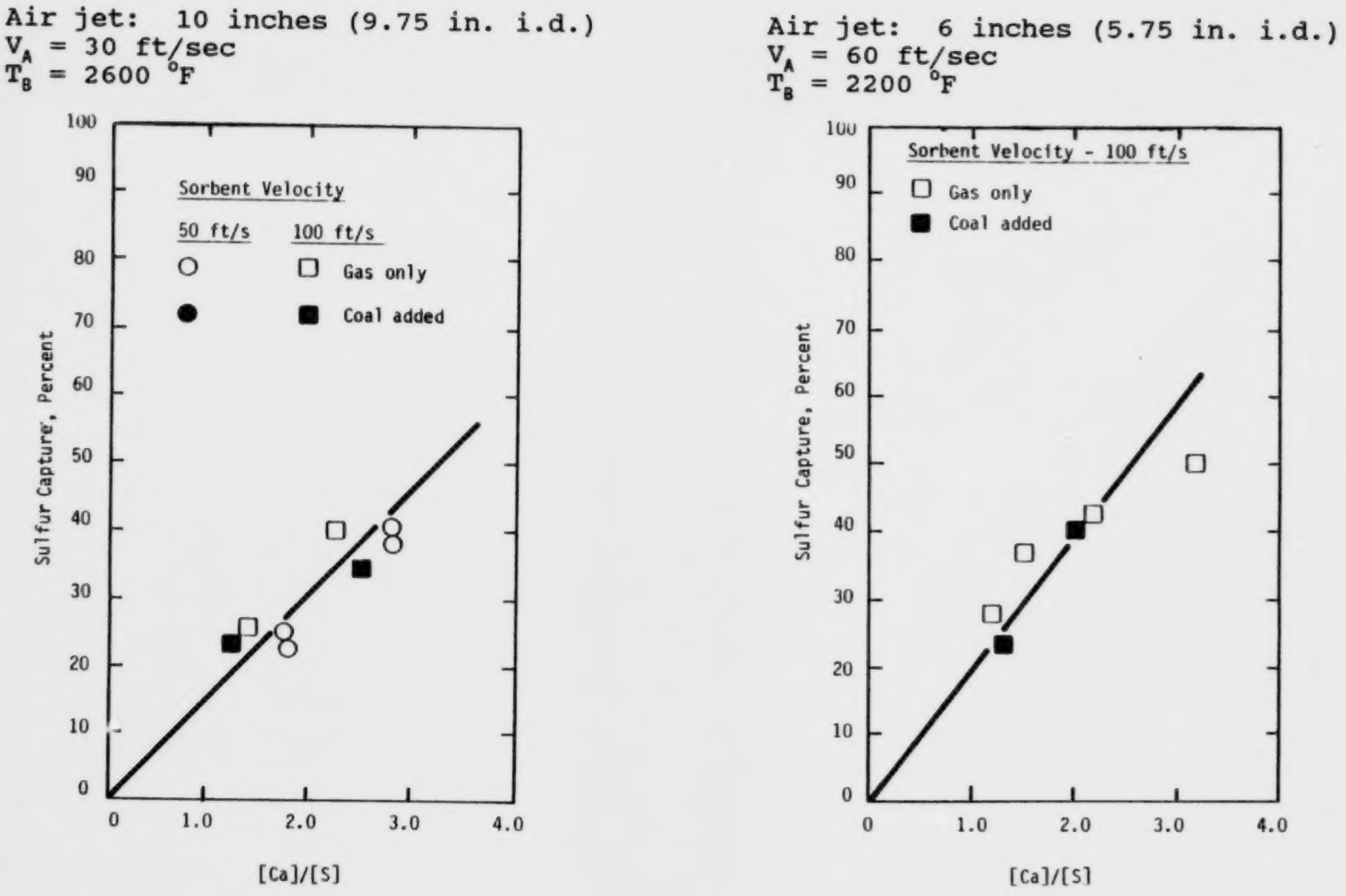
Air jet: 10 inches (9.75 in. i.d.)
V_A = 30 ft/sec
T_B = 2600 °F

Air jet: 6 inches (5.75 in. i.d.)
V_A = 60 ft/sec
T_B = 2200 °F

Figure 8-13. Effect of coal ash on SO_2 capture in gas flames -- 10-inch and 6-inch double concentric jets (co-flow, uniform flow conditions)

burner wall to avoid destruction of the pipe, rather than extending 3 feet into the furnace as with the large jets. (Injection flush with the firing wall -- together with the relatively low mass of jet air and rapid mixing in the single-pipe case -- would result in the sorbent from the single-pipe jets seeing a peak temperature close to the background temperature.)

To test a range of sorbent heating rates and peak temperatures, the test matrix for this single-pipe series addressed three sorbent jet velocities V_S (25, 50 and 100 ft/sec) and three background temperatures T_B (2200, 2600 and 2800 °F). Again, Vicron limestone was used in all tests.

Figure 8-14 shows SO_2 capture versus Ca/S molar ratio for jets of all three velocities for a background temperature of 2200 °F. SO_2 removal was similar for injection velocities of 50 and 100 ft/sec (about 30 percent removal at Ca/S = 2); however, removals were much lower for the low injection velocity of 25 ft/sec. The reduced removal at low velocity would presumably be due to one of three possible causes: 1) exposure of the sorbent to a higher peak temperature, thus reducing reactivity; 2) reduced residence time in the sulfation temperature window; or 3) reduced sorbent heating rate, causing lower reactivity. Concerning the first possible cause, all three of these jets should have exposed the sorbent to approximately the same peak temperature:

a) a jet of a given diameter will reach the same temperature in a given distance, regardless of its velocity; the amount of background gas entrained is proportional to jet mass, so higher-velocity (higher-mass) jets entrain proportionately more background gas. Thus, the high-velocity jets could not "punch" the sorbent through to cooler temperatures farther away from the firing wall.

b) The mass of jet injection air is sufficiently small for all of these single-pipe jets, such that the higher-velocity jets should not significantly influence the background temperature in the furnace, as happened with the large double concentric jets.

Fuel: Natural gas + SO_2
Sorbent: Vicron 45-3
T_B = 2200 °F
Furnace exit temp: 1795 °F (V_s = 25 ft/sec)
1830 °F (V_s = 50 ft/sec)
1822 °F (V_s = 100 ft/sec)
Sorbent jet: 1-inch single pipe

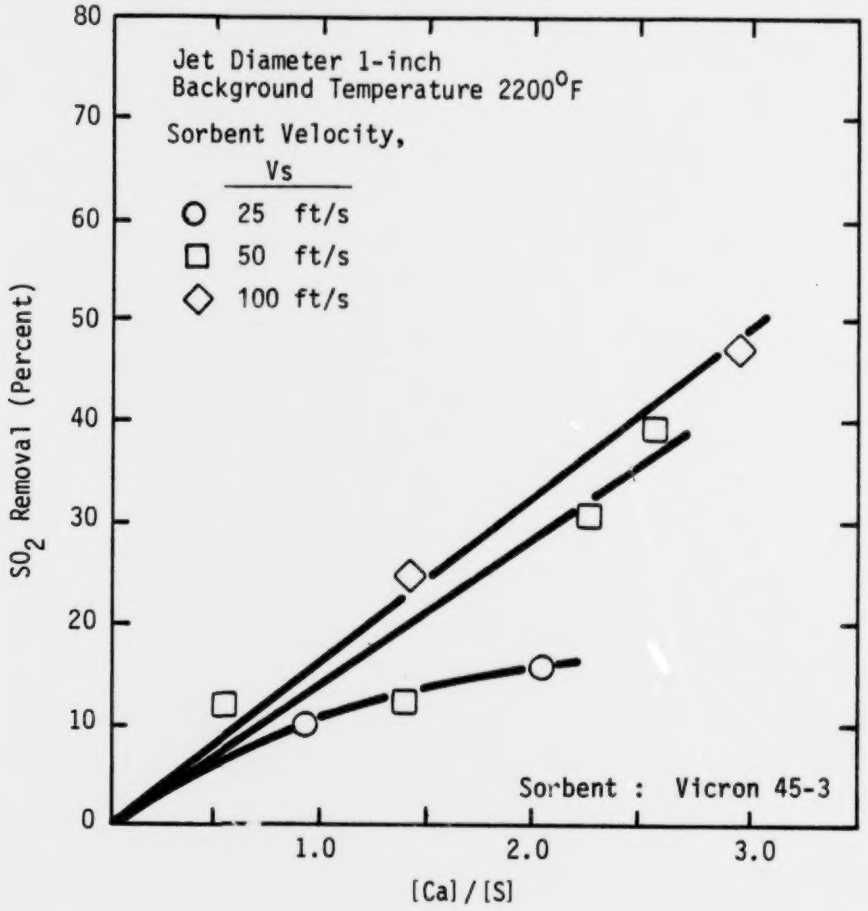

Figure 8-14. SO_2 capture with single-pipe sorbent jet at 2200 °F background temperature -- effect of sorbent injection velocity

Concerning the second possible cause listed above, it is believed that the sorbent in all jets was exposed to similar time/temperature histories:

a) comparison of the furnace exit temperatures for the three runs (see notes on top of Figure 8-14) shows that they are similar, suggesting that, in all cases, the sorbent passed through a similar temperature window in the furnace (from T_B to T_{exit}).

b) while the faster jets might intuitively be expected to give the sorbent somewhat less residence time in the furnace, the large recirculation zone at the back wall of the SWS probably gave the sorbent from all of these jets a similar residence time sufficiently extended to wash out any residence time effects that might otherwise be created by jet velocity.

Since these three jets thus should have seen similar peak temperatures and similar time/temperature histories, the major difference between them would appear to be the third possible cause listed above, the sorbent heating rate. (A fast jet and a slow jet will heat to the same temperature in the same distance; the fast jet will just cover that distance, and thus heat up, more rapidly.)

The results in Figure 8-14 appear to offer the clearest suggestion to date in this study that increases in heating rate might increase sorbent performance, all other factors being equal. This result prompted further heating rate experiments on single-pipe (and small double concentric) jets, addressing a variety of sorbents in addition to Vicron. These additional experiments are described in Section 9. Unfortunately, sufficient measurements were not made in the Figure 8-14 tests to verify: the actual heating rates experienced in each run; the actual sorbent reactivities (surface areas) attained; and the actual time/temperature profiles, including peak temperatures. Again -- because of the recirculation zone at the rear wall of the SWS, creating unknown sorbent residence time in the furnace -- it was not possible to insert a known time/temperature history into available mathematical models for the purpose of back-calculating the effective sorbent reactivities/surface areas attained. (This recirculation zone would be less pronounced with the smaller, single-pipe jets than it was with the large, double concentric jets, but was still present.)

For the 100 ft/sec sorbent jet velocity, tests were made at the three background temperatures T_B. These results are shown in Figure 8-15. SO_2 removal decreased sharply as the background temperature increased from 2200 to 2800 °F. Removals at Ca/S = 2 fell from about 30 percent to about 15 percent with the increase in temperature. Since these small jets mix rapidly, the sorbent particles probably saw peak temperatures approximately equal to the background temperatures. The drop in capture with increasing T_B further illustrates the need to avoid high sorbent temperatures; the deactivation caused by increased peak temperature would seem to have overwhelmed any benefit of increased heating rate that would have resulted from the higher T_B.

8.3 Double Concentric Jets in Cross-Flow

For sorbent injection in the upper furnace, remote from the burner, it is likely that the jet will often be issuing through the furnace wall perpendicular to the main furnace gas flow. Such jets in cross-flow have different characteristics from jets issuing into co-flowing streams, as addressed in this study up to this point. The cross-flow jet entrains furnace gas as it penetrates across the flow, and as it does, it is bent towards the downstream direction of the main gas flow. The key characteristics of cross-flow jet behavior are the path of the jet, as defined by its center-line trajectory, and its entrainment in relation to the distance along its curved path. Cross-flow jets were tested briefly in this study to determine how differences in cross-flow jet properties, relative to co-flowing jets, might influence the effect of jet parameters on sorbent performance.

Fuel: Natural gas + SO_2
Sorbent: Vicron 45-3
Furnace exit temp: 1822 °F (T_B = 2200 °F)
2210 °F (T_B = 2600 °F)
2386 °F (T_B = 2800 °F)
Sorbent jet: 1-inch single pipe
V_s = 100 ft/sec

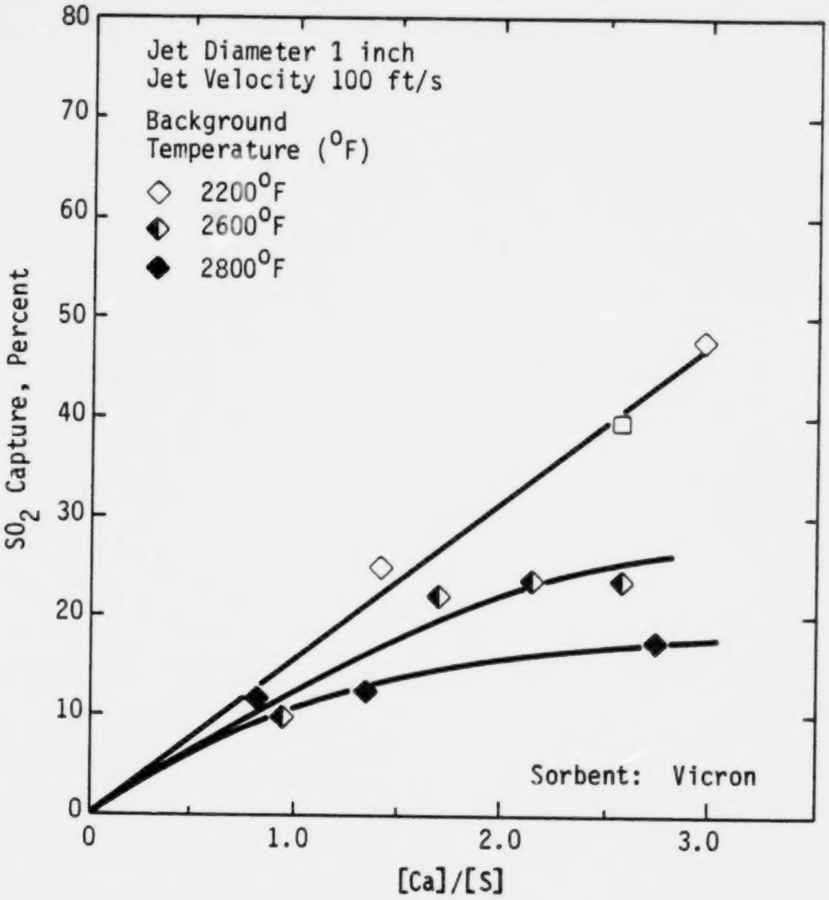

Figure 8-15. SO_2 capture with single-pipe sorbent jet at injection velocity of 100 ft/sec -- effect of background temperature.

In these studies, double concentric sorbent jets were injected into the SWS in cross-flow at a distance of five feet downstream of the firing wall, as illustrated in Figure 7-10. The background temperature in all cases was about 2200 °F at the point of injection, simulating the injection conditions that might be used with upper furnace injection. The outer, annular air jet of the double concentric jet was 4 inches in diameter; the inner (sorbent) jet had a diameter of 1 inch. During these tests, the SWS was operating in the uniform-flow mode, with the six gas-fired burners on the firing wall, burning natural gas doped with SO_2.

The test matrix for the cross-flow experiments is shown in Table 7-5. The primary variables were the annular air jet velocity V_A and the sorbent jet velocity V_S, along with the sorbent feed rate. In one run, V_A was zero -- i.e., the jet was operating as a single-pipe sorbent jet with no annular air.

The SO_2 captures obtained with these jets is shown in Figure 8-16 as a function of the calcium-to-sulfur molar ratio. The results show only small differences in capture between all of the jet velocity combinations tested. Capture was about 25 percent at Ca/S = 2. The co-axial air jet surrounding the sorbent jet in most of the runs would have been expected to delay mixing of the sorbent jet with hot gas, and thus possibly protect the sorbent from overheating. However -- since the one single-pipe test gave the same performance as the double concentric tests -- it is apparent that, at the relatively low background temperature of 2200 °F, protection of Vicron limestone from overheating is not a problem.

The 4-inch annular air jet was small enough that it did not create the substantial cooling of the SWS bulk gases, as had the 6- to 12-inch air jets tested earlier. This is demonstrated by the fact that the furnace exit temperatures were about the same for the double concentric and single-pipe tests (see note on top of Figure 8-16).

Fuel: Natural gas + SO_2
Sorbent: Vicron 45-3
T_B = 2200 ° F
Furnace exit temp: 1863 °F ($V_A = V_s$ = 25 ft/sec)
1866 °F (V_A = 25, V_s = 50 ft/sec)
1817 °F ($V_A = V_s$ = 50 ft/sec)
1868 °F (V_A = 0)
Annular air jet: 4 inches diameter (3.75 in. i.d.)
Sorbent jet: 1 inch diameter

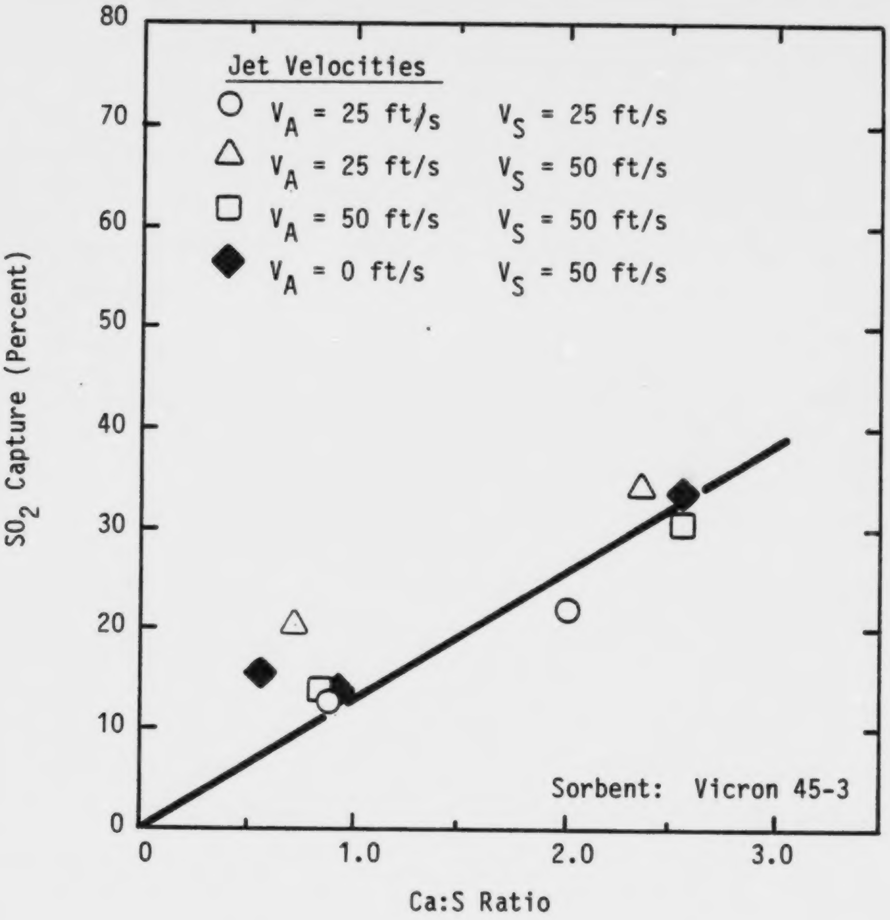

Figure 8-16. SO_2 capture with double concentric jet in cross-flow -- effect of air and sorbent jet velocities.

It is possible that the double concentric jets (of various velocities) might have reduced peak sorbent temperature, or reduced the heating rate, or improved sorbent dispersion, relative to the single-pipe jet. However, in view of the comparable SO_2 removal performance for all of the jets, it is apparent that any such effects were being masked -- perhaps by the unknown residence time at favorable sulfation temperature in the unavoidable recirculation zone at the back of the SWS.

To further assess the possible effects of sorbent dispersion with the various jets tested here, the center-line trajectories of these jets has been estimated using an empirical correlation for the trajectory as a function of the jet-to-stream momentum flux ratio. The equation for the trajectory is given by Patrick (3) as:

$$\frac{y}{d} = J^{.43} \left(\frac{x}{d}\right)^{.38}$$

where y is cross stream penetration of the jet
x is downstream distance of the jet
d is jet diameter
J is jet-to-stream momentum flux ratio, $J = \frac{\rho_j V_j^2}{\rho_\infty V_\infty^2}$

and ρ_j is jet density
ρ_∞ is cross stream density
V_j is jet velocity
V_∞ is cross stream velocity

Figure 8-17 shows the estimated center-line trajectories of the jets studied here. To make these predictions, the double concentric jets were replaced with equivalent single-pipe jets of the same mass and momentum flux. These calculations predict that all of these jets penetrate completely across the SWS furnace and impinge on the opposite wall before they reach the exit of the

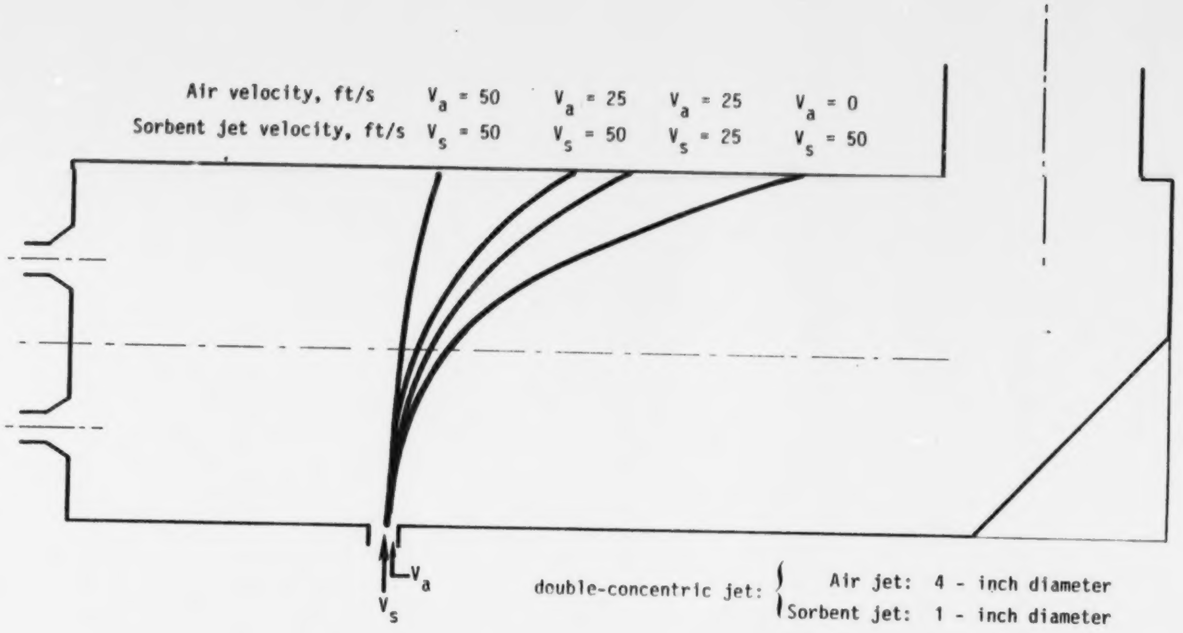
Air velocity, ft/s
Sorbent jet velocity, ft/s
V_a = 50 V_s = 50
V_a = 25 V_s = 50
V_a = 25 V_s = 25
V_a = 0 V_s = 50
V_a
V_s
double-concentric jet:
Air jet: 4 - inch diameter
Sorbent jet: 1 - inch diameter

Figure 8-17. Estimated center-line trajectories of cross-flow jets tested in SWS furnace.

furnace. Thus, the jets would concentrate the sorbent to one side of the furnace, providing inadequate dispersion of the sorbent over the furnace cross-section immediately downstream of the injection point. It is thus possible that inadequate sorbent dispersion in the temperature regime near the injection point limited the overall SO_2 capture of all of these jets. Poor dispersion could have contributed to masking any SO_2 capture differences that might otherwise have resulted from different thermal histories or differences in reactivity caused by the different jets.

9.0 SORBENT HEATING RATE STUDIES WITH SMALL JETS

The tests described in this section were specifically designed to investigate the influence of initial sorbent heating rate on SO_2 capture and, by inference, on sorbent reactivity. Since peak sorbent temperature also influences reactivity, peak temperature is included as a variable in the test matrix. (Since the residence time-at-temperature history of the sorbent in the SWS, as well as the reactivity, can affect the measured SO_2 captures -- and since this history necessarily varied for the different test conditions -- a mathematical sulfation model was used in an effort to separate out the reactivity vs. residence time effects, as discussed in Section 9.4.)

To achieve higher heating rates -- and to achieve more effective control of the heating rate -- these experiments were conducted with small jets. Most of the testing was conducted with 2-inch diameter (sometimes 1-inch diameter) single-pipe sorbent jets. Limited testing was also carried out with a 4-inch double concentric jet containing a 1-inch sorbent jet (Section 9.3). For the single-pipe jet tests, the SWS was operated in the co-flowing configuration illustrated in Figure 7-5.

The testing reported here comprised Tests 7, 8 and 9 in Table 7-3 (with the matrix for Tests 7 and 8 presented in more detail in Table 7-4). The desired variations in heating rate and peak temperature were achieved by using different combinations of jet diameter, jet velocity, and background furnace gas temperature, as detailed in Table 7-4. The calculations used to derive the desired jet diameters, velocities and background temperatures were discussed in conjunction with Figures 7-6 through 7-9. The background temperatures used are representative of sorbent injection into the upper furnace region, remote from the burners.

As shown, the calculations suggest that a doubling of the sorbent jet velocity should double the heating rate, all other factors being equal. A faster jet will reach the same temperature in the same distance as a slower jet, but will cover that distance more quickly and will hence heat more quickly. Smaller-diameter jets will heat more rapidly because of their smaller mass. And a higher background temperature will increase heating rate by increasing the delta-T between the background and the jet. The background temperature also affects the peak temperature seen by the sorbent.

Five different sorbents were tested in this heating rate study: Vicron limestone (10 μm mass mean); D3002 dolomite; two hydrated calcitic limes, hydrated at atmospheric pressure (Colton and Longview); and Genstar Type-S pressure-hydrated dolomitic lime.

9.1 SO_2 Capture Results with 2-Inch Single-Pipe Jets

Most of the heating rate testing was conducted with 2-inch diameter single-pipe jets. The 2-inch jets were tested at two different jet velocities (50 and 100 ft/sec) for three different background temperatures (2500, 2600 and 2800 °F). These conditions were calculated to yield estimated peak sorbent temperatures in the jet of 2040, 2100 and 2250 °F, respectively. All five of the sorbents listed previously were tested in the 2-inch jets.

SO_2 capture results for Vicron limestone are given in Figure 9-1. The figure shows SO_2 capture versus calcium-to-sulfur ratio for the three different background temperatures; in each case the results for two velocities are shown, representing different sorbent heating rates. It can be seen that there are slight differences in SO_2 capture with velocity, although in two cases (2500 °F and 2800 °F background temperatures), the data are limited, making interpretation difficult. For the case of the 2600 °F

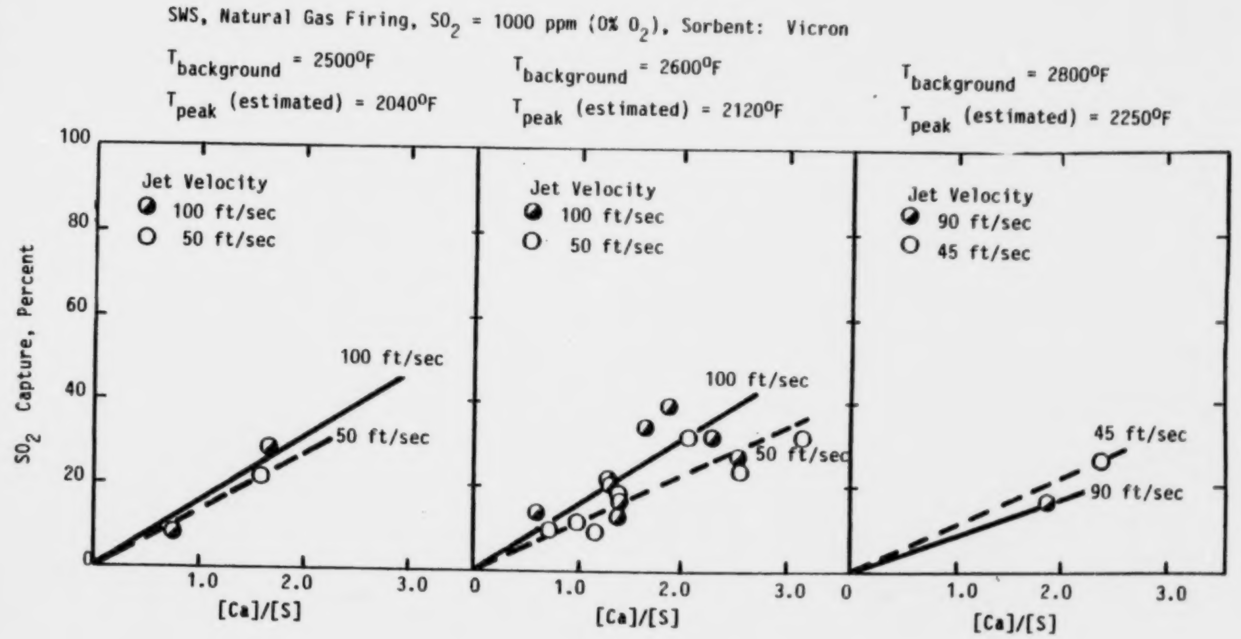

Figure 9-1. SO_2 capture with Vicron limestone injected through a 2-inch single-pipe jet -- heating rate studies.

background temperature, there are more data, but the data show considerable scatter. This scatter may reflect slight changes in experimental technique, since these particular data points were measured during different tests that were conducted some months apart. Regression lines through the data for the 2600 °F case suggest that the capture was higher at the higher injection velocity (31 percent compared to 23 percent at Ca/S = 2.0). As discussed in Section 9.4, this difference in capture could be due to heating rate differences between the two velocities, or to other effects. The effect of temperature on capture was relatively small for this sorbent over the range tested.

Figure 9-2 shows SO_2 capture versus calcium-to-sulfur ratio for Colton Lime for the same velocities and background temperatures. Again, these results show only small differences in SO_2 capture between the two different jet velocities. At the high and low temperatures, the low-velocity jet (i.e., the slower heating rate) gave the higher capture, whereas at the intermediate temperature, the higher-velocity jet gave the highest capture. The best SO_2 capture was obtained at the intermediate background temperature (2600 °F), giving 50 percent capture at Ca/S = 2.0 for the 100 ft/sec jet. This is considerably higher than was obtained with Vicron, which only gave 31 percent SO_2 removal, and is in line with results from other investigations (4) which show that the atmospheric hydrates are more reactive and produce higher SO_2 capture than pulverized limestone.

Figure 9-3 shows SO_2 capture versus calcium-to-sulfur ratio for Longview Lime. Longview and Colton limes are both calcitic atmospheric hydrates, and so could be expected to have similar sulfur capture potential under the same thermal and mixing conditions. The results in Figure 9-3 show Longview Lime to give slightly higher capture, and also to have a different shape of SO_2 capture versus calcium-to-sulfur curve. Except for one case,

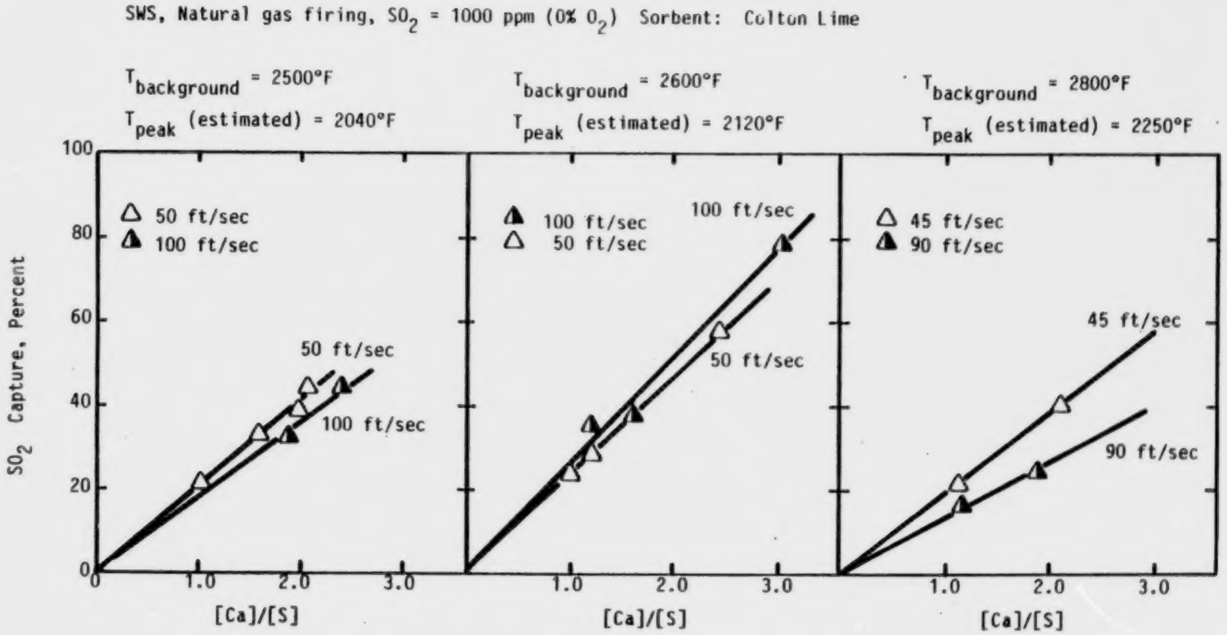

Figure 9-2. SO_2 capture for Colton atmospheric-pressure calcitic hydrate injected through 2-inch single-pipe jet -- heating rate studies.

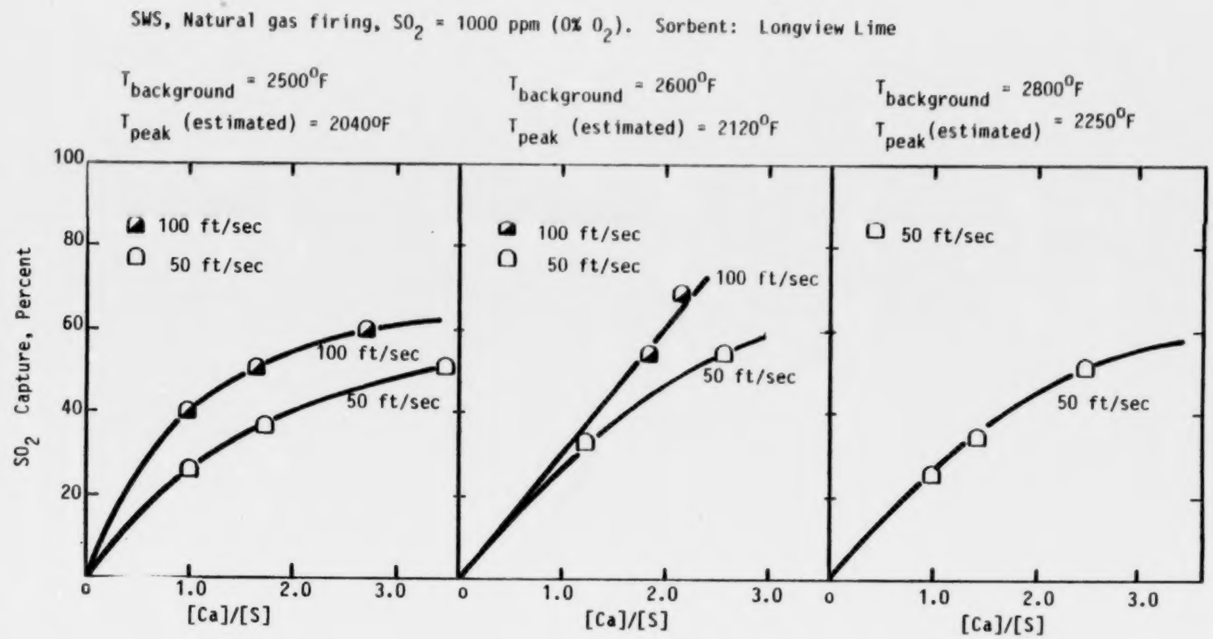

Figure 9-3. SO_2 capture for Longview atmospheric-pressure calcitic hydrate injected through 2-inch single-pipe jet -- heating rate studies.

capture with Longview Lime increases rapidly at low Ca/S and then falls to a slower rate of increase at high Ca/S. This different response may be a result of different sorbent pore size distribution within the particles, or different reactivity characteristics between the two sorbents.

For Longview Lime, capture was always higher with the higher-velocity jet. This implies that there could have been an impact of sorbent heating rate on sorbent reactivity, with higher heating rates leading to higher reactivity and overall capture. The highest capture obtained was again for the jet injected at 100 ft/sec into a background temperature of 2600 °F, giving 60 percent capture at Ca/S = 2.0.

Figure 9-4 shows SO_2 capture versus calcium-to-sulfur ratio for D3002 dolomite. The dolomite achieved higher capture than either limestone or calcitic atmospheric hydrate, as was expected from previous investigations showing the superiority of dolomites over limestones. The best capture was achieved when injecting into the intermediate background temperature of 2600 °F at 100 ft/sec, giving 70 percent SO_2 capture at Ca/S = 2.0. The effect of injection velocity was noticeable with this sorbent, showing increased capture at the higher velocity for the two low-temperature cases. However, this result was reversed for the high temperature case, as it was for the Vicron and Colton Lime (Longview Lime was not tested at that condition). Possibly at the higher temperature, the faster heating rate leads to a longer time for the sorbent at temperatures which cause the sorbent to sinter and lose reactivity.

The SO_2 capture results for S-Type pressure hydrated dolomitic lime are given in Figure 9-5. This sorbent produced the highest capture of all the sorbents tested here. This was expected because the pressure hydrates have been found to produce high captures in

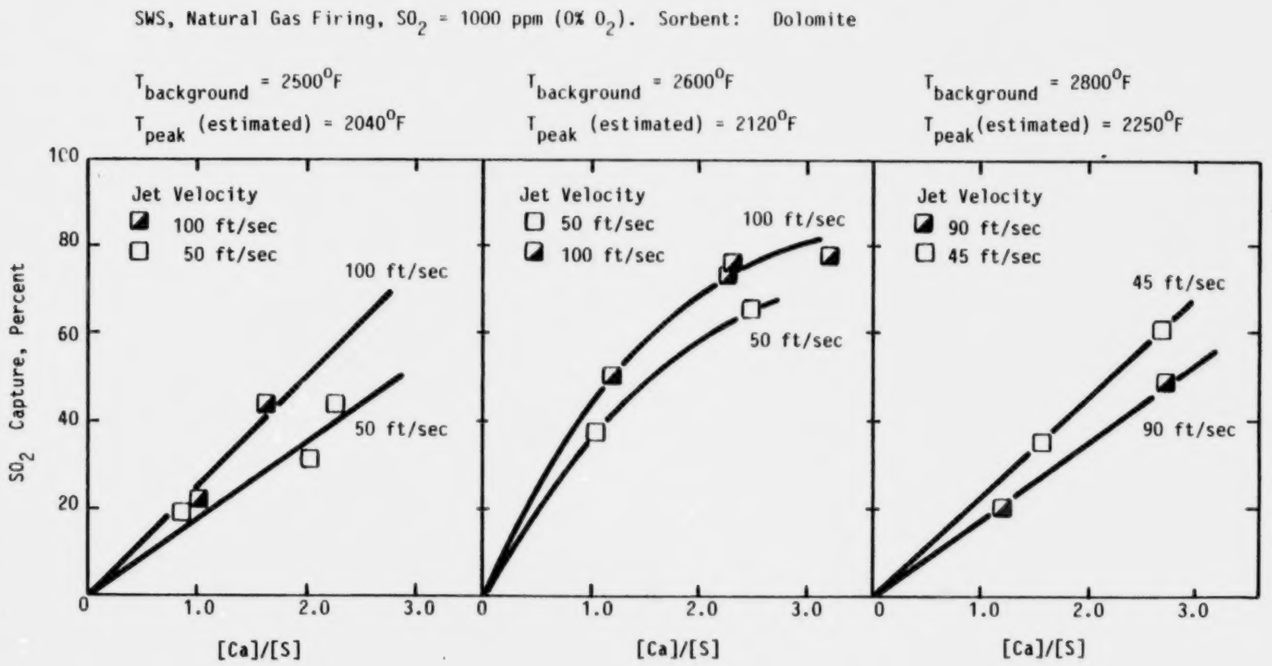

Figure 9-4. SO_2 capture for D3002 dolomite injected through 2-inch single-pipe jet -- heating rate studies.

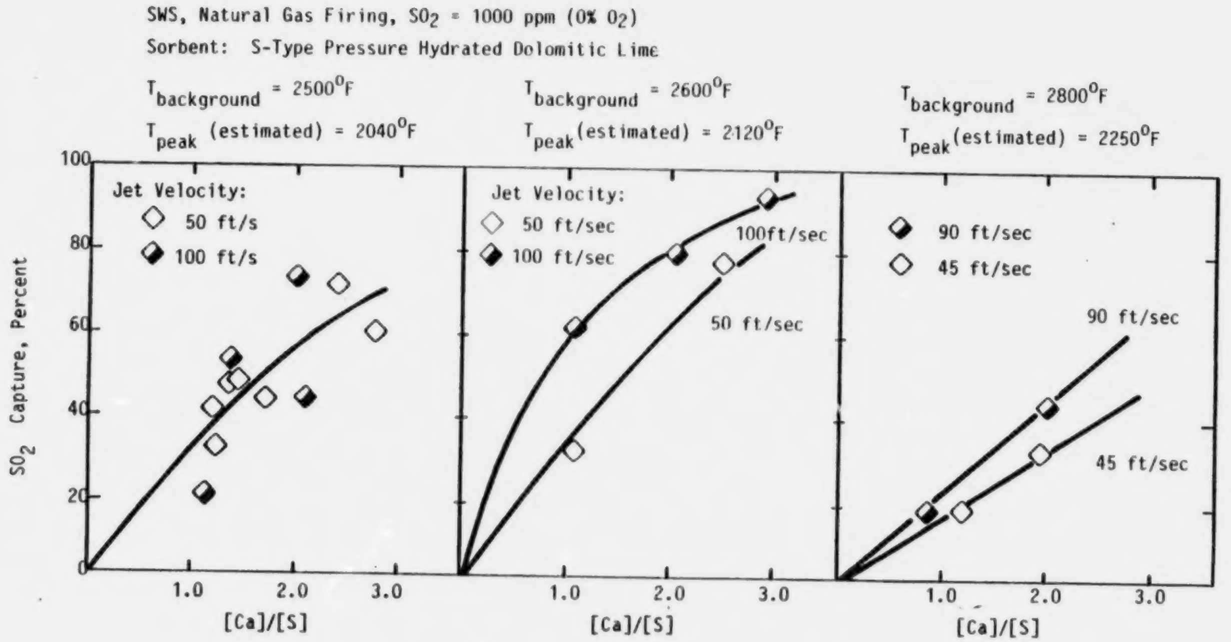

Figure 9-5. SO_2 capture for Genstar Type-S dolomitic pressure hydrate injected through 2-inch single-pipe jet -- heating rate studies.

other experimental investigations. For this sorbent, the effect of increasing jet velocity and hence heating rate was to increase SO_2 capture; the exception was for the lowest background temperature case, where the results were too scattered to determine if there was an effect of heating rate. The highest capture was obtained at the intermediate background temperature (2500 ^{o}F) at 100 ft/sec, producing SO_2 captures of 80 percent at Ca/S = 2.0.

The SO_2 capture results for the 2-inch jets are summarized in Table 9-1, showing SO_2 capture at Ca/S = 2.0 for the different temperature levels and heating rates studied. Also shown in this table is the measured peak temperature, as described later in Section 9.4. There does not appear to be a consistent pattern with regard to the possible effect of heating rate, except at the intermediate background temperature (2600 ^{o}F). For that injection temperature, the higher heating rate consistently produced higher SO_2 capture. (Again, as discussed in Section 9.4, it is not certain that SO_2 capture differences between the jets of different velocities can in fact be ascribed to differences in heating rate.) The 2600 ^{o}F background temperature also produced the highest captures, suggesting that the optimum peak temperature is about 2250 - 2300 ^{o}F (the peak temperature produced by this background temperature).

9.2 SO_2 Capture Results For 1-Inch Single-Pipe Jets

The tests using 1-inch jets were intended to provide a comparison between jets of different diameter having the same heating rate and peak temperature, and to extend the range of heating rates studied (producing one very high heating rate case). Because of the different influence of furnace conditions on the jets, the peak temperatures experienced by the sorbents were not the same in all cases. Thus the interpretation of these results is difficult.

TABLE 9-1. SO_2 CAPTURE RESULTS FOR 2-INCH JETS

Background Temperature °F		2500		2600		2800	
Peak temperature (estimated), °F		2040		2120		2250	
Heating Rate*		1	2	1	2	1	2
Peak Temperature (measured) °F		2220	2180	2290	2250	2510	2430
SO_2 Capture @ Ca/S = 2.0 (Percent)	Sorbent						
	Vicron	27	31	23	31	22	17
	Colton Lime	41	35	46	51	38	27
	Longview Lime	40	54	47	61	45	NA
	Dolomite	36	50	59	70	46	35
	S-Type	56	56	63	80	33	44

* HR1: Temperature rises from 300°F to 2000°F in 0.12 seconds.
HR2: Temperature rises from 300°F to 2000°F in 0.05 seconds.

Figure 9-6 shows the SO_2 capture versus calcium-to-sulfur ratio for three sorbents: Vicron limestone, Longview atmospheric hydrate, and Type-S pressure hydrate. For each sorbent, results are shown for three different heating rates resulting from different jet diameter/jet velocity combinations. In all cases, the peak sorbent temperature was in the range of 2400 - 2510 °F. This is above the optimum temperature for SO_2 capture; at these temperatures, the sorbents probably had their reactivity reduced through sintering, thus masking any heating rate effects.

The variations in capture for the different conditions shown in Figure 9-6 show no apparent trends with either heating rate or peak sorbent temperature. It is not possible to separate the effects of the two parameters, both of which varied for each jet configuration. The comparison is made more difficult because capture was affected by the low reactivity of the sorbent because of the high peak temperatures.

9.3 Small-Diameter Co-Axial Jets

Experiments were also conducted with co-axial jets having a 4-inch outside diameter and a 1-inch sorbent jet on the axis. The sorbents tested with these double concentric jets were: Vicron limestone, Longview atmospheric hydrate, and Type-S pressure hydrate. The annular air velocity V_A was 60 ft/sec for all cases; for the Type-S, 100 ft/sec was also tested. The sorbent velocity V_S was varied from 150 ft/sec down to zero; at $V_S = 0$, the sorbent was added to the annular air, and the jet was thus similar to a 4-inch single-pipe, dilute-phase jet. The purpose of these tests was to further investigate the influence of the sorbent jet velocity in double concentric jets, because this had been found to be important in tests in the LWS furnace (described in the separate companion report on this internally-staged burner project).

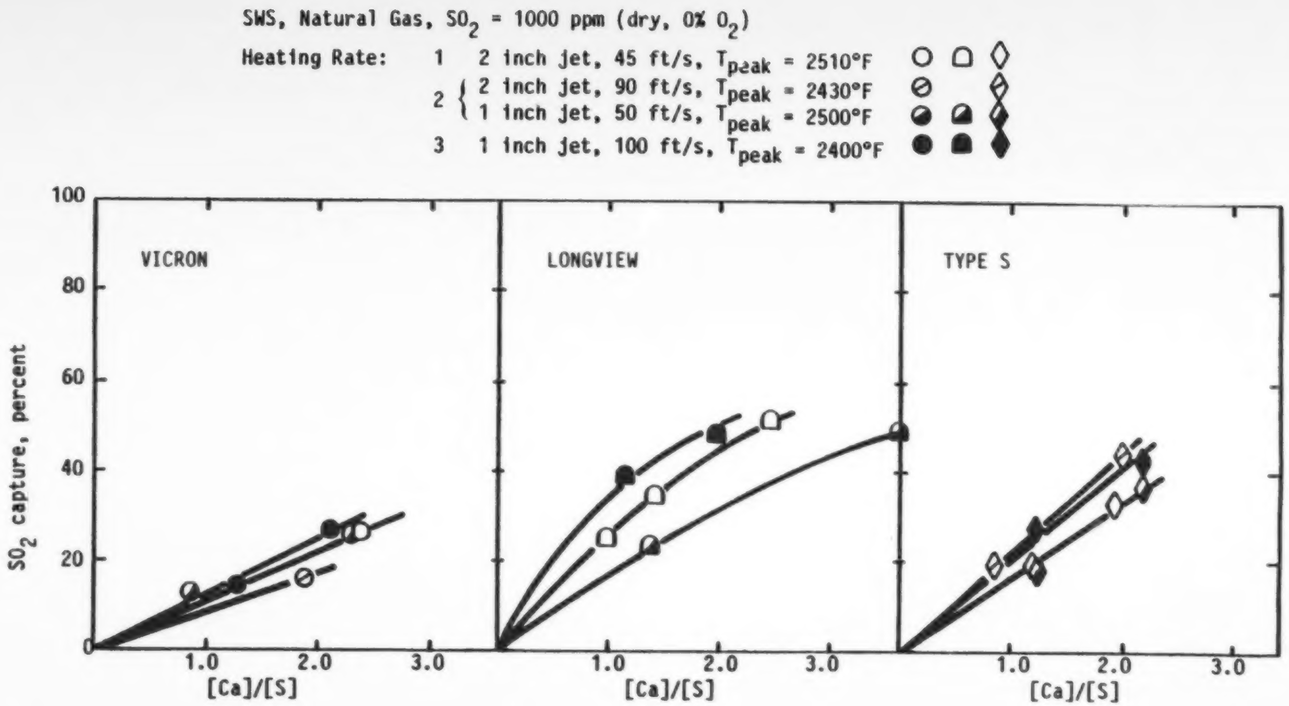

Figure 9-6. Effect of heating rate and peak temperature on SO_2 capture in 1-inch single-pipe jets (Vicron limestone, Longview atmospheric hydrate and Type-S pressure hydrate) -- heating rate studies.

These jets were found to mix very rapidly with the surrounding furnace gas, as shown by the measured temperatures described in Section 9.4. On investigation, it was found that this injector produced a strongly swirling flow in the coaxial air jet. This is thought to be the reason for the higher entrainment rate observed with this particular double concentric jet. Because of the higher rate of temperature increase, these jets subject the sorbent to heating rates and peak temperatures more typical of the single-pipe jets that were tested; hence, the results with this particular 4-inch double concentric jet are not directly comparable to the other coaxial jet studies described in Section 8. Nevertheless, the results with this 4-inch jet provide some data on the effect of changing the sorbent velocity.

The SO_2 capture for coaxial jets using Vicron limestone is shown in Figure 9-7, showing the effect of changing the sorbent velocity. SO_2 capture is in the range of 18 to 23 percent at Ca/S = 2.0. Although the data are limited, the regression lines suggest that capture is increased as the sorbent velocity is increased. This could be caused by changes in jet mixing rates resulting from internal turbulence in the jet due to the shear between the inner and outer flows.

Figure 9-8 shows SO_2 capture for Longview atmospheric hydrate. Here there are more data, but it has considerable scatter. The SO_2 capture is 55 to 60 percent at Ca/S = 2.0 for the double concentric jets, but for the dilute phase jet ($V_S = 0$), it was only about 35 percent at Ca/S = 2.0. There appears to be a big advantage here in protecting the sorbent by surrounding it with the co-flowing air jet. However, the SO_2 capture with the 2-inch single-pipe jet in Section 9.1 was similar to that achieved with these coaxial jets, so that the coaxial jet is not a necessary means of obtaining high captures for upper furnace injection conditions.

Fuel: Natural gas + SO_2 (baseline SO_2 without sorbent = 1000 ppm dry, 0% O_2)
Sorbent: Vicron 45-3 limestone
Annular air jet: 4-inches (double concentric, with 1-inch coaxial sorbent jet)
Annular air velocity V_A: 60 ft/s

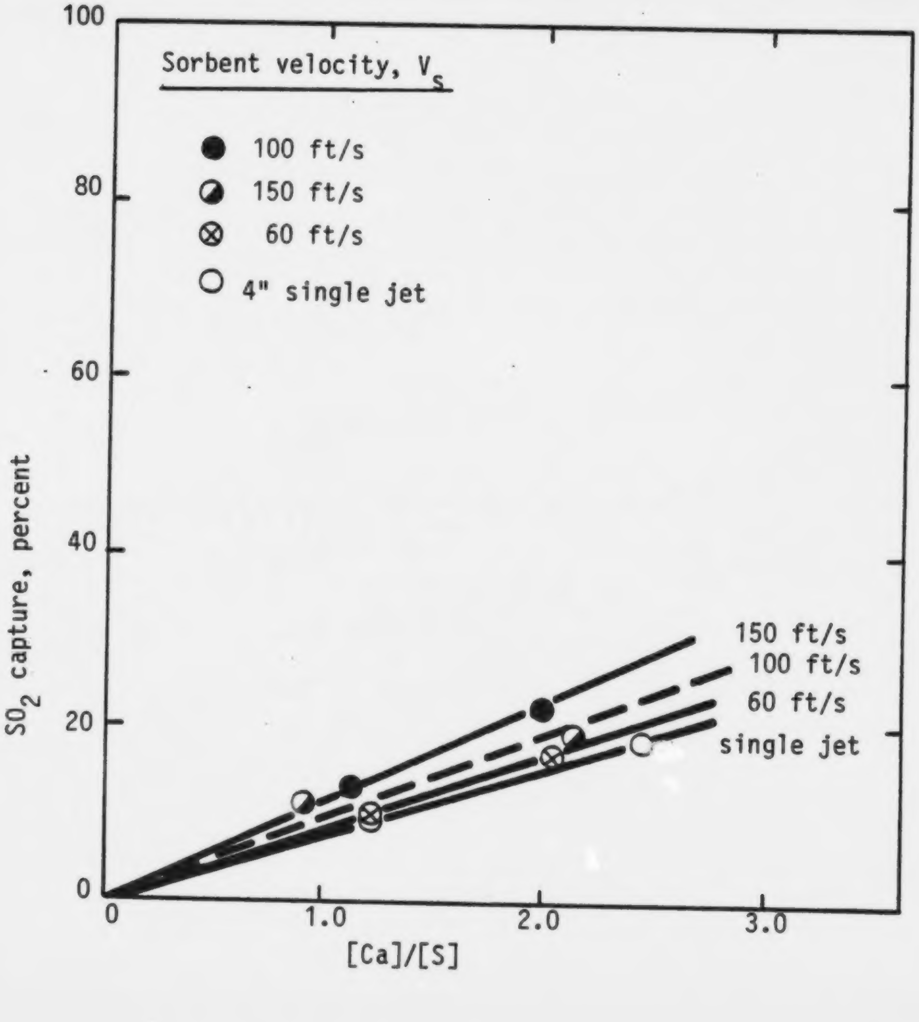

Figure 9-7. SO_2 capture with Vicron limestone injected through 4-inch double concentric jet -- heating rate study.

Fuel: Natural gas + SO_2 (baseline SO_2 without sorbent = 1000 ppm dry, 0% O_2)
Sorbent: Longview atmospheric calcitic hydrate
Annular air jet: 4 inches (double concentric, with 1-inch coaxial sorbent jet)
Annular air velocity V_A: 60 ft/s

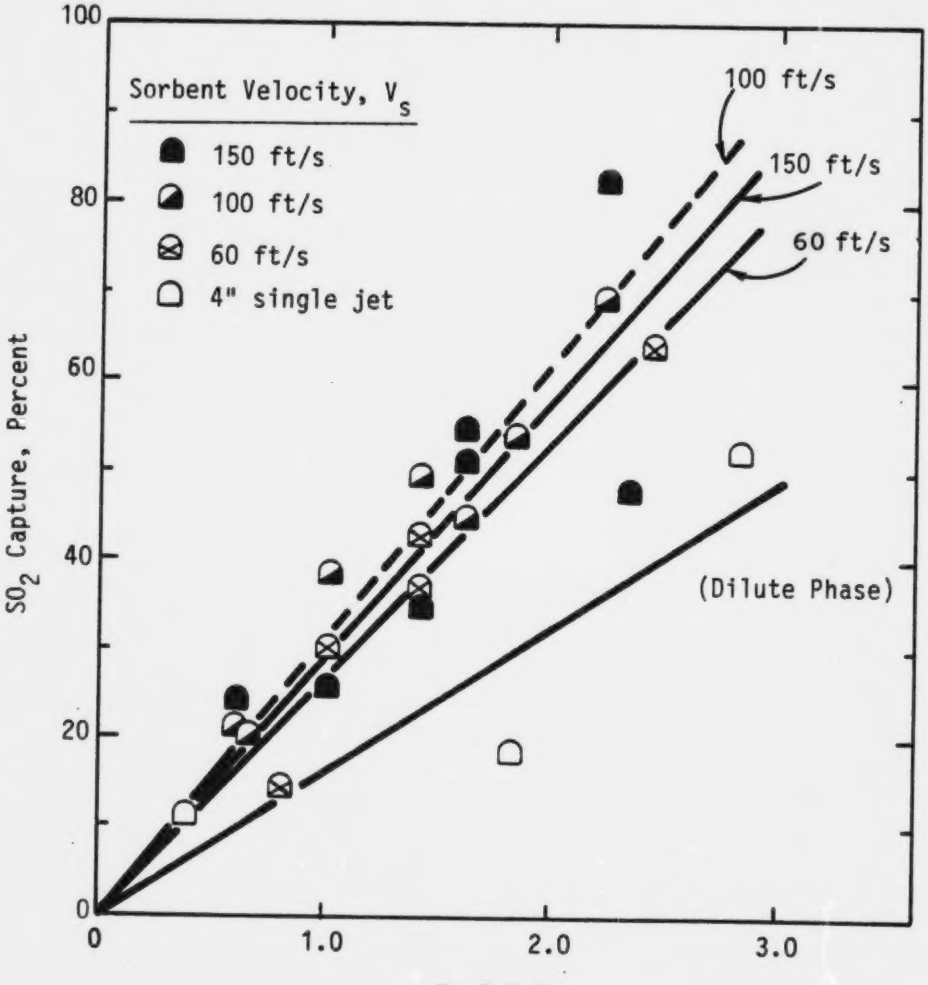

Figure 9-8. SO_2 capture with Longview atmospheric calcitic hydrate injected through 4-inch double concentric jet -- heating rate studies.

Figure 9-9 shows SO_2 capture for the Type-S sorbent. In this case, two different air velocities V_A were tested: 60 ft/sec and 100 ft/sec. The higher-V_A case produced the higher SO_2 capture, close to 90 percent at Ca/S = 2.0, compared with captures in the range of 55 to 70 percent for the lower velocity. Within these bands, the data scatter prevents identification of a specific effect of sorbent velocity V_S. Compared to the 2-inch jets, the 100 ft/sec coaxial jet produced higher capture (approximately 90 percent at Ca/S = 2.0, compared with 80 percent for the 2-inch jet). The reason for this improvement is not clear, but one possibility is that the higher jet mass flow, coupled with the increased entrainment rate of the swirling jet, more rapidly produced uniform mixing and dispersion of the sorbent over the furnace gas.

9.4 Temperature Measurements In Jets

During these heating rate tests, a number of temperature profiles were measured in the SWS in an effort to determine the true peak temperature experienced by the jets, and to confirm the entrainment constant that is used in the jet equations to estimate bulk jet temperature histories. A typical temperature distribution in a jet is shown in Figure 9-10 for a 2-inch jet issuing into a background gas temperature of 2500 °F at 50 ft/sec. This figure shows the expected development of Gaussian type jet temperature profiles. In a number of cases, only the temperatures along the jet centerline were measured. At least one temperature survey was conducted for each of the jet configurations studied in the heating rate test matrix. These measured temperatures showed higher peak temperatures than those estimated when the test matrix was drawn up (Figures 7-6 through 7-9). Table 9-2 shows the peak sorbent temperatures actually measured (the highest bulk mean temperature detected along the jet) for each of the jets studied. These measured temperatures should be compared with the calculated peak

Fuel: Natural gas + SO_2 (baseline SO_2 without sorbent = 1000 ppm dry, 0% O_2)
Sorbent: Genstar Type-S dolomitic pressure hydrate
Annular air jet: 4 inches (double concentric, with 1-inch coaxial sorbent jet)
Annular air velocity V_A: 60 and 100 ft/s

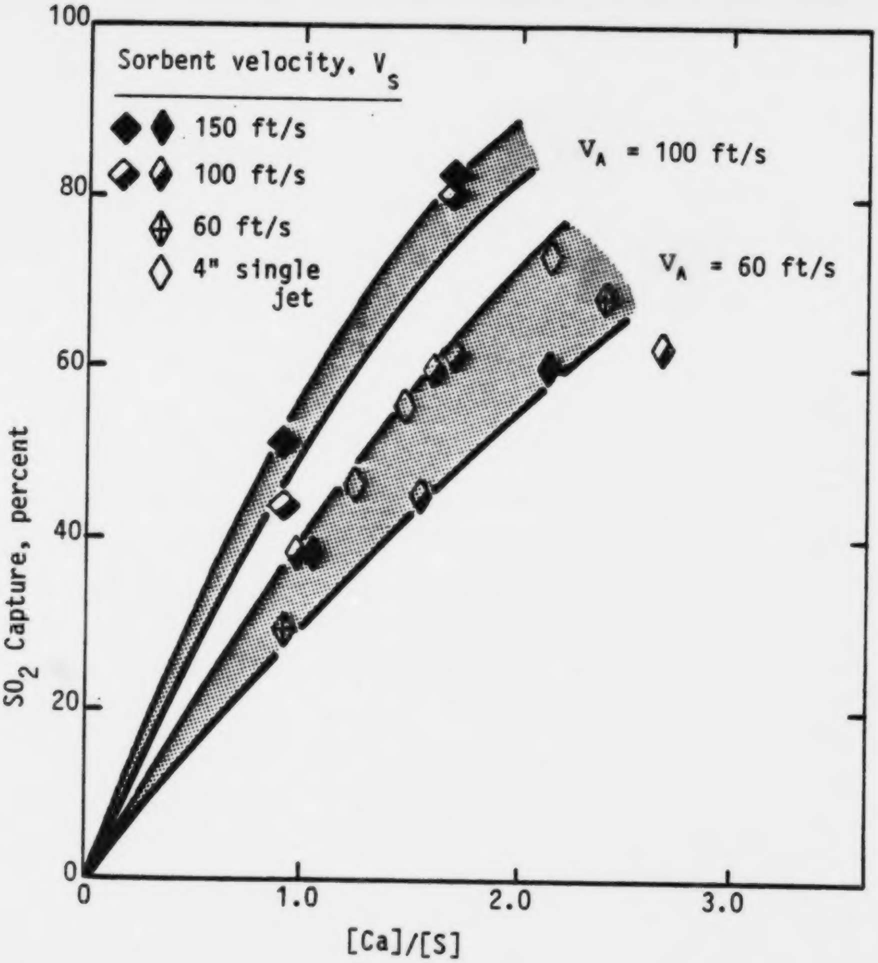

Figure 9-9. SO_2 capture with Genstar Type-S dolomitic pressure hydrate injected through 4-inch double concentric jet -- heating rate studies.

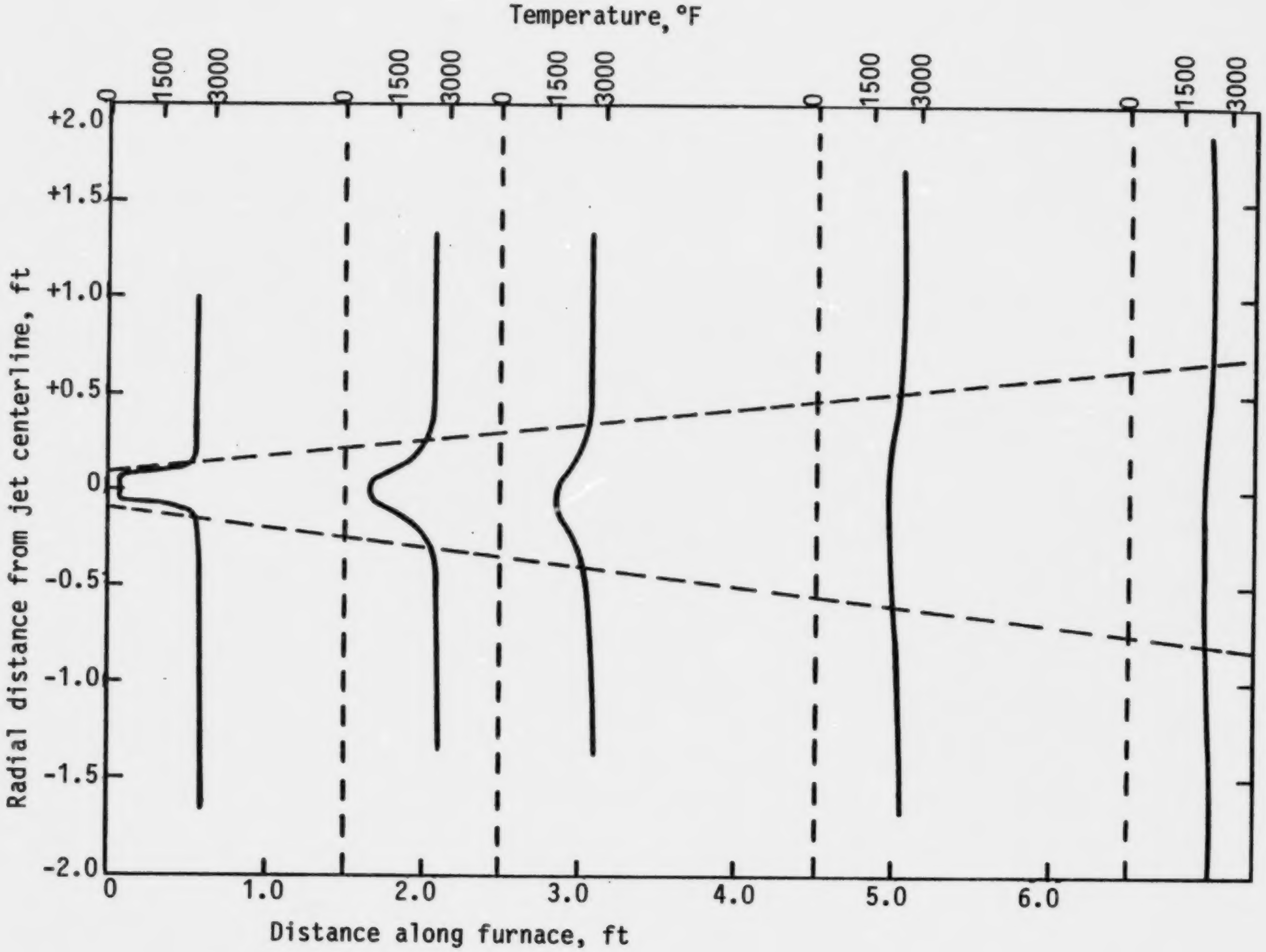

Figure 9-10. Temperature distribution measured in 2-inch jet (jet velocity = 50 ft/sec; background temperature 2500°F).

TABLE 9-2. PEAK SORBENT TEMPERATURES MEASURED DURING JET TEMPERATURE SURVEYS

Background Temperature, °F			2500	2600	2800
Peak Sorbent Temperature, °F	Jet Configuration				
	Diameter inch	Velocity ft/sec			
	2"	50	2220	2290	
		100	2180	2250	
		45			2510
		90			2430
	1"	50		2500	
		100		2400	
	4"x 1" coaxial	60		2280	

temperatures presented in, e.g., Table 7-4. The measured temperatures were up to 250 F° higher than had been estimated. The biggest differences were observed with the low velocity jets -- 2-inch at 45 ft/sec, and 1-inch at 50 ft/sec. It is likely that these jets were the most affected by the general turbulence level in the furnace. The measured temperature profiles also showed that the jet temperatures rose much faster than had been expected from the predictions made from the simple jet theory when developing the test matrix. Hence, the measured temperature data were used to make an estimate of the mass entrainment rates actually occurring in the furnace.

Using the assumption that the temperature profiles were Gaussian in form, the bulk mean temperature at each axial position was estimated from the center-line and background temperatures measured at each position. The predicted temperature for jets entraining gas that is falling in temperature along the jet is given approximately by:

$$T_x = T_o + \left(1 - \frac{x_o}{x}\right)(T_b - T_o) - \frac{bx}{2}$$

$$\text{where} \quad x_o = \frac{d_o}{k\left(\frac{\rho_\infty}{\rho_o}\right)^{1/2}}$$

and T_x is mean jet temperature at distance x from the nozzle

T_o is initial jet temperature

T_b is background temperature at jet nozzle

b is rate of decay of background temperature with distance

d_o is jet diameter

P_o, P_{oo} are densities of jet and surroundings, respectively

k is the jet entrainment constant.

On rearranging, the above equation becomes:

$$\frac{T_b - T_o}{T_b - T_x - \frac{bx}{2}} = k\left(\frac{\rho_\infty}{\rho_0}\right)^{1/2}\frac{x}{d_o}$$

and the entrainment constant k can be obtained from the slope of the line obtained by plotting

$$\frac{T_b - T_o}{T_b - T_x - \frac{bx}{2}} \quad \text{versus} \quad \frac{x}{d_o\left(\frac{\rho_0}{\rho_\infty}\right)^{1/2}}$$

The temperature data for all the jets measured is plotted in this way in Figure 9-11. This shows considerable scatter, but nevertheless produces a satisfactory correlation from which the entrainment coefficient can be found. Note that two correlations were obtained: one for the 1-inch and 2-inch jets, the other for the 4-inch coaxial jet. The coaxial jet entrained much faster than the single jet, which was not expected; on investigation it was found that this large jet had a degree of swirl imparted to it as a result of the particular double-concentric inlet arrangement.

For the single jets, the line of best fit gave an entrainment coefficient k = 0.47, compared with the standard coefficient for entrainment in a quiescent atmosphere of k = 0.32 (Ricou and Spalding (5)). This higher entrainment rate is apparently the result of increased turbulence in the jet, probably carried downstream from the gas flames used to generate the high-temperature gas flow.

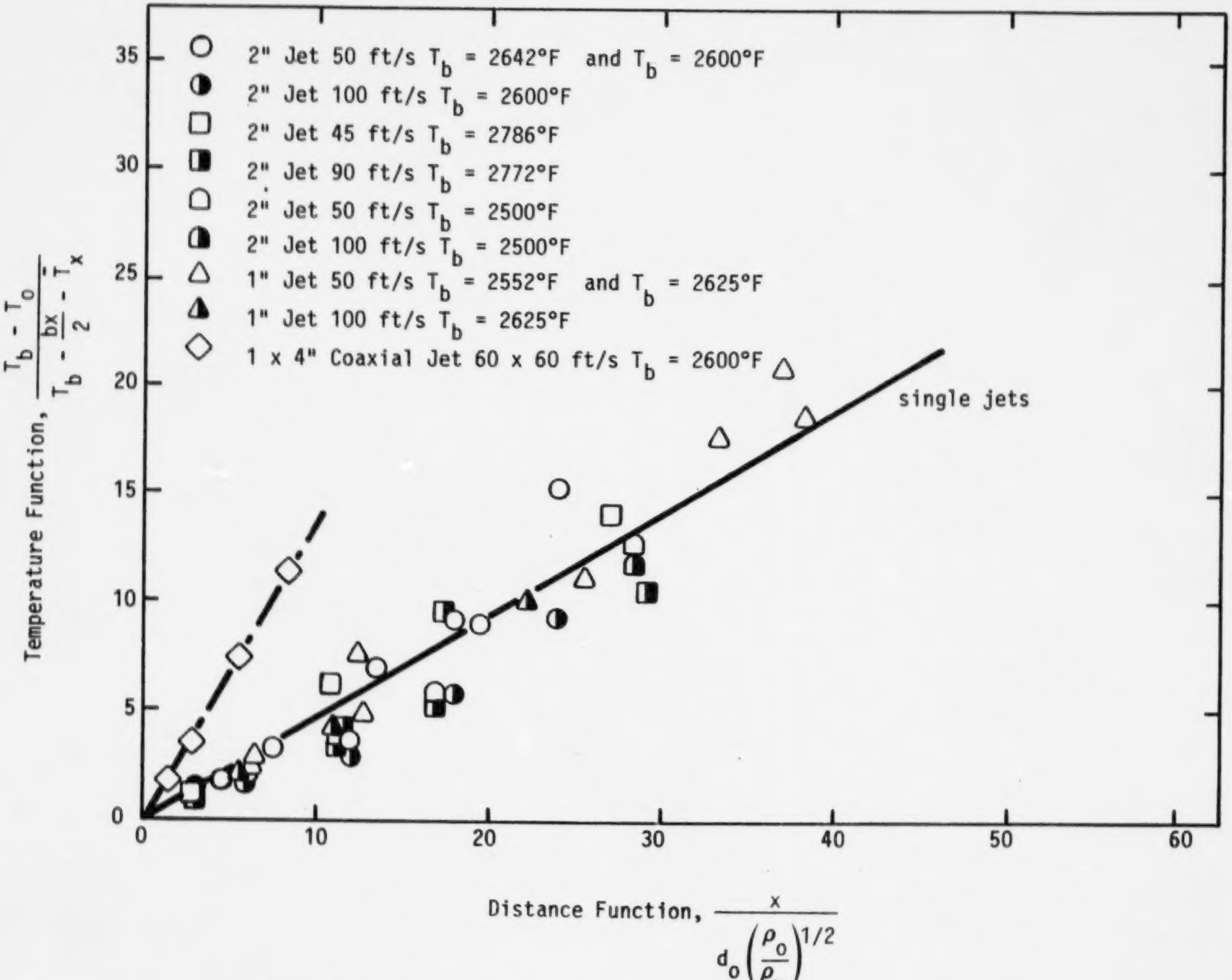

Figure 9-11. Change in mean temperature with distance along jet.

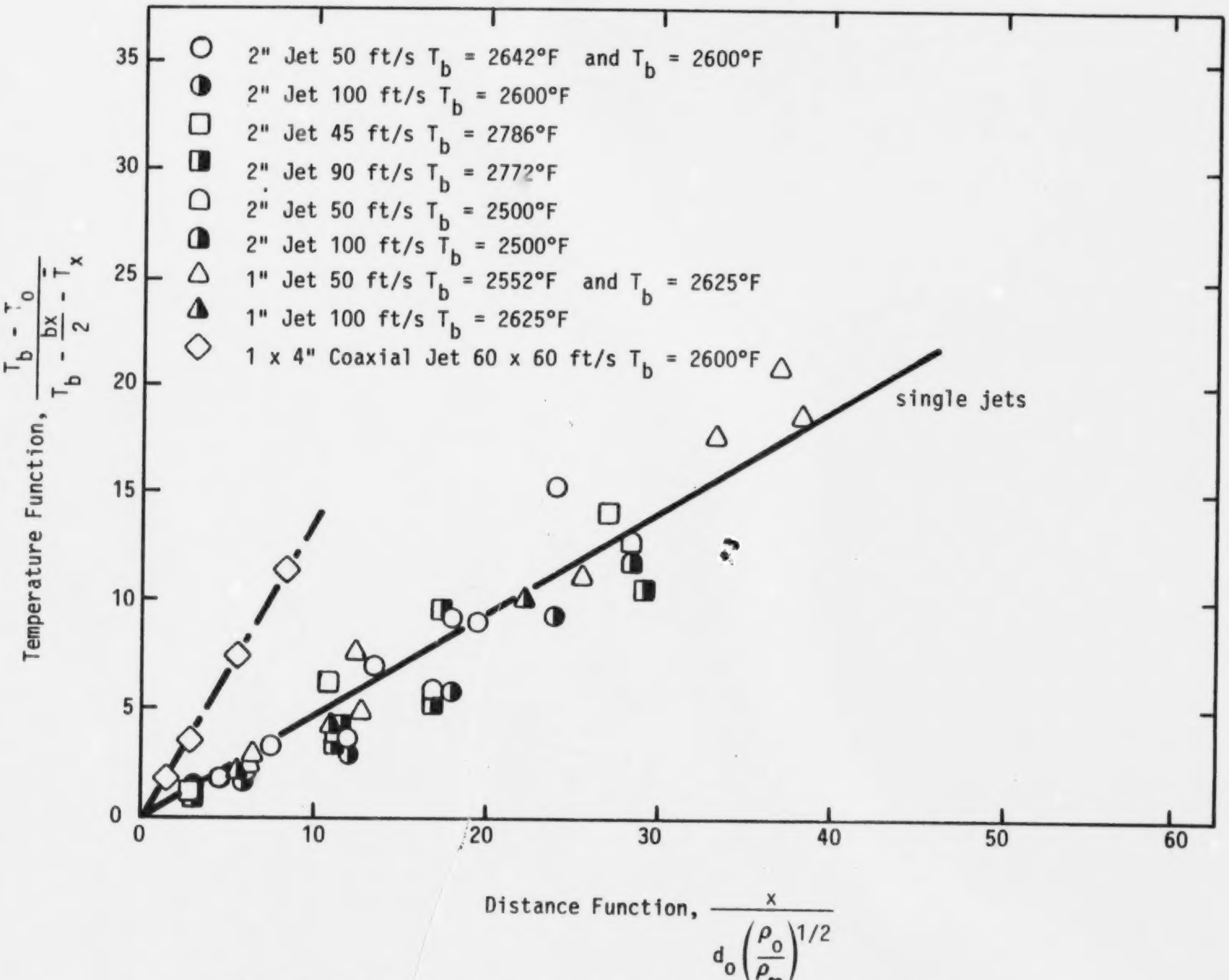

Figure 9-11. Change in mean temperature with distance along jet.

Using this derived jet entrainment coefficient, and gas flow and temperature measurements in the SWS, it was possible to reconstruct the average temperature-versus-time and Ca/S ratio-versus-time relationships for each of the jet configurations tested in the SWS. To make this calculation, the SWS was divided into four regions: (i) the jet region, which comprised the cylindrical part of the furnace where jet entrainment took place; (ii) a mixing region at the furnace exit, where it was assumed that the jet/gas mixing was completed; and (iii) and (iv), two different segments of the duct work between furnace exit and the gas sampling port.

Figures 9-12 and 9-13 show the calculated temperature and concentration histories for 2-inch jets issuing into 2500 °F background temperature at 50 ft/sec and 100 ft/sec, respectively. Also shown are measured gas temperatures for comparison. These figures show that the overall residence time of sorbent in the sulfation temperature window is of the order of 2.5 seconds, with the residence time in the jet region being 0.65 or 0.35 seconds. Thus, the heating up time for the sorbent in the jet represents a comparatively short time in relation to the overall residence time in the sulfation temperature window.

In terms of the temperature history of sorbent in each of these cases, the differences in residence time in the sulfation window may not be significant. However, there is a considerable difference between the concentration histories (i.e., the effective Ca/S in the jet vs. time) for the two different jet velocities. The higher-velocity jet has a larger mass flow, and hence it entrains more furnace gas in a given distance. Because the sorbent flow is the same in both cases, the calcium-to-sulfur ratio in the high-velocity jet falls more rapidly towards its well-mixed level, as shown in Figures 9-12 and 9-13.

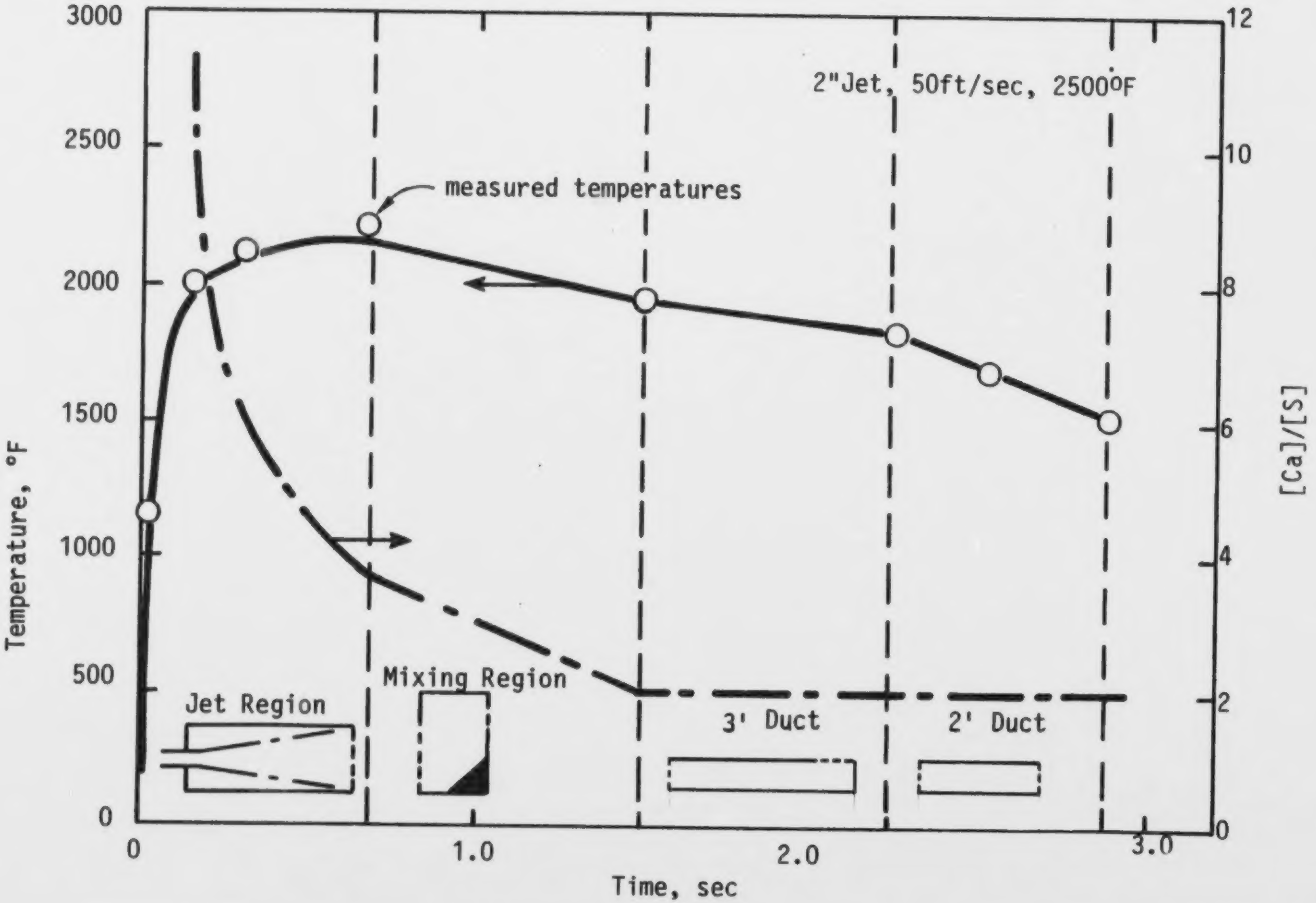

Figure 9-12. Estimated temperature and Ca/S ratio histories for 2-inch jet injected at 50 ft/s into SWS with 2500°F background temperature.

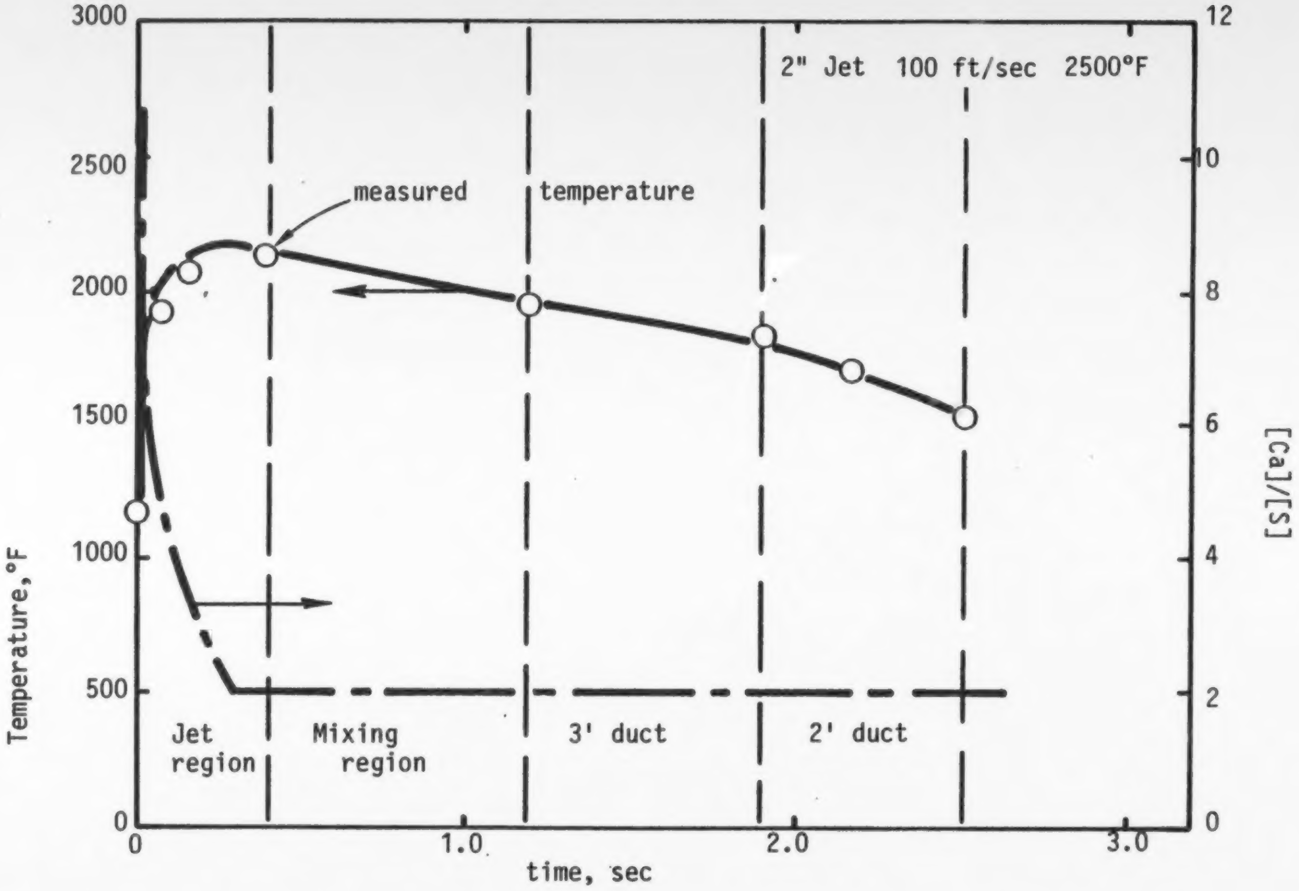

Figure 9-13. Estimated temperature and Ca/S ratio histories for 2-inch jet injected at 100 ft/sec into SWS with 2500°F background.

In an attempt to determine whether the different temperature and concentration histories were sufficient to account for changes in SO_2 capture, use was made of the sulfation model of Silcox et al (6) to predict SO_2 capture for each of these temperature histories. To do this, the model was modified to take account of the variation in effective Ca/S ratio as well as the variation in temperature. The SO_2 capture versus time predictions for Vicron limestone injection into a background temperature of 2500 °F at 50 and 100 ft/sec at Ca/S = 2.0 are shown in Figure 9-14. This shows that the high-velocity jet produces a slightly higher capture even though the sorbent had a shorter overall residence time in the furnace. Also shown on this plot is a second prediction for the 50 ft/sec jet, but assuming that the Ca/S ratio had fallen instantly to its well mixed value. Capture for the completely mixed case was much higher, showing the significance of the overall mixing on the course of the sulfur capture process. This is not surprising since sulfation can only occur as the reactants are brought together. In the jet, the sorbent initially has no sulfur contact, but gradually develops it as the jet entrains the surrounding flue gas. Thus the sulfation reaction is delayed and limited by the time taken for the sorbent and the SO_2 to mix adequately.

Table 9-3 shows the result of predictions for the other sorbents. The surface areas used for these calculations were based on data of Slaughter (7) for surface areas developed at a temperature of 2200 °F (approximately the peak temperature for the 2500 °F background case). These predictions consistently showed an increase in SO_2 capture for the higher jet velocity. Also shown are the measured SO_2 captures for these cases, which, as discussed before, show inconsistent changes with change in jet velocity. In some cases, the model predictions matched the measured capture closely; in other cases, there were significant differences. The model should be used as an indicator only, especially in view of these differences between measured and predicted results. Never-

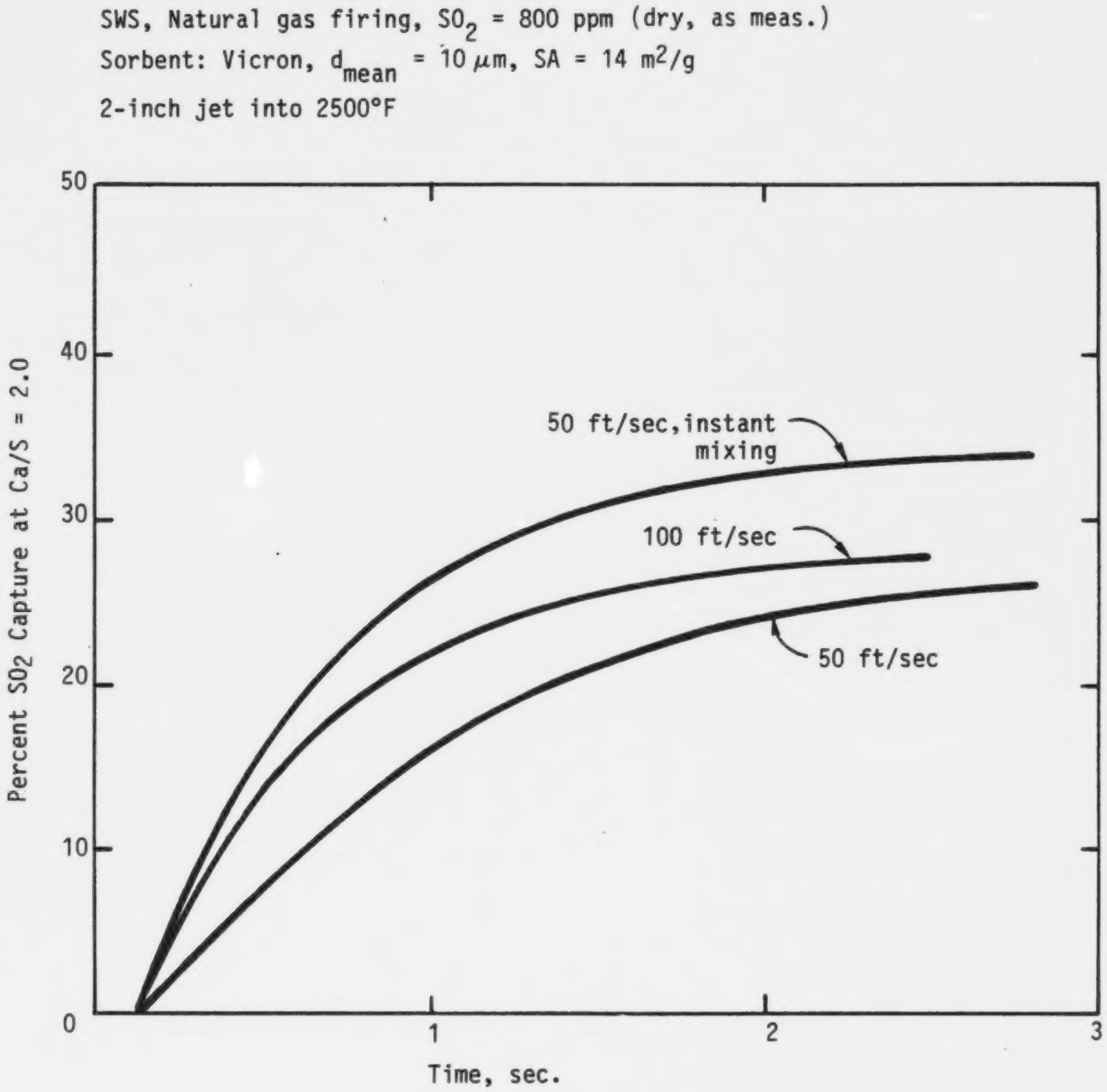

Figure 9-14. SO_2 captures predicted for 2-inch single-pipe jets at jet velocities of 50 and 100 ft/sec, based upon sulfation model of Silcox et al. (6).

TABLE 9-3. SUMMARY OF JET SULFUR CAPTURE PREDICTIONS: EFFECT OF JET VELOCITY ON SO_2 CAPTURE.

Sorbent	Vicron		Colton Lime		Dolomite		S-Type	
Mean diameter, m	10		4		10		2	
Surface area , m^2/g *	14		12		23		23	
SO_2 capture at Ca/S = 2.0**	Predicted	Measured	Predicted	Measured	Predicted	Measured	Predicted	Measured
Jet velocity 50 ft/s	25.8	27	24.6	41	37.3	36	42.2	56
Jet velocity 100 ft/s	27.6	31	26.0	35	40.5	50	45.7	56

* Surface area based on the data of Slaughter (5) at 2200°F
** 2-inch jet issuing into 2500°F furnace gas

theless, the model illustrates that only small differences in SO_2 capture could be expected at the different jet velocities purely on the basis of velocity impacts on the thermal and concentration histories of the sorbent. The large and inconsistent differences actually measured could therefore be the result of changes in sorbent reactivity. However, it cannot be said from these results that changes in heating rates of the sorbent were in fact the cause of the changed reactivity. It may be that heating rate affects sorbent reactivity, but it is also very likely that the reactivity was affected by differences in peak temperature experienced by the sorbent for the different jets as a result of non-systematic variations of entrainment and mixing.

9.5 Effect of Temperature On SO_2 Capture

The 2-inch jet test matrix was designed to study separately the effects of heating rate and peak temperature on SO_2 capture for a range of sorbents. As discussed previously in Section 9.4, the temperature measurements showed that the jets entrained faster and reached higher temperatures than had been estimated when the test matrix was drawn up. The temperatures achieved by each of the jet configurations, based on measurements, was given in Table 9-2; these have been used in comparing the effects of temperature on SO_2 capture.

Figure 9-15 shows SO_2 capture plotted as a function of measured peak temperature for each of the sorbents tested for the two different sorbent heating rates. Apart from Vicron at the low heating rate, these plots show a peak in SO_2 capture at the intermediate temperature, corresponding to a peak sorbent temperature of about 2300 °F. This is close to the optimum peak temperature identified from other experimental investigations. In terms of peak SO_2 capture, the sorbents rank in the order (from best to worst): dolomitic pressure hydrate; dolomite; atmospheric-

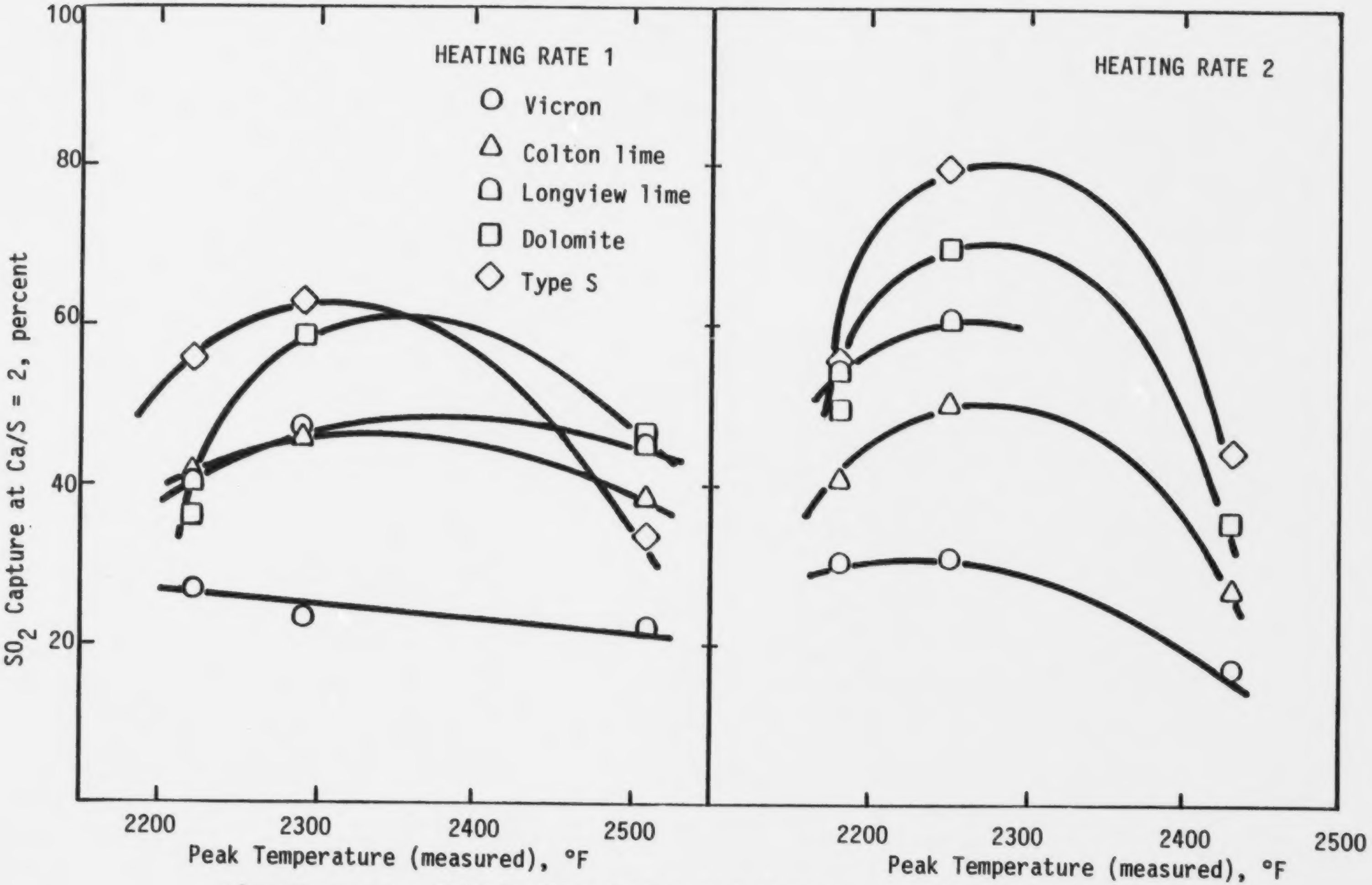

Figure 9-15. Effect of peak sorbent temperature on SO_2 capture at different sorbent initial heating rates.

pressure calcitic hydrates; and Vicron limestone. Again, this is the ranking that has been observed in previous experimental investigations.

The possible effect of initial heating rate can be observed by comparing the two plots in Figure 9-15. At the optimum temperature, there appears to be a definite increase in SO_2 capture at the higher heating rate for all the sorbents tested. It should be noted that the measured increase in capture is higher than could be expected from the effects of changing the overall thermal and concentration histories of the sorbent, as discussed in Section 9.4. At temperatures above or below the optimum, there are only small differences in capture for the different heating rates; in some cases the higher heating rate produced the lower capture. It is probable that heating rate effects were masked by other factors for temperatures away from the optimum. At high temperatures excessive sintering of the sorbent could cause loss of reactivity, and could reduce or eliminate any advantage of high heating rate. Conversely, at the lower temperatures, sintering would not be a factor in limiting sorbent reactivity, but the low temperature levels would limit the rate of sulfation and again minimize the effect of changes in reactivity caused by the different heating rates. Thus, it is plausible to expect that any effect of heating rate on sorbent reactivity will only become significant at temperatures which are close to the optimum for overall sulfur capture. In this context, the results presented in Figure 9-15 suggest that increasing the initial heating rate of the sorbent might produce an increase in overall SO_2 capture, particularly with the higher-reactivity sorbents.

9.6 Sorbent Surface Area

In order to obtain a more direct measure of the influence of temperature and heating rate on sorbent reactivity, tests were conducted where sorbent was injected into an SO_2-free furnace atmosphere, and sorbent samples were collected from the gas at the furnace exit. Solid samples were collected for each of the five sorbents tested for at least some of the jet configurations, including the 1-inch and 2-inch single-pipe jets, and the 4-inch x 1-inch co-axial jets. These samples were analyzed for specific surface area using the B.E.T. technique.

Table 9-4 shows the sorbent surface areas obtained from these solid samples. Also shown is the measured peak temperature in the jet for each configuration. The jets are listed in ascending order of heating rate, the lowest being the 1" x 4" co-axial jets at 60 ft/sec, up to the highest heating rates, produced by the 1-inch jets at 100 ft/sec. These data have been plotted as a function of peak sorbent temperature in Figure 9-16 for each of the sorbent types. The different amount of shading on the symbols indicates the sorbent heating rate. The figure shows that, as expected, sorbent surface area decreases as the peak temperature seen by the sorbent is increased in the temperature range considered. Generally, the ranking of the sorbents in terms of surface area was the same as had been observed from the SO_2 capture results, i.e., Vicron gave the lowest surface area, followed by the calcitic atmospheric hydrates (Colton and Longview), then dolomite, and finally the dolomitic pressure hydrate, Type-S. This trend of surface area versus peak temperature, and the ranking of the sorbents, is the same as has been observed in other experimental investigations at bench-scale, see for example Greene et al. (8). Furthermore, the absolute values of surface area are in line with other experimental data.

The results for the different heating rates shown in Figure 9-16, indicate that there was little apparent influence of heating rate on the sorbent surface area generated during these tests. The weighted mean sorbent heating rate is difficult to define for a

TABLE 9-4. SORBENT SURFACE AREAS MEASURED AT FURNACE EXIT FOR DIFFERENT JET CONFIGURATIONS

Jet Configuration	Peak Temp. °F	Sorbent Surface Area, m^2/g *				
		Vicron	Colton Lime	Longview Lime	Dolomite	Type S
1"x4" coaxial jets;						
Va=60 Vj = 0 ft/s	2280	7.7		9.1		24.5
Vj = 60		7.4		8.9		26.4
Vj = 100		9.1		11.2		26.7
Vj = 150		9.3		11.3		26.4
2" jet; 50 ft/s	2220	9.23				
	2290		7.71	10.2	13.4	23.8
2" jet; 45 ft/s	2510					16.7
2" jet; 100 ft/s	2180	10.8				
	2250			11.1	15.5	25.5
2" jet; 90 ft/s	2430	5.2	6.4		10.1	19.7
1" jet; 50 ft/s	2500	4.7		4.3		16.3
1" jet; 100 ft/s	2400	6.8		7.6		20.7

* All samples taken at end of furnace, where temperature was approximately 2000°F.

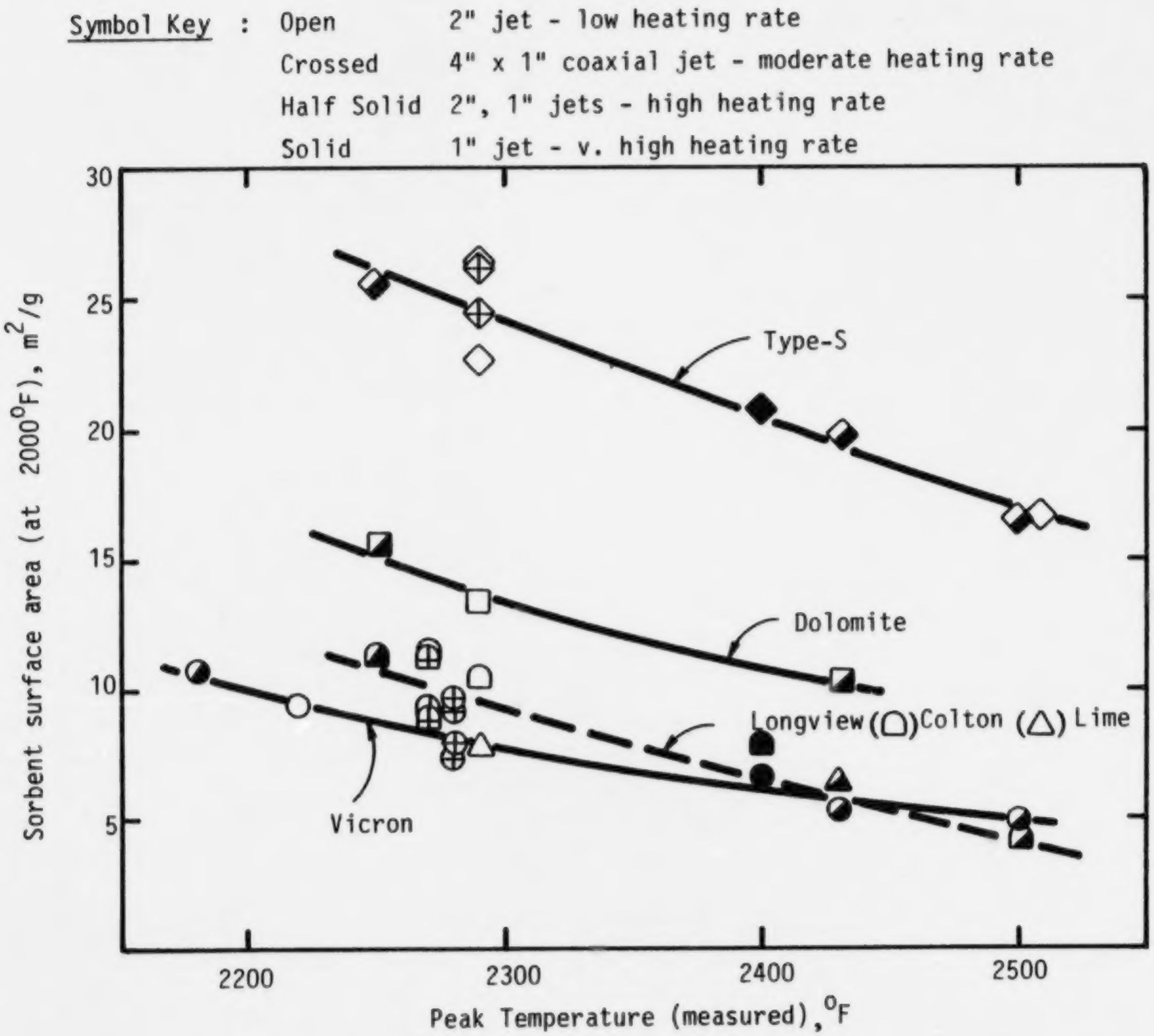

Figure 9-16. Effect of peak temperature and heating rate on sorbent surface area.

practical jet injection situation, because sorbent at the edge of the jet will be heated faster than sorbent in the center of the jet. Defining the heating rate as the average rate of increase of the jet mean temperature up to a temperature of 2000 °F, the heating rates studied here varied from a low of 15000 F°/sec to a high of 60,000 F°/sec, i.e., over a four-fold range. Over this range, the effect on sorbent surface area appears to be small, much less than the observed variations due to peak temperature.

A more detailed surface area survey was conducted for the Longview Lime sorbent injected into 2600 °F background temperature. This consisted of taking surface area samples on the center-line of the jet at different axial distances from the nozzle, as well as samples on either side of the jet axis at an axial distance of 6 ft, corresponding to the point where the jet reached its peak temperature. The survey was taken for the 2-inch jet at both 50 and 100 ft/sec, giving two different heating rates.

The results of these surveys are given in Figure 9-17, which shows both the surface area and the temperature of the jet at each sample location. The hydrate appears to have started with a surface area of the order of 20 m^2/g before injection, which then fell steadily as the jet temperature increased, reaching the final surface area of 10-11 m^2/g at furnace exit. This loss of surface area appears to be the effect of sorbent sintering. (Since no SO_2 was present in the furnace gases, no area loss would have occurred due to the sulfation reaction.) The temperature effect is also illustrated by the samples that were taken off-axis. The temperature off-axis was about 100-200 F° higher than on the center-line, and sorbent at those locations would have experienced higher temperatures during its passage through the furnace to that location. The surface areas off-axis were lower than on the centerline, as would be expected. The differences between the results for the two jets are relatively small, supporting the previous conclusion that

2" Single Parallel Jet, T_b = 2600^{o}F, Sorbent Longview

Sorbent Velocity \ Distance From End of Jet	2 ft	4 ft	6 ft	8 ft
50 ft/s	15.31 m^2/g 1526^{o}F	16.41 m^2/g 1904^{o}F	(-6") 12.11 m^2/g 2390^{o}F	10.20 m^2/g 2316^{o}F
			(℄) 15.07 m^2/g 2245^{o}F	
			(+6") 10.94 m^2/g 2318^{o}F	
100 ft/s	18.28 m^2/g 1130^{o}F	13.74 m^2/g 1769^{o}F	(-6") 10.27 m^2/g 2300^{o}F	11.10 m^2/g 2192^{o}F
			(℄) 13.58 m^2/g 2084^{o}F	
			(+6") 13.14 m^2/g 2327^{o}F	

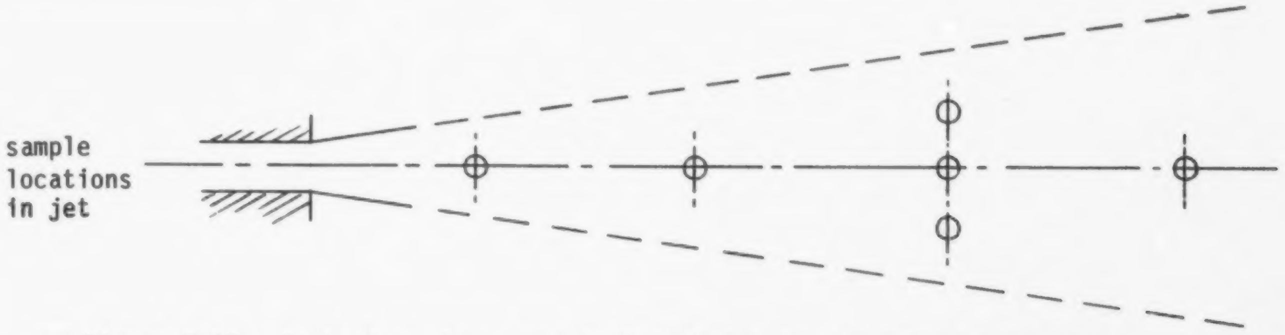

Figure 9-17. Sorbent surface area in 2-inch jet for Longview Lime sorbent.

heating rate was not an important influence on surface area in these investigations.

9.7 Summary of Sorbent Heating Rate Studies

The main objective of this part of the study was to see if the rate of heating sorbent during the calcination phase had an influence on sorbent reactivity, thus offering a means to improving SO_2 capture by tailoring sorbent jet injection conditions to give optimum heating rates.

In practical sorbent injection configurations, sorbent is injected into the furnace gas as a two-phase mixture of sorbent in a carrier gas, usually air, by means of turbulent jets. Thus, heating rates, and the thermal histories of the sorbent, can be altered by changing the jet injection configurations. The three factors that have the greatest influence on sorbent thermal history are furnace gas temperature, jet diameter and jet velocity. The furnace temperature and jet diameter define the spatial distribution of temperature within the jet, as a result of jet entrainment. Velocity determines the heating rate because it defines the time required for the jet fluid to move through the temperature field. In this series, sorbent heating rate and peak sorbent temperature were varied independently by changing furnace temperature and jet velocity. Changes in reactivity were inferred by changes in SO_2 capture, and in some cases by measurement of surface area of sorbent samples taken in the absence of SO_2 in the furnace gas.

The results of the SO_2 measurements showed that changes in capture occurred when the heating rate was increased but the results were not consistent. By comparing captures in terms of the peak temperature experienced by the sorbent, it was shown that there was a strong dependence of capture on peak temperature, as had been observed in other bench and pilot-scale experimental investigations. The optimum peak temperature in these experiments appeared to be about 2300 °F, slightly higher than observed previously.

Sorbent heating rate appeared to have an influence on capture when the peak temperature was in the range for optimum capture (around 2300 °F), and in that situation increasing the particle heating rate gave a slight improvement in overall SO_2 capture. Above or below the optimum temperature, there was no consistent influence of heating rate.

Attempts were made to predict the SO_2 capture, using an available sulfation model, taking account of the full temperature and concentration history of the sorbent in the jet and through the furnace exit ducting to the sampling port. Although not quantitatively exact, this modeling approach showed that there could be a slight increase in SO_2 capture with increased jet velocity resulting from the effect the jet velocity had on the thermal and concentration histories of the sorbent. However, the differences were smaller than the observed impact of heating rate on SO_2 capture, suggesting that some of this effect was caused by changes in sorbent reactivity.

Sorbent surface area samples were taken at the exit of the furnace for a large number of injection and furnace conditions. These surface areas matched well with measurements obtained in other experimental facilities, showing the same ranking of sorbents and trend of decreasing surface area with increasing temperature. However, the data showed only small variations with sorbent heating rate, suggesting that the final surface area was not influenced by the initial heating rate. Surface areas measured at intermediate locations along the path of the jet were higher than the final surface area, indicating that high surface areas are initially generated during calcination, and then progressively destroyed by sintering processes. Thus, even though there was no heating rate effect on final surface area, it is possible that heating rate affected the initial sorbent surface area, to produce the observed increase in overall SO_2 capture.

10.0 CLOSE-COUPLED PRECALCINER INVESTIGATION

The purpose of this investigation was to examine the possibility of generating high reactivity sorbent using a close-coupled, high temperature precalciner which would generate very high heating rates in the sorbent and then quench the sorbent before it overheated and particle sintering began. Four precalciners were used in these tests: long and short versions of precalciners made from standard alumina refractory and from chrome refractory. The chrome refractory versions were tested to see if chromium might act as a catalyst in either generating high sorbent reactivity or in promoting SO_2 capture.

In all cases the precalciner was connected to the SWS furnace by a pipe ending in a 2 inch jet on the furnace axis. The jet velocity varied between 100 and 200 ft/sec and the jet temperature varied between 800 and 2000°F. These variations occurred because of the different amounts of heat added to the jet fluid in the precalciner. The sorbent used in all cases was limestone (Vicron). In all cases a test was also conducted where the sorbent bypassed the precalciner, which was left operating so that the jet conditions in the SWS remained the same.

10.1 SO_2 Capture With The Precalciners

10.1.1 Regular Refractory, Long Version

For this version, flame temperatures (in the precalciner) of 2000°F and 2600°F were tested with SWS furnace background temperatures of 2300°F and 2500°F. Figure 10-1 shows the results of these tests. The high temperature case (2500°F) gave SO_2 capture of about 20 percent at Ca/S = 2.0. This is little different from the capture that could be expected from conventional sorbent injection. The low temperature case (2000°F) gave slightly higher capture of 25 percent at Ca/S = 2.0. This may have been the result of the lower temperatures in both the precalciner and the furnace producing less sorbent sintering. When the precalciner was bypassed the SO_2 capture fell to about 17 percent at Ca/S = 2.0. These captures indicate that the sorbent was

SWS, Uniform flow configuration
SWS Fuel: Natural gas doped with SO_2,
initial flue gas SO_2 = 1000 ppm
(dry, corrected to 0% O_2)
Sorbent: Vicron 45-3 limestone
Precalciner: Standard alumina refractory,
long version

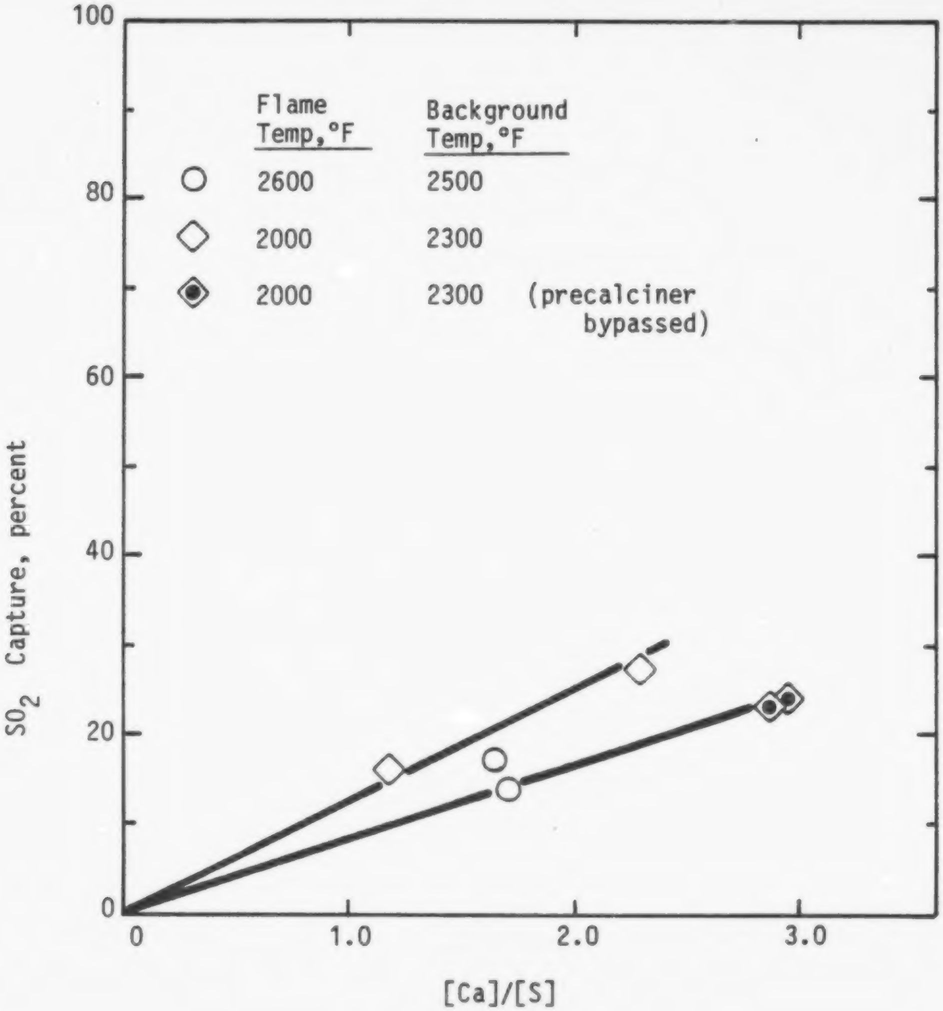

Figure 10-1. SO_2 capture with Vicron limestone using close-coupled precalciner -- standard alumina refractory, long version.

being overheated, probably because of the high initial jet temperature leading to higher peak sorbent temperatures than with the conventional injection jets.

10.1.2 Regular Refractory, Short Version

The short version of the precalciner was tested to see if reducing the residence time of the sorbent in the high temperature calciner would be beneficial. Figure 10-2 shows SO_2 capture achieved with the short precalciner. With a precalciner temperature of 2900°F and a furnace background temperature of 2400°F, SO_2 capture at Ca/S = 2.0 was about 31 percent. This was a noticeable improvement over the long precalciner case. With the precalciner bypassed, the capture fell to about 25 percent, indicating that the precalciner was having some benefit. However, these captures were not any better than those achieved with conventional sorbent injection.

10.1.3 Chrome Refractory, Long Version

This version was tested with flame temperatures of 2500, 2900 and 3000°F, all with a SWS background temperature of 2300°F. Figure 10-3 shows the SO_2 capture achieved with this precalciner. Capture ranged between 20 and 30 percent at Ca/S = 2.0. At the upper limit of this range was the capture with the precalciner bypassed, and at the lower limit was the case with the low (2500°F) precalciner temperature. It appears that increasing the precalciner temperature improved the capture, but no more than if the precalciner was bypassed.

10.1.4 Chrome Refractory, Short Version

SO_2 capture results for the short version chrome refractory precalciner are given in Figure 10-4. The conditions tested were precalciner temperatures of 2000°F, 2500°F and 2900°F, all injecting into the SWS with a background temperature of 2300°F. The SO_2 captures fall in a wide band, ranging from 25 to 45 percent at Ca/S = 2.0. The bypass case gave the lowest

SWS, Uniform flow configuration
SWS Fuel: Natural gas doped with SO_2,
initial flue gas SO_2 = 1000 ppm
(dry, corrected to 0% O_2)
Sorbent: Vicron 45-3 limestone
Precalciner: Standard alumina refractory,
short version

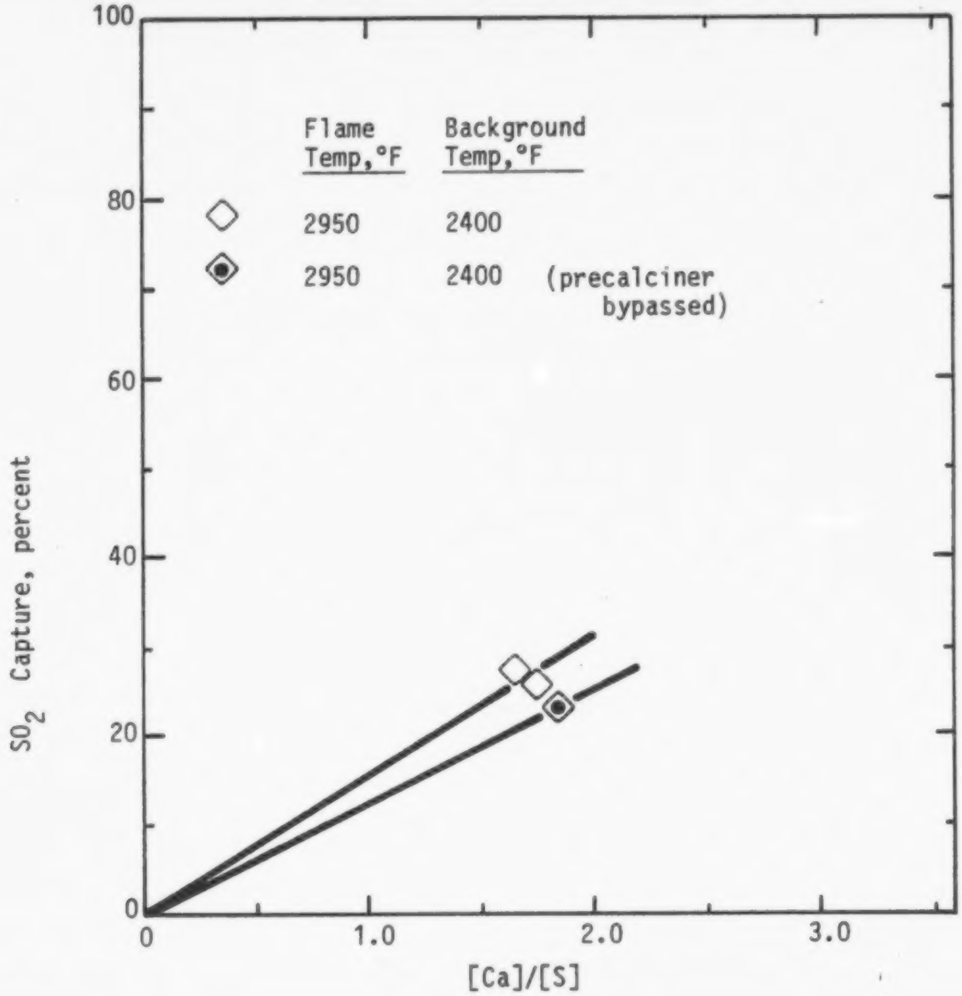

Figure 10-2. SO_2 capture with Vicron limestone using a close-coupled precalciner -- standard alumina refractory, short version.

SWS, Uniform flow configuration
SWS Fuel: Natural gas doped with SO_2,
initial flue gas SO_2 = 1000 ppm
(dry, corrected to 0% O_2)
Sorbent: Vicron 45-3 limestone
Precalciner: Chromium refractory, long version

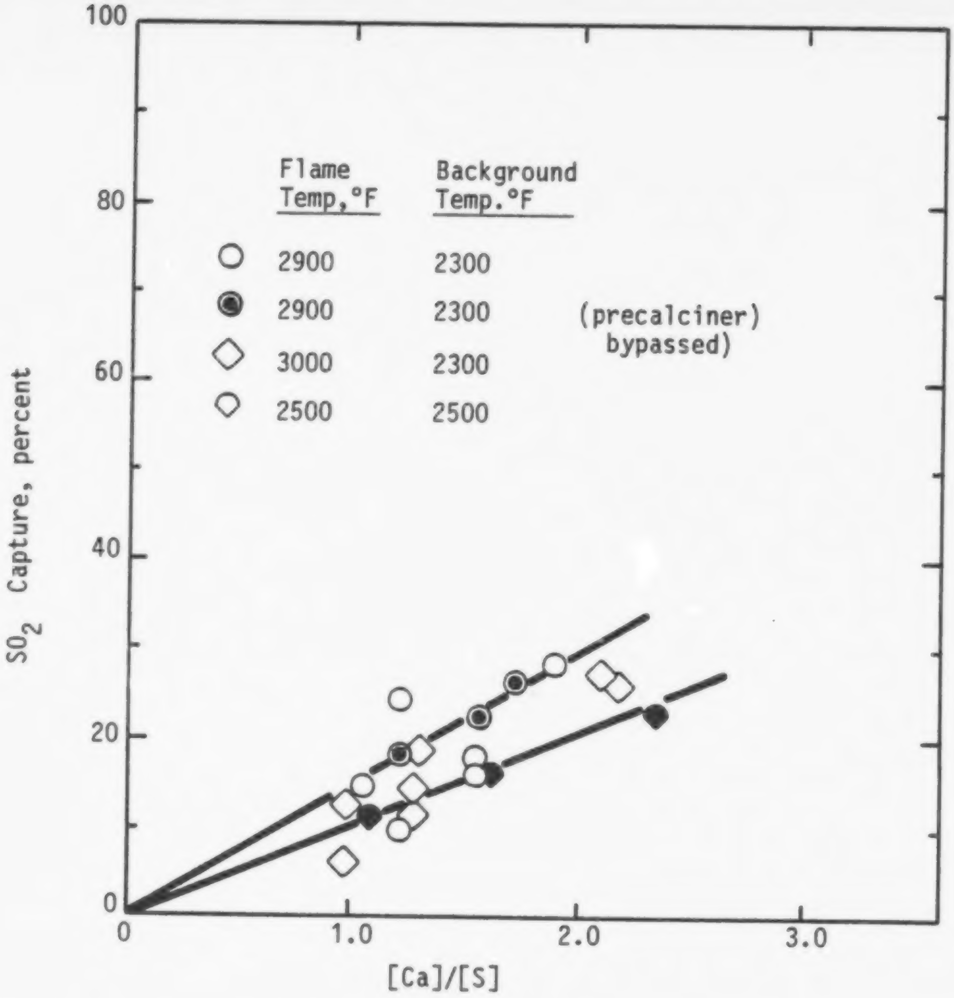

Figure 10-3. SO_2 capture with Vicron limestone using a close-coupled precalciner -- chromium refractory, long version.

SWS, Uniform flow configuration
SWS Fuel: Natural gas doped with SO_2,
initial flue gas SO_2 = 1000 ppm
(dry, corrected to 0% O_2)
Sorbent: Vicron 45-3 limestone
Precalciner: Chromium refractory, short version

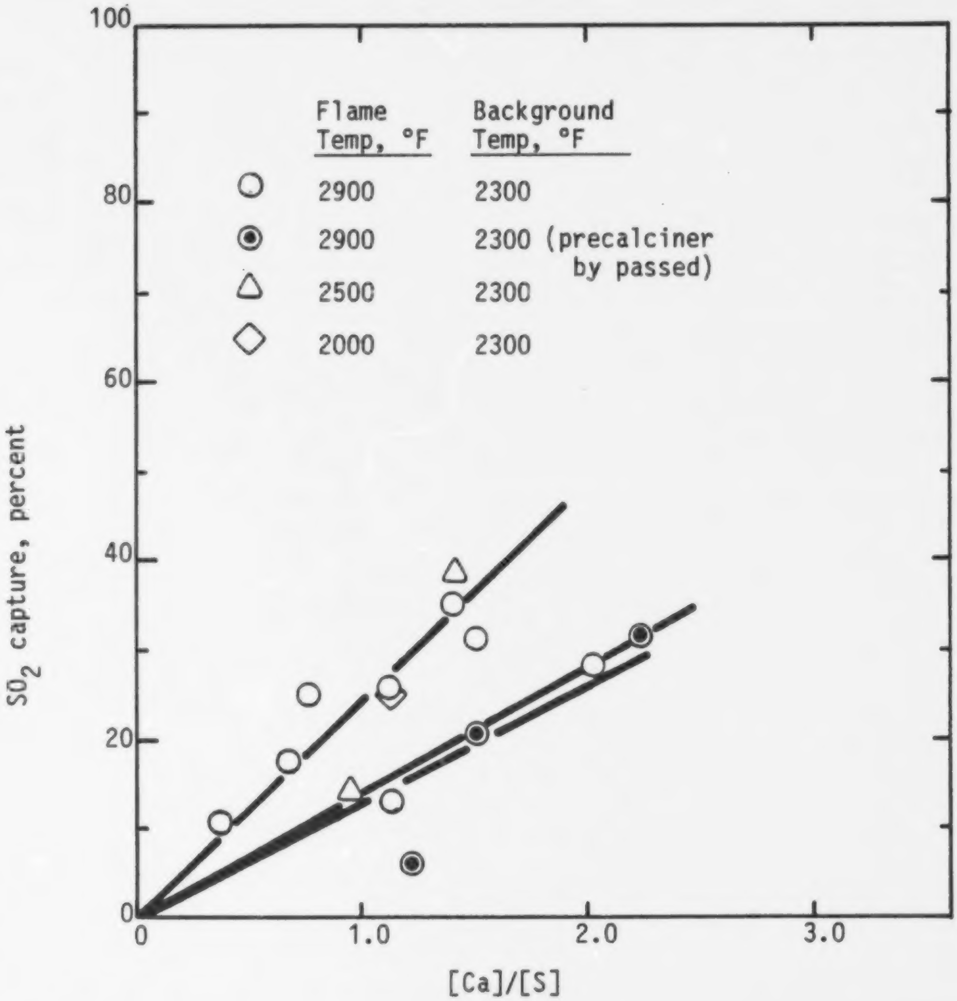

Figure 10.4. SO_2 capture with Vicron limestone using close-coupled precalciner -- chromium refractory, short version.

capture at about 30 percent, similar to the bypass case for the long chrome precalciner. Capture generally improved with the precalciner in use, suggesting that the short version of the chrome refractory precalciner may have produced higher sorbent reactivity than with conventional sorbent injection.

10.2 Sorbent Surface Areas

During the precalciner tests, a small number of sorbent samples were taken under selected conditions for surface area measurement. All operating conditions were kept the same as for the SO_2 measurements except the SO_2 doping to the gas flame in the furnace was turned off. Surface area samples were taken at the exit of the SWS furnace, but in some cases samples were also taken from the jet nozzle, to measure the amount of surface area development in the precalciner itself.

Table 10-1 summarizes the results of the surface area measurements. Surface areas of furnace exit were in the range of 5 - 10 m^2/g, which is typical for Vicron sorbent subject to peak temperatures around 2300°F (see Figure 9-16). Surface areas generated with the precalciner bypassed were essentially the same as those generated when the sorbent passed through the precalciner.

The effect of the precalciner can be seen from the samples taken at the jet exit with and without the sorbent bypass. With sorbent bypass, the surface area at the jet exit was 0.9 m^2/g, which is close to the raw sorbent surface area of 0.6 m^2/g. However, with sorbent passing through the precalciner, the surface area at the jet exit rose to about 4.0 m^2/g, with a further increase to the furnace exit. Thus, the precalciner contributed only part of the surface area developed by the sorbent, and because there was a further increase in surface area in the furnace, the sorbent could not have been calcined completely or extensively sintered in the precalciner.

In these tests the precalciner did not achieve its objective of generating a high sorbent surface area prior to injection into the furnace.

TABLE 10-1. SORBENT SURFACE AREAS GENERATED WITH CLOSE-COUPLED PRE-CALCINER (VICRON SORBENT)

Precalciner	T_{flame}, ^{o}F	T_{back}, ^{o}F	Surface area, m^2/g	
			Jet Exit	Furnace Exit
No-Chrome (Short)	2900	2400	NA	10.21
bypassed*			NA	8.11
Chrome (Short)	2900	2300	NA	9.76 6.52
bypassed*			NA	5.21
Chrome (long)	2900	2300	3.5	8.6
bypassed*			0.9	10.9
Chrome (long)	3000	2300	4.2	4.8

* In these cases the precalciner was still operating, but the sorbent was bypassed.

Perhaps it is not feasible to significantly increase the initial surface area/reactivity of limestones by controlled, high-heating-rate precalcination on-site followed by immediate injection into the furnace. Perhaps the calcination/surface area development/sintering/sulfation processes occur in such a manner that controlled precalcination cannot provide significantly greater surface areas (or, at least, significantly greater SO_2 captures) than does injection of the raw limestone directly into the furnace at optimal peak temperatures. On the other hand, possibly the problem in this study was simply that the sorbent was not adequately mixed with the hot gases in the experimental precalciner, and/or did not reach a high enough temperature before being quenched and leaving the precalciner, or did not achieve a high enough heating rate. More work would be needed to fully understand the thermal behavior of the precalciner, and the potential for developing high sorbent surface areas through use of an on-site, close-coupled precalciner beside a utility boiler.

11.0 CONCLUSIONS FROM SORBENT JET INVESTIGATIONS

These sorbent jet investigations were conducted in two phases. The first phase mainly investigated large diameter co-axial (double-concentric) jets which were intended to simulate the situation where sorbent was injected along the axis of the tertiary air jet of a DMB burner. The second phase concentrated on small diameter jets, as might be used for upper furnace sorbent injection, looking at the possibility of enhancing sorbent reactivity by changing sorbent heating rates through adjustment of jet injection conditions. The main conclusions from these studies are discussed separately below.

11.1 Large Diameter Jet Studies

In the SWS furnace, the large diameter jets (6, 10 and 12-inch diameter) mixed so slowly with the surrounding furnace gas that the sorbent experienced a peak temperature that was approximately equal to the furnace exit temperature. The highest temperatures seen by the sorbent in these tests was about 2000°F, well below the optimum for SO_2 capture. The SO_2 capture was found to be relatively insensitive to changes in jet aerodynamics.

Tests on sorbent jets without the coaxial air jet showed that these small diameter sorbent jets gave SO_2 captures that were sensitive to furnace background temperature and jet aerodynamic parameters. These jets produced peak sorbent temperatures close to the background furnace gas temperature at the injection point and it was found that the best capture was obtained at the lowest background temperature, 2200°F. Increasing the jet velocity increased SO_2 capture, and since this increased sorbent heating rates for the same peak sorbent temperature, it is thought that increased sorbent heating rate may have led to improved sorbent reactivity.

The comparison between single sorbent jets and double-concentric jets having the same inner (sorbent) jet parameters showed that SO_2 capture was improved when the sorbent jet was blanketed by the outer air flow. Thus the double-concentric jet offers a potential means of protecting sorbent where injection into high temperature zones is unavoidable.

Measurements of sorbent surface area development along a jet showed that high surface areas developed at temperatures below about 1700°F, but as peak temperature was increased, the surface area was reduced, presumably through sintering and grain growth. Although the surface area at higher temperatures was lower, similar SO_2 captures were obtained, showing the competition between the different process variables: lower peak temperatures gave higher surface areas but reduced sulfation reaction rates, whereas higher peak temperatures gave reduced surface area but higher sulfation reaction rates.

Tests on crossflow sorbent jets showed little sensitivity to jet injection parameters, but this may have been caused by jet over-penetration across the furnace, causing poor sorbent diopersion.

11.2 Sorbent Heating Rate Studies

Sorbent heating rate and peak sorbent temperature were varied independently by changing furnace temperature and jet velocity. The SO_2 capture for all the sorbents tested was found to be sensitive to peak sorbent temperature, with the higher reactivity sorbents showing the greater sensitivity. Maximum SO_2 capture was found with peak sorbent temperatures in the range 2250 - 2350°F. The effect of heating rate was not consistent over the full range of temperatures tested, but at temperatures producing maximum SO_2 capture, the higher heating rate consistently produced higher SO_2 capture. Sulfation modelling studies indicate that this increase does not appear to be solely the result of changes in the thermal and concentration history of the sorbent between tests; thus, it could be the result of heating rate effects on sorbent reactivity.

Surface area samples taken without any SO_2 doping in the furnace gas showed that surface area developed to a maximum along the jet and then decayed as the sorbent was held at high temperature. Sorbent surface areas taken at the end of furnace showed a trend of decreasing surface area with increasing temperature as has been found in other investigations. There was no observable influence of heating rate on final surface area of sorbent at furnace exit. The surface area values for each sorbent and the relative ranking of sorbents were also in line with results from other investigations. The ranking of sorbents (in order of increasing surface area and reactivity) was: limestone (Vicron), calcitic atmospheric hydrates, dolomite and pressure hydrated dolomitic lime (Type-S).

The close-coupled precalciner tests investigated four different versions of the precalciner, to study the effects of calciner temperature and residence time, and the possible influence of chromium in the refractory as a reactivity promoter. The SO_2 capture results did not show any improvement over the case where the sorbent was allowed to bypass the precalciner, except for the short residence time chrome refractory system. Surface area measurements on sorbent taken from both jet exit and furnace exit, showed that the sorbent was only partially calcined in the pre-calciner, with final calcination completed in the furnace. Surface area at the end of the furnace was the same with or without the precalciner. These tests showed that, under the precalciner conditions studied, the use of the precalciner did not produce any improvement in capture over conventional sorbent injection.

12.0 REFERENCES

1. Akiyama, T., "The Reduction of NO_x Emissions from Burners for Coal and Oil-Fired Boilers by Burner Modifications," AP-6 Trials Report, International Flame Research Foundation, IJmuiden, The Netherlands, Document No. F37/a/5, March 1980.

2. Payne, R., T. Akiyama and J. Witkamp, "Studies on Pollutant Emission Characteristics of a Number of Oil-Fired Combustors," American Flame Research Committee Symposium on NO_x Reduction, Newport Beach, CA, 1980.

3. Patrick, M. A., "Experimental Investigation of Mixing and Flow in a Round Turbulent Jet Injected Perpendicularly into a Main Stream," Journal of the Institute of Fuel, September 1967, pp. 425-431.

4. McCarthy, J. M., S. L. Chen, J. C. Kramlich, W. R. Seeker, and D. W. Pershing, "Reactivity of Atmospheric and Pressure Hydrated Sorbents for SO_2 Control," in Proceedings: 1986 Joint Symposium on Dry SO_2 and Simultaneous SO_2/NO_x Control Technologies, Volume 1, EPA-600/9-86-029a, October 1986 (NTIS No. PB87-120465).

5. Ricou, F. P., and D. B. Spalding, "Measurements of Entrainment by Axisymmetrical Turbulent Jets," Journal of Fluid Mechanics, Vol. 11, Part 1, 1961, pp. 21-32.

6. Silcox, G. D., D. M. Slaughter, and D. W. Pershing, "High-Temperature Sulfation Studies in an Isothermal Reactor: A Comparison of Theory and Experiment," Twentieth Symposium (International) on Combustion, The Combustion Institute, August 1984, pp. 1357-1364.

7. Slaughter, D. M., G. D. Silcox, P. M. Lemieux, G. H. Newton, and D. W. Pershing, "Bench-Scale Evaluation of Sulfur-Sorbent Reactions," in Proceedings: First Joint Symposium on Dry SO_2 and Simultaneous SO_2/NO_x Control Technologies: Volume 1, EPA-600/9-85-020a, July 1985 (NTIS No. PB85-232353).

8. Greene, S. B., S. L. Chen, W. D. Clark, M. P. Heap, D. W. Pershing, and W. R. Seeker, "Bench-Scale Process Evaluation of Reburning and Sorbent Injection for In-Furnace NO_x/SO_x Reduction," report prepared for the U. S. Environmental Protection Agency by Energy and Environmental Research Corp., EPA-600/7-85-012, March 1985 (NTIS No. PB85-185890).

APPENDIX A

QUALITY ASSURANCE: SWS INVESTIGATIONS

A.0. CRITICAL MEASUREMENTS

The experiments discussed in this report were performed in accordance with the quality assurance guidelines set forth in the Quality Assurance Project Plan for this program. The Quality Assurance Plan was submitted to EPA on April 29, 1983. This appendix describes the specific tests conducted to determine the precision and accuracy levels for the critical measurements in this program. Critical measurements are those which directly affected the results and conclusions in this report. The critical measurements were:

- Fuel flow rates
- Sorbent flow rates
- Combustion air preheat temperatures
- Furnace exit gas species composition
- Solids composition

Table A-1 summarizes the precision, accuracy and completeness for these critical measurements. The QA goals for the most critical measurements were met during these tests. In the following sections, each measurement is briefly described and the various QA checks are discussed.

A.1 Fuel Flow Rate

The fuel flow rate was monitored continuously during the tests with calibrated instruments. The flow rates of three fuels used during these tests (gas, oil, coal) were monitored with the following instruments:

- Coal flow rate with volumetric twin-screw-type feeder
- Oil flow rate with factory calibrated rotameter
- Gas flow rate with factory calibrated rotameter

TABLE A-1. PROGRAM OBJECTIVES FOR MEASUREMENT PRECISION ACCURACY AND COMPLETENESS.

PARAMETER	MEASUREMENT METHOD	PRECISION: % REL. STANDARD DEVIATION		ACCURACY, %		COMPLETENESS, %	
		ACTUAL	GOAL	ACTUAL	GOAL	ACTUAL	GOAL
Fuel Flow Rate							
Coal	Volumetric Feeder	-	5	-	5	90	90
Oil	Rotameter						
Gas	Rotameter						
Sorbent Flow Rate	Volumetric Feeder	10	10	-	10	90	90
Burner/Sorbent Carrier Air Flow Rates	Venturi Flowmeter	3.6	4	4.20	5	90	90
Combustion Air Preheat Temp.	Thermocouples	2.5	5	2.5	5	90	90
Gas Species	Continuous Monitors	-	2		20	>90	90
NO/NO_x	Chemiluminescense			9.9			
CO	NDIR			-			
CO_2	NDIR			2.9			
SO_2	UV			6.0			
O_2	Paramagnetic			19.2			
Furnace Exit Temperature	Suction Pyrometer	2.5	5	2.5	5	90	90
Solids Comp.							
Carbon	Perkin Elmer 240B	1.1	5	5.6	5	>90	90
Hydrogen		0.9		4.1			
Nitrogen		7.7		15.9			
Ash	ASTM	2.3		2.2			
Sulfur	Leco SC32	3.0		7.4			
Heating Value	ASTM	0.08		0.8			

The coal feeder was calibrated by operating the feeder system at constant feed rate and determining the mass of coal collected in a measured time period. A calibration graph showing the mass flux of coal as a function of feeder speed setting was produced as shown in Figure A-1. Preground and dried coal was supplied to the feeder from large storage bunkers. The rotameter used for oil flow rate measurement was also calibrated in a similar manner as described above. The calibration of the flowmeter used for gas flow measurement was checked against a laminar flow element.

As an independent check on the fuel flowrate, the fuel composition, the composition of combustion products in the exhaust and the measured air flow rates were used to calculate the thermal heat input into the furnace. This was routinely compared with the calculated heat input based on fuel heating value and mass flowrate for oil or gas. This procedure, commonly called "fuel-check" was performed every test day before the testing commenced. This procedure allowed to check the proper operation of the SWS systems and to identify any problems. The checks this procedure provided include:

- Gas sampling system leak check
- Combustion air measurement system check
- Fuel flow rate measurement check
- Furnace leak check

The results of these fuel checks performed during the test period are shown in Figures A-2 and A-3. The two heat input rates calculated as described above were within 5% of each other allowing testing to proceed. No tests were conducted unless the "oil check" was within 10%.

A-2. Sorbent Flow Rate

Sorbent flow rates were measured by a screw-type volumetric feeder similar to that used for the coal flow rate measurement. The feeder was calibrated as described for coal feeder.

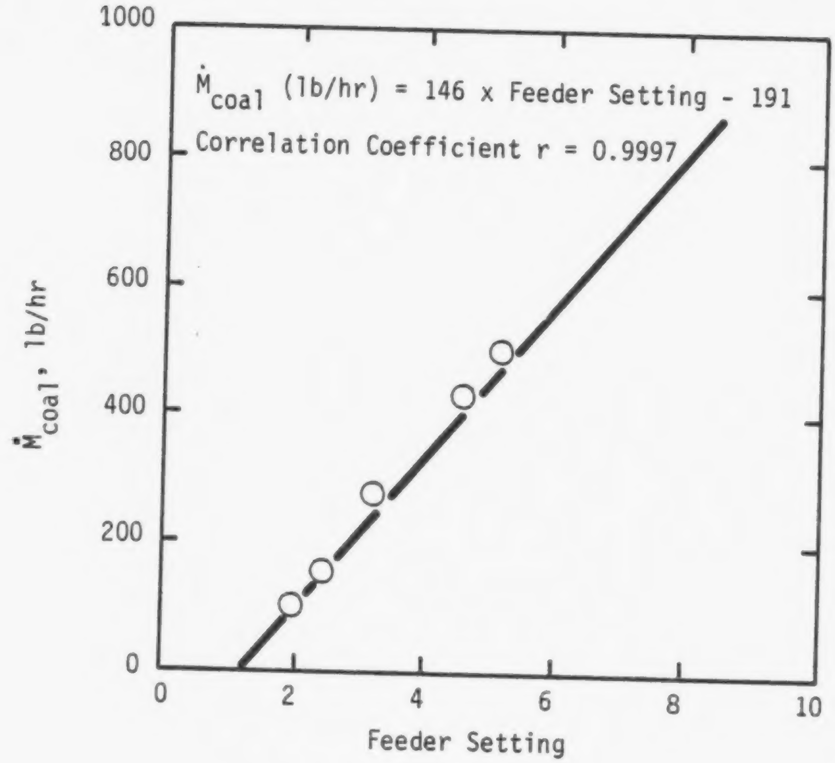

Figure A-1. Coal feeder calibration for Utah coal.

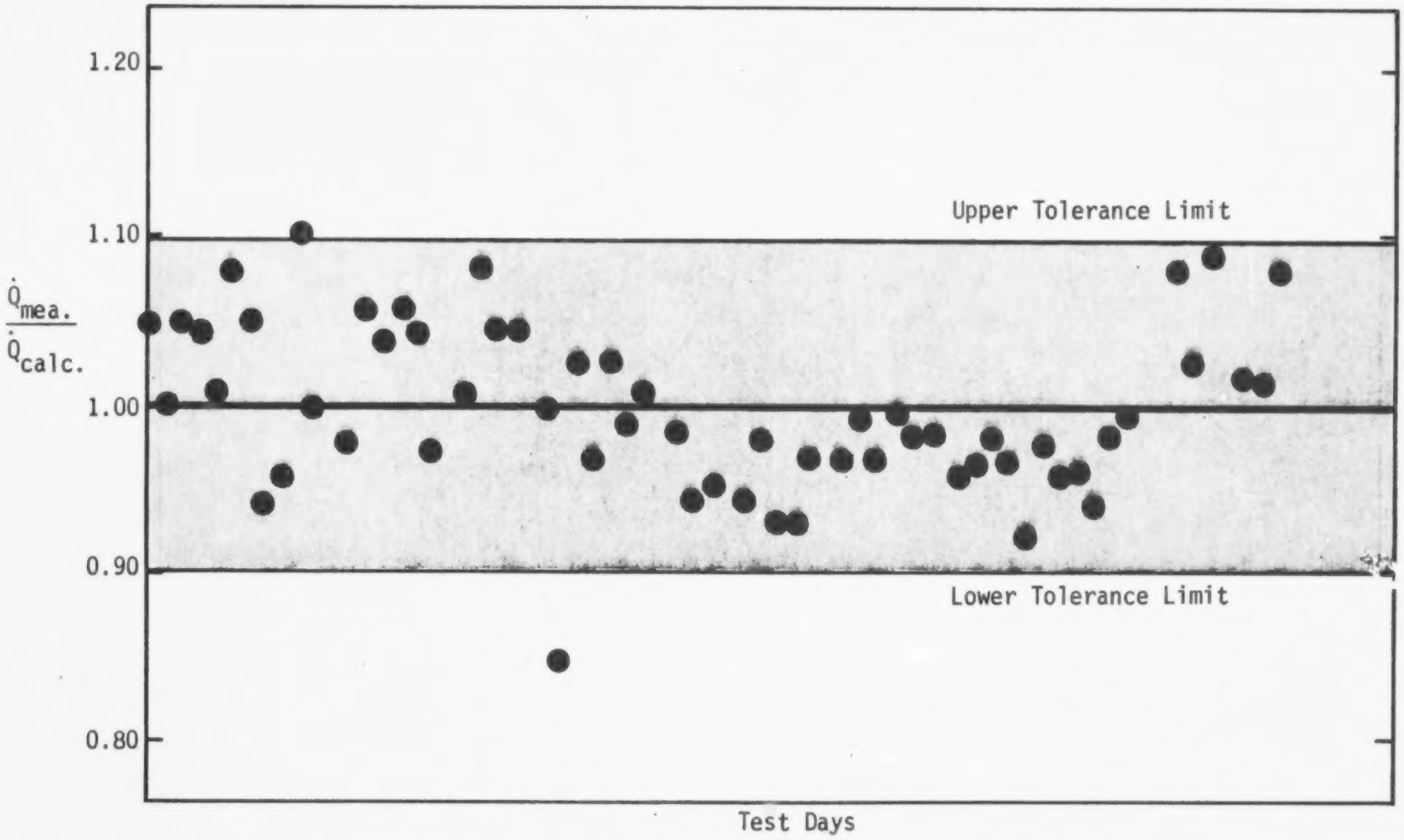

Figure A-2. "Fuel Check" during the burner test series.

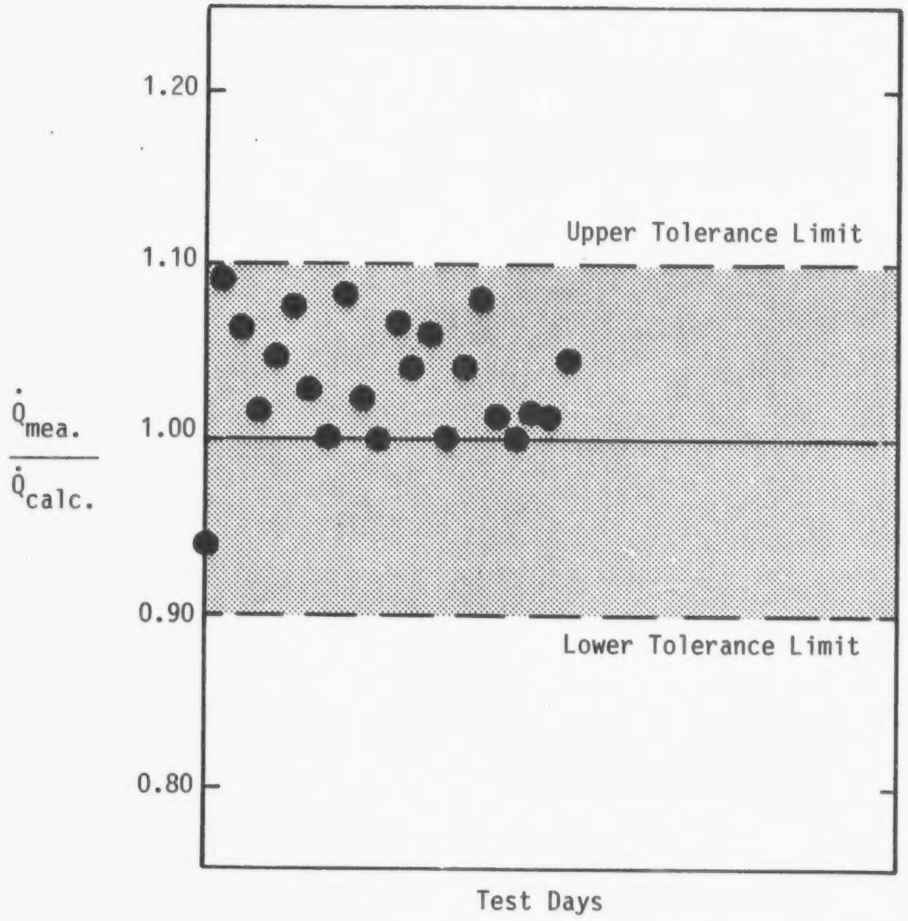

Figure A-3. "Fuel check" during jet experiment series.

A.3 Burner/Sorbent Carrier Air Flowrates

The preheated combustion air flowrates to various burner passages were measured with calibrated venturi flowmeters. These flowmeters are routinely calibrated before each test series. A comparison of these calibration checks before this series of tests showed an agreement with the previous calibrations of same venturis within 4%. The air flowrates were determined from the measured pressure drops in the venturi and the air temperature according to

$$M = K\rho_0\sqrt{\Delta P/T} \tag{A-1}$$

Where M is the mass flow of air, ΔP is the venturi pressure drop in inches of H_2O, T is the absolute temperature in ^oR and K is the dimensional venturi calibration constants listed in Table A-2.

A.4 Gas Species Measurement

Concentrations of NO_x, CO, CO_2, O_2 and SO_2 were measured at the exit of the SWS furnace. A water cooled sample probe was located at the center of the exhaust duct before the flue gases entered the air preheater. The sample train and the SWS analytical systems are shown in Figures A-4a and A-5 respectively. The sample, withdrawn from the stack, was passed through water condensers and filters and was pumped into the continuous monitors for NO_x, CO and O_2 concentration measurements. Because of the active particulates present in the sample stream in most tests, a separate sampling train was used for SO_2 measurement. The SO_2 sampling train is schematically shown in Figure A-4b. A phase discrimination probe, shown in Figure A-6 was utilized to minimize the contact of active particulate with the gas stream.

The continuous monitor instruments used for gas species composition listed in Table A-3. Instruments were operated according to EPA Performance Standards 2 and 3. Each instrument was calibrated by two gases: a zero gas and a span gas at approximately 90 percent of span. Instrument calibrations were performed every two hours during testing. Calibration gases were

TABLE A-2. SWS VENTURI FLOWMETER CALIBRATIONS

Calibration Date	Venturi Calibration Constant, K*				
	Venturi #1	Venturi #2	Venturi #3	Venturi #4	Venturi #5
10/31/83	5626	8778	8707	7711	8427
01/07/84	5044	8448	7764	7216	7826
10/01/84	5218	8448	8437	7132	7826
04/03/85			7575	7630	
Average	5296	8558	8120	7422	8026
Standard Dev.	244	155	466	252	258
Rel. St. Dev, %	4.60	1.82	5.74	3.40	3.22

* $\dot{M} = K\rho_{o}\sqrt{\Delta P/T}$

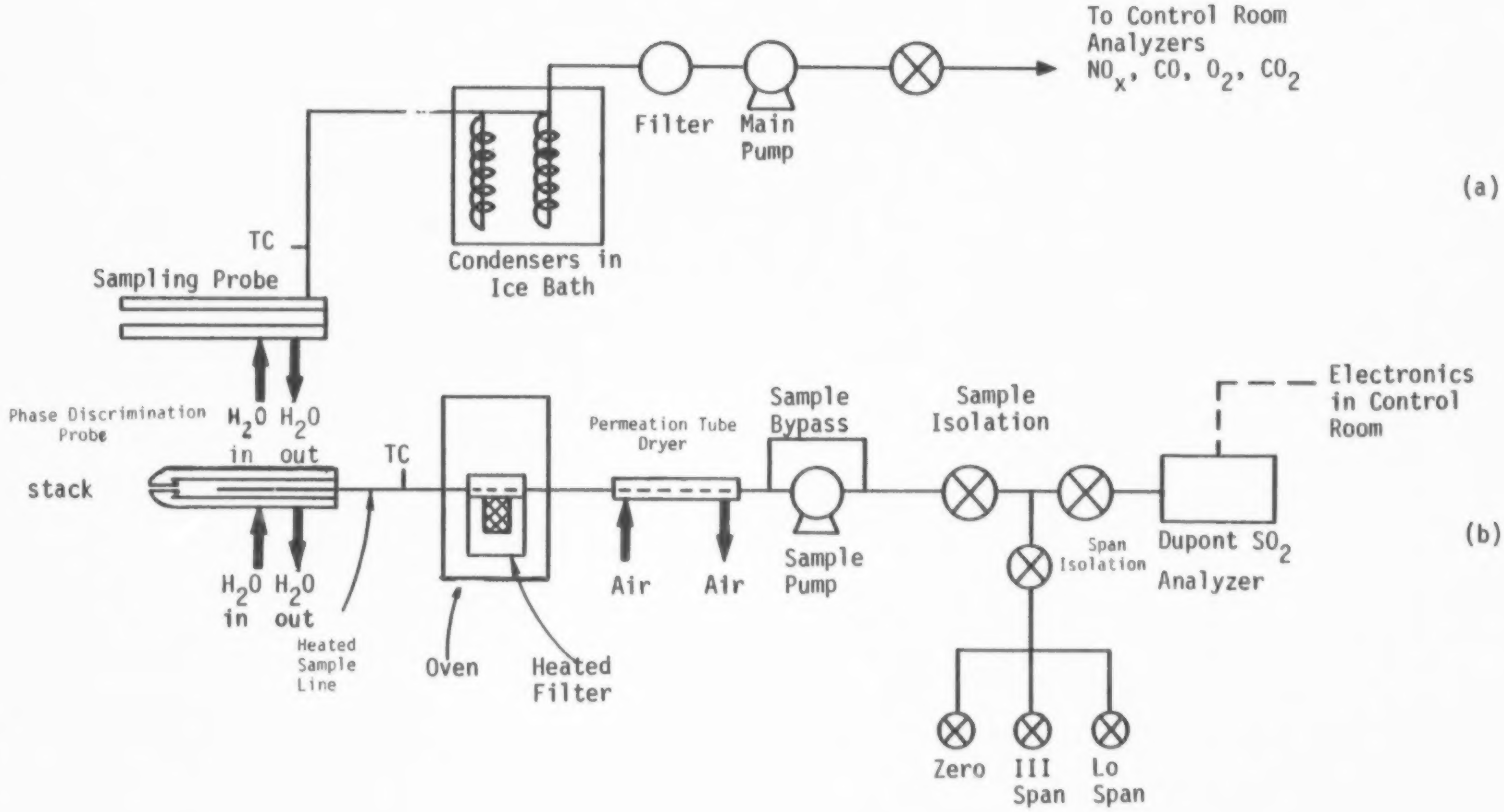
To Control Room
Analyzers
NO_x, CO, O_2, CO_2
Filter
Main Pump
(a)
TC
Sampling Probe
Condensers in Ice Bath
Phase Discrimination Probe
H_2O in
H_2O out
stack
TC
H_2O in
H_2O out
Heated Sample Line
Oven
Heated Filter
Permeation Tube Dryer
Air
Air
Sample Bypass
Sample Pump
Sample Isolation
Span Isolation
Dupont SO_2 Analyzer
Electronics in Control Room
(b)
Zero
III Span
Lo Span

Figure A-4. Schematic of SWS sampling system.

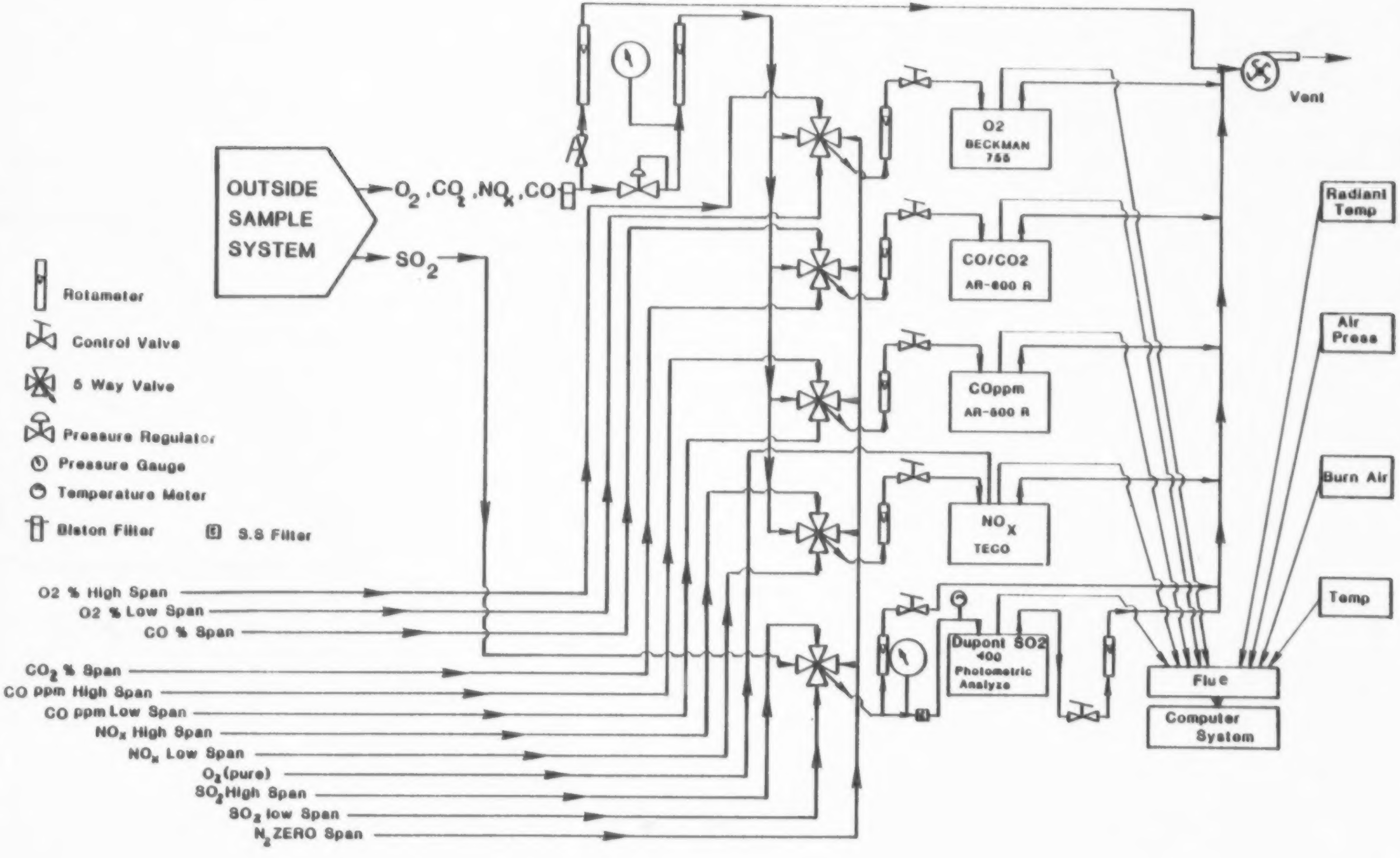
OUTSIDE SAMPLE SYSTEM
O_2, CO_2, NO_x, CO
SO_2
Vent
O2 BECKMAN 755
CO/CO2 AR-600 R
COppm AR-500 R
NO_x TECO
Dupont SO2 400 Photometric Analyze
Radiant Temp
Air Press
Burn Air
Temp
Flue
Computer System
Rotameter
Control Valve
5 Way Valve
Pressure Regulator
Pressure Gauge
Temperature Meter
Biston Filter
S.S Filter
O2 % High Span
O2 % Low Span
CO % Span
CO_2 % Span
CO ppm High Span
CO ppm Low Span
NO_x High Span
NO_x Low Span
O_2(pure)
SO_2 High Span
SO_2 low Span
N_2 ZERO Span

Figure A-5. SWS Furnace Analytical System

TABLE A-3. CONTINUOUS GAS ANALYSERS

Gas Measured	Detection Principle	Manufacturer	Model No.	Range
NO, NO_x	Chemiluminescent	Thermo Electron Corp. (TECO)	10 AR	0-1000 ppm
CO	Nondispersive Infrared (NDIR)	Anarad, Inc.	AR500R	0-500 ppm
CO_2	Nondispersive Infrared (NDIR)	Anarad, Inc.	AR500R	0-25 percent
O_2	Paramagnetic	Taylor Servomex	Type OA 272	0-10 percent
SO_2	UV Absorption	DuPont	400	0-5000 ppm

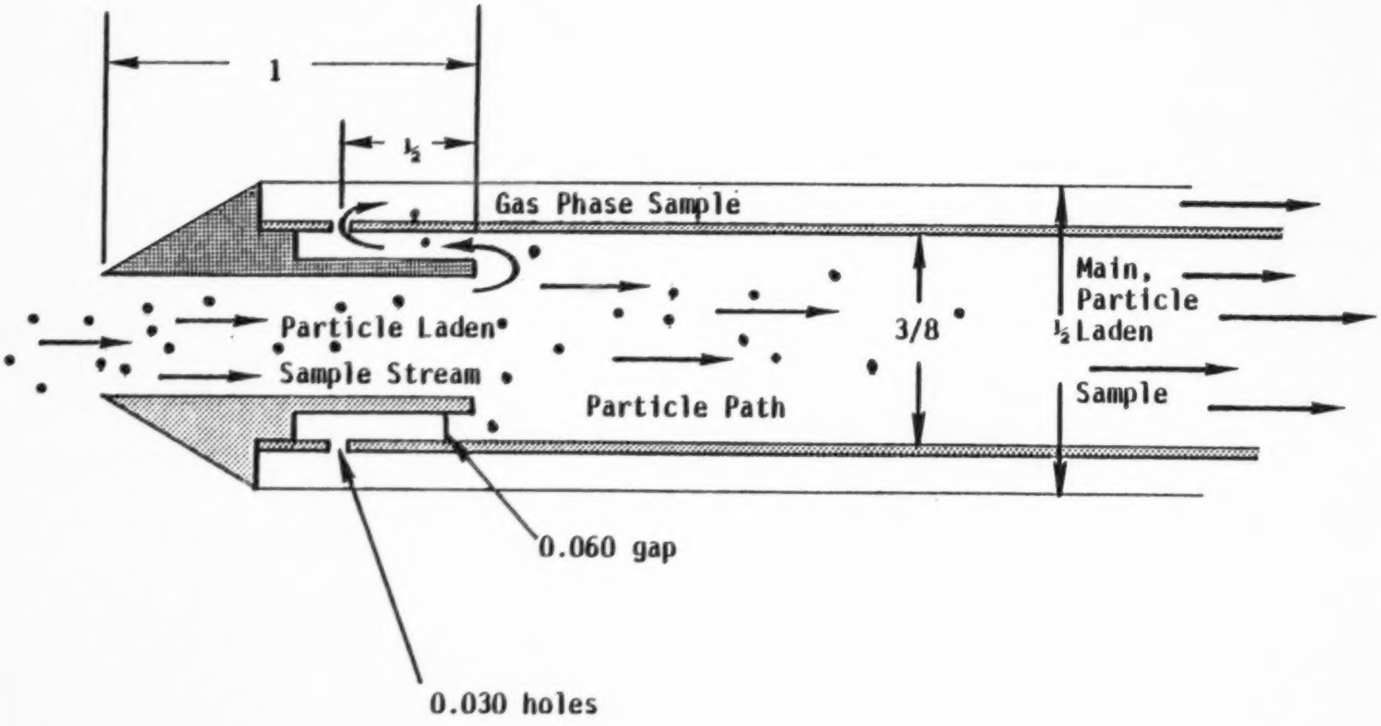
1
½
Gas Phase Sample
Particle Laden
Sample Stream
Particle Path
3/8
Main,
Particle
½ Laden
Sample
0.060 gap
0.030 holes

Dimensions: Inches

Figure A-6. Phase discrimination probe.

certified standard grade mixtures, compared by the manufacturer to primary standard gas mixtures (NBS traceable, gravimetrically prepared).

A series of Quality Assurance checks were carried out before this series of tests commenced. Instrument performance tests were conducted to determine the relative accuracy, calibration error and 2 hour drift. Table A-4 summarizes these results. The relative accuracy was determined by comparing the instrument values to values obtained using EPA Reference Methods. There is currently no performance specification for the CO monitor or standard reference method for CO determination, but calibration error and 2-hour drift tests were conducted in accordance with the guidelines for the other analyzers. The results showed that all of the instruments were within EPA specifications for the relative accuracy.

A.5 Furnace Exit Temperature

The furnace exit temperature and the gas temperatures in the furnace were measured with single shield suction pyrometers. Figure A-7 shows the tip construction of the suction pyrometer. K and S-type thermocouples were used in these pyrometers depending on the temperature levels. These thermocouples were manufactured according to the ASTM standards. The error limits for K-type thermocouple are ± 2.2°C or ± 0.75% of the reading (whichever is greater). The error limits for S-type thermocouple are ± 1.5°C or ± 2.5% of the measured temperature (whichever is greater). These pyrometers were calibrated to determine the optimum suction gas flowrate for temperature measurements. The calibration curve is shown in Figure A-8. During temperature measurements the suction flowrates were monitored by an orifice meter in the suction stream. In all tests, the suction flow rate was such that the pressure drop across the orifice flowmeter was kept above 0.20 inches of H_2O.

A.6 Solids Composition

Coal and ash samples were analyzed in EER's laboratory for carbon, hydrogen, nitrogen, ash, and moisture using a Perkin Elmer 240B elemental

TABLE A-4. INSTRUMENT PERFORMANCE TESTS SUMMARY

Instrument/ Manufacturer	Relative Accuracy		Calibration Error			2-Hour Drift Test			
	%	EPA Spec	Mid	High	EPA Spec	Zero	EPA Spec	Cali- bration	EPA Spec
O_2--Beckman	19.2	≤20	.26	2.32	≤5.0	.24	≤0.4	.30	≤0.4
CO_2--Anarad, Inc.	2.9	≤20	.08	0.31	≤5.0	.42	≤0.4	1.00	≤0.4
SO_2--DuPont	5.99	≤20	4.05	1.47	≤5.0	8.73	≤2.0	1.46	≤2.0
NO/NO_x--TECO	9.88	≤20	1.59	1.89	≤5.0	.38	≤2.0	2.4	≤2.0
CO--Anarad, Inc.	-	-	2.17	2.46	-	1.15	-	1.08	-

Note: O_2 & CO_2--EPA Method 3 (Orsat)

$SO_@$--EPA Method 6

NO_x--EPA Method 7

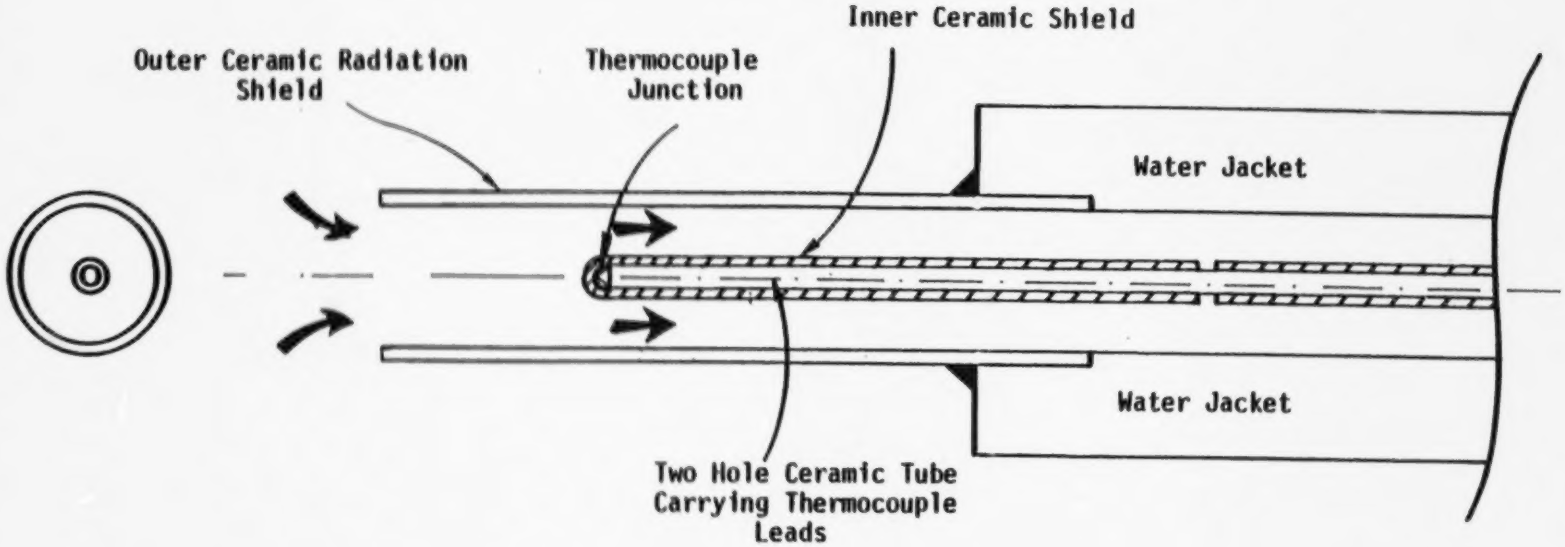
Inner Ceramic Shield
Outer Ceramic Radiation Shield
Thermocouple Junction
Water Jacket
Water Jacket
Two Hole Ceramic Tube Carrying Thermocouple Leads

Figure A-7. Suction pyrometer tip construction.

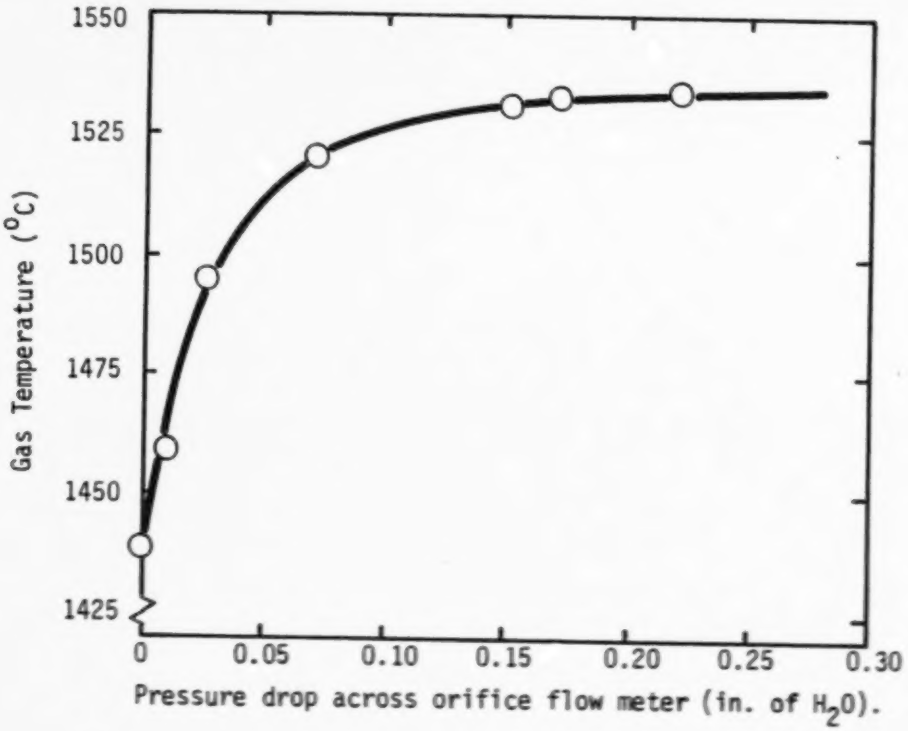

Figure A-8. Suction flowrate calibration for suction pyrometer.

analyzer, and for sulfur using a Leco SC32 sulfur analyzer. Coal samples were analyzed for heating value by Hazen Research, Inc. EER routinely determines precision and accuracy by analyzing replicate and standard samples. Results are monitored using quality control charts. Audit samples from EPA's Environmental Monitoring and Support Laboratory were sent to Hazen Research on a blind basis. Results of the analysis of 10 samples over the past 3 years have shown only 1 analysis to be outside the 2 percent accuracy levels. Two audit samples analyzed in replicate by Hazen showed precision of less than 0.2 percent. Audit results for the coal heating value are shown in Figure A-9. Audit results of EER's analysis for sulfur are shown in Figure A-10. An inter-laboratory comparison with Hazen Research to evaluate the precision and accuracy of EER's carbon, hydrogen, nitrogen, and ash analyses are shown in Table A-5. All values were within the QA goals except carbon and nitrogen. These values exceeded the goals due to the low levels of the measurements. The overall precision and accuracy were adequate to satisfy the needs of the program.

A.7 Summary of Quality Assurance Procedures

A summary of these quality assurance procedures is presented in Table A-6.

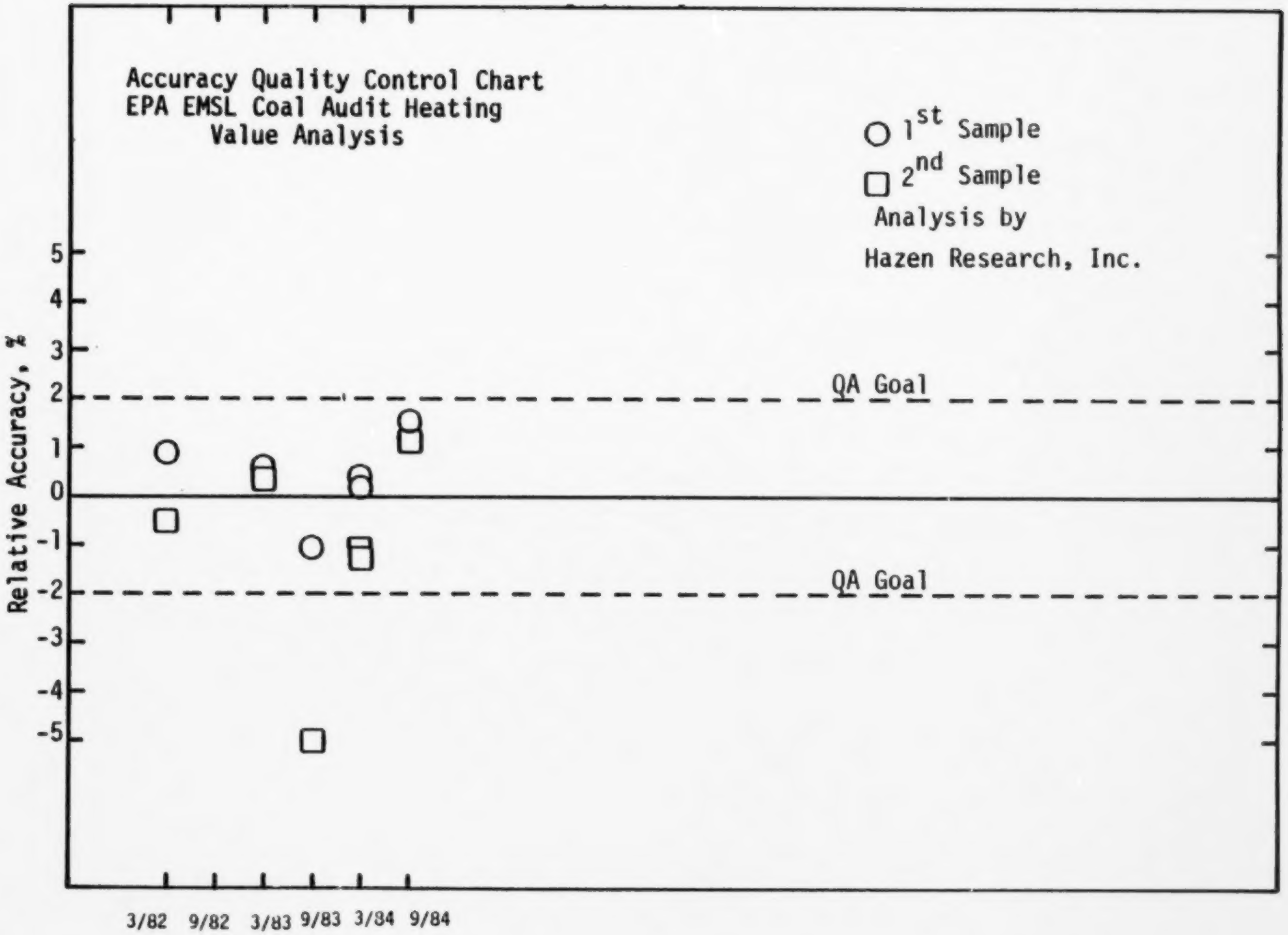

Figure A-9. Relative accuracy of heating value determinations.

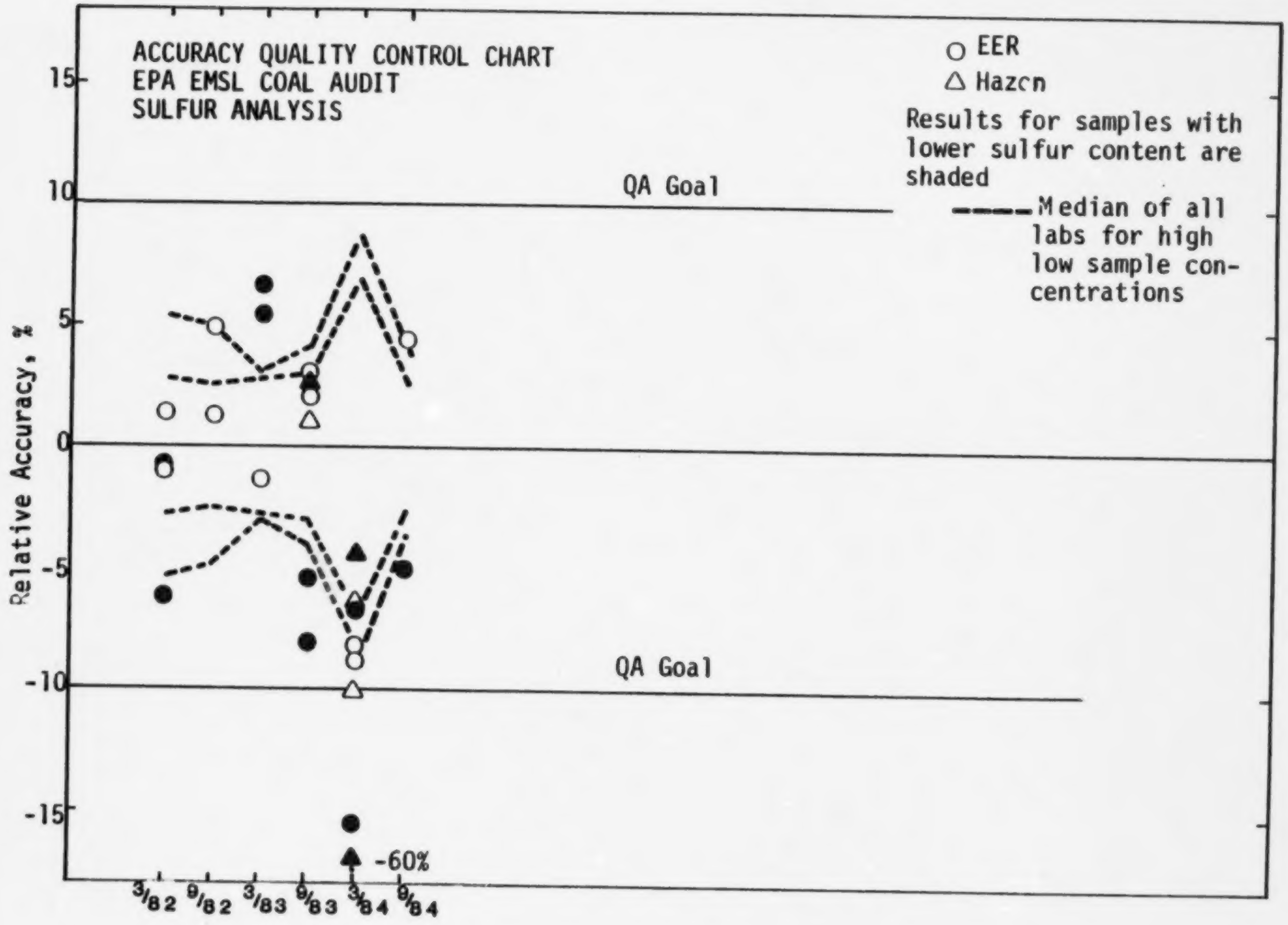

Figure A-10. Relative accuracy of coal sulfur.

TABLE A-5. SOLIDS ANALYSIS INTER-LABORATORY COMPARISON

	PARAMETER	EER ANALYSIS				STANDARD DEVIATION	HAZEN ANALYSIS	ACCURACY (%)
		1	2	3	AVG			
10-9-84 SAMPLE NO 115604	C	62.71	61.83	-	62.270	1.0	65.79	5.35
	H	4.10	4.17	-	4.140	1.2	4.00	3.38
	N	0.91	0.88	-	0.895	2.4	0.76	17.80
	Ash	8.85	8.46	8.86	8.720	2.6	8.99	3.00
10-9-84 SAMPLE NO 115610	C	63.60	62.18	-	62.890	1.6	66.41	5.30
	H	4.26	4.22	-	4.240	0.7	4.26	0.47
	N	1.05	0.85	-	0.950	14.9	0.78	21.80
	Ash	7.93	7.44	7.85	7.740	3.4	7.97	2.90
10-9-84 SAMPLE NO 115641	C	59.90	60.42	-	60.160	0.6	64.20	6.29
	H	4.04	4.09	-	4.065	0.9	3.75	8.40
	N	0.91	0.84	-	0.875	5.7	0.82	6.71
	Ash	11.60	11.46	-	11.530	0.9	11.62	0.77

AVG.	C	H	N	Ash
RELATIVE PRECISION,(%)	1.1	0.9	7.7	2.3
RELATIVE ACCURACY,(%)	5.65	4.08	15.44	2.22

TABLE A-6. SUMMARY OF QUALITY ASSURANCE PROCEDURES

PARAMETERS	MEASUREMENT METHODS	QUALITY CONTROL CHECK	FREQUENCY
Burner Settings	Direct Inspection		
Air Distribution	Calibrated Venturi Flowmeter	Verify calibration of venturi	Beginning and end of test series
Air Preheat Temperature	Thermocouples	Inspect thermocouple, replace as needed	Prior to each test day
Fuel Flow Rate	Mass Balance	Oil Check	Prior to each test day
Combustor Wall Temperature	Thermocouples	Check-out equipment	Prior to each test day
Furnace Exit Gas Temperature	Suction Pyrometer	Inspect thermocouple and shield, replace as needed	Prior to each test day
NO/NO_x	Continuous Monitor Chemiluminescence	EPA Performance Specification 2 Relative Accuracy Test	Beginning and end of tests
CO	Continuous Monitor NDIR	Check-out instruments and align electronics	Weekly
CO_2	Continuous Monitor NDIR	EPA Performance Specification 3 Relative Accuracy Test	Beginning and end of tests
SO_2	Continuous Monitor UV	EPA Performance Specification 2 Relative Accuracy Test	Beginning and end of tests
O_2	Continuous Monitor Paramagnetic	EPA Performance Specification 3 Relative Accuracy Test	Beginning and end of tests
HC	Continuous Monitor FID	Check-out instruments and align electronics	Weekly
In-Flame Gas Species	Grab Sample - GC/FID Continuous Monitor	EPA Performance Specification 2&3 Relative Accuracy Tests	Weekly
Particulate Mass Loading	EPA Method 5	EPA Audit Procedure, EPA-600/4-77-027b	Every fourth test
Solid Composition	Ultimate and Proximate Analyses (ASTM)	Spiked Samples, Replicate Samples	One per batch Three every other batch
Sorbent Feed Rate	Volumetric Feeder	Verify calibration	Weekly
Fuel Size Distribution	ASTM Method	Inspect screens, surrogate sample	Each test; one every tenth batch
Flame Characteristics	Color Video and Direct Inspection	Check-out equipment	Prior to use